The Control and Detection of Biomolecules Using Functional DNA

By

Aysha Ali

UNIVERSITY OF BIRMINGHAM

A thesis submitted to the

University of Birmingham

for the degree of

DOCTOR OF PHILOSOPHY

School of Chemistry

College of Engineering and Physical Science

University of Birmingham

October 2018

UNIVERSITY OF BIRMINGHAM

University of Birmingham Research Archive

e-theses repository

Abstract

Deoxyribonucleic acid (DNA) is the most important component of life and has many uses beyond the realm of natural biology. Synthetic oligonucleotide chemistry has allowed for the development of novel DNA based biotherapeutic and biosensing platforms that aim to overcome challenges faced within these fields. The versatility of synthetic DNA in the control and detection of biomolecules was investigated in this thesis using three topics:

1. The synthetic modification of the backbone of a thrombin binding aptamer (TBA). Thrombin is an important enzyme involved in the process of blood clotting and TBA competitively binds to thrombin at the same site as fibrinogen, disrupting the process of blood clotting. The TBA folds into a G-quadruplex formation and this structure is disrupted upon intramolecular photo-induced dimerisation of the two anthracene modifications. As a result, a switchable system was developed that allowed the reversible photo-control of thrombin activity using anthracene photochromism.

2. The synthetic modification, with one anthracene monomer, of the backbone of an oligonucleotide that probed for a Thymine (T) to Adenine (A) point variation in the BRAF gene, a known mutation in certain cancers. Genomic samples were amplified and successfully probed for the T or A point variant using fluorescence spectroscopy. The probe generated a linear dependence fluorescence plot, using synthetic DNA targets, to allow for the quantification of the allelic ratio of T to A within a sample of genomic DNA.

3. The bioconjugation of oligonucleotide probes to the M13-bacteriophage was utilised to design an assay, based on linear dichroism spectroscopy, for two potato virus strains. The assay was able to detect double stranded DNA targets at 0.03 nM, a level competitive with other detections methods that do not require amplification, and was further developed to detect two viral strains at once.

I dedicate this thesis to my mum, who has sacrificed everything to make me who I am today.

Acknowledgements

I would like to start by thanking my supervisors, the most important factors in me being able to get through this PhD; Professor James Tucker and Professor Timothy Dafforn. Jim and Tim, the dynamic duo, thank you for giving me this opportunity. My sincerest gratitude to Jim for trusting my biochemistry background in being able to complete a chemistry PhD. You never once questioned my abilities and that gave me the confidence to trust myself. Tim, without your positivity and enthusiasm for science I think I would have given up on lab work after my undergraduate degree. You have always had your offices open for me and tried to provide support in whatever way possible, especially when life was pretty tough for me. I will forever be grateful for having the best supervisors a student could ask for.

I am not even sure where to start with thanking the Tucker group. Haydn Little, Holly Andrews, Francia Allabush, Klaudia Englert and Media Ismail; thank you for being there from the beginning and being such awesome friends and teachers. Ed Wilkinson, Georgina Leck, and Charlotte Farrow; Sorry, (secretly not sorry), for all the times I have distracted you but I hope I've been of some help to your PhD degrees. Thank you to the past members of the group, in particular Huy Nguyen, John Kedge, David Kershaw and Ben Cross. A special mention to my adopted supervisor Dr Jean-Louis Duprey. Thank you for your knowledge, honesty, friendship and support. My PhD would not have been the same without you. Thank you to Chi and the analytical facility for always going above and beyond for us. Thank you to the Grainger and Cox groups; Russel Wood, Nick Cundy and Connor Prior for your laughs, coffee breaks, advice, and chemistry knowledge in our fourth floor office. Thank you to the Paco group for sharing your office with us and thank you to Daniel Gill for making the last few months bearable.

The Dafforn group and all the members of the seventh floor of Biosciences past and present, hats off to you for putting up with me for 6 years: Richard Logan, Rosemary Parslow, Steve Hall, Charles Moore-Kelly, Richard Meek, Julia Kraemer, Ian Cadby, Matthew Tridgett,

Timothy Knowles, Pooja Sridhar and Gareth Hughes. Zoe Stroud, a special thanks to you for being my PhD side-kick and always being willing to go on a sanity holiday with me, as if time in the lab with me was not enough. Here is to a lifetime of drinking coffee together! A big thank you to our collaborators at SASA, especially David Kenyon, Christophe Lacomme and Craig Douglas, for their enthusiasm, wisdom and contribution to my final PhD project.

Dr. Kasra Razmkhah, I never thought I would find such a life-long friend during one of my placements. You helped me believe that I could spend the next 3 years doing Chemistry. Your knowledge is incredible, and your tour guide skills of Tehran are even better. I cannot wait to see you in Iran again to continue the adventures of Kaz and Aysha. To the MIBTP 2014 cohort, we made it! Liam Riley and Niki Anthoney, I would not be where I am without you two. You two are more than family to me. Some of my best friends who have stuck by me for more than just these four years; Eleni Webb, Pippa Mitchell, Becca Gardner, Joy Hipwell, Joanna Hubbard, Jake Hyslop, Sven Kalinda and Grace Greggory. Thank you to Hamid Afshar for being my best friend throughout my time in Birmingham. I love you all so much.

To the Ghuman family. You have been my Birmingham family and have accepted me with open arms into all parts of your life. Harlene you have been a rock in my life. Without you and the hours of bench talk I don't know where I'd be right now. You're a hero and I don't think I could have asked for a better sister. Thank you for giving us Curren, I'm so excited to be Aunty Aysha to him for the rest of his life.

Mum you have been through so much in life and yet you have been the most loving, kind, solid mum that I could have ever asked for. You have made me who I am today and I am so proud to be writing the acknowledgements for my thesis because I know how much this means to you.

I am thankful to so many of you I have come across in the past four years because you are all the reason I've made it through the past 4 years smiling.

Table of Contents

Abbreviations

Abbreviations

2D	Two-dimensional
3D	Three-dimensional
6-FAM	6-Fluorescein
6K1	Second 6 Kilodalton Protein
AeT	Anthracenylethynyl
AeeT	Anthracenylbuta-1,2-diynyl
ATP	Adenosine triphosphate
ALISA	Aptamer-linked Immunosorbent Assay
APS	Ammonium Persulfate
ASO	Antisense Oligonucleotide
AuNP	Gold Nanoparticle
BDPs	Base Discriminating Probes
BSA	Bovine Serum Albumin
CD	Circular Dichroism
cDNA	Complementary deoxyribonucleic acid
CEF	Chick Embryo Fibroblasts
CIb	Cylindrical Inclusion Body
CP	Coat Protein
CPG	Controlled Pore Glass
CRC	Colorectal Cancer
Cy3	Cyanine 3
Cy5	Cyanine 5
DASH	Dynamic Allele-Specifc Hybridisation
DGGE	Denaturing Gradient Gel Electrophoresis
DHPLC	Denaturing High Performance Liquid Chromatography
DCM	Dichloromethane
DMSO	Dimethylsulfoxide
DMT	Dimethoxytrityl
DNA	Deoxyribose Nucleic Acid
dNTPs	Deoxynucleotide Triphosphates
dsDNA	Double Stranded DNA
E. coli	Escherichia coli
EDTA	Ethylenediaminetetraacetic Acid
ELISA	Enzyme-Linked Immunosorbent Assay
EM	Electron Microscopy
EMSA	Electrophoretic Mobility Shift Assay

ES-MS	Electrospray Mass Spectrometry
ESI	Electrospray Ionisation
FRET	Förster Resonance Energy Transfer
G4	G-quadruplex
H-bonds	Hydrogen Bonds
HC-Pro	Helper Component Proteinase
HPLC	High Performance Liquid Chromatorgraphy
HPV	Human Papilloma Virus
HIV	Human Immunodeficiency Virus
LB	Lysogeny Broth
LD	Linear Dichroism
M13	M13 Bactriophage
MM	Malignant Melanoma
MRI	Magnetic Resonance Imaging
MS	Mass Spectrometry
Native-PAGE	Native Polyacrylamide Gel Electrophoresis
NIa	Nuclear Inclusion Protein a
NIb	Nuclear Inclusion Protein b
O/N	Overnight
P1	First Protein
P3	Third Protein
PAGE	Polyacrylamide Gel Electrophoresis
PCR	Polymerase Chain Reaction
PEEK	Polyetheretherketone
PEG	Polyethylene Glycol
PIPO	Potyviridae Open Reading Frame
PMSA	Prostate-Specific Membrane Antigen
PNA	Peptide Nucleic Acid
PolyT	Poly Thymine
PVA	Potato Virus A
PVX	Potato Virus X
PVY	Potato Virus Y
Q-PCR	Quantitative Polymerase Chain Reaction
RNA	Ribose Nucleic Acid
RP-HPLC	Reversed Phase High Performace Liquid Chromatography
RT	Room Tempeature
SEC	Size Eclusion Chromatography
SELEX	Systematic Evolution of Ligands by Exponential Enrichment

Stat3	Signal Transducer and Activator of Transcription 3
SMCC	Succinimidyl 4-(N-maleimidomethyl)cyclohexane-1-carboxylate
SNPs	Single Nucleotide Polymorphisms
SOC	Super Optimal Broth with Catabolite Repression
ssDNA	Single Stranded DNA
ssRNA	Single Stranded RNA
TBA Buffer	Thrombin Binding Aptamer Buffer
TBA	Thrombin Binding Aptamer
TBE	Tris/Borate/EDTA
TCA	Trichloroacetic acid
TCEP	Tris-(2-Carboxyethyl)phosphine
TEAA	Triethylammonium Acetate
TEMED	Tetramethylethylenediamine
T_m	Melting Temperature
TOF	Time of Flight
UV	Ultraviolet
UV-Vis	Ultraviolet-visible
VEGF	Vascular Endothelial Growth Factor
VPg	Viral Genome Linked Protein
VT-CD	Variable Temperature Circular Dichroism
WT	Wild-type

DNA Bases

A	Adenine
C	Cystosine
G	Guanine
T	Thymine
U	Uracil

Chapter 1 - Introduction

1.1 Introduction

This chapter serves as an introduction to three specific applications of synthetic deoxyribonucleic acid (DNA); therapeutics, genomic point variation detection, and viral DNA detection. As this thesis covers three diverse projects, where the common theme is the use of modified DNA oligonucleotides, this review will cover:

- A basic background on DNA

- DNA modifications, specifically anthracene modification of oligonucleotides

- The different uses of synthetic DNA, specifically DNA aptamers and DNA-based detection systems.

1.2 Structure and applications of synthetic DNA

1.2.1 DNA structure

Within living cells our hereditary information is stored in chromosomes that primarily consist of DNA, a macromolecular polymer. However, to understand how this information is stored it is important to explore the building blocks of DNA. A DNA polymer consists of long repeating units of nucleotides, with nucleotides made up of a deoxyribose sugar, an organic base and a phosphate group. The deoxyribose sugar contains hydroxyl groups that are able to undergo condensation reactions with the bases and the phosphates to build a nucleic acid monomer. The backbone of DNA is comprised of these deoxyribose sugars covalently linked by phosphate groups (**Figure 1.1**). Each deoxyribose sugar molecule has a nitrogen-containing base attached, of which there are four different types. The nucleobases are the purines, adenine (A) and guanine (G), and the pyrimidines, cytosine (C) and thymine (T) (**Figure 1.2**). Ribonucleic acid (RNA) is similar to DNA, but utilises a ribose sugar instead and replaces T nucleobases with uracil (U).[1]
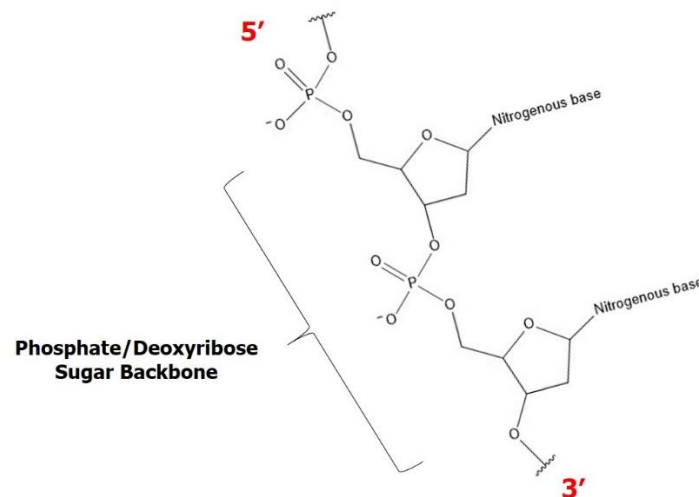
Figure 1.1 *A basic view of a dinucleotide consisting of a deoxyribose sugar, a nitrogenous base and a phosphate group covalently bonded to another nucleotide by a phosphodiester bond.*
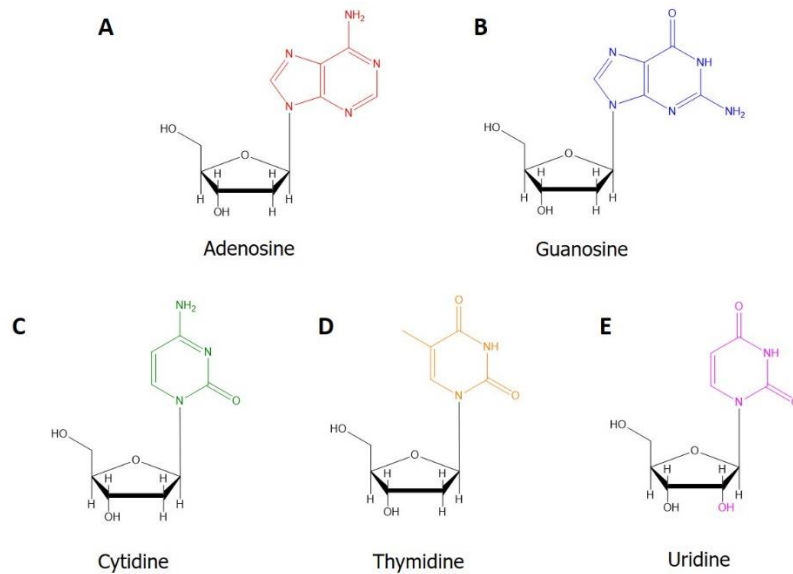
Figure 1.2 *The four different nucleosides found in DNA:* **A)** *Adenosine,* **B)** *Guanosine,* **C)** *Cytidine,* **D)** *Thymidine and in RNA* **E)** *Uridine.*

The directionality of DNA comes from the 5'- and 3'- ends of a single DNA strand, where the 5'- end contains a free phosphate group attached to the 5'- carbon whereas the 3'- end contains a free hydroxyl group from the 3'- sugar in the final base. Two single strands of DNA (ssDNA) are linked by base pairing between the bases to form an anti-parallel double-helical structure, with an A base pairing with a T base via two hydrogen bonds (H-bonds) and a G pairing with a C bases via three H-bonds (**Figure 1.3**). The order of these nucleobases within DNA encodes the hereditary information mentioned earlier and in living cells, this code is read and translated into amino acids, which then form peptides and proteins.
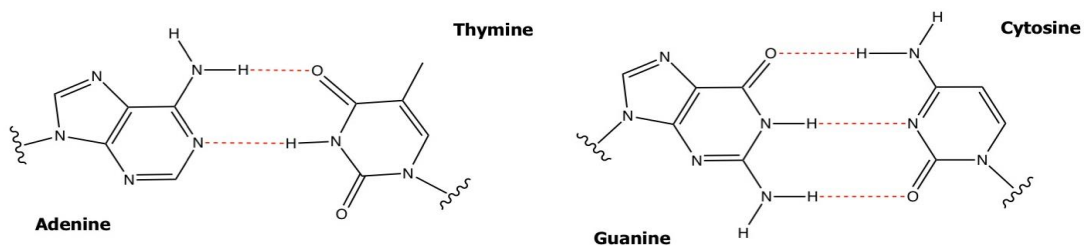
Figure 1.3 *The A and T base pair held together by two H-bonds (left) and the G and C base pair held together by three H-bonds (right). The H-bonds are shown in red.*

The double helical nature of DNA was first hypothesised by Watson and Crick in 1953.[2] This led to the discovery of three main types of DNA secondary structure; A-DNA, B-DNA and Z-DNA forms (**Figure 1.4**). B-DNA is the most common form of DNA found in biology and has a right-handed helical structure. The B-form has distances of 0.34 nm between each base pair, a contributing factor to the folding of the strands. The DNA structure is often described of as a "ladder", however, the glycosidic bonds that hold the deoxyribose sugar and the bases are not at fixed 90° angles like the rungs on a ladder resulting in asymmetric grooves when the strand folds into a helix thus creating the major and minor grooves seen within a DNA double-helix. The A-form of DNA is also a right-handed double helix but with a shorter distance (reduced to 0.26 nm) between nucleotides, resulting in a more compact helix. The Z-form of DNA forms a left-handed helix and normally occurs when there are repeats of purines and pyrimidines present (preferentially poly(G:C)).[3]
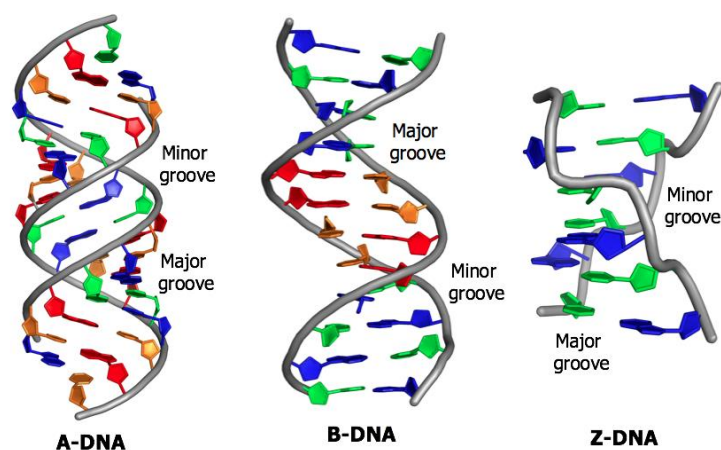
Figure 1.4 *The three main structures of duplexed DNA helices; the right handed A-DNA helix (left), the right handed B-DNA helix (middle) and the left handed Z-DNA helix (right).*

Research into the structure of DNA and individual nucleotides has been strengthened by the development of automated synthesis of short single strands of DNA (known as oligonucleotides) from which the fields of DNA nanotechnology,[4] synthetic biology,[5] medicine[6] and forensics[7] have greatly benefited. The next section will discuss the role of both single stranded DNA (ssDNA) and double stranded DNA (dsDNA) as a scaffold in nanotechnology, and the many uses they have outside of the cellular environment.

1.3 Aptamers

The ability of short ssDNA to form complex 3D structures has led to the development of new molecular recognition elements, known as aptamers.[21-24] DNA or RNA aptamers are short oligonucleotides that can bind proteins, small molecules and other cellular targets (**Figure 1.5**). DNA and RNA normally form duplexes by hybridisation to complementary sequences. However, through the formation of other secondary structures, interactions with different targets can be engineered. This is done using a technique called the Systematic Evolution of Ligands by Exponential Enrichment (SELEX) which selects sequences with high specificity and high affinity for the desired target.[8]
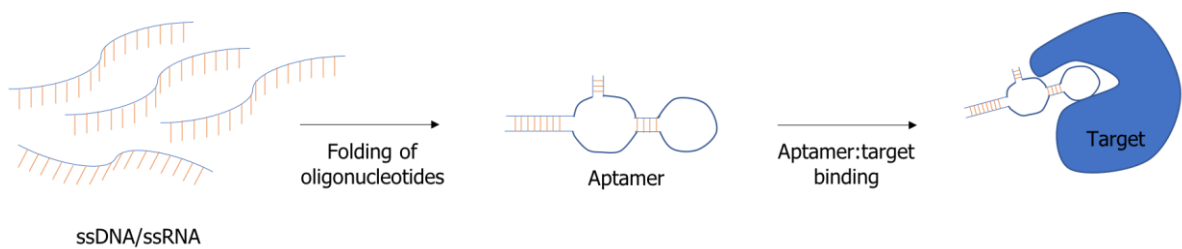
Figure 1.5 *Aptamer ssDNA/ssRNA strands self-complement and fold into 3D structures which then bind to the desired the target molecule.*

1.3.1 Systematic Evolution of Ligands by Exponential Enrichment (SELEX)

The SELEX procedure involves the construction of an RNA or DNA library consisting of nucleotide strands that contain two constant regions flanking a randomised region (**Figure 1.6**).[9] The randomised regions of the strands are the areas of interest for target binding and can be of a variable length and the constant regions are the sites where primers will bind for subsequent amplification steps (**Step 1, Figure 1.6**). The library is then incubated with the target molecule (**Step 2, Figure 1.6**) and any non-binding strands are washed away (**Step 3, Figure 1.6**).[9]
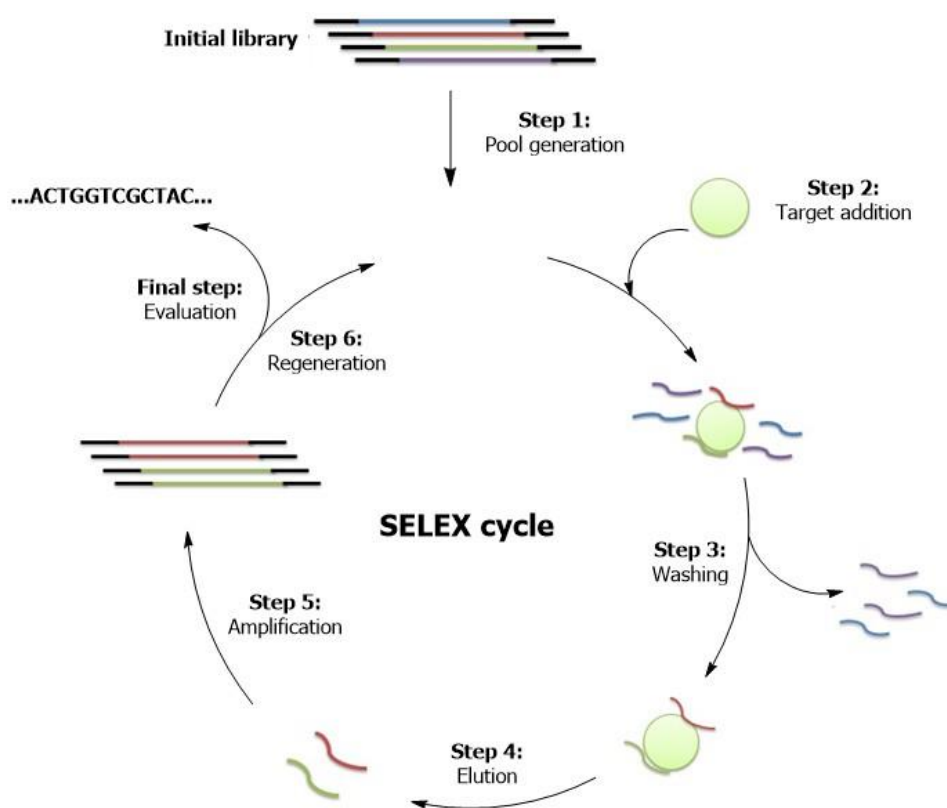
Figure 1.6 *One cycle of SELEX involving;* **step 1**: *pool generation,* **step 2**: *target addition,* **step 3**: *wash and removal of unbound   sequences,* **step 4**: *elution of bound sequences,* **step 5**: *amplification of bound sequences and* **step 6**: *regeneration and evaluation of sequences specific to the target ligand.*

The resulting nucleotide sequences that are specific to the target of interest are eluted (**Step 4, Figure 1.6**) and amplified (**Step 5**, **Figure 1.6**) using polymerase chain reaction (PCR) (**Section 1.6.2**).[10] Reverse transcriptase PCR is used for the generation of RNA aptamers.[11] After the PCR process, a pool of aptamer sequences with some binding affinity to the target molecule is

generated. The strands are then used in the next round of the SELEX cycle. Subsequent pools are treated under increasingly rigorous conditions such as changed buffer conditions, reaction volumes, and incubation times, to produce aptamers sequences with higher binding affinities to the target molecule.[12]

Cell-SELEX is used when the target is a whole cell rather than a biomolecule and the target for the aptamer will likely be a protein on the surface of the cell. The process of cell-SELEX requires specialist equipment as a cell cannot easily be immobilised onto a surface. The "counter selection" process that will rid the pool of aptamers that have non-selectively bound to the surface of the cell, or those aptamers that are bound to areas that are also found in many other cells. This adds another layer of complication to SELEX. However, the power of successful aptamer generation to a cell is greater than that for simple biomolecular targets.[13-14]

1.4 Synthetic DNA modification

Often, the standard four nucleobases are not enough to gain full access to the potential that oligonucleotides hold. For example, the detection of biomolecules is aided by using oligonucleotides tagged with fluorophores and the modification of aptamers can add extra functionality. In this section different modifications of DNA will be discussed, in particular, a base replacement by an anthracene phosphoramidite, will be considered in detail.

The modification of the backbone of an oligonucleotide strand is one of the easiest modifications that can be done during, or post, synthesis. A phosphorothioate modification, discovered by Eckstein in 1966,[15] is an example of one such backbone modification (**Figure 1.7**). The modification exchanges an oxygen group for a sulphur group in the phosphate backbone but conserves the negative charge. The modification has been used in order to improve the stability of oligonucleotide therapeutics as the strands become less likely to be recognised by nucleases in the body.[16]

Phosphate backbone in natural DNA   Phosphorothioate DNA modification
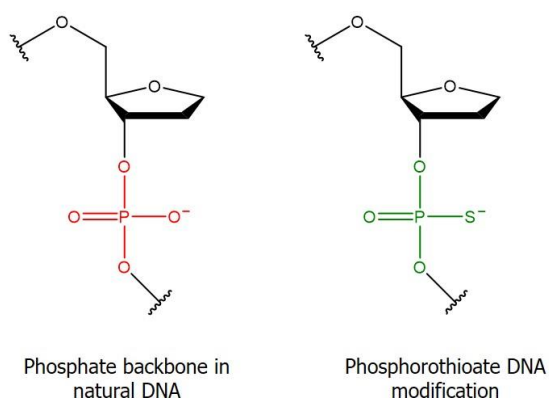
Figure 1.7 *The phosphorothioate backbone modification to protect the DNA strand from nuclease degradation.*

Conjugate linker groups, such as thiol modifications, are readily available as phosphoramidites and can be end strand modifications that are incorporated onto the 5'- or 3'- end of an oligonucleotide during synthesis. These modifications allow the conjugation of the strands to nanoparticles and other biomolecules.[17]

Many other chemical modifications of oligonucleotides exist but for the purpose of this thesis the focus will be on partial backbone replacement of DNA with non-nucleosidic groups. This involves

the replacement of the sugar unit within DNA with a chemical linker. An example of this is the

replacement of the sugar-phosphate backbone within DNA using M-(2-aminoethyl)glycine creating

a peptide nucleic acid (PNA) (**Figure 1.8**). These PNA strands are able to hybridise both DNA and

RNA in a similar manner to the hybridisation of DNA-DNA or DNA-RNA.[18]
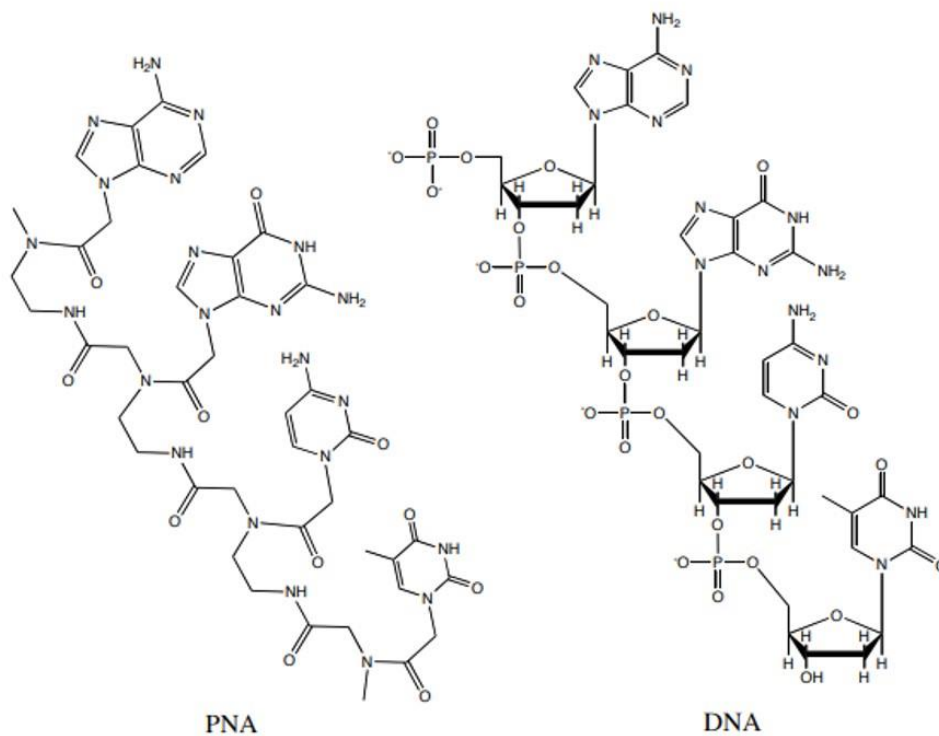
Figure 1.8 The structure of a single strand of PNA with the standard A, T, C, G nitrogenous bases (left) versus the structure of DNA (right).

The deoxyribose sugar within a nucleotide can be replaced with chemical modifications while maintaining the phosphate groups thus allowing the formation of phosphodiester linkages between the modified bases and the canonical bases during chemical synthesis of oligonucleotides. This is the case when the modifications involve alkyl based acyclic linkers that mimic the ribose of a nucleotide. An amino acid group linked to a diethanolamine backbone was synthesised by Saito *et al.*, for the introduction of two pyrene molecules to an oligonucleotide strand (**Figure 1.9A**).[19] The amino acid linker group enabled the stereochemical control of the modifications within the oligonucleotide. Bashkin *et al.*, utilised serinol to attach terpyridine sites (**Figure 1.9B**), that coordinate metals, to RNA. This allowed for the study of copper dependent RNA cleavage.[20]
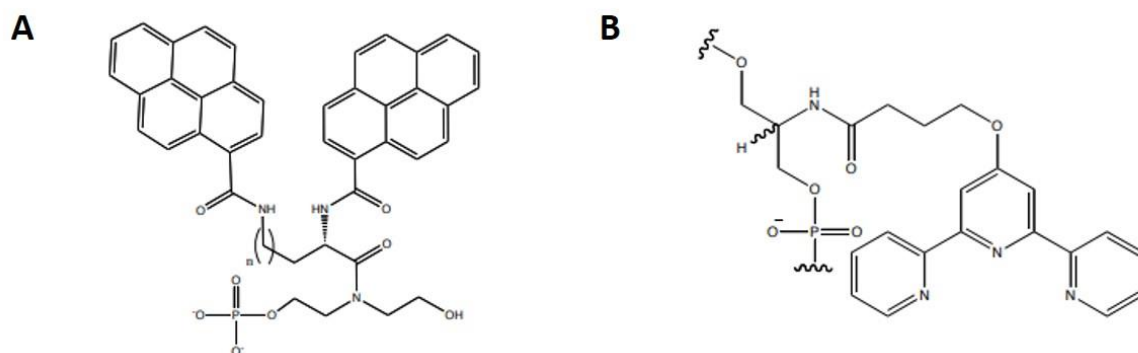
Figure 1.9 A) *The two pyrene modifications that were linked to an L-amino acid with a phosphate group in order to be tethered to oligonucleotides and **B)** The serinol linker attached to a terpyridine modification also synthesised with a phosphate group.*

1.4.1 Anthracene

Anthracene, commonly used due to its photochromic properties, is a conjugated, cyclic organic compound made of 3 benzene rings fused together.[21-22] The aromatic properties of the molecule give rise to its characteristic absorption (300-400 nm) and fluorescence (400-500 nm) spectra.[23] Anthracene has been utilised in this project as both a photochemical moiety incorporated into oligonucleotide aptamers (**Chapter 3**) and a fluorescent tag in an oligonucleotide probe (**Chapter 4**).

Anthracene is a chemical with many uses and has the ability to; fluoresce, form excimers, intercalate, and dimerise. Anthracene crystals have long been known to be efficient organic scintillators for the detection of radiation and have the ability to distinguish between neutrons and gamma rays. Ionising radiation energy can be absorbed by anthracene crystals which will fluoresce as the system relaxes back down to the ground state becoming the basis of photomultiplier scintillation counters.[24-25] The anthracene ring is capable of undergoing a Diels-Alder reaction with a singlet oxygen dienophile to form endoperoxides.[26-27] When the system is exposed to UV irradiation the endoperoxide reverts back to anthracene and a singlet oxygen species. Recently, these reactions have been used to release singlet oxygen species into tumour cells to cause cell apoptosis for photodynamic cancer therapy.[28]

The ability of anthracene to intercalate into DNA has been harnessed for anticancer therapy. The intercalation events can be monitored by the photophysical changes to the anthracene once it is bound to the DNA, using both UV-visible and fluorescence spectroscopy.[29] Anthracyclines are a class of anthracene drugs that have previously been used in cancer therapy. They intercalate and inhibit both DNA and RNA synthesis and in turn prevent the replication of the cancer cells.[30-31]

Anthracene can also be covalently linked to nucleotides as a reporter molecule to introduce specificity and increased duplex stability for fluorescence sensing applications. Anthracene has previously been attached to the 2'- position of the deoxyribose sugar resulting in an increase in the stability of dsDNA duplexes formed as the anthracene intercalates into the duplex.[32] The sensing properties of anthracene will be discussed in detail in **Chapter 4**.

Anthracene photochromism is an important physical property that has been effectively explored within supramolecular systems (**Chapter 3**). Briefly, anthracene photodimerisation has been used

to control biological events and to create higher order DNA nanostructures. Anthracene ligated onto the 5'- or 3'- ends of single strands of DNA have been used by Ihara and co-workers to make DNA-anthracene conjugates. The anthracene molecules were only able to efficiently form dimerised photoadducts when the oligonucleotide strands they were conjugated to were fully complementary (**Figure 1.10**). The study demonstrated the ability of photodimerisation of DNA-anthracene conjugates to discriminate between base differences within segments of oligonucleotides.[33]

Finally, anthracene monomers can be incorporated into the backbone of oligonucleotides as base mimics using solid phase oligonucleotide synthesis by covalently attaching the anthracene to a non-nucleosidic scaffold.[34] The Tucker group has previously used a serinol linker to introduce anthracene modifications into DNA.[34] However, the serinol linker resulted in stereoisomeric mixtures being incorporated into the strands.[35] A threoninol linker is now used to generate oligonucleotides with anthracene modifications where the stereochemistry can be chosen as the linker is available as both the L(RR) or the D(SS) form allowing the production of two diastereomeric phosphoramidites (**Figure 1.11**). This threoninol modification becomes the basis for both the photochemical and fluorescence studies of anthracene within DNA for binding and detection in this project. The specific anthracene uses in this thesis will be discussed in detail in **Chapter 3** (photochemical properties) and **Chapter 4** (fluorescence properties).
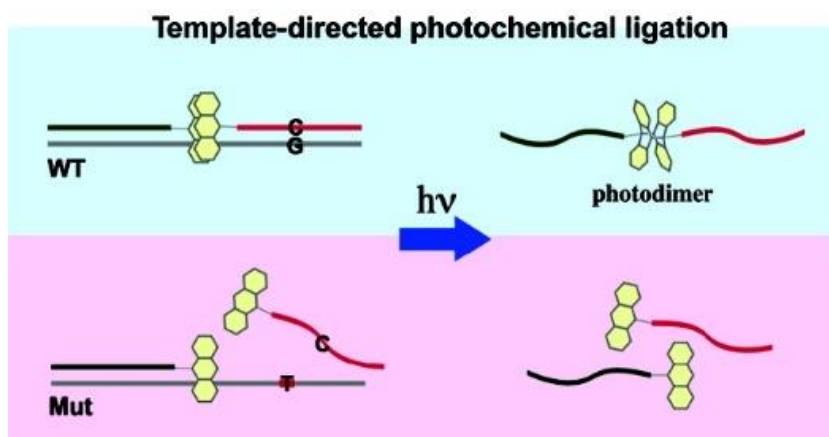
Figure 1.10 *Research by Ihara et al., demonstrating the detection of base changes in ssDNA using DNA probes conjugated to anthracene modifications at either the 5'- or 3'- ends of the strands. If the strands had fully complementary base sequences then photodimerisation of the anthracenes using UV light was possible and if a base variation was present then photodimerisation of the anthracenes was not possible.*[36]

L-threoninol (*R,R*) linker   D-threoninol (*S,S*) linker
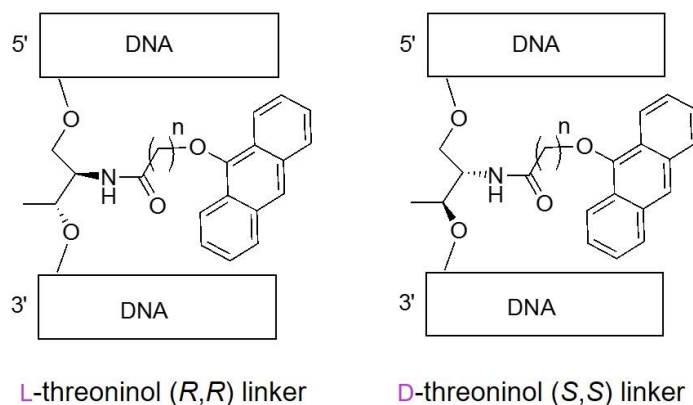
Figure 1.11 *a) D-threoninol (S,S) and b) L-threoninol (R,R) linkers incorporated as a base into the middle of an oligonucleotide strand.*

14

1.5 Applications of synthetic DNA

A number of key aspects make synthetic oligonucleotides attractive for varying roles. For example, it is possible that aptamers could substitute for antibodies as the production of antibodies is expensive[37-38] and slow compared to the synthesis of an aptamer using the DNA synthesis phosphoramidite method (**Chapter 2**). In addition, DNA can be easily modified and functionalised using a DNA synthesiser and this provides a means to improve functionality, stability and binding of the strands to their targets.[39-40] DNA has been used in a range of applications including analytical research, medicine, nanotechnology and the diagnosis of disease, some of which will be explored next.[41]

1.5.1 DNA in self-assembly and nanotechnology

The field of DNA nanotechnology aims to harness the specificity displayed by the chemical properties of DNA to create materials that are highly ordered. The Watson-Crick base pairing brings specificity to the system and the ability to chemically synthesise oligonucleotides has meant the information encoded by DNA can be used to design and programme libraries of short ssDNA that can assemble into specific arrangements, thus allowing for the precise location of each component within a system to be controlled. Seeman et al. applied a branched DNA junction, referred to as the Holliday junction (

Figure *1.12*) seen naturally during DNA replication, to create larger oriented two-dimensional (2D)[42] and subsequently three-dimensional (3D) DNA structures using synthetic DNA.[43]
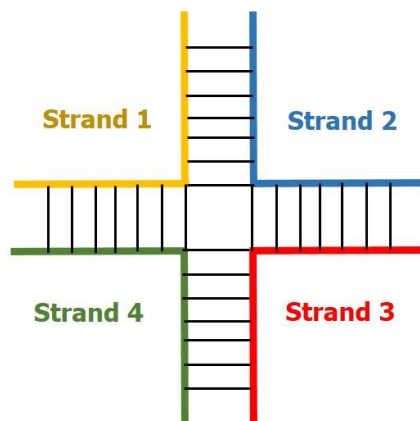
Figure 1.12 *The design of a Holliday junction by Seeman et al. using synthetic oligonucleotide strands. In this example, four oligonucleotide strands are designed to have complementary base pairing to one other leading to the formation of the Holliday junction, a branched junction commonly seen during DNA replication.*

An example of the uses of these DNA scaffolds can be seen in the research by Kiehl *et al*. furthered to create a 2D DNA scaffold based on gold nanoparticles.[44] The nanoparticles were functionalised with an oligonucleotide that was complementary to one motif on a three component DNA scaffold, and this generated a gold-based nanoscale circuit that could be used for nanoelectronics (**Figure 1.13**). Stulz *et al*. have worked on modified deoxyuridine containing porphyrin rings to create nanometre scale DNA-porphyrin arrays.[45] Eleven tetraphenyl porphyrins were covalently attached in a row sitting in the major grove of a double stranded helix. These structures were also evaluated for their ability to act as electron wires.[46]
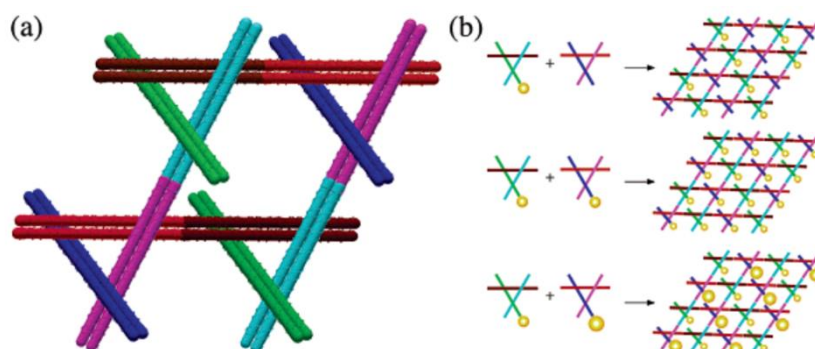
Figure 1.13 a) the three component DNA array that leaves one motif (the green or blue) to bind to a gold nanoparticle and *b)* the motifs seen in green and blue binding to an oligonucleotide functionalised onto a gold nanoparticle forming a 2D array that can function as a semiconductor.[44]

1.5.1.1 DNA origami

The field of DNA origami was introduced by Rothemund in 2006 to simplify the design and creation of higher order DNA assemblies.[47] The creation of large scale DNA structures requires the use of many oligonucleotide strands that rely on multiple binding reactions to assemble correctly. However, DNA origami involves the use of readily available ssDNA, (e.g. the viral M13 bacteriophage genome), and short staple oligonucleotide strands to create a desired nanostructure. The viral DNA acting as a scaffold increases the efficiency of the folding and results in the assembly forming more entropically favourable. The M13 bacteriophage DNA sequence, and the design of required origami, is entered into a computer programme, and the programme calculates the length, sequence and number of oligonucleotide staple strands required to create the larger DNA origami structure (**Figure 1.14**).[47]
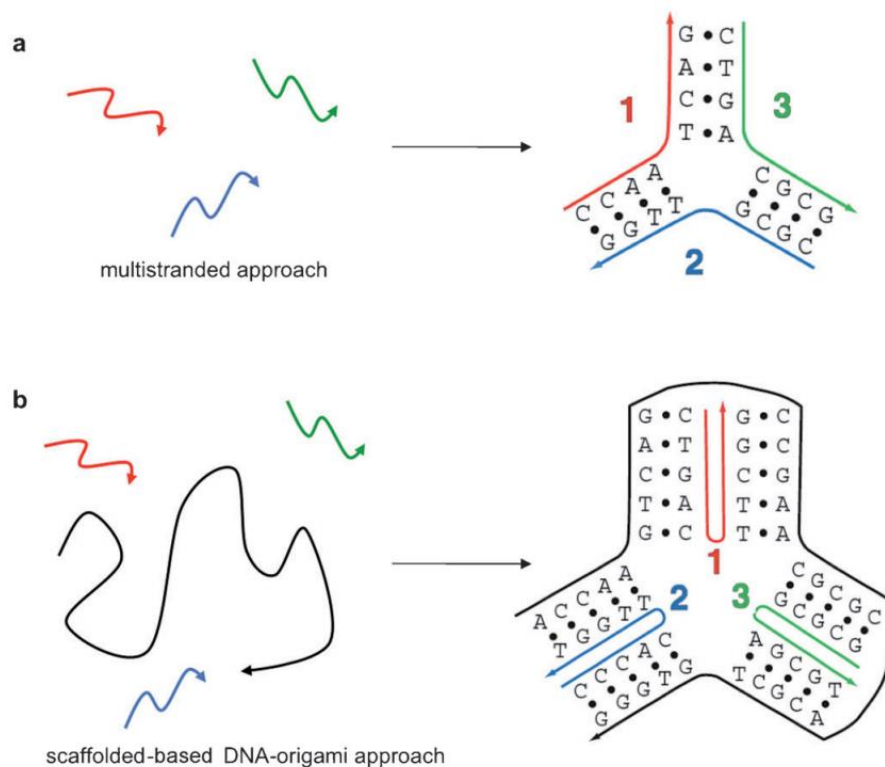
Figure 1.14 *The idea behind Rothemund's DNA origami approach **a)** the multistranded approach using a number of short staple strands to create a higher order structure. The more complicated the design of the 2D or 3D structure the higher the number of staple strands required to create the structure. **b)** the scaffolded-based DNA-origami approach which will require a smaller number of staple strands, when compared to the multistrand approach, the more complicated the structure becomes.[48]*

One earlier application of DNA origami involved the formation of liquid crystal DNA structures that allowed the structural determination of membrane proteins using nuclear magnetic resonance (NMR). William Shih *et al.* created helical nanotubes using DNA that formed liquid crystals that increased the stability of membrane proteins when present with the detergents normally used to solubilise membrane proteins. This increased stabilisation allowed a more accurate determination of the backbone residual dipolar couplings of the proteins using NMR.[49] Since, DNA origami has been used for many applications, for example; the study of biochemical process,[50] the creation of molecular motors,[51] the generation of thermally stable materials,[52] metal based nanostructures,[53] and drug delivery.[54]

1.5.2 DNA-based drug delivery

For a drug delivery method to be successful it must be; non-toxic to the host, able to transverse across cell membranes, show specificity to the target cell, and it must provide protection to the drug molecule against degradation. Self-assembled DNA nanostructures are promising drug delivery platforms as they are capable of fulfilling many of these requirements while being compatible with cellular environments and biodegradable. As mentioned earlier, DNA can be programmed to self-assemble into a tetrahedron, by complementary base pairing of four or more oligonucleotide strands.[55] These structures are rigid and stable and can provide a means to deliver drugs into cells and the structures can be loaded with drug molecules using intercalation or DNA bioconjugation.[56] For example, Kim *et al*. created a DNA tetrahedron made of four oligonucleotides, one of which contained a Cyanine 5 (Cy5) dye for visualisation purposes. The tetrahedron was then loaded with doxorubicin, a DNA intercalating drug used to treat cancer (**Figure 1.15**). Breast cancer cells often become resistant to doxorubicin and these findings demonstrated that DNA tetrahedron structures linked to doxorubicin were able to be internalised by these resistant cells.[57] Since then, researchers have established that DNA nanostructures are biocompatible,[58] resist enzymatic degradation, and increase the likelihood of drug delivery and retention by a cell.[59-60]
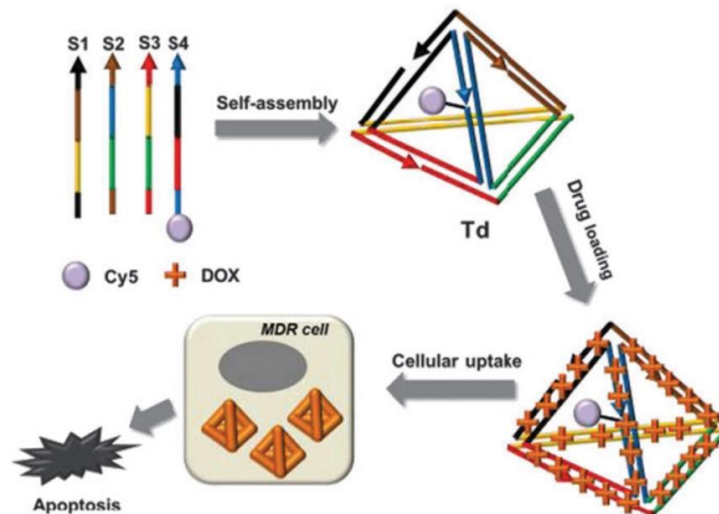
Figure 1.15 *Four oligonucleotides, one linked to a Cyanine 5 (Cy5) dye forming a self-assembled tetrahedron that is intercalated with doxorubicin (DOX). The DOX loaded tetrahedron is internalised by multidrug resistant (MDR) cells causing cell death.[57]*

As described above, aptamers generated using cell-SELEX can be selected to bind to receptors and proteins found on the biological membranes of cells. These aptamers can be internalised by the target cell or transport particular drugs to these cells. An example of this has been carried out by Min *et al*.[61] using two aptamers generated against prostate-specific membrane antigen (PMSA). An aptamer was generated for PMSA(+) cancerous cells. The aptamer was complexed with an anticancer leukaemia drug, doxorubicin, and introduced into the cells successfully. **Figure 1.16** demonstrates research by Zhang *et al*.,[62] to create a Poly-Aptamer-Drug system that was more effective than its single aptamer counterpart in causing cell apoptosis by successfully delivering doxorubicin to cells. The aptamer drug scaffold had a 40 fold greater binding affinity for the cancerous cells than the aptamer alone.
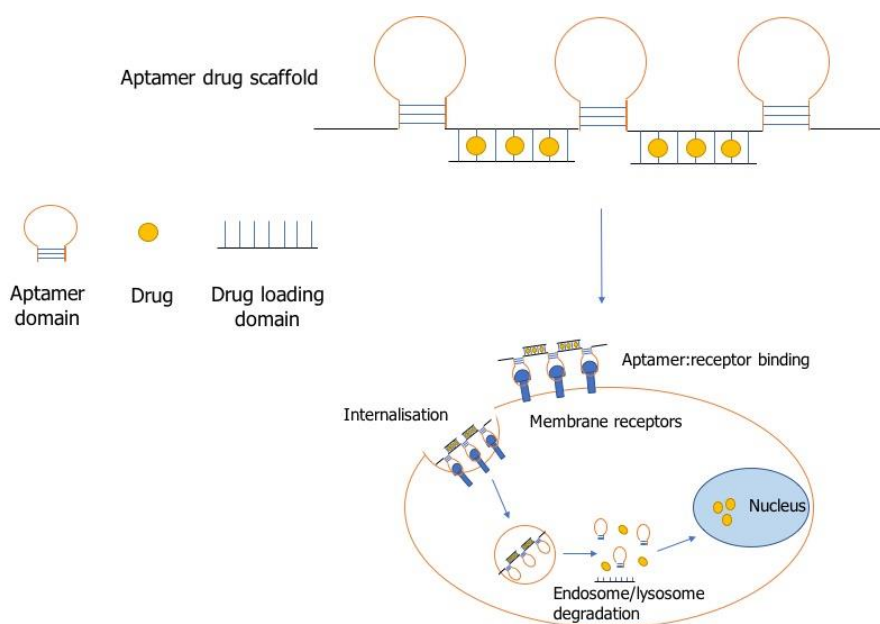
Figure 1.16 *The use of a poly-aptamer to deliver drugs to cells. The particular aptamer-drug scaffold is based oligonucleotide strand that contains aptamer domains and drug loading domains. The aptamer is generated against receptors on the cell surface that are able to be internalised and from here the substituents are broken down and the drug is released to either have its effect in the cytoplasm or the nucleus.[62]*

1.5.3 DNA-based therapy

The use of synthetic oligonucleotides in drug development is actively becoming a platform for disease therapy, some examples of such are antisense oligonucleotides (ASOs). To introduce ASOs, the process of transcription needs to be understood. Converting the genome into its resulting phenotypic proteins begins by transcription whereby DNA is converted into messenger RNA (mRNA). This mRNA is utilised as the information to produce the proteins in a cell by a process called translation (**Figure 1.17**).[63]
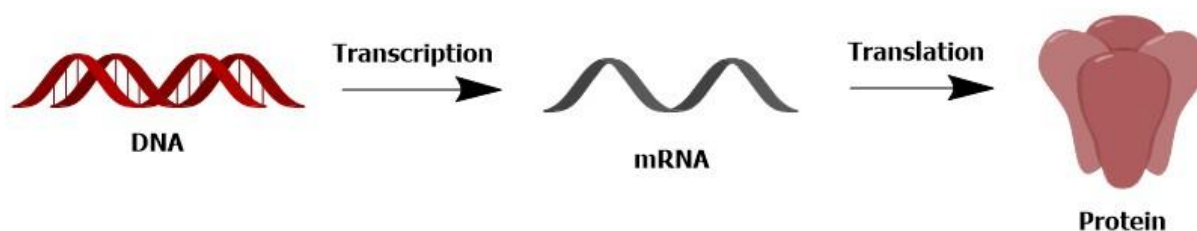
Figure 1.17 *The process of transcription and translation leading to the production of a protein.*

An mRNA strand must be single stranded for the translation process and the most common function of ASOs is to bind to mRNA to inactivate this process.[64] In 1978, the first ASO was described by Stephenson and Zamecnik. The ASO inhibited Rous sarcoma virus replication in chick embryo fibroblasts (CEF) by blocking the viral replication pathway.[65] Many ASOs have been developed since this discovery, for the treatment of diseases such as Duchenne muscular dystrophy[66] and familial hypercholesterolemia.[67] The aptamer therapeutics field is expanding and currently of great interest as an aptamer will bind to their target with high specificity and this allows the production of therapeutics that are able to discriminate between proteins that are evolutionarily related and contain domains that are structurally similar.[68-69] Vascular endothelial growth factor (VEGF) is implicated in vision related diseases and the aptamer Pegpleranib, in combination with an anti-VEGF antibody, has improved vision in patients compared to those administered with the antibody alone.[70] NU172, an aptamer against thrombin, the protein involved in the formation of a blood clot, is in clinical trials as a potential anticoagulant.[71]

1.6 DNA based detection systems

Since the advent of DNA sequencing a large number of sequences are now available for the use in DNA based detection methods. A DNA probe is a short single stranded DNA that has a complementary sequence to a target sequence of interest. These sequences may be those of a point variant, mutation, or sequences that are molecular markers of disease and infection.[72-73] The probes can contain labels that are visualised using appropriate analysis techniques. A particular focus will be on the detection of molecular marker base changes, known as point variants, within DNA-based detection systems (**Chapter 4**).

1.6.1 Aptamer-based sensors

The folding properties of aptamers, and their binding selectivity, make them attractive for the development of diagnostics. Research has shown that aptamer-based sensors can be developed using electrochemical or fluorescence-based methods in order to translate an aptamer:target complex into a signal that can be measured. Electrochemical sensors are available that are able to detect molecules such as adenosine triphosphate (ATP),[74-75] and thrombin.[76] Electrochemical sensors are cost effective, rapid, sensitive and require simple instrumentation. Certain fluorescence-based detection methods that are discussed in this section are applicable to aptamer sensors. For example, the concept of molecular beacons can be applied to aptamers as the structural change in an aptamer upon target binding can be detected using förster resonance energy transfer (FRET).[77-78] An enzyme-linked immunosorbent assay (ELISA), the immunological detection technique that uses antibodies for the detection of biomolecules, can also be modified to be an aptamer-linked immobilised sorbent assay (ALISA).[79]

1.6.2 Polymerase Chain Reaction

Probe technology is highly specific to the disease or pathogen being identified but requires high concentrations of target and therefore some sort of amplification technique for the DNA of interest.[80] PCR is a specialised DNA amplification technique that uses DNA probe technology to overcome the problem of needing large quantities of DNA for the detection of target DNA.[81] The standard PCR reaction is designed to amplify, detect or clone a known nucleic acid sequence.[82-83]
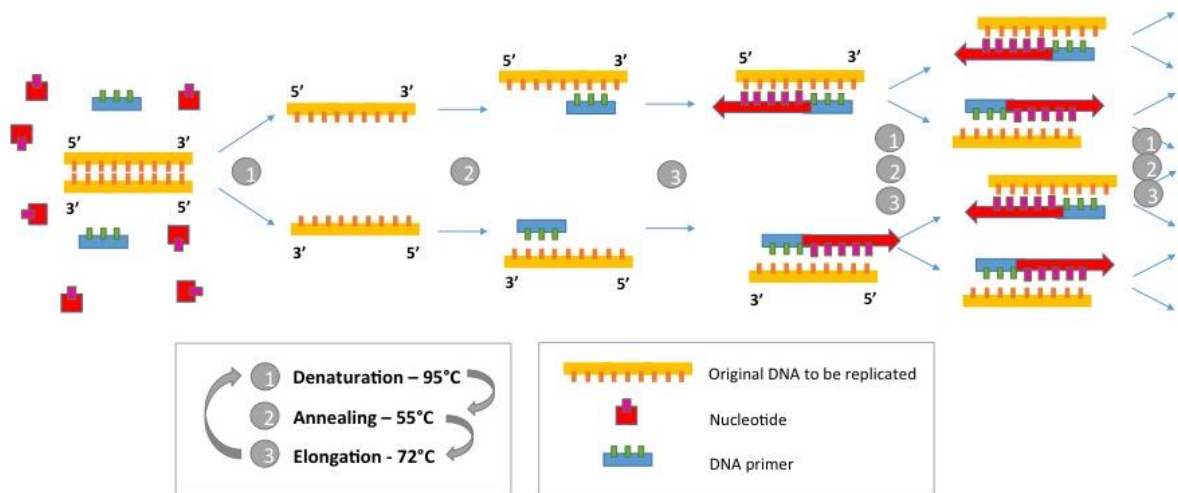
Figure 1.18 *The method of PCR depicted with example temperatures that can be used at each stage of the process.*

A cycle of PCR (**Figure 1.18**) contains 3 steps and this cycle is usually repeated between up to 40 times until optimum amplification of target is thought to be reached. The reaction components consist of:

- Template DNA from host organism
- DNA polymerase for the elongation of the new DNA strands
- Primers that are essentially short DNA probes that will bind to the forward or reverse side of the template DNA sequence. These are used to initiate the PCR reaction.
- Free nucleotides that are used by the DNA polymerase to create the new strand of DNA.

The **first** step involves heating, to 95°C, the double stranded DNA causing denaturation and separation of the two strands. The **second** step will see the temperature decreased to 45-75°C to allow the primers to anneal to the template DNA strand. In the **third** and final step, the DNA

polymerase extends the forward primer using the free nucleotides until the reverse primer is reached and this step occurs at approximately 72°C.[84]

There are many alternative PCR assays all serving specific functions, for example, quantitative PCR (Q-PCR)[85] and reverse transcriptase PCR. Q-PCR is used to provide real-time information on the amount of dsDNA produced in a PCR cycle and relies on a dsDNA binding dye that only fluoresces upon binding of a DNA duplex. The fluorescence emission intensity of the reaction is proportional to the amount of PCR product formed. TaqMan probes (**Section 1.6.8**) are based on Q-PCR technology.

Reverse transcriptase PCR is useful when the target contains a genome that is made of RNA, which is common for viral targets, and therefore conventional PCR techniques need to be modified for the amplification of regions within RNA. In a similar reaction that occurs in a cell, the RNA is converted to a complementary DNA strand (cDNA) in a step prior to conventional PCR that is then used to amplify the cDNA.[86]

1.6.3 Denaturing high performance liquid chromatography (DHPLC)

DHPLC is a traditional approach for the detection of point variants in genes. High performance liquid chromatography (HPLC) is a column based separation technique used for the purification or analysis of oligonucleotides in research and industry[87] and DHPLC is based on ion pair reversed-phase HPLC (RP-HPLC) (**Chapter 2**). The reaction starts with a PCR reaction that amplifies the DNA with the point variant, and some wild-type (WT) DNA in separate tubes, and post-amplification the products from the two tubes are mixed together. The resulting solution is heated to denature the DNA and is cooled to allow the dsDNA to re-anneal and the mixture will contain some homoduplexes and some heteroduplexes[88] (**Figure 1.19**). The detection of any point variants within the PCR products is done by passing the samples through a reversed-phase high purity liquid chromatography (RP-HPLC) column and when a heteroduplex is present the sample will be retained on the RP-HPLC column to a greater extent than the homoduplex samples.[89-90] The chromatogram produced will show an elution profile that is different for the homozygous sequence compared to that of the strands with the point variant.
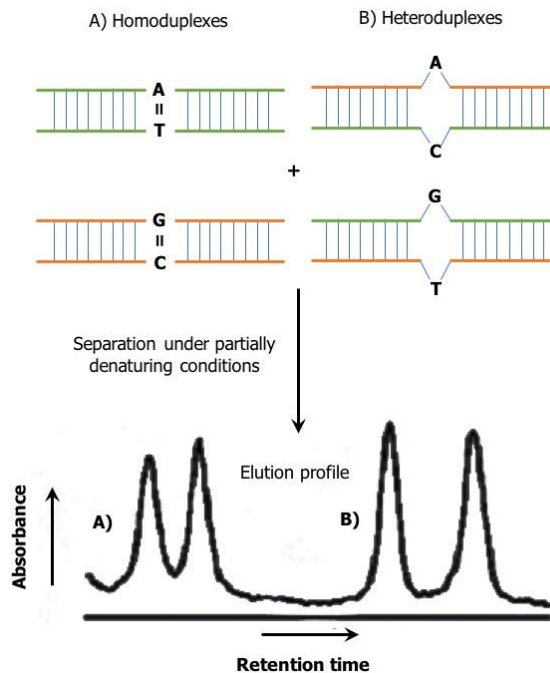
Figure 1.19 *The homoduplexes and heteroduplexes formed after the mixing and heat annealing of PCR amplification products from mutant and WT DNA. Next is an example of their respective HPLC elution profiles.*

1.6.4   Denaturing gradient gel electrophoresis

Denaturing gradient gel electrophoresis (DGGE) was first developed by Lerman *et al.*[91-92] and is also an analytical technique used in the detection of point variants within DNA. Similarly to DHPLC, DGGE is used to separate PCR products but using gel electrophoresis rather than RP-HPLC.[93] Standard gel electrophoresis (**Chapter 2**) uses polyacrylamide gels to separate DNA, which is negatively charged, using an electric field. The DNA will move towards a positive electrode through a mesh that is created by the polymerisation of the polyacrylamide. The speed of movement through the gel is dependent on the size of the DNA strands.

The amplified DNA from a PCR reaction is run on a gel using a chemical denaturant at one concentration resulting in the melting temperature of the DNA to be lower as the DNA duplexes are less stable. A temperature gradient is then applied to the gel and the DNA strands will denature to varying extents. As the DNA is under an electric field and a thermal gradient, the strands will reach a branching state. In other words, the DNA has not fully denatured, but the strands are partially double stranded and partially single stranded.[93] This branching will disrupt the movement of the DNA through the gel (**Figure 1.20**). Similar to the DHPLC technique, a mixture of SNP DNA and wild-type DNA will create mismatched heteroduplexes and some homoduplexes. The heteroduplexes will reach the branching point much faster, and at lower temperatures than the homoduplexes, as the DNA duplex is already destabilised due to the mismatch. This allows the gel separation of sequences with only one base difference.

Denaturation

0 % ⟶ 100 %

Partially
melted
WT

Partially
melted
mutant

Double
strand
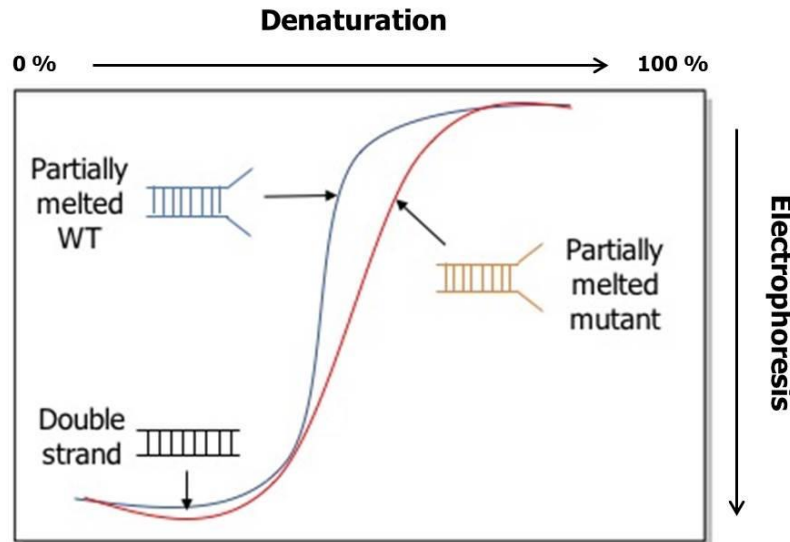
Electrophoresis

Figure 1.20 *A diagrammatic represenation of DGGE to show the denaturation gradient (above), from 0 to 100%, of the samples which is perpendicular to the direction of the gel electrophoresis (below). The denaturant gradient allows for the strands to reach a branching point similar to that in DHPLC and then the strands are separated using gel electrophoresis. At low denaturant concentration (left) the DNA fragment remains double stranded, but as the concentration increases (moving right) the DNA fragment begins to denature, creating a branched molecule. At very high concentrations of denaturant, the DNA fragment can completely melt, creating two single strands.*

1.6.5 Dynamic allele-specific hybridisation

Dynamic allele-specific hybridisation (DASH) relies on the heating and monitoring of a DNA duplex as it denatures. The target strand is initially amplified using PCR and one primer will contain a biotin modification. The strand amplified using this primer will be bound to the well on a plate using streptavidin and if the correct sequence is present it will form a duplex with the target gene.

A dsDNA intercalating dye will be added to the plate and the intensity of emission of the dye will be relative to the proportion of duplex present.[94] When the correct buffer conditions are present, but there is a point variant present, the melting temperature (T_m) (**Chapter 2**) of the strand will decrease considerably. The dye fluorescence will then be monitored as the duplex is denatured. If the fluorescence decreases rapidly then the strand has a lower T_m than expected and it is not forming a duplex as well as it should be. The technique requires precise standardisation of the reaction conditions to ensure the varying denaturation temperatures, and therefore the point variations, can be detected.[94]

1.6.6 Molecular beacons

A molecular beacon is a single stranded oligonucleotide probe that forms a hairpin structure. These probes use the phenomenon of FRET, whereby the energy from an absorbed photon is transferred by a donor to an acceptor chromophore resulting in a fluorescence quenching effect on the donor and an increase in emission of the acceptor.[95] The beacons are approximately 15 to 20 nucleobases long and the loop part of the hairpin acts as the probe (**Figure 1.21**). The 5'- and 3'- ends of the probe, also known as the stems, are where the strands are modified with a fluorophore and a quencher. When the probe is not bound to a target the loop structure keeps the fluorescence quenched as the fluorophore and quencher are in close proximity.[96] When the strand binds its complementary target the hairpin structure will undergo a conformational change and the fluorophore will begin to fluoresce again (**Figure 1.21**). If more than one sequence of DNA is to be detected, each molecular beacon can be labelled with a different fluorophore that produces a different fluorescent colour. This means the molecular beacons can be used in multiplex assays.[97]
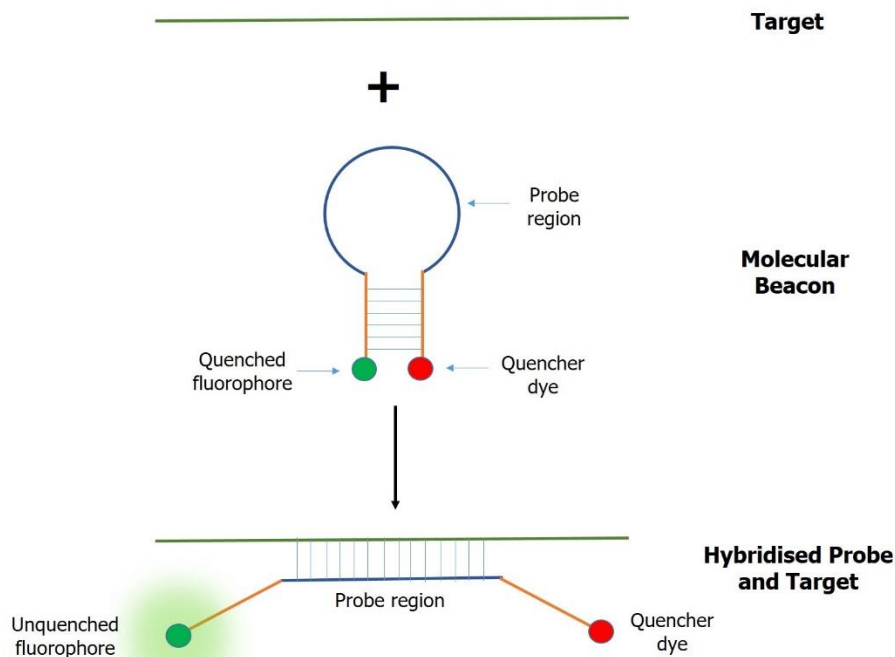
Figure 1.21 *The concept of a molecular beacon assay whereby any fluorescence from the fluorophore on the probe is quenched while the target is not present as the fluorophore remains in close proximity to the quencher dye. The probe becomes fluorescent upon hybridisation with the target strand as the fluorophore and the quencher dye are now further apart.*

Molecular beacons have also been employed for point variation detection.[98] The detection system utilises different fluorophores in order to give read-outs of different colours.[97] The hairpin motif of molecular beacons increases the specificity of the probes to their targets. This allows the detection of targets with only one nucleobase difference. The molecular beacon with the fluorophore completely complementary to the target will give a characteristic fluorescent colour.[98]

1.6.7 DNA Microarrays

Microarray technology is a field of bioinformatics that has allowed the detection of nucleotide samples to become a more high-throughput process.[99] A microarray is a biochip that contains DNA attached to a solid surface. This can allow large sets of data to be generated on a high number of genetic samples allowing scientists to research genetic variation in a much less labour-intensive manor.[100] This information can be useful for evolutionary studies or the diagnosis of disease. Each spot of DNA will be contain a small amount, normally picomoles, of a specific oligonucleotide probe. The complementary target binding and forming a duplex with the probe will be quantifiable by the use of labels, such as fluorophores, present on the targets. The main purpose of microarray technology is to probe the expression of many genes all at once. However, the technology reverses the process of normal probing techniques. In a normal diagnostic assay an unknown mixture is probed by a pre-labelled probe and one target is focused upon. In contrast, a microarray chip is coated with probes in specific known positions. If the target solution, tagged with a fluorophore, contains a sequence that is complementary to the probe on the surface of the chip DNA hybridisation will occur and the target will now be bound to the probe (**Figure 1.22**). The targets that have not hybridised to the probes are washed away before the chip is imaged to quantify for any successfully formed probe:target duplexes.[101]
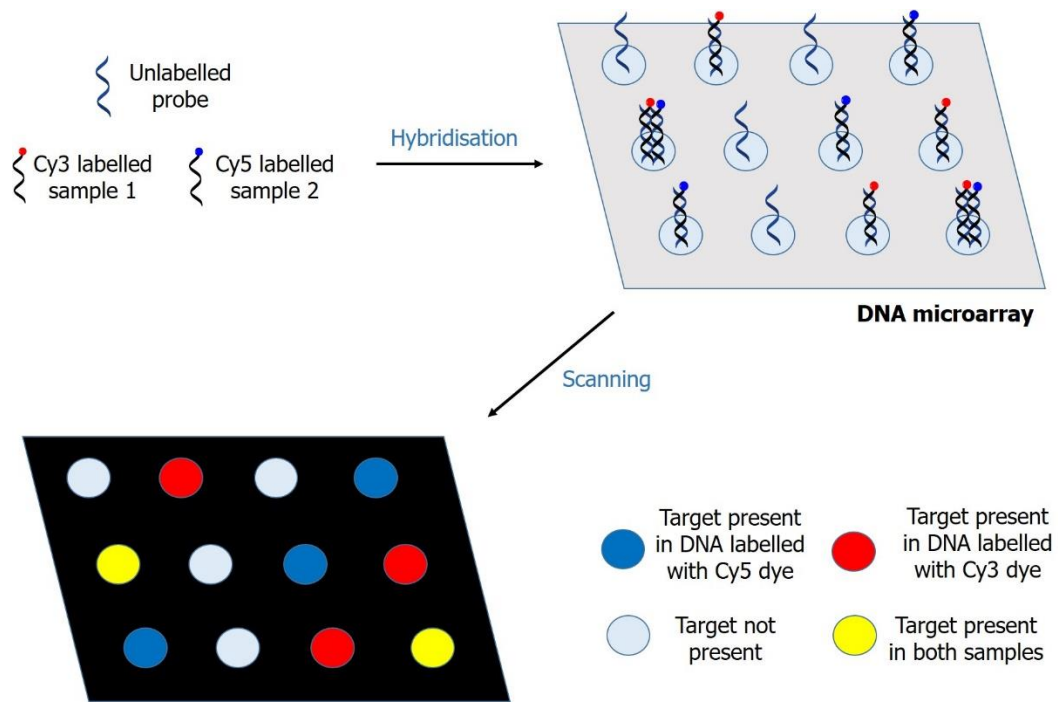
Figure 1.22 *The principle behind microarray technology where unlabelled probes are spotted onto a DNA microarray surface. Samples that are linked to different dyes (e.g. Cyanine 3 (Cy3) and Cy5) are hybridised to the probes and the microarray is read by a fluorescence scanner. If the target is present then there will be a fluorescence read-out of either; one colour corresponding to the target gene being present in only one sample or a mixture of colours indicating both samples contain the target gene.*

Array technology for the detection of point variants uses the same approach as DNA microarrays however both the WT and mutant variant of the disease being detected must be probed for.[102-104] For routine point variant analysis microarrays have replaced more laborious processes, such as DHPLC discussed above, for analysis as the method is a high-throughput alternative.[105-106]

1.6.8 TaqMan™ probe

TaqMan probes were first introduced in 1991 by Gelfand *et al.*[107] for their 5' nuclease activity and further established for allelic discrimination by Lee *et al.*[108] The principle behind the TaqMan probes also relies on FRET, in a similar manner to molecular beacons, and the fluorescence intensity increase demonstrates a variation in the distance between a fluorophore and a quencher. Q-PCR is utilised for the monitoring of the fluorescence increase while a PCR reaction is occurring to amplify a target. The specific sequence of events that occur during the traditional TaqMan detection assay are as follows (**Figure 1.23**):

1) A fluorophore is attached to the 5'- end of an oligonucleotide probe that has been designed for the detection of the target of interest and a corresponding quencher is attached to the 3'- end. The probes are not extendable by the Taq polymerase as they lack a free hydroxyl group.

2) During a PCR reaction a DNA polymerase is required for the amplification of the nascent strand. The DNA polymerase used in a TaqMan reaction is the Taq polymerase which has 5' –> 3' exonuclease activity. While the Taq polymerase is extending the primer, it will come across the probe with the quencher and fluorophore.

3) The Taq polymerase will cleave the nucleotides on the probe base by base in order for the extension of the strand to occur resulting in the being released and the fluorescence emission is monitored. Every time a cycle of PCR occurs, and the right target is present, the fluorescence will increase proportionally to the product. If the probe is not bound, then there will be no increase in fluorescence.
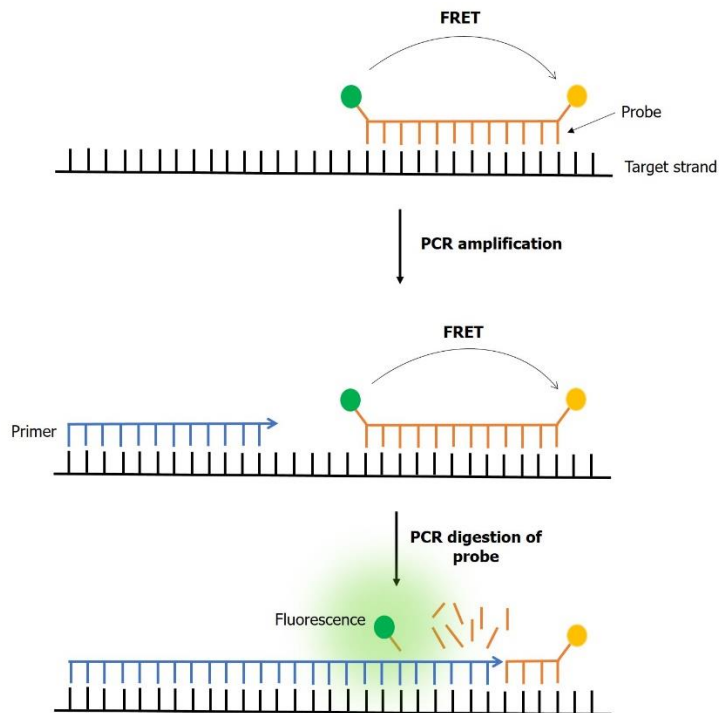
Figure 1.23 *The process of a TaqMan sensing reaction. The probe binds its complementary target strand and as the process of PCR takes place the probe gets digested and fluorescence is seen.*

For point variation detection there are two probes present with two different fluorophores. Each is complementary to a different point variant sequence. The probes will only bind if they are completely complementary to the target sequence. Using Q-PCR it can be seen which fluorophore is fluorescing and therefore which point variant is present. The probe must be completely complementary to the bases in the target otherwise the melting temperature of the resulting duplex will be lower, and this will result in less efficient binding preventing the exonuclease activity of the polymerase.[109] As the technique is based on PCR, each point variant reaction requires optimisation and therefore it is difficult to probe more than a few point variants at a time.[110] However, researchers have developed assays where the reaction has detected up to seven point variations at once.[111]

1.6.9 The benefits of DNA based diagnostics

The unique merits that oligonucleotides hold against their immunological counterparts are that they have high thermal stability, they are cheap to produce, and have many applications due to their high specificity for their targets. The production of monoclonal antibodies is costly and requires highly specialised techniques such as mammalian cell culture.[38] The production process requires the use of antibodies to test the performance of the antibodies that have been generated leading to an expensive production cycle. Oligonucleotides are easily synthesised in great quantities and can be modified without the risk of structural changes that could lead to low affinity binding to target. DNA detection systems have also become less painstaking than some of the traditional processes discussed in this chapter due to the development of bioinformatics and more automated processes that can handle large amounts of data. Oligonucleotide aptamers can also bind to a diverse range of systems, for example ions and small molecules ligands, which cannot be recognised by antibodies. For this reason, oligonucleotides are promising competitors to antibodies for the use in medical and other biological applications.[39]

Although the use of DNA comes with many advantages there are some limitations that must be taken into consideration. An oligonucleotide drug will have a much larger mass than its small molecule counterparts and therefore it may be more difficult to deliver the oligonucleotide therapeutic into cells. As discussed earlier in the introduction, DNA carries a charge and therefore will not cross a cell membrane barrier, again making it difficult to deliver the DNA into cells.[59, 112] When using DNA as a diagnostic the sequence of the target molecule must be known beforehand and this means unknown diseases and targets cannot be detected. During DNA and RNA amplification events it is possible to get false positive results as the reactions are highly sensitive and are highly prone to contamination events.[113]

1.7 Thesis aims

1. Biotherapeutics is a field that is ever expanding, and as diseases become resistant to readily available drugs, and other diseases remain incurable, there will always be a market for novel biotherapeutic research. The ability to cost-effectively synthesise oligonucleotide aptamers to many different targets and introduce synthetic modifications using solid-phase DNA synthesis into aptamers has meant many researchers are exploring the use of these as therapeutics. The first part experimental chapter of this thesis will explore a novel modification introduced into an aptamer for the control of a key blood clotting protein known as thrombin (**Chapter 3**).

2. The developed world requires sensing platforms, that are increasingly more sensitive and rapid, that enable new ways to detect and tackle disease in a patient specific manner and developing countries require sensing platforms that allow for the rapid detection of biomolecules in a cheap and portable manner. The broadening of biological detection methods from the traditional immunoassay based designs to being more DNA oriented is becoming the future of biological sensing and this thesis will explore two different methods to explore; a) the detection of point variants using a method that allows for the determination of the ratio of one base to another (**Chapter 4**) and b) the detection of a potato virus using a novel linear dichroism (LD) and M13 bacteriophage based detection system (**Chapter 5**).

3. Before delving into the research conducted in these PhD projects **Chapter 2** will outline the key instrumentation and techniques that are required to undertake the research in **Chapters 3**, **4**, and **5**. **Chapter 6** will cover the methods used within this thesis to experimentally develop and test the aims of this thesis.

1.8 References

1. Neidle, S., The Building-Blocks of DNA and RNA. In *Principles of Nucleic Acid Structure*, Academic Press: 2008; pp. 20-37.

2. Watson, J. D.; Crick, F. H. C., Molecular Structure of Nucleic Acids: A Structure for Deoxyribose Nucleic Acid. *Nature* **1953,** *171*, pp. 737-738.

3. Dickerson, R. E., DNA structure from A to Z. In *Methods in enzymology*, Academic Press: 1992; Vol. 211, pp. 67-111.

4. Jones, M. R.; Seeman, N. C.; Mirkin, C. A., Programmable materials and the nature of the DNA bond. *Science* **2015,** *347*, pp. 1260901.

5. Kosuri, S.; Church, G. M., Large-scale de novo DNA synthesis- technologies and applications. *Nature Methods: Focus on Synthetic Biology* **2014,** *11*, pp. 499-507.

6. Hu, Q.; Li, H.; Wang, L.; Gu, H.; Fan, C., DNA Nanotechnology-Enabled Drug Delivery Systems. *Chemical reviews* **2018**.

7. Jobling, M. A.; Gill, P., Encoded evidence: DNA in forensic analysis. *Nature Reviews Genetics* **2004,** *5*, pp.739.

8. Tuerk, C.; Gold, L., Systematic evolution of ligands by exponential enrichment: RNA ligands to bacteriophage T4 DNA polymerase. *Science* **1990,** *249*, pp. 505.

9. Ray, P.; Viles, K. D.; Soule, E. E.; Woodruff, R. S., Application of aptamers for targeted therapeutics. *Arch Immunol Ther Exp* **2013,** *61*, pp. 255-71.

10. Bayrac, A. T.; Sefah, K.; Parekh, P.; Bayrac, C.; Gulbakan, B.; Oktem, H. A.; Tan, W., In Vitro Selection of DNA Aptamers to Glioblastoma Multiforme. *ACS Chemical Neuroscience* **2011,** *2*, pp. 175-181.

11. Adler, A.; Forster, N.; Homann, M.; Goringer, H. U., Post-SELEX chemical optimization of a trypanosome-specific RNA aptamer. *Combinational Chemistry & High Throughput Screening* **2008,** *11*, pp. 16-23.

12. Fitzwater, T.; Polisky, B., A SELEX primer. *Methods in enzymology* **1996,** *267*, pp. 275-301.

13. Ohuchi, S., Cell-SELEX Technology. *BioResearch Open Access* **2012,** *1* (6), pp. 265-272.

14. Guo, K.; Paul, A.; Schichor, C.; Ziemer, G.; Wendel, H. P., CELL-SELEX: Novel perspectives of aptamer-based therapeutics. *International Journal of Molecular Sciences* **2008,** *9*, pp. 668-678.

15. Eckstein, F., Nucleoside Phosphorothioates. *Journal of the American Chemical Society* **1966,** *88*, pp. 4292-4294.

16. Gan, R.; Wu, X.; He, W.; Liu, Z.; Wu, S.; Chen, C.; Chen, S.; Xiang, Q.; Deng, Z.; Liang, D.; Chen, S.; Wang, L., DNA phosphorothioate modifications influence the global transcriptional response and protect DNA from double-stranded breaks. *Scientific Reports* **2014,** *4*, pp. 6642.

17. Hermanson, G. T., Chapter 3 - The Reactions of Bioconjugation. *Bioconjugate Techniques (Third Edition)*, Ed. Academic Press: 2013; pp. 229-258.

18. Egholm, M.; Buchardt, O.; Christensen, L.; Behrens, C.; Freier, S. M.; Driver, D. A.; Berg, R. H.; Kim, S. K.; Norden, B.; Nielsen, P. E., PNA hybridizes to complementary oligonucleotides obeying the Watson-Crick hydrogen-bonding rules. *Nature* **1993,** *365*, pp. 566-8.

19. Okamoto, A.; Ichiba, T.; Saito, I., Pyrene-Labeled Oligodeoxynucleotide Probe for Detecting Base Insertion by Excimer Fluorescence Emission. *Journal of the American Chemical Society* **2004,** *126*, pp. 8364-8365.

20. Trawick, B. N.; Osiek, T. A.; Bashkin, J. K., Enhancing sequence-specific cleavage of RNA within a duplex region: incorporation of 1,3-propanediol linkers into oligonucleotide conjugates of serinol-terpyridine. *Bioconjugate chemistry* **2001,** *12*, pp.900-5.

21. Cruickshank, D., A detailed refinement of the crystal and molecular structure of anthracene. *Acta Crystallographica* **1956,** *9*, pp. 915-923.

22. Robertson, J. M., The crystalline structure of anthracene. A quantitative X-Ray investigation. *Proceedings of the Royal Society of London. Series A, Containing Papers of a Mathematical and Physical Character* **1933,** *140*, pp. 79-98.

23. Novaira, A. I.; Avila, V.; Montich, G. G.; Previtali, C. M., Fluorescence quenching of anthracene by indole derivatives in phospholipid bilayers. *Journal of Photochemistry and Photobiology B: Biology* **2001,** *60*, 25-31.

24. Wright, G. T., Absolute Scintillation Efficiency of Anthracene Crystals. *Proceedings of the Physical Society.* **1955,** *68*, pp. 929-937.

25. Schuster, P.; Brubaker, E., Investigating the Anisotropic Scintillation Response in Anthracene through Neutron, Gamma-Ray, and Muon Measurements. *IEEE Transactions on Nuclear Science* **2016,** *63*, pp. 1942-1954.

26. Atherton, J. C. C.; Jones, S., Diels–Alder reactions of anthracene, 9-substituted anthracenes and 9,10-disubstituted anthracenes. *Tetrahedron* **2003,** *59*, pp. 9039-9057.

27. Aubry, J.-M.; Pierlot, C.; Rigaudy, J.; Schmidt, R., Reversible Binding of Oxygen to Aromatic Compounds. *Accounts of Chemical Research* **2003,** *36*, pp. 668-675.

28. Kolemen, S.; Ozdemir, T.; Lee, D.; Kim, G. M.; Karatas, T.; Yoon, J.; Akkaya, E. U., Remote-Controlled Release of Singlet Oxygen by the Plasmonic Heating of Endoperoxide-Modified Gold Nanorods: Towards a Paradigm Change in Photodynamic Therapy. *Angewandte Chemie International Edition* **2016,** *55*, pp. 3606-3610.

29. Kumar, C. V.; Asuncion, E. H., DNA binding studies and site selective fluorescence sensitization of an anthryl probe. *Journal of the American Chemical Society* **1993,** *115* (19), 8547-8553.

30. Weiss, R. B., The anthracyclines: will we ever find a better doxorubicin? *Seminars in oncology* **1992,** *19*, pp. 670-86.

31. de Silva, S. A.; Zavaleta, A.; Baron, D. E.; Allam, O.; Isidor, E. V.; Kashimura, N.; Percarpio, J. M., A fluorescent photoinduced electron transfer sensor for cations with an off-on-off proton switch. *Tetrahedron Letters* **1997,** *38*, pp. 2237-2240.

32. Yamana, K.; Aota, R.; Nakano, H., Oligonucleotides having covalently linked anthracene at specific sugar residue: Differential binding to DNA and RNA and fluorescence properties. *Tetrahedron Letters* **1995,** *36*, pp. 8427-8430.

33. Ihara, T.; Mukae, M.; Tabara, M.; Kitamura, Y.; Jyo, A., Photochemical ligation between anthracene-DNA conjugates and its analytical application to gene analysis. *Nucleic Acids Symposium Series* **2005,** *49*, pp. 41-42.

34. Moran, N.; Bassani, D. M.; Desvergne, J.; Keiper, S.; Lowden, P. A. S.; Vyle, J. S.; Tucker, J. H. R., Detection of a single DNA base-pair mismatch using an anthracene-tagged fluorescent probe. *Chemical Communications* **2006,** pp. 5003-5005.

35. Reynolds, M. A.; Beck, T. A.; Hogrefe, R. I.; McCaffrey, A.; Arnold, L. J.; Vaghefi, M. M., A non-nucleotide-based linking method for the preparation of psoralen-derivatized methylphosphonate oligonucleotides. *Bioconjugate chemistry* **1992,** *3*, pp. 366-374.

36. Ihara, T.; Fujii, T.; Mukae, M.; Kitamura, Y.; Jyo, A., Photochemical ligation of DNA conjugates through anthracene cyclodimer formation and its fidelity to the template sequences. *Journal of the American Chemistry Society* **2004,** *126*, pp. 8880-1.

37. Shaughnessy, A. F., Monoclonal antibodies: magic bullets with a hefty price tag. *BMJ : British Medical Journal* **2012,** pp. *345*.

38. Couchman, J. R., Commercial antibodies: The good, bad, and really ugly. *Journal of Histochemistry and Cytochemistry* **2009,** *57*, pp. 7-8.

39. Parashar, A., Aptamers in therapeutics. *Journal of Clinical and Diagnostic Research* **2016,** *10*, pp. BE01-BE06.

40. Sun, H.; Zhu, X.; Lu, P. Y.; Rosato, R. R.; Tan, W.; Zu, Y., Oligonucleotide aptamers: new tools for targeted cancer therapy. *Molecular Therapies Nucleic Acids* **2014,** *3*, pp. 182.

41. Song, K.; Lee, S.; Ban, C., Aptamers and their biological applications. *Sensors* **2012,** *12*, pp. 612-631.

42. Seeman, N. C., Nucleic acid junctions and lattices. *Journal of theoretical biology* **1982,** *99*, pp. 237-47.

43. Chen, J. H.; Seeman, N. C., Synthesis from DNA of a molecule with the connectivity of a cube. *Nature* **1991,** *350*, pp. 631-3.

44. Zheng, J.; Constantinou, P. E.; Micheel, C.; Alivisatos, A. P.; Kiehl, R. A.; Seeman, N. C., Two-dimensional Nanoparticle Arrays Show the Organizational Power of Robust DNA Motifs. *Nano Letters* **2006,** *6*, pp. 1502-1504.

45. Fendt, L.; Bouamaied, I.; Thöni, S.; Amiot, N.; Stulz, E., DNA as supramolecular scaffold for porphyrin arrays on the nanometer scale. *Journal of the American Chemical Society* **2007,** *129*, pp. 15319-15329.

46. Stulz, E., Nanoarchitectonics with Porphyrin Functionalized DNA. *Accounts of Chemical Research* **2017,** *50*, pp. 823-831.

47. Rothemund, P. W. K., Folding DNA to create nanoscale shapes and patterns. *Nature* **2006,** *440*, pp. 297.

48. Saccà, B.; Niemeyer, C. M., DNA Origami: The Art of Folding DNA. *Angewandte Chemie International Edition* **2012,** *51*, pp. 58-66.

49. Douglas, S. M.; Chou, J. J.; Shih, W. M., DNA-nanotube-induced alignment of membrane proteins for NMR structure determination. *Proceedings of the National Academy of Sciences* **2007,** *104* , pp. 6644.

50. Rajendran, A.; Endo, M.; Sugiyama, H., Single-Molecule Analysis Using DNA Origami. *Angewandte Chemie International Edition* **2012,** *51*, pp. 874-890.

51. Yang, Y.; Goetzfried, M. A.; Hidaka, K.; You, M.; Tan, W.; Sugiyama, H.; Endo, M., Direct Visualization of Walking Motions of Photocontrolled Nanomachine on the DNA Nanostructure. *Nano Letters* **2015,** *15* (10), pp. 6672-6676.

52. Pillers, M. A.; Lieberman, M., Thermal stability of DNA origami on mica. *Journal of Vacuum Science & Technology* **2014,** *32*, pp. 040602.

53. Shen, B.; Linko, V.; Tapio, K.; Kostiainen, M. A.; Toppari, J. J., Custom-shaped metal nanostructures based on DNA origami silhouettes. *Nanoscale* **2015,** *7*, pp. 11267-11272.

54. Ahmadi, Y.; De Llano, E.; Barišić, I., (Poly)cation-induced protection of conventional and wireframe DNA origami nanostructures. *Nanoscale* **2018,** *10*, pp. 7494-7504.

55. Dunn, K. E.; Dannenberg, F.; Ouldridge, T. E.; Kwiatkowska, M.; Turberfield, A. J.; Bath, J., Guiding the folding pathway of DNA origami. *Nature* **2015,** *525*, pp. 82.

56. Ramakrishnan, S.; Ijäs, H.; Linko, V.; Keller, A., Structural stability of DNA origami nanostructures under application-specific conditions. *Computational and Structural Biotechnology Journal* **2018,** *16*, pp. 342-349.

57. Kim, K. R.; Kim, D. R.; Lee, T.; Yhee, J. Y.; Kim, B. S.; Kwon, I. C.; Ahn, D. R., Drug delivery by a self-assembled DNA tetrahedron for overcoming drug resistance in breast cancer cells. *Chemical communications* **2013,** *49*, pp. 2010-2.

58. Li, J.; Fan, C.; Pei, H.; Shi, J.; Huang, Q., Smart drug delivery nanocarriers with self-assembled DNA nanostructures. *Advanced materials* **2013,** *25*, pp. 4386-96.

59. Pinheiro, A. V.; Han, D.; Shih, W. M.; Yan, H., Challenges and opportunities for structural DNA nanotechnology. *Nature Nanotechnology* **2011,** *6*, pp. 763-72.

60. Wang, A. Z.; Langer, R.; Farokhzad, O. C., Nanoparticle delivery of cancer drugs. *Annual Review of Medicine* **2012,** *63*, pp. 185-98.

61. Min, K.; Jo, H.; Song, K.; Cho, M.; Chun, Y. S.; Jon, S.; Kim, W. J.; Ban, C., Dual-aptamer-based delivery vehicle of doxorubicin to both PSMA (+) and PSMA (-) prostate cancers. *Biomaterials* **2011,** *32*, pp. 2124-32.

62. Zhang, Z.; Ali, M. M.; Eckert, M. A.; Kang, D.; Chen, Y. Y.; Sender, L. S.; Fruman, D. A.; Zhao, W., A polyvalent aptamer system for targeted drug delivery. *Biomaterials* **2013,** *34*, pp. 9728-9735.

63. Alberts, B.; Johnson, J. L.; Raff, M.; Roberts, K.; Walter, P., *Molecular biology of the cell*. 6th ed.; W. W. Norton & Company: **2014**.

64. Lundin, K. E.; Gissberg, O.; Smith, C. I., Oligonucleotide Therapies: The Past and the Present. *Human gene therapy* **2015,** *26* (8), 475-85.

65. Zamecnik, P. C.; Stephenson, M. L., Inhibition of Rous sarcoma virus replication and cell transformation by a specific oligodeoxynucleotide. *Proceedings of the National Academy of Sciences* **1978,** *75*, pp. 280-284.

66. Mendell, J. R.; Rodino-Klapac, L. R.; Sahenk, Z.; Roush, K.; Bird, L.; Lowes, L. P.; Alfano, L.; Gomez, A. M.; Lewis, S.; Kota, J.; Malik, V.; Shontz, K.; Walker, C. M.; Flanigan, K. M.; Corridore, M.; Kean, J. R.; Allen, H. D.; Shilling, C.; Melia, K. R.; Sazani, P.; Saoud, J. B.; Kaye, E. M., Eteplirsen for the treatment of Duchenne muscular dystrophy. *Annals of Neurology* **2013,** *74*, pp. 637-647.

67. Raal, F. J.; Santos, R. D.; Blom, D. J.; Marais, A. D.; Charng, M.-J.; Cromwell, W. C.; Lachmann, R. H.; Gaudet, D.; Tan, J. L.; Chasan-Taber, S.; Tribble, D. L.; Flaim, J. D.; Crooke, S. T., Mipomersen, an apolipoprotein B synthesis inhibitor, for lowering of LDL cholesterol concentrations in patients with homozygous familial hypercholesterolaemia: a randomised, double-blind, placebo-controlled trial. *The Lancet* **2010,** *375*, pp. 998-1006.

68. Doudna, J. A.; Cech, T. R.; Sullenger, B. A., Selection of an RNA molecule that mimics a major autoantigenic epitope of human insulin receptor. *Proceedings of the National Academy of Sciences of the USA* **1995,** *92*, pp. 2355-9.

69. Mahlknecht, G.; Maron, R.; Mancini, M.; Schechter, B.; Sela, M.; Yarden, Y., Aptamer to ErbB-2/HER2 enhances degradation of the target and inhibits tumorigenic growth. *Proceedings of the National Academy of Sciences of the USA* **2013,** *110*, pp. 8170-8175.

70. Drolet, D. W.; Green, L. S.; Gold, L.; Janjic, N., Fit for the Eye: Aptamers in Ocular Disorders. *Nucleic Acid Therapeutics* **2016,** *26*, pp. 127-146.

71. Buff, M. C. R.; Schäfer, F.; Wulffen, B.; Müller, J.; Pötzsch, B.; Heckel, A.; Mayer, G., Dependence of aptamer activity on opposed terminal extensions: improvement of light-regulation efficiency. *Nucleic Acids Research* **2010,** *38*, pp. 2111-2118.

72. Lee, S.; Jo, H.; Her, J.; Lee, H. Y.; Ban, C., Ultrasensitive electrochemical detection of engrailed-2 based on homeodomain-specific DNA probe recognition for the diagnosis of prostate cancer. *Biosens Bioelectron* **2015,** *66*, pp. 32-8.

73. Heller, M. J., DNA microarray technology: devices, systems, and applications. *Annual Review of Biomedical Engineering* **2002,** *4*, pp. 129-53.

74. Liu, X.; Li, W.; Xu, X.; Zhou, J.; Nie, Z., Electrochemical aptamer sensor for small molecule assays. *Methods in Molecular Biology* **2012,** *800*, pp. 119-32.

75. Zuo, X.; Song, S.; Zhang, J.; Pan, D.; Wang, L.; Fan, C., A target-responsive electrochemical aptamer switch (TREAS) for reagentless detection of nanomolar ATP. *Journal of the American Chemical Society* **2007,** *129*, pp. 1042-3.

76. Zhang, S.; Zhou, G.; Xu, X.; Cao, L.; Liang, G.; Chen, H.; Liu, B.; Kong, J., Development of an electrochemical aptamer-based sensor with a sensitive Fe3O4 nanopaticle-redox tag for reagentless protein detection. *Electrochemistry Communications* **2011,** *13*, pp. 928-931.

77. Tan, X.; Chen, W.; Lu, S.; Zhu, Z.; Chen, T.; Zhu, G.; You, M.; Tan, W., Molecular Beacon Aptamers for Direct and Universal Quantitation of Recombinant Proteins from Cell Lysates. *Analytical chemistry* **2012,** *84*, pp. 8272-8276.

78. Stojanovic, M. N.; de Prada, P.; Landry, D. W., Aptamer-based folding fluorescent sensor for cocaine. *Journal of the American Chemical Society* **2001,** *123*, pp. 4928-31.

79. Vivekananda, J.; Kiel, J. L., Anti-Francisella tularensis DNA aptamers detect tularemia antigen from different subspecies by Aptamer-Linked Immobilized Sorbent Assay. *Labortatory Investigation* **2006,** *86*, pp. 610-8.

80. Yang, S.; Rothman, R. E., PCR-based diagnostics for infectious diseases: uses, limitations, and future applications in acute-care settings. *The Lancet Infectious Diseases* **2004,** *4*, pp. 37-48.

81. Cadwell, R. C.; Joyce, G. F., Randomization of genes by PCR mutagenesis. *PCR Methods and Applications* **1992,** *2*, pp. 28-33.

82. Garibyan, L.; Avashia, N., Research techniques made simple: Polymerase chain reaction (PCR). *The Journal of Investigative Dermatology* **2013,** *133*, pp. e6-e6.

83. Bell, J., The polymerase chain reaction. *Immunology Today* **1989,** *10* (10), 351-355.

84. Bartlett, J. M.; Stirling, D., A short history of the polymerase chain reaction. *Methods of Molecular Biology* **2003,** *226*, pp. 3-6.

85. Gofflot, S.; Deprez, M.; el Moualij, B.; Osman, A.; Thonnart, J. F.; Hougrand, O.; Heinen, E.; Zorzi, W., Immunoquantitative PCR for prion protein detection in sporadic Creutzfeldt-Jakob disease. *Clinical Chemistry* **2005,** *51*, pp. 1605-11.

86. Santos, C. F.; Sakai, V. T.; Machado, M. A. A. M.; Schippers, D. N.; Greene, A. S., Reverse transcription and polymerase chain reaction: principles and applications in dentistry. *Journal of Applied Oral Science* **2004,** *12*, pp. 1-11.

87. Huber, C. G.; Oefner, P. J.; Bonn, G. K., High-Resolution Liquid Chromatography of Oligonucleotides on Nonporous Alkylated Styrene-Divinylbenzene Copolymers. *Analytical Biochemistry* **1993,** *212*, pp. 351-358.

88. Nagamine, C. M.; Chan, K.; Lau, Y. F., A PCR artifact: generation of heteroduplexes. *American Journal of Human Genetics* **1989,** *45*, pp. 337-339.

89. Troedsson, C.; Lee, R. F.; Stokes, V.; Walters, T. L.; Simonelli, P.; Frischer, M. E., Development of a denaturing high-performance liquid chromatography method for detection of protist parasites of metazoans. *Applied and Environmental Microbiology* **2008,** *74*, pp. 4336-45.

90. Liu, W.; Smith, D. I.; Rechtzigel, K. J.; Thibodeau, S. N.; James, C. D., Denaturing high performance liquid chromatography (DHPLC) used in the detection of germline and somatic mutations. *Nucleic Acids Research* **1998,** *26*, pp. 1396-1400.

91. Lerman, L. S.; Fischer, S. G.; Hurley, I.; Silverstein, K.; Lumelsky, N., Sequence-determined DNA separations. *Annual Reviews in Biophysics and Bioengineering* **1984,** *13*, pp. 399-423.

92. Fischer, S. G.; Lerman, L. S., Length-independent separation of DNA restriction fragments in two-dimensional gel electrophoresis. *Cell* **1979,** *16*, pp. 191-200.

93. Khan, A. S.; Freedman, R.; Byerley, W.; Leonard, S., Temperature gradient gel electrophoresis analysis of the beta-NGF gene in schizophrenia. *Journal of Psychiatry and Neuroscience* **1995,** *20*, pp. 199-209.

94. Howell, W. M.; Jobs, M.; Gyllensten, U.; Brookes, A. J., Dynamic allele-specific hybridization. *Nature Biotechnology* **1999,** *17*, pp. 87.

95. Förster, T., *Delocalized Excitation and Excitation Transfer*. Florida State University: 1965.

96. Tyagi, S.; Kramer, F. R., Molecular beacons in diagnostics. *F1000 Medicine Reports* **2012,** *4*, pp. 10.

97. Vet, J. A. M.; Majithia, A. R.; Marras, S. A. E.; Tyagi, S.; Dube, S.; Poiesz, B. J.; Kramer, F. R., Multiplex detection of four pathogenic retroviruses using molecular beacons. *Proceedings of the National Academy of Sciences of the United States of America* **1999,** *96*, pp. 6394-6399.

98. Tyagi, S.; Bratu, D. P.; Kramer, F. R., Multicolor molecular beacons for allele discrimination. *Nature Biotechnology* **1998,** *16*, pp. 49.

99. Alwine, J. C.; Kemp, D. J.; Stark, G. R., Method for detection of specific RNAs in agarose gels by transfer to diazobenzyloxymethyl-paper and hybridization with DNA probes. *Proceedings of the National Academy of Sciences of the United States of America* **1977,** *74*, pp. 5350-5354.

100. Taub, F. E.; DeLeo, J. M.; Thompson, E. B., Sequential comparative hybridizations analyzed by computerized image processing can identify and quantitate regulated RNAs. *DNA* **1983,** *2*, pp. 309-27.

101. Seidel, C., Introduction to DNA Microarrays: A Network-Based Approach. In *Analysis of Microarray Data*, Ed. Wiley-VCH. 2008.

102. Dutt, A.; Beroukhim, R., Single nucleotide polymorphism array analysis of cancer. *Current Opinion in Oncology* **2007,** *19*, pp. 43-49.

103. Cutler, J. A.; Mitchell, M. J.; Greenslade, K.; Smith, M. P.; Savidge, G. F., A rapid and cost-effective method for analysis of three common genetic risk factors for thrombosis. *Blood Coagulation and Fibrinolysis* **2001,** *12*, pp. 33-6.

104. Gunderson, K. L.; Steemers, F. J.; Lee, G.; Mendoza, L. G.; Chee, M. S., A genome-wide scalable SNP genotyping assay using microarray technology. *Nature Genetics* **2005,** *37*, 549.

105. Matsuzaki, H.; Dong, S.; Loi, H.; Di, X.; Liu, G.; Hubbell, E.; Law, J.; Berntsen, T.; Chadha, M.; Hui, H.; Yang, G.; Kennedy, G. C.; Webster, T. A.; Cawley, S.; Walsh, P. S.; Jones, K. W.; Fodor, S. P. A.; Mei, R., Genotyping over 100,000 SNPs on a pair of oligonucleotide arrays. *Nature Methods* **2004,** *1*, pp. 109.

106. Jaluria, P.; Konstantopoulos, K.; Betenbaugh, M.; Shiloach, J., A perspective on microarrays: current applications, pitfalls, and potential uses. *Microbial Cell Factories* **2007,** *6*, pp. 4-4.

107. Holland, P. M.; Abramson, R. D.; Watson, R.; Gelfand, D. H., Detection of specific polymerase chain reaction product by utilizing the 5'----3' exonuclease activity of Thermus aquaticus DNA polymerase. *Proceedings of the National Academy of Sciences* **1991,** *88*, pp. 7276-7280.

108. Lee, L. G.; Connell, C. R.; Bloch, W., Allelic discrimination by nick-translation PCR with fluorogenic probes. *Nucleic Acids Research* **1993,** *21*, pp. 3761-3766.

109. McGuigan, F. E.; Ralston, S. H., Single nucleotide polymorphism detection: allelic discrimination using TaqMan. *Psychiatric Genetics* **2002,** *12*, pp. 133-6.

110. Syvanen, A. C., Accessing genetic variation: genotyping single nucleotide polymorphisms. *Nature Reviews Genetics* **2001,** *2*, pp. 930-42.

111. Lee, L. G.; Livak, K. J.; Mullah, B.; Graham, R. J.; Vinayak, R. S.; Woudenberg, T. M., Seven-color, homogeneous detection of six PCR products. *Biotechniques* **1999,** *27*, pp. 342-9.

112. Tørring, T.; Gothelf, K. V., DNA nanotechnology: a curiosity or a promising technology? *F1000prime reports* **2013,** *5*, pp. 14-14.

113. Vaneechoutte, M.; Van Eldere, J., The possibilities and limitations of nucleic acid amplification technology in diagnostic microbiology. *Journal of Medical Microbiology* **1997,** *46*, pp. 188-194.

Chapter 2 - Techniques

2.1 Oligonucleotide Synthesis

The first chemical synthesis of a dinucleotide was performed in 1955 by Michelson and Todd.[1] This led to the development of the phosphoramidite method[2-3] for the automated synthesis of oligonucleotides up to 100 nucleotides long. This automated approach allows for the incorporation of modified bases, providing these modifications can undergo phosphitylation, into oligonucleotide strands. Standard solid support oligonucleotide synthesis occurs in the opposite fashion to DNA biosynthesis whereby the cycle occurs in a 3'- to 5' direction. The stepwise procedure in phosphoramidite approach (**Scheme 2.1**) of oligonucleotide synthesis will be discussed next.

Start here
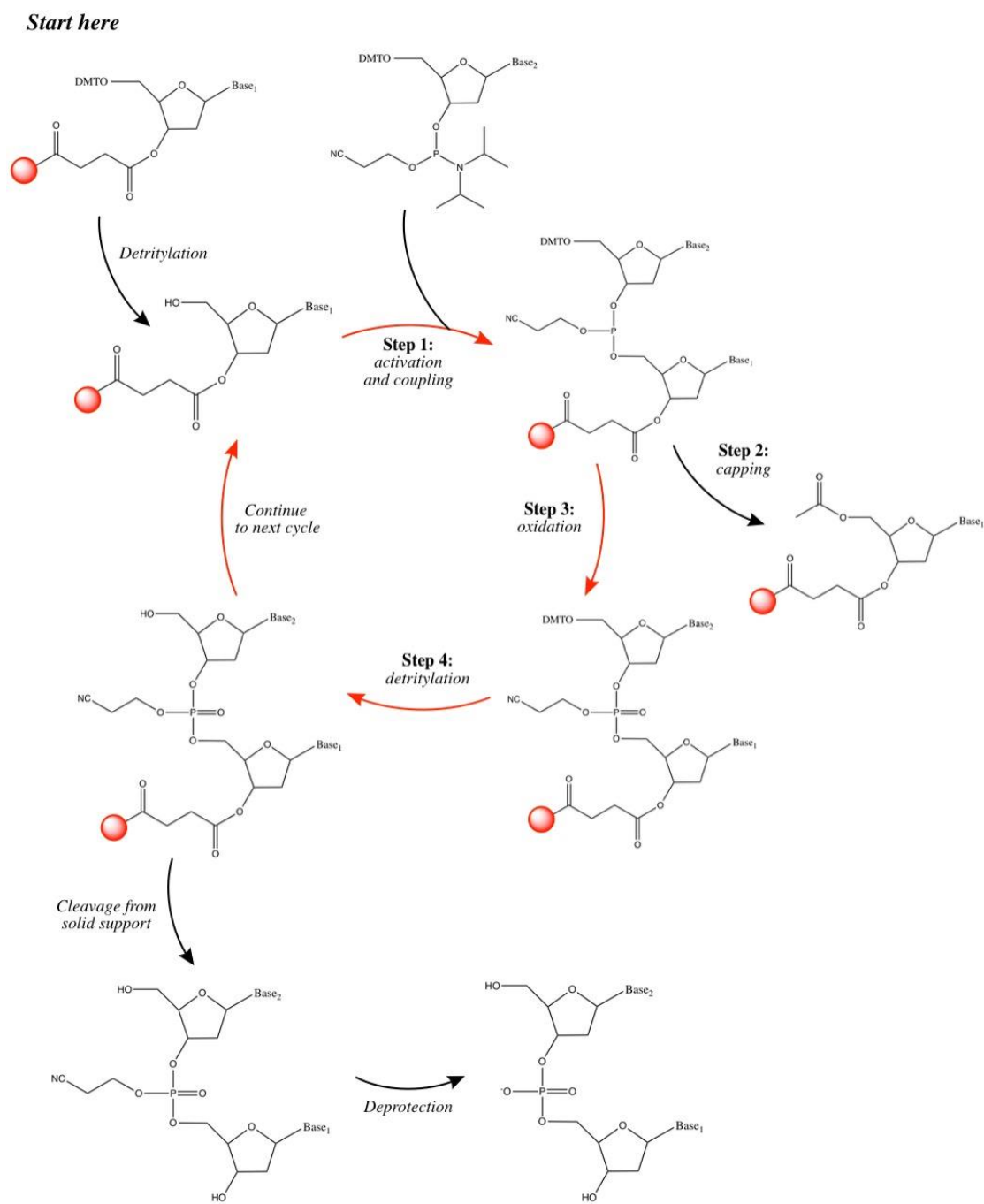
Scheme 2.1 *The solid-phase oligonucleotide synthesis cycle.*

2.1.1 Detritylation

The first nucleoside is attached with a succinate linker, on the 3'- end, to a column containing a control

pore glass (CPG) resin and this nucleoside has a 4,4'-dimethoxytrityl (DMT) protecting group. This

protecting group stops the nucleosides from polymerising while being bound to the solid support resin.

The DMT must be removed by a detritylation step (**Scheme 2.2**), using trichloroacetic acid (TCA) in

dichloromethane (DCM), in order for oligonucleotide synthesis to be possible.[4]
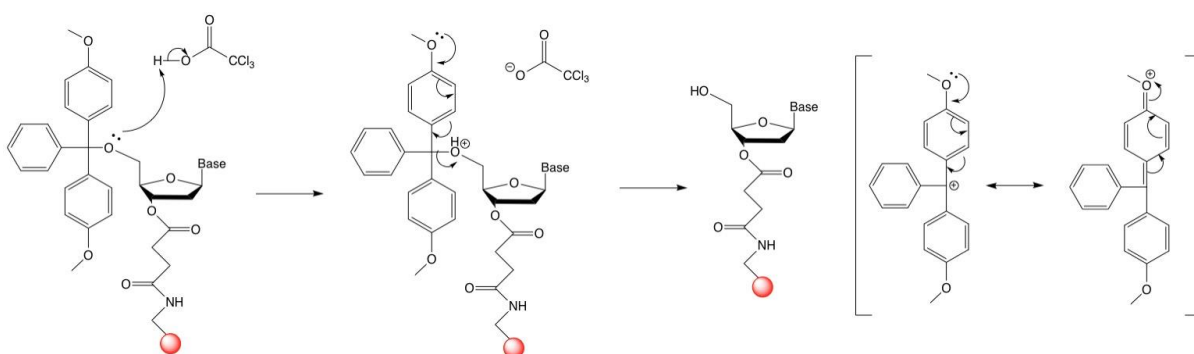
Scheme 2.2 *The detritylation of the 5'-OH group achieved using trichloroacetic acid (TCA).*

2.1.2 Activation and Coupling

The incoming phosphoramidite base is added, along with an activator, to the column. The phosphoramidite is added in excess to allow the reaction to go to completion. The activator protonates the diisopropylamino group on the base to convert it into a good leaving group. The phosphoramidite reacts with the free 5'- hydroxyl group on the resin bound nucleoside and a new phosphorus-oxygen bond form. This results in a phosphite triester and a free diisopropylamino group. (**Scheme 2.3**).[4]
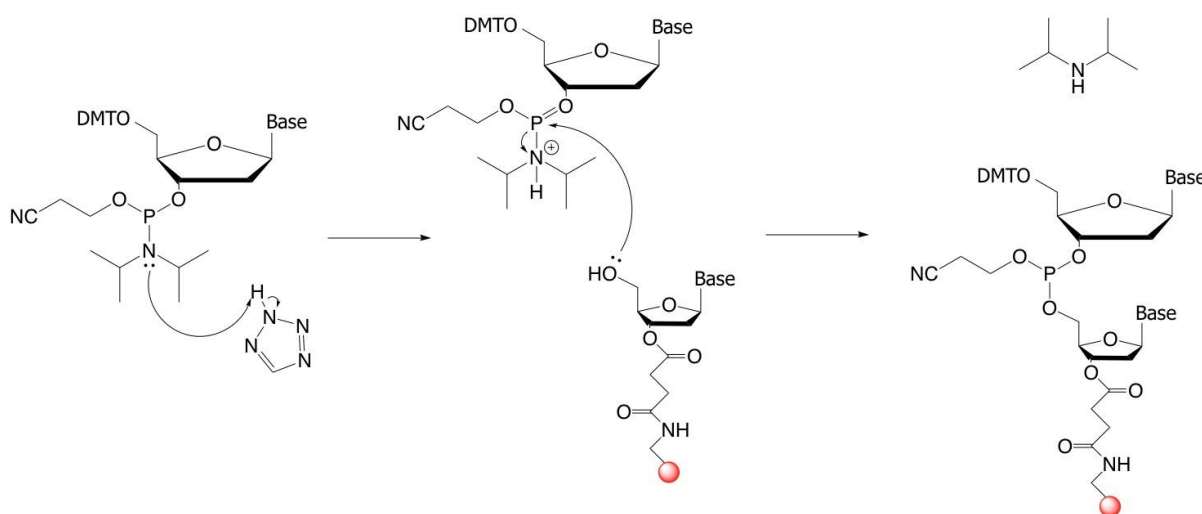
Scheme 2.3 *The activation of the phosphoramidite and subsequent coupling to the next nucleoside phosphoramidite base.*

2.1.3 Capping

As coupling reactions are not always at a yield of 100%, the reaction can leave unreacted 5'-hydroxyl groups from the sugar on the nucleoside functionalised onto the solid support resin. To avoid any incoming phosphoramidite reacting with the CPG bound base, a capping step is introduced. This step avoids unwanted base deletions within the synthesis cycle. The capping step involves blocking the free 5'-hydroxyl groups by an acetylation reaction (**Scheme 2.4**).[4]
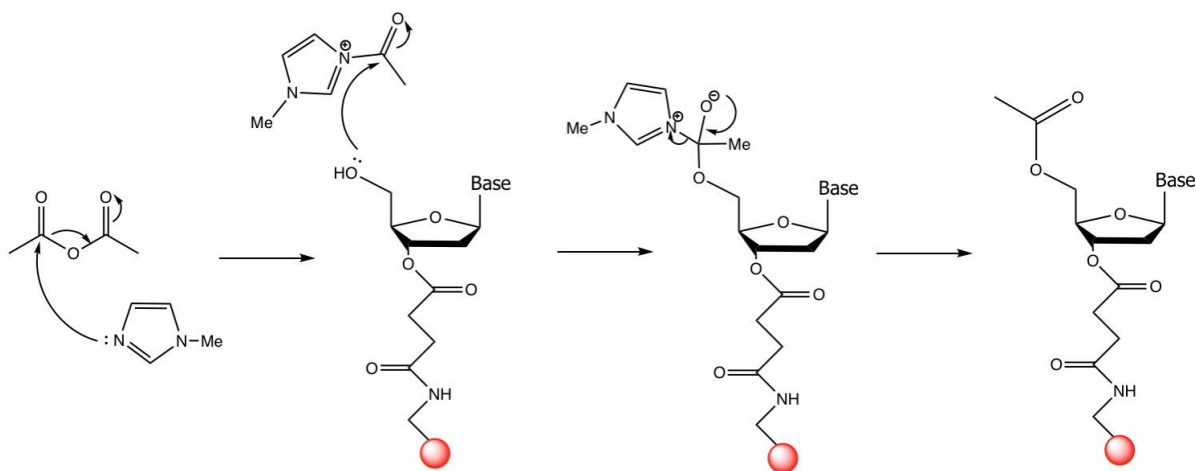
Scheme 2.4 *Acetylation of unreacted 5'-hydroxyl groups on the CPG resin bound base.*

2.1.4 Oxidation

The phosphate triester (P(III)) formed in the coupling reaction is unstable to acidic conditions that are present in the following steps of DNA synthesis. Therefore, the P(III) is converted to a more stable P(V) by an oxidation reaction using iodine while also being exposed to pyridine and water. The phosphotriester is now protected with a 2-cyanoethyl functional group (**Scheme 2.5**) ensuring no undesirable reactions take place later in the cycle.[4]
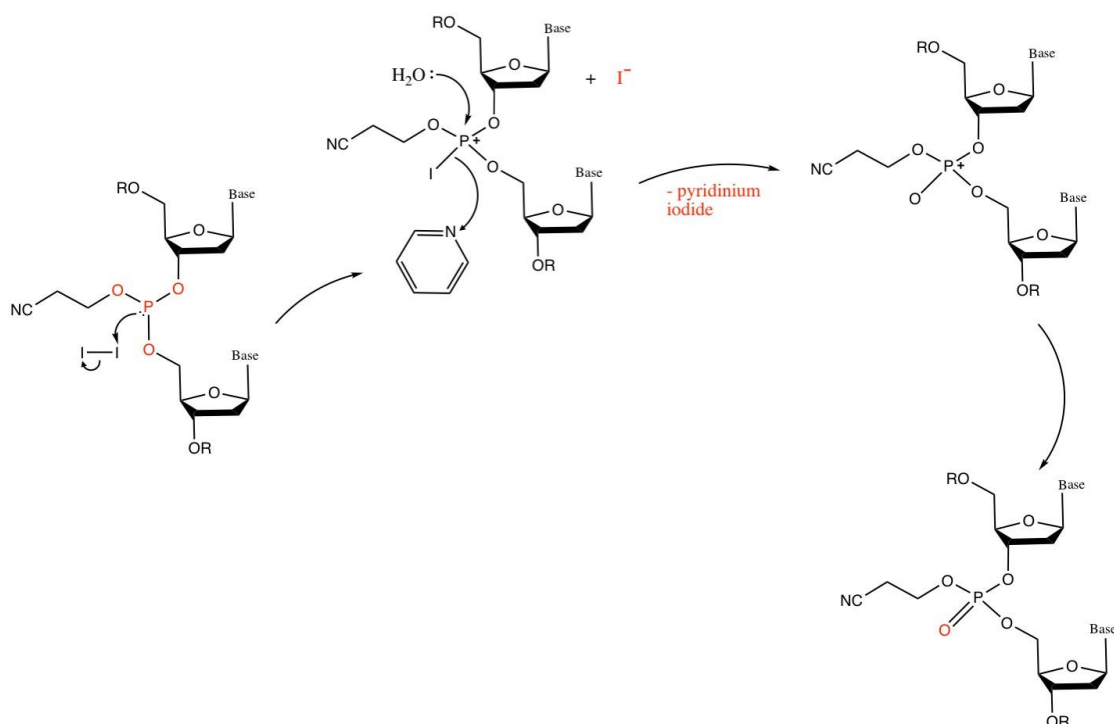
Scheme 2.5 The oxidation step to convert the phosphitetriester into a phosphotriester group.

2.1.5 Detitrylation

Another DMT protecting group is present at the 5'- end of the growing oligonucleotide strand and must be removed in order for the synthesis cycle to continue. The deprotection step is carried out using trichloroacetic acid (TCA) and can be used to monitor the stepwise yield, i.e. the coupling efficiency, of the synthesis as the free DMT carbocation produced as a result of this reaction absorbs light at 495 nm.[4]

These steps are then repeated, as seen in **Scheme 2.1** The solid-phase oligonucleotide synthesis cycle. until the required oligonucleotide strand of a specified length has been synthesised.

2.1.6 Cleavage of oligonucleotide from CPG resin and deprotection

After the correct length of oligonucleotide has been synthesised it is cleaved from the CPG solid support. A common linker used for attaching the nucleotide to the solid support is a succinyl linker that holds the 3'- end of the strand to the resin and is cleaved with concentrated ammonium hydroxide (**Scheme 2.6**).[4] However, other linkers, such as the UnyLinker™ have also been developed.[5]

The oligonucleotide, which is now in concentrated ammonium hydroxide, is heated to 60 °C for the removal of any protecting groups on the adenine, guanine or cytosine bases. Finally, the ammonium hydroxide is evaporated, leaving the newly synthesised oligonucleotide.[4]
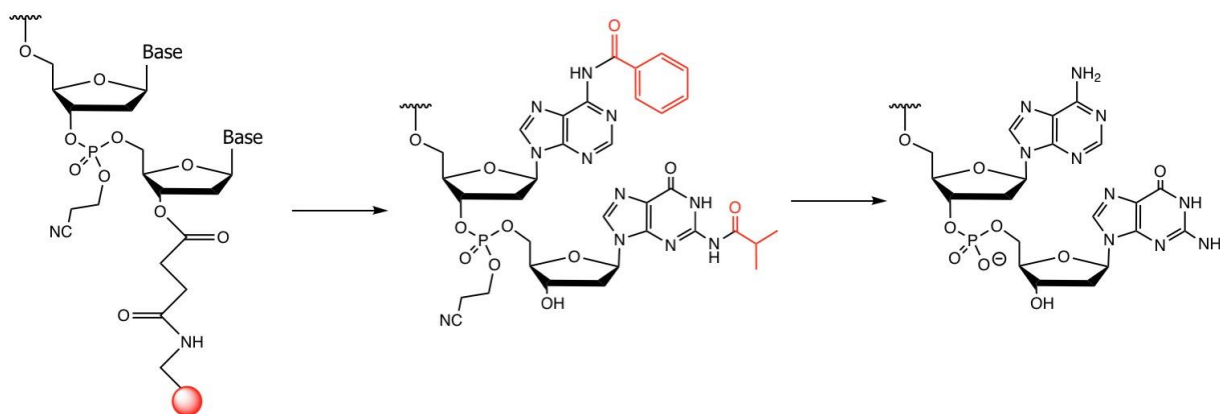
Scheme 2.6 *The cleavage of the succinyl linker from the CPG solid support resin leaving.*

2.2 High performance liquid chromatography

High performance liquid chromatography (HPLC) is a purification and analytical technique based on column chromatography, and uses both a solid-phase and mobile-phase in order to separate molecules.[6] The compounds are separated by their relative polarity by sending the compound in a liquid mobile-phase (e.g. hexane) through a column with a solid-phase (e.g. silica). If the molecule that is flowing through the column has higher polarity, it will interact with the polar solid-phase more than if the molecule has lower, or no, polarity. The molecules with lower polarity will be interacting with the mobile-phase and will come through the column first. While the molecules flow through the columns the absorbance or fluorescence of the samples can be monitored to distinguish which peak is to be collected. This monitoring also allows for the determination of how pure the collected fractions are.

Reversed-phase HPLC (RP-HPLC) differs from conventional HPLC in that the silica used in the solid-phase is covered with long-chain aliphatic hydrocarbons.[7] These convert the stationary solid-phase from polar to non-polar and the mobile-phase utilised in becomes polar (e.g. water). The polar mobile-phase then enables the separation of the products as any non-polar compounds will be attracted to the hydrocarbons on the silica *via* van der Waals' forces. The more hydrophilic polar molecules will remain in the mobile-phase and will be eluted first. RP-HPLC is commonly used to separate oligonucleotides and peptides.[8]

2.2.1 Ion-pair RP-HPLC

Ion pair RP-HPLC, established by Schill and Eksborg in 1973,[9] is used when an improved separation of polar compounds is required, as is often the case with oligonucleotides. As discussed above, ionic compounds are not retained well by a standard RP-HPLC column. The ion pair allows improved retention of the polar compounds by adding another layer of resolution to the separation and purification process. The ionic pair reagent will have a hydrophilic head and a hydrophobic tail. The head will interact with the solid-phase and the tail will interact with the mobile-phase. The polar samples will form an "ionic-pair" with the ion pair reagent and the polar sample will exchange with the counter ion of the buffer

that has been retained by the solid-phase, thus resulting in greater retention of the sample. The work in this thesis relied on the purification of oligonucleotides using ion pair RP-HPLC. The mobile phase used for the purification of these strands was the ion-pair reagent TEAA, in water, at pH 7.[10] The separation used a gradient of TEAA buffer against different levels of the non-polar solvent acetonitrile. The gradients used in this research can be seen in **Chapter 6**.

2.3 Size Exclusion Chromatography

Size exclusion chromatography (SEC) is another biomolecular separation technique that allows for the separation of biomolecules from other smaller molecules present within a sample.[11] Similarly to HPLC, the column contains a solid-phase matrix consisting of porous beads such as the dextran polysaccharide, Sephadex[12] and the pore sizes of these columns will vary from 20 − 300 μm. The mobile phase will create a partition while moving through the solid-phase where the larger molecules present within the sample will end up outside the pores and will end up flowing straight through the column. This is known as the void volume (V_0). The elution volume (V_1), is the total volume of mobile-phase required for the separation process. When smaller molecules are present they will enter the pores of the beads and elute in later fractions from the column. The elution volume of the smaller fractions between V_0 and V_1 is denoted as V_e.[13]

2.4 Mass Spectrometry

Mass spectrometry (MS) is an analytical technique that measures the mass-to-charge ratio of samples for the identification and quantification of molecules. For the samples to be analysed they require either a positive or negative charge and these ionised analytes are created using an ion source and are accelerated towards a magnetic field. The magnetic field deflects the charged analytes to different degrees depending on their mass/charge ratio, thus creating an ion beam by which a sample can be detected and identified. A mass spectrometer can be used to study the size of molecules or it can be useful for the identification of impurities within a sample.

The main method used in order to ionise the samples within this thesis was negative mode electrospray ionisation (ESI). ESI uses a fine needle that has an electric field in order to ionise and simultaneously inject the sample into the mass spectrometer. ESI mass spectrometry and HPLC are often combined in analytical to create automated systems for the analysis of molecules.

2.5 Spectroscopy

The electromagnetic spectrum can be used to give quantitative information about molecules within a system by using the ability of matter to absorb and/or emit photons of light. During photo-excitation a molecule can absorb a single photon of light resulting in an electron being pushed from an initial ground state electron density to a higher energy state (**Figure 2.1**).[14] The Jablonski diagram shows the different absorbance and relaxation process that can occur when a molecule absorbs a photon of light. For the purpose of the work in this thesis the focus in this chapter will mainly be on absorption and fluorescence. Two other relaxation processes, seen in **Figure 2.1**, are intersystem crossing and decay via phosphorescence. A reference describing these phenomenon is included here for the reader.[15]
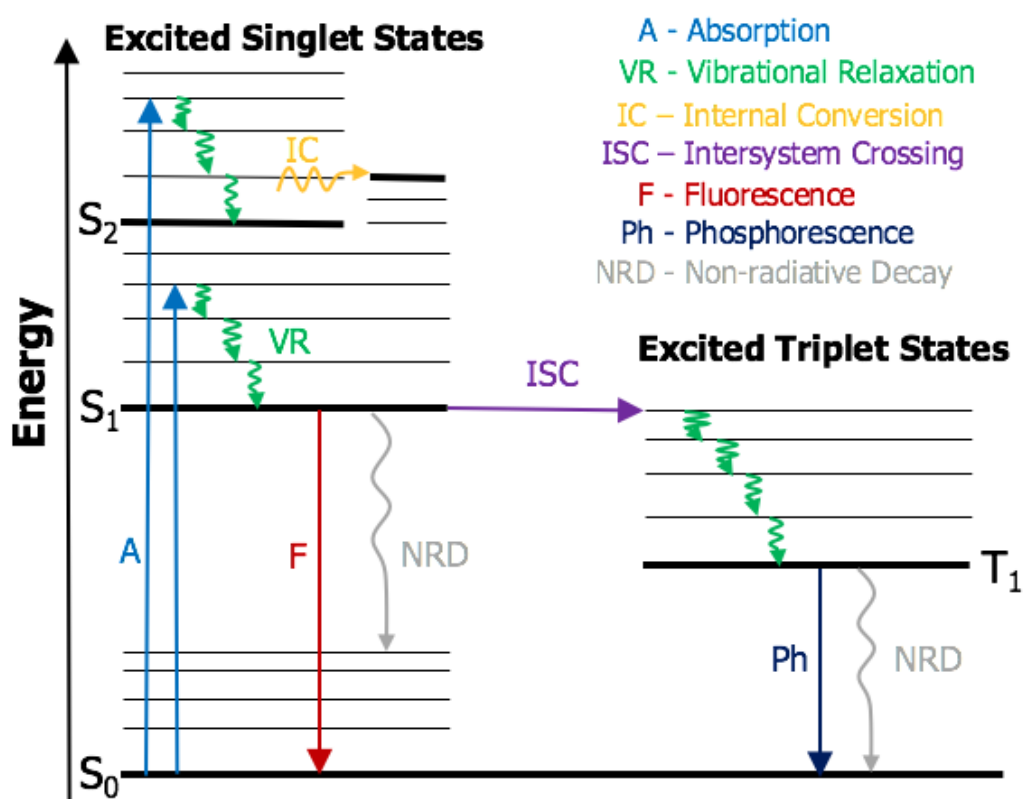
Figure 2.1 *A Jablonksi diagram that demonstrates the energy transfer process involved in the varying absorption and emission processes that an occur upon absorbance of a photon of light.[15]*

2.5.1   Ultraviolet visible spectroscopy

Ultraviolet visible spectroscopy (UV-vis) is an absorption-based technique that is often used to determine the quantity of molecules present within a sample. The measurement is based on how much light at any given wavelength between 170-800 nm is absorbed by a molecule. When any molecule absorbs a photon of light, at a certain wavelength, the energy of the molecule will increase by the following equation (**Equation 2.1**):

$$\Delta E = h\nu = hc/\lambda$$

Equation 2.1 *The equation for the energy of a given molecule after absorbing a specific wavelength of light; where ΔE is the change in energy, h is Planck's constant, ν is the frequency of light, c is the speed of the light and λ is the wavelength of the light that is being absorbed.*

The transmittance, which is the variable monitored by spectrophotometers, is the difference of light that is incident on the molecule versus the light that is transmitted by the molecule and this is described by **Equation 2.2**. Where I_0 is the light which is incident upon the molecule and I is the light that is transmitted, and therefore reaching the spectrophotometer detector.

$$T = \frac{I}{I_0}$$

Equation 2.2 *The transmittance equation relating the monitoring of the light incident on the molecules versus the light that is transmitted by the molecules.*

If there is some light being absorbed by the sample the light being transmitted will be lower in intensity than that of the incident light. The transmittance is lowest when a solution is absorbing more light of particular wavelengths. Therefore, a useful calculation is the amount of light that is being absorbed by the sample. The wavelength of light that is most strongly absorbed by the sample is known as lambda max (λ_{max}). The calculation of an absorbance is defined by the log of the transmittance (**Equation 2.3**).

$$A = log\left(\frac{I_0}{I}\right)$$

Equation 2.3 The absorbance can be defined by the light transmittance equation.

Where **A** is the consequent calculated absorbance that is displayed as an absorbance curve. The Beer-Lambert law is an equation that can then be used to relate the absorption of a substance to its extinction coefficient, the pathlength of the sample and the concentration (**Equation 2.4**).

$$A = \varepsilon\, l\, c$$

Equation 2.4 *The Beer-Lambert law.*[15]

Within the equation, *A* relates to the absorbance of the sample, the extinction coefficient is represented by the ε, *l* is the path length and *c* is the concentration of the substance of interest within the sample. The concentration is measured in mol dm^{-3} and the pathlength is measure in cm. The extinction coefficient is a value that accounts for how strongly a molecule is absorbing light at a certain wavelength. The resulting units for the extinction coefficient are $mol^{-1}\,dm^3\,cm^{-1}$.

2.5.1.1 UV-vis transmission assays

The transmittance of UV-vis light, at a given wavelength, can give important information about the interactions between biomolecules. The percentage of UV-vis light transmitted through a molecule is a measure of the turbidity of a sample and can give information about the formation of complexes such as a blood clot involving thrombin and fibrinogen. As the sample becomes more turbid, less UV-vis light is transmitted and absorbed resulting in more light being scattered. The blood clotting interaction assay used in **Chapter 3**[16] functions by measuring the magnitude of scattered UV-vis light, at 450 nm, versus the light that is absorbed and transmitted through a sample containing thrombin and fibrinogen.[17-18] As the two interact and fibrinogen is converted to fibrin, a thick clot forms and the amount of light transmitted through the sample decreases over time.

2.5.1.2 UV-vis thermal denaturation studies

The H-bonding causing the formation of the double stranded duplex structure of deoxyribonucleic acid (DNA) (**Chapter 1**) can be dissociated by a method known as denaturation by varying the pH conditions or temperature of the DNA solution. The temperature at which half the DNA in a solution has denatured is known as the melting temperature (T_m).[19] When the temperature of the sample is increased the duplex strand will begin to separate. The T_m is dependent on the buffer the DNA is present in and also the base sequence of the two strands and gives an indication of the stability of a double stranded duplex. Complementary strands will display higher T_m temperatures as will strands high in G:C base pairs as they will contain three H-bonds as opposed to the A:T base pair that is held together with two H-bonds.[20] The thermal denaturation process is monitored using UV-vis spectroscopy as ssDNA strands will absorb more strongly at 260 nm than dsDNA duplexes (**Figure 2.2**).
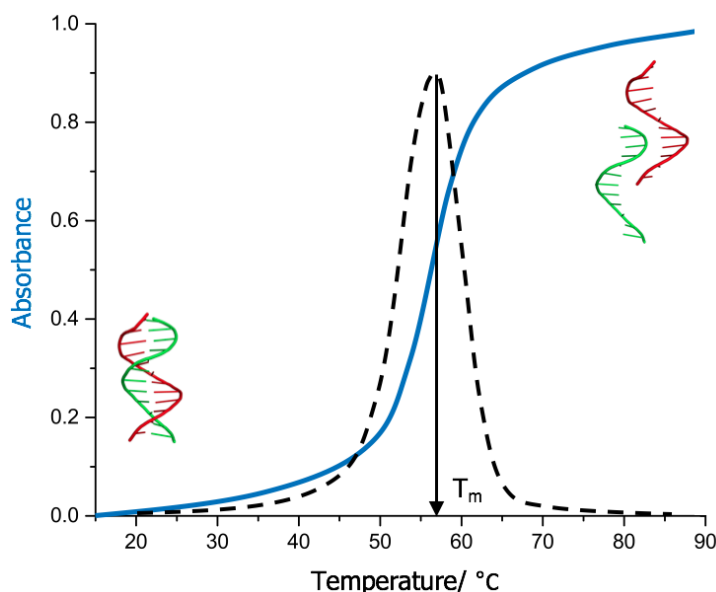
Figure 2.2 An example of a thermal melting curve of dsDNA monitored using UV-vis spectroscopy. As the temperature is increased the absorbance of the DNA at 260 nm increases as the duplexes are beginning to denature. The blue line represents the thermal melting curve and the dashed lines show the first derivative that gives the calculated T_m value.

2.5.2 Fluorescence Spectroscopy

Fluorescence is a fundamental luminescence process occurring with molecules that are rigid and often conjugated in structure. The process involves a photon of light being absorbed by a fluorophore and the fluorophore going to a higher electronic state, e.g. S_1 or S_2 (**Figure 2.1**). The molecule will then relax, in a rapid process known as internal conversion, from a higher vibrational state to the lowest vibrational state in S_1. The molecule will then relax back down to the ground state (S_0). During this relaxation process a detectable photon of light can be released and this is known as fluorescence.[15] Another luminescence phenomenon, phosphorescence, occurs when molecules in S_1 go through a spin conversion, called intersystem crossing, to the triplet state (T_1). The emission that results from the relaxation of a molecule from T_1 to S_0 is known as phosphorescence.

During fluorescence, the wavelength of the photon that is emitted will have a higher wavelength, i.e. lower energy, than the photon that has been absorbed. A reason for this is due to the energy lost during internal conversion down to the lowest vibrational level of S_1 before fluorescence occurs. This difference in wavelength between the fluorescence and absorption is called the Stokes shift.[21] Kasha's rule states that a molecule will give the same fluorescence emission spectrum irrespective of the excitation wavelength used[22] and the reason behind this phenomenon is similar to that of the Stokes shift. As all fluorescence is occurring from the lowest vibrational level of S_1 the fluorescence becomes independent of the wavelength of excitation. The fluorescence intensity of a molecule is commonly measured using a spectrofluorometer and the fluorescence emission spectrum is a depiction of the wavelength distribution of emission at one wavelength.

The quantum yield of a fluorophore is defined as ratio of photons that are emitted compared to the number of photons that have been absorbed by the molecule. If a fluorophore has a large quantum yield it will give the brightest fluorescence emission.[15]

2.5.2.1 *Sangar DNA sequencing*

Sangar DNA sequencing is the process of determining the nucleotide sequence of an isolated region of a DNA strand and utilises fluorescence spectroscopy. The sequencing begins by transferring a DNA sample to a multi-well plate where the sequencing reaction will take place. A reaction mix is added to the well containing; free nucleotides, a DNA polymerase, DNA primers for the region of interest, and fluorescently modified terminator bases. Similarly to PCR, the sample is heated to allow the denaturation of the DNA duplex. Next, the sample is cooled to allow the annealing of the primers to the ssDNA. The DNA polymerase binds to the primer:DNA duplex region and begins to elongate the strand using the unlabelled nucleotides in the reaction mix. The elongation continues until a terminator base is added and this cycle is repeated enough to produce DNA fragments of all possible lengths to give a full read-out of the DNA sequence. The newly synthesised fragments are separated by length using capillary electrophoresis and the shorter DNA fragments will move through the capillary faster than the longer strands. The fluorescence emission from the terminator base will be monitored, giving a different fluorescence colour for each different terminator base. The DNA sequencer will then monitor the fluorescence of these bases giving the sequence of the DNA strand.[23] The process of DNA sequencing has revolutionised our knowledge on genomic DNA and how disease is detected and in light of newer techniques it is becoming a more cose-efficient process.[24-25]

2.6 Linear Dichroism Spectroscopy

Linear Dichroism (LD) is another spectroscopic technique that utilises the absorbance of linearly polarised light by a species to provide information about its orientation against a predefined orientation axis.[26] Molecules that can be aligned against a linear axis will absorb linearly polarised light to different degrees dependent upon whether the absorbing chromophores are oriented parallel to the polarised light beam, or, whether the chromophores are perpendicular to that of the linearly polarised light beam.[27-28]

The difference of absorption of parallel polarized light ($A_{||}$) and perpendicular polarized light ($A_{\perp}$) compared to the predefined orientation direction is calculated to give LD spectra using a spectrophotometer using the following equation (**Equation 2.5**):

$$LD = A_{\parallel} - A_{\perp}$$

Equation 2.5 *The LD equation established by Norden et al., that relates parallel absorbed linearly polarised light versus perpendicular absorbed linearly polarised light to the resulting LD signal.*[29-30]

If a molecule cannot be aligned against the predefined orientation axis, i.e. the degree of alignment (S) is 0, the sample will not give rise to an LD signal. However, if the chromophores within an oriented sample are aligned more parallel to the predefined orientation axis the sample will give a positive LD signal and a negative signal will be generated when the chromophores align more perpendicular to the orientation axis. When the degree of alignment is equal to 1 the sample has perfect orientation with the orientation axis and will give a very strong LD signal. As a result, the absorbance given in the LD spectra will change depending on the degree of alignment between the polarised light and the transition dipole moment of the chromophores on the sample.[27]

2.6.1 Alignment of samples for the use of LD

Linear dichroism can be used for molecules that can be orientated artificially along a linear plane.[27] Samples require a method of artificial orientation against the predefined orientation axis that enables the full potential of LD to be utilised. The alignment of samples that are not intrinsically aligned can be achieved through varying techniques. The three main techniques are squeezed gel, stretch film or shear flow alignment.[27]

Although there are many methods of orienting the sample, the method focused on within this project is Couette shear flow orientation (**Figure 2.4**) which uses the viscous drag resulting from a solution flowing between thin walls of a Couette cell to orient long structures (**Figure 2.3**).
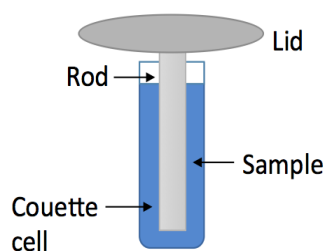
Figure 2.4 *A Couette flow cell used to align samples for shear flow linear dichroism.*
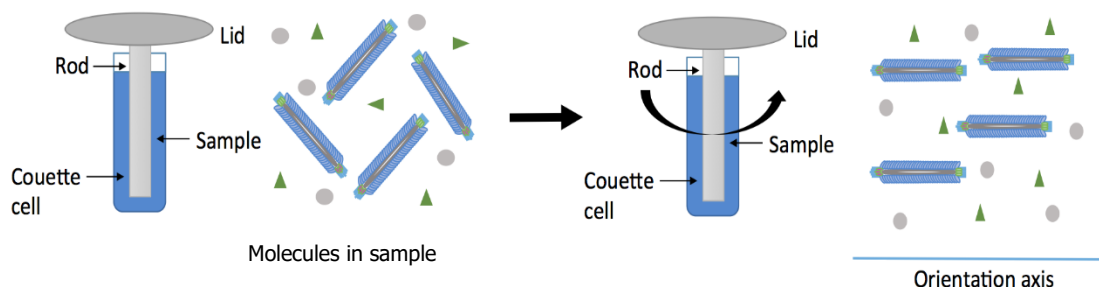
Figure 2.3 *A diagram depicting the process of Couette flow alignment of a system for detection by linear dichroism.*

2.7 Circular Dichroism Spectroscopy

The electromagnetic spectroscopic method for studying chiral molecules is known as circular dichroism (CD). Biomolecules are often chiral and fold into secondary and tertiary structures. These highly organised structures, in combination with the chirality of each subunit within the biomolecule, will give a defined CD signal.[27, 30]

The definition of CD is the difference between the absorption of circularly polarised, right-handed (A_r) or left-handed (A_l) light by a molecule.[27] The equation for CD can be seen below (**Equation 2.6**).

$$CD = A_l - A_r$$

Equation 2.6 *The equation that allows for the measurement of a CD signal.*

CD signals can be monitored when a biomolecule is absorbing one direction of circular polarised light more than the other direction in a similar manner to linearly polarised light in LD spectroscopy. The resulting spectra can have both a positive and a negative signal. The positive signal is as a result of the molecule absorbing A_l more than A_r and the negative signal is due to a greater absorbance of A_r light.[27]

DNA is a chiral molecule that folds into a helix in a very specific manner dependent upon the sugar-phosphate backbone and the stacking of the base-pairs. The three different morphological structures of DNA were discussed in the introduction (**Chapter 1**) and all three of these arrangements, B, Z and A, will give different CD signals.[31] The right-handed double stranded DNA helix of B-DNA will give a maximum at ~275 nm and a minimum at ~245 nm. The more compact A-DNA right-handed helix gives a maximum at ~270 nm and a minimum at ~230 nm. Lastly, Z-DNA, a left-handed helical structure will give a small minimum at 290 nm, a broad minimum between 220 and 260 nm and a maximum at ~280 nm.[27, 32-33]

In this project CD was used to study the structure of a modified G-quadruplex aptamer (**Chapter 3**). Although CD cannot provide atomic information about chiral structures it can allow the discrimination between the different structures and any topological arrangements, giving an indication of any structural changes when any chemical modifications are introduced into an aptamer.[34] When a G-quadruplex takes on a parallel orientation the absorbance maximum can be seen to be approximately 260 nm and the minimum is seen at ca. 240 nm. For an anti-parallel G-quadruplex the maximum will be seen at ca. 290 nm and the minimum at ca. 260 nm (**Figure 2.5**).[34]
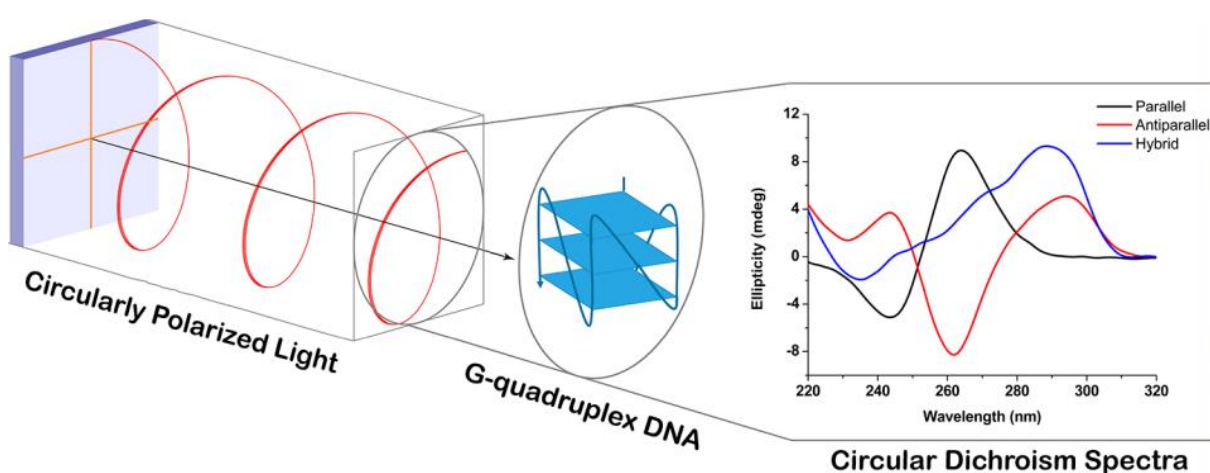
Figure 2.5 *The typical circular dichroism spectra expected after the absorbance of circularly polarised light from a sample of G-quadruplex DNA.[35]*

2.8 Gel Electrophoresis

Electrophoretic separation of molecules in gels is dependent upon their mass/size, shape and charge. A gel polymer is set using either acrylamide or agarose and an electric field is applied to the gel once it has been loaded with sample.[36] The gel is placed in an electrophoresis chamber where an electrical field will pull any samples that contain a negative charge towards an electrode with a positive charge (**Figure 2.6**).[37] Molecules which carry a high charge or are lesser in mass will move faster through the gel and conversely the molecules which carry a smaller charge and are larger in size will move slower through the gel, thus separating the components in a mixture. This technique will separate negatively charged molecules, like oligonucleotides that are negatively charged as a result of the phosphate backbone.
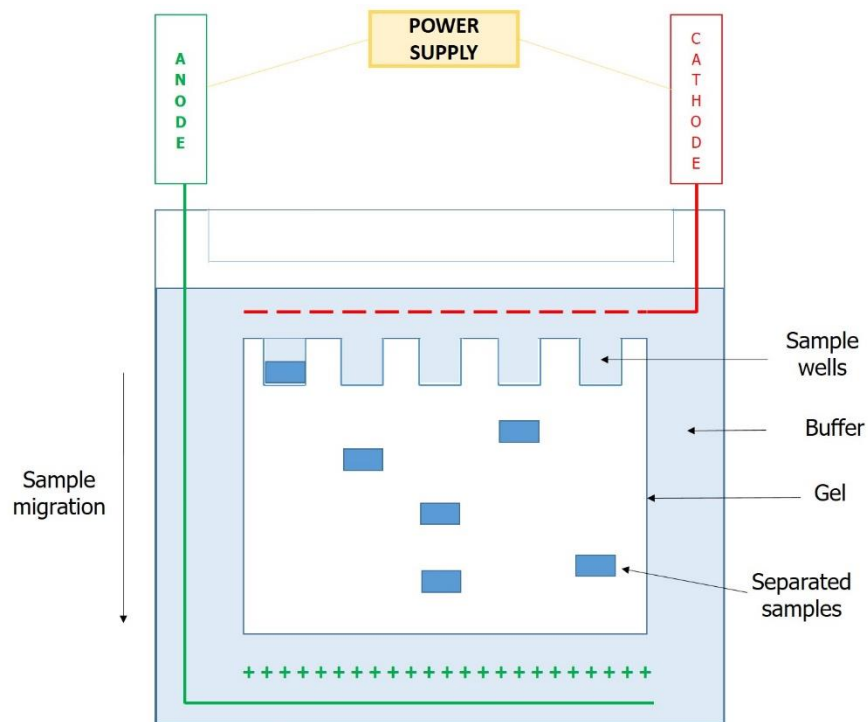
Figure 2.6 A typical gel electrophoresis set-up where negatively charged samples will move through the gel towards a positive electrode.

Several of the techniques discussed in the introduction involved the use of gel electrophoresis and the specific gel electrophoresis techniques utilised in this thesis are discussed in this section:

2.8.1 Agarose gel electrophoresis

Agarose gel electrophoresis is the conventional gel separation method used with larger biomolecules, such as genomic DNA fragments between 0.5 – 25 kb long, as the pore size of an agarose gel is larger than the pore size of an acrylamide gel.[36] The size of the agarose gel pores will depend on the agarose concentration used and the migration of the molecules will depend on the running buffer and/or voltage used to run the gel. The samples are run with a dye that will allow for visualisation of the bands once the gel has been stopped, a traditional DNA dye being ethidium bromide. [38] Ethidium bromide intercalates with DNA fragments and can be visualised using UV-vis gel illuminators and bands will be seen where there has been separation of the sample.

In **Chapter 4** agarose gel electrophoresis was used as a diagnostic tool to analyse fragments of DNA amplified from polymerase chain reactions (PCR) in order to determine the success of the PCR reaction.

2.8.2 Polyacrylamide Gel Electrophoresis (PAGE)

Smaller DNA fragments, such as short oligonucleotides, synthesised using solid-phase DNA synthesis are commonly visualised using acrylamide rather than agarose gels. The resulting pore sizes of the acrylamide matrix is smaller and sufficient for shorter strands of DNA than that of the larger mesh created when agarose is polymerised.[39] Similarly to an agarose gel the pore size of the acrylamide can be modified by changing the concentration of acrylamide used or by changing the amount of crosslink agents, (Tetramethylethylenediamine (TEMED) or ammonium persulphate (APS)), used.

There are two main categories of polyacrylamide gels that are used to separate DNA fragments; native polyacrylamide gels and denaturing polyacrylamide gels.[37] Native gels will contain no denaturing agents allowing for the separation of double stranded DNA (dsDNA) without disrupting the helical

structure held together by the hydrogen bonds discussed in the introduction (**Chapter 1**). A denaturing gel will introduce a denaturant such as urea or fomamide in order to disrupt the double stranded helical structure. A native gel allows the study of DNA in its native helical structure and denaturing gels allow for the study of single stranded DNA (ssDNA). The main technique used within this thesis was native PAGE as the research focused on short single stranded oligonucleotides.

Native polyacrylamide gels are undertaken using buffers that have high conductance, such as tris-borate-EDTA (TBE) buffer,[40] in order to reduce the likelihood of a gel from overheating if run for a long period of time, reducing the chance of any DNA secondary structure denaturation.

Similarly to agarose gels, the separated bands on a polyacrylamide gel will be visualised at the end of a gel run. Within this thesis the Diamond™ Nucleic Acid Dye was used as it is known for its low toxicity to the user, rapid staining time, and has high DNA sensitivity. The dye is excited at 495 nm, a longer wavelength than DNA, which will also mean that the DNA strands will not be damaged by the UV light typically used for visualisation.

2.8.3 *Electrophoretic Mobility Shift Assay*

An electrophoretic mobility shift assay (EMSA) is a native polyacrylamide gel separation technique that is commonly used to study the interactions between DNA and proteins.[41] Different mixtures of DNA:protein will be used throughout the gel by adding the same concentration of DNA in all the samples while adding increasing concentrations of the protein of interest. The DNA:protein complex will move through the gel slower than the unbound DNA, which will migrate to the bottom of the gel while the complex will stay near the top of the gel. Gels can be stained for DNA in a similar manner to that in **Section 2.9.2.** The protein will be stained using a protein stain, such as coomassie brilliant blue, after the DNA has been visualised. Coomassie dyes[42] work by binding to either the basic amino acid residues or the hydrophobic amino acid residues in proteins that are present within the sample allowing the proteins to be visualised. The visualisation can be done by eye but a picture can be taken using a normal camera to record the bands and compare them to the corresponding DNA stain image.

2.9 References

1. Michelson, A. M.; Todd, A. R., Nucleotides part XXXII. Synthesis of a dithymidine dinucleotide containing a 3′ : 5′ -internucleotidic linkage. *Journal of the Chemical Society* **1955**, pp. 2632-2638.

2. Matteucci, M. D.; Caruthers, M. H., Synthesis of deoxyoligonucleotides on a polymer support. *Journal of the American Chemical Society* **1981,** *103*, pp. 3185-3191.

3. Caruthers, M. H.; Beaucage, S. L.; Becker, C.; Efcavitch, J. W.; Fisher, E. F.; Galluppi, G.; Goldman, R.; deHaseth, P.; Matteucci, M.; McBride, L., Deoxyoligonucleotide synthesis via the phosphoramidite method. *Gene Amplification and Analysis* **1983,** *3*, pp. 1-26.

4. Brown, T.; Brown, T. J., Nucleic Acids Book. 2013. http://www.adtbio.co./nucleic-acids-book (accessed 20 July 2015).

5. Ravikumar, V. T.; Kumar, R. K.; Olsen, P.; Moore, M. N.; Carty, R. L.; Andrade, M.; Gorman, D.; Zhu, X.; Cedillo, I.; Wang, Z.; Mendez, L.; Scozzari, A. N.; Aguirre, G.; Somanathan, R.; Berneès, S., UnyLinker: An Efficient and Scaleable Synthesis of Oligonucleotides Utilizing a Universal Linker Molecule: A Novel Approach To Enhance the Purity of Drugs. *Organic Process Research & Development* **2008,** *12*, pp. 399-410.

6. Huber, C. G.; Oefner, P. J.; Bonn, G. K., High-Resolution Liquid Chromatography of Oligonucleotides on Nonporous Alkylated Styrene-Divinylbenzene Copolymers. *Anal Biochem* **1993,** *212*, pp. 351-358.

7. Ashman, K.; Bosserhoff, A.; Frank, R., High-speed preparative reversed-phase high-performance liquid chromatography of synthetic oligonucleotides. *Journal of Chromatography* **1987,** *397*, pp. 137-140.

8. Snyder, L. R.; Glajch, J. L., JJ Kirkland Practical HPLC Method Development. Wiley, New York: 1988.

9. Eksborg, S.; Schill, G., Ion pair partition chromatography of organic ammonium compounds. *Analytical chemistry* **1973,** *45*, pp. 2092-2100.

10. Gilar, M.; Fountain, K. J.; Budman, Y.; Neue, U. D.; Yardley, K. R.; Rainville, P. D.; Russell Ii, R. J.; Gebler, J. C., Ion-pair reversed-phase high-performance liquid chromatography analysis of oligonucleotides: Retention prediction. *Journal of Chromatography A* **2002,** *958*, pp. 167-182.

11. Barth, H. G.; Jackson, C.; Boyes, B. E., Size Exclusion Chromatography. *Analytical chemistry* **1994,** *66*, pp. 595-620.

12. Kuga, S., Pore size distribution analysis of gel substances by size exclusion chromatography. *Journal of Chromatography A* **1981,** *206*, pp. 449-461.

13. Mori, S.; Barth, H. G., Fundamental concepts In Size Exclusion Chromatography, Eds. Springer Berlin Heidelberg, 1999; pp 11-29.

14. Ball, D. W., *Modern Spectroscopy* Fourth ed.; John Wiley & Sons, Inc.: New York, 2004; Vol. 50, p 2469-2470.

15. Lakowicz, J. R., *Principles of Fluorescence Spectroscopy*. Springer **2006**; Vol. 3, pp. 960.

16. Clauss, A., Rapid physiological coagulation method in determination of fibrinogen. *Acta Haematologica* **1957,** *17*, pp. 237-46.

17. Miesbach, W.; Schenk, J.; Alesci, S.; Lindhoff-Last, E., Comparison of the fibrinogen Clauss assay and the fibrinogen PT derived method in patients with dysfibrinogenemia. *Thrombosis Research* **2010,** *126*, pp. e428-e433.

18. Mackie, I. J.; Kitchen, S.; Machin, S. J.; Lowe, G. D. O., Guidelines on fibrinogen assays. *British Journal of Haematology* **2003,** *121*, pp. 396-404.

19. Wartell, R. M.; Benight, A. S., Thermal denaturation of DNA molecules: A comparison of theory with experiment. *Physics Reports* **1985,** *126*, pp. 67-107.

20. Russell, A. P.; Holleman, D. S., The thermal denaturation of DNA: average length and composition of denatured areas. *Nucleic Acids Research* **1974,** *1*, pp. 959-978.

21. Stokes, G. G., On the change of refrangibility of light. *Philosophical Transactions of the Royal Society of London* **1852,** *142*, pp. 463-562.

22. Kasha, M., Characterization of electronic transitions in complex molecules. *Discussions of the Faraday Society* **1950,** *9*, pp. 14-19.

23. Gomes, A.; Korf, B., Chapter 5 - Genetic testing techniques. In *Pediatric Cancer Genetics*, Robin, N. H.; Farmer, M. B., Eds. Elsevier: 2018; pp 47-64.

24. Smith, L. M.; Sanders, J. Z.; Kaiser, R. J.; Hughes, P.; Dodd, C.; Connell, C. R.; Heiner, C.; Kent, S. B. H.; Hood, L. E., Fluorescence detection in automated DNA sequence analysis. *Nature* **1986,** *321*, pp. 674.

25. Bumgarner, R., DNA microarrays: Types, applications and their future. *Current protocols in molecular biology* **2013,** pp. *0 22*.

26. Rodger, A., Linear dichroism. *Methods in enzymology*, Academic Press: **1993**; Vol. 226, pp. 232-258.

27. Norden, B.; Rodger, A.; Dafforn, T. R., *Linear Dichroism and Circular Dichroism: A textbook on Polarized-Light Spectroscopy*. 1 ed.; Royal Society of Chemistry: **2010**.

28. Kliger, D. S.; Lewis, J. W.; Randall, C. E., Chapter 2 - Polarization properties of light. *Polarized Light in Optics and Spectroscopy*, Kliger, D. S.; Lewis, J. W.; Randall, C. E., Eds. Academic Press, **1990**; pp. 9-26.

29. Nordén, B.; Rodger, A.; Dafforn, T. R., *Linear Dichroism and Circular Dichroism*. The Royal Socetry of Chemistry: London, 2010.

30. Nordén, B., Applications of linear Dichroism Spectroscopy. *Applied Spectroscopy Reviews* **1978,** *14*, pp. 157-248.

31. Johnson, W. C., Secondary Structure of Proteins Through Circular Dichroism Spectroscopy. *Annual Review of Biophysics and Biophysical Chemistry* **1988,** *17*, pp. 145-166.

32. Albinsson, B.; Kubista, M.; Norden, B.; Thulstrup, E. W., Near-ultraviolet electronic transitions of the tryptophan chromophore: linear dichroism, fluorescence anisotropy, and magnetic circular dichroism spectra of some indole derivatives. *The Journal of Physical Chemistry* **1989,** *93*, pp. 6646-6654.

33. Dodero, V. I.; Quirolo, Z. B.; Sequeira, M. A., Biomolecular studies by circular dichroism. *Frontiers in Biosciences (Landmark Ed)* **2011,** *16*, pp. 61-73.

34. Burge, S.; Parkinson, G. N.; Hazel, P.; Todd, A. K.; Neidle, S., Quadruplex DNA: sequence, topology and structure. *Nucleic Acids Research* **2006,** *34*, pp. 5402-15.

35. Carvalho, J.; Queiroz, J. A.; Cruz, C., Circular Dichroism of G-Quadruplex: a Laboratory Experiment for the Study of Topology and Ligand Binding. *Journal of Chemical Education* **2017,** *94*, pp. 1547-1551.

36. Rabilloud, T., *Proteome Research: Two-Dimensional Gel Electrophoresis and Identification Methods*. **2000**.

37. Peters, T. N., *Gel electrophoresis of proteins: A practical approach* Second ed.; Oxford University Press, **1991**; Vol. 19, pp. 39-39.

38. Karsten, U.; Wollenberger, A., Improvements in the ethidium bromide method for direct fluorometric estimation of DNA and RNA in cell and tissue homogenates. *Analytical Biochemistry* **1977,** *77*, pp. 464-70.

39. Matthew, R. W.; Ralph, R., Electrophoresis of nucleic acids. In *Route Maps in Gene Technology*, **2009**.

40. Bisen, P. S., *Laboratory Protocols in Applied Life Sciences*. 1 ed.; CRC Press: Boca Raton, **2014**; pp. 1826.

41. Hellman, L. M.; Fried, M. G., Electrophoretic mobility shift assay (EMSA) for detecting protein-nucleic acid interactions. *Nature protocols* **2007,** *2*, pp. 1849-1861.

42. Neuhoff, V.; Arold, N.; Taube, D.; Ehrhardt, W., Improved staining of proteins in polyacrylamide gels including isoelectric focusing gels with clear background at nanogram sensitivity using Coomassie Brilliant Blue G-250 and R-250. **1988,** *9* , pp. 255-26

Chapter 3 – Photoactivated manipulation of the thrombin binding aptamer

3.1 Introduction

Biomolecules offer exquisite molecular recognition properties that can be exploited for therapeutic and diagnostic applications. For example, the use of antibodies has revolutionised diagnostics through the Enzyme Linked Immunosorbent Assay (ELISA) and other related technologies. The same molecules are now also central to drug discovery, with approximately 70 monoclonal antibody products expected to be on the global pharmaceutical market by 2020.[1] However, almost all of the current examples provide recognition processes that are difficult to control. For example, once the interaction between a biomolecule and an antibody has occurred, it can be difficult to reverse the interaction under physiological conditions. The ability to control biomolecules and their binding properties are particularly important in research for therapeutic purposes.[2-3]

As discussed in **Chapter 1**, short single stranded DNA (ssDNA) aptamers are able to bind to many different biomolecular targets including; DNA, proteins, cells, and small molecules.[3-5] A powerful way to control bimolecular binding events is by incorporating photoreactive functional groups, such as anthracene, into DNA. The incorporation of two anthracene groups into the architectural framework of a DNA strand provides a means for controlling DNA binding through anthracene photodimerisation. This photodimerisation process is central to this chapter whereby we demonstrate a novel system in which anthracene groups are incorporated into an aptamer to switch on and off a biomolecular recognition event that controls an enzymatic output.

3.2 Anthracene photochemistry

The uses of anthracene are reviewed in the introduction (**Chapter 1**) of this thesis and further information can be found in a recent review by Damme and Prez.[6] This chapter will focus on the photochemical properties demonstrated by two molecules of anthracene.

A phenomenon discovered by Fritzsche in 1867, two molecules of anthracene are capable of photodimerisation upon irradiation with Ultra-Violet (UV) light at 365 nm (± 5nm).[7-8] They undergo a $4\pi+4\pi$ pericyclic cycloaddition reaction whereby one anthracene is in its photochemically excited state and the other is in its ground state. As a result, two new covalent bonds are formed resulting in two anthracene molecules becoming one photodimer. The reaction is reversible when the photodimer is exposed to heat or UV-vis light of a shorter wavelength. The dimerisation reaction can also be reversed by mechanical stress and thus anthracene has also been used as a mechanophore.[9]

Supramolecular chemistry has benefited from the photochemical properties of anthracene as the reversible photodimerisation of two anthracenes can result in significant structural changes in a system. In recent work by Hizal et al., photoinduced polymerisation reactions using anthracene modified polymers have been employed to generate larger biopolymer assemblies.[10] Onal and co-workers found that telechelic (2-anthryl)-1-phenylethe-capped polyisobutylene polymer samples reversibly quadrupled in size when irradiated with light at 365 nm.[11]

Other photochemical uses of anthrcene can be seen in research by the Beyeler group. They reported the synthesis of rhenium complexes that contained two anthracene groups to demonstrate a novel molecular switch (**Figure 3.1**). The anthracene units were linked to 2,2'-bipyridine, and in their open form, they acted as quenchers of the luminescence from metals complexed to the bipyridine centre. However, when the anthracenes were irradiated with visible light, intramolecular photodimerisation caused the loss of the quenching properties due to the disrupted nature of the extended anthracene π system.[12]
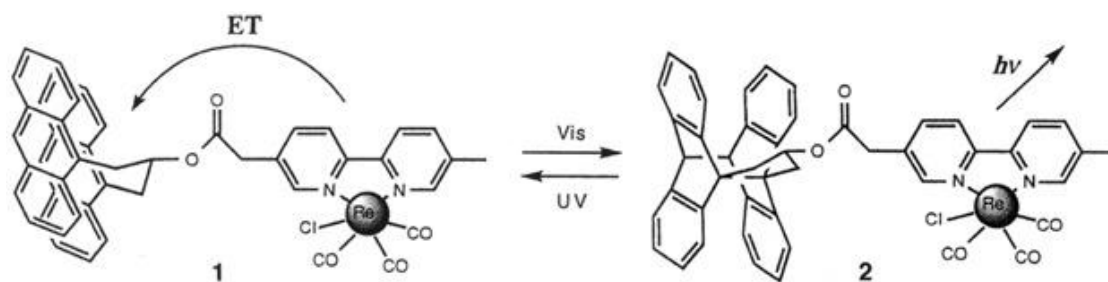
Figure 3.1 *Rhenium complexed bipyridine linked to two anthracene monomers. The forward reaction shows the anthracene dimerisation reaction after exposure to visible light allowing the metals to luminesce and the reverse occurs with exposure of the system to UV light.*[12]

The control of sodium ion transport across a phospholipid bilayer has been described using a calix[4]arene ester modified with two anthracene groups. The calix[4]arene ester was found to bind and carry Na^+ across a membrane when the anthracenes were in their monomeric form. However, upon photodimerisation the process was inactivated.[13]

More recently within the Tucker group, anthracene photodimerisation was used to create a light controlled peptide-DNA binding system by the introduction of an anthracene group into two DNA-binding peptides derived from a transcription factor. The photodimerisation of the two anthracenes was only possible when the correct DNA target was present, with improved DNA binding affinity seen after the anthracene had formed a photodimer.[14]

3.3 The control of DNA duplex formation

Similar approaches can be applied to oligonucleotides modified with anthracene for gaining photocontrol over DNA duplex formation.[15] The carbon 9 (C9) functionalisation of an anthracene with a D-Threoninol linker (discussed in **Chapter 1**) group has previously allowed its incorporation into oligonucleotides using phosphoramidite chemistry.[16-17] Functionalisation at this position leads to a pair of products upon photodimerisation: a head-to-tail or head-to-head dimer (**Figure 3.2**) with the former being more stable for steric reasons.[18]
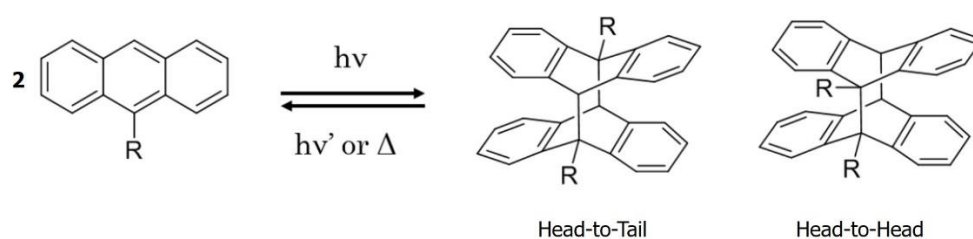
Figure 3.2 *The photodimerization of two anthracene monomers functionalised at the C9 position in presence of UV-vis light. The resulting products are two products; head-to-tail and head-to-head dimers.*

The Tucker group demonstrated the functionalisation of an oligonucleotide with two anthracene groups did not disrupt hybridisation to its target strand (**Scheme 3.1**) with the resulting duplex still able to form the common B-DNA structure discussed in **Chapter 1**.[19]
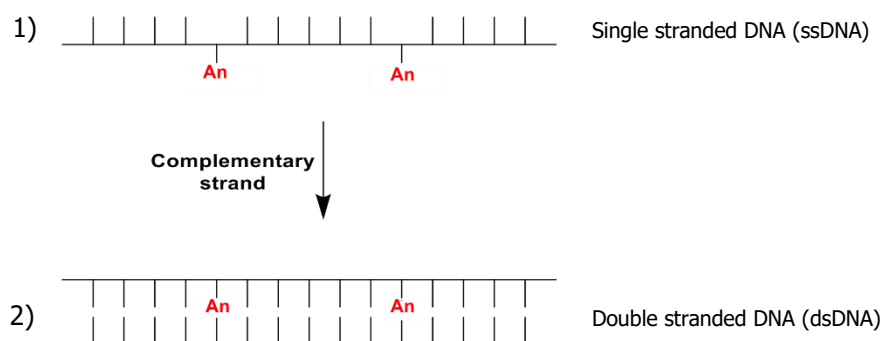
Scheme 3.1 *1) The incorporation of two anthracene monomers (represented by the red **An**) as base replacements into a single strand of DNA and 2) the successful formation of a dsDNA duplex of the anthracene modified single strand with its complementary strand.*

However, once the two anthracene groups within the oligonucleotide had undergone photodimerisation the strand was no longer able to form a duplex due to the lack of conformational flexibility (**Scheme 3.2**). The photodimerisation was found to be reversible by heating the sample to 80 °C, which allowed duplex formation to occur again.[19]
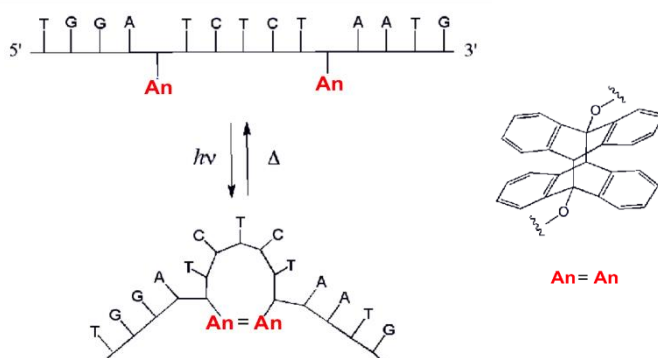
Scheme 3.2 *The photodimerisation of the two anthracene (**An**) groups changing the structure of the oligonucleotide enough to prevent duplex formation. A 365 nm bandpass filter was used in order to protect the DNA from UV-vis damage.*

The work in this chapter builds upon this previous study with the aim to establish whether or not anthracene photodimerisation is able to modulate the binding behaviour of ssDNA aptamers towards biomolecules such as proteins.[20]

3.4 Thrombin

The haemostasis process is an essential part of blood clotting. When injury to a blood vessel occurs there are many cofactors, proteins and enzymes involved that must be activated in order for thrombosis to take place. Human α-thrombin, an enzyme from the family of serine proteases, is a vital protein involved in the process of blood coagulation at the site of blood vessel injury. As well as being involved in the formation of a blood clot, thrombin is also involved in other processes during the haemostasis and is able to bind and have an effect on many substrates. This study focuses on α-thrombin as the two other forms of the protein, β-thrombin and γ-thrombin, are less active.[21] Thrombin naturally exists as the precursor pro-thrombin and is proteolysed when the coagulation cascade is triggered.[22]

Thrombin has two anion binding exosites, one of which (exosite I) binds fibrinogen. Exosite II is known to be the heparin, an anticoagulant, binding site.[23] During the formation of a blood clot thrombin causes the production of fibrin from fibrinogen, and is incorporated into the forming clot.[22] This conversion involves the proteolytic cleavage of the N-terminal peptides of fibrinogen forming fibrin. These fibrin monomers form cross-links and their aggregation forms the fibres seen in a blood clot. Thrombin is also involved in the activation of itself through cofactors such as XI, VIII and V (**Figure 3.3**) and stimulates the aggregation of platelets by cleaving membrane bound protease receptors.[24-25] The first crystal structure of the protein was solved in 1989 by Bode *et al*. in a complex with D-Phe-Pro-Arg-chloromethylketon (PPACK).[26] Further research has resulted in crystal structures where the specific active sites and other anionic binding sites have been studied (**Figure 3.4**).
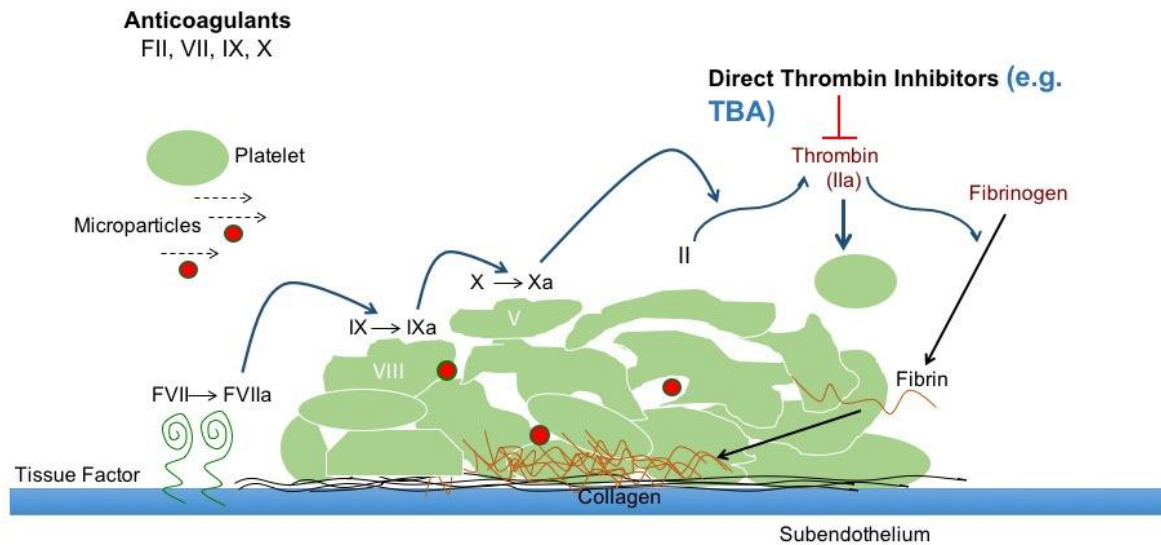
Figure 3.3 *A diagrammatic representation of the coagulation cascade. Upon stimulation of the cascade varying coagulation factors (FVII, FVIIa, IX, IXa, X, and Xa) cause the formation of thrombin (IIa) from prothrombin (II) which in turn causes the formation of fibrin from fibrinogen. Direct thrombin inhibitors such as the thrombin binding aptamer (discussed in the next section) can block this process.*
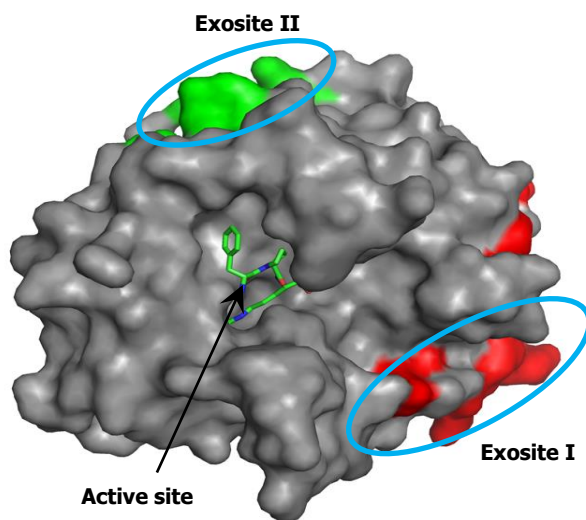
Figure 3.4 *The crystal structure of α–human thrombin (grey). The two exosites, exosite I (red) and exosite II (green) are circled in blue. The active site in this solid surface image is bound to PPACK, an inhibitor of thrombin. The active site contains a serine protease.*[23]

3.4.1 The thrombin binding aptamer

One aptamer with particularly interesting biological activity is the aptamer that targets α-thrombin, the thrombin binding aptamer (TBA).[20, 27] The aptamer was first discovered by Bock *et al*. in an attempt to develop inhibitors of thrombin.[27] TBA is a 15 base long oligonucleotide (**Figure 3.5B**) that has a G-quadruplex (G4) tertiary structure that is formed by oligonucleotides with high guanine (G) base content. The G4 structure assembles when four G residues, in close proximity, form a G-quartet structure by Hoogsteen base pairing (**Figure 3.5A**).[28] A G4 can arrange into three main conformations; parallel, antiparallel and a hybrid of the two.[29-30] The glycosidic bonds between the deoxyribose sugar and the G residues in the parallel conformations are in the *anti*-orientation. In the *anti*-orientation the sugar ring and therefore any hydrogen bonding occurs away from the sugar ring and the glycosidic bonds in the *sin*-orientation are in the opposite direction. The antiparallel G4 structures contain both the *sin*- and the *anti*-conformations.[28]

The regulation of many biological pathways, in both eukaryotes and microorganisms, depend upon these G4 structures and can be found in extended poly-G sequences of telomeres that form tetrameric G4 structures. These telomeres ensure that the chromosome does not unravel.[31] Aptamers with a G4 structure have been found to bind to targets that are able to inhibit pathways such as signal transduction and transcription in cells. The G4 structure is able to structurally respond to external stimuli, for example ions, making it a good signal transducer. For example, G4 oligonucleotides have been selected by Tweardy *et al*. as inhibitors of the signal transducer and activator of transcription 3 (Stat3) that is known for contributing to head and neck cancer.[32] The TBA folds into an anti-parallel G4 structure[33] (**Figure 3.5B**) in the presence of K^+ ions, as shown by the crystal structure of the aptamer solved by Krauss *et al*. (**Figure 3.6**).[20, 34-37] The potassium cation is oriented equidistant between the two planes of the two G-tetrads.[28] TBA binds to thrombin at exosite I, the fibrinogen binding site, via the two TT loops present at the top of the aptamer.[38] The formation of a complex between TBA and thrombin competitively inhibits the binding of fibrinogen to thrombin, thereby inhibiting the process of blood coagulation.[27, 39]
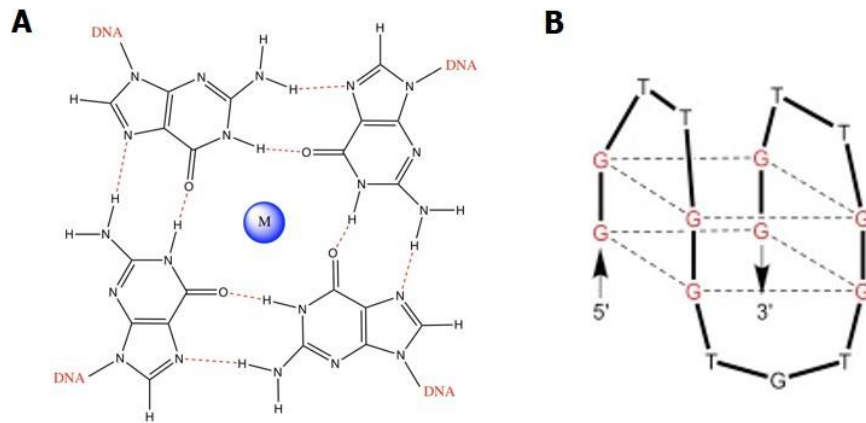
Figure 3.5 A) *The Hoogsten base hydrogen bond pairing of four guanine residues forming a G-quartet in the presence of a monovalent cation, such as K+, causing the folding of TBA, and* **B)** *Two G-quartets come together to form the anti-parallel G4 structure of the TBA.*
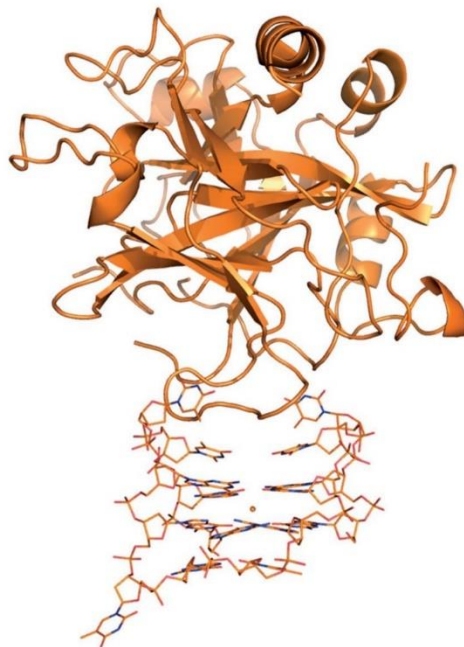
Figure 3.6 *The crystal structure of TBA, in the presence of a potatssium ion coordinated in the centre of the TBA structure, bound to thrombin at exosite I as determined by Krauss et al.[37]*

3.4.2 Control of TBA binding

The presence of an aptamer that blocks thrombin and hence blood clotting has implications for a number of thrombotic disorders.[40] Traditional anti-coagulants, (e.g. Heparin or Warfarin), which prevent the formation of unwanted blood clots can often result in side effects.[41] For example, reduction in clotting capability means that wound healing is severely compromised at injury sites away from the site where anticoagulation is required. If a patient undergoing anticoagulation therapy should require an invasive surgical procedure the potential for significant bleeding has to be considered and one solution to this issue would be to remove the anticoagulation therapy. Unfortunately, for current therapies this relies on cessation of the medication, while relying on the clearance systems of the body to reduce the systemic concentration of the anticoagulant. A more effective solution to this issue would be to have an anticoagulant therapy that could be applied in a specific area and deactivated locally within the body.

Due to the importance of thrombin in blood clotting, gaining control of TBA has been of interest in recent research. For example, Clever *et al.* introduced chiral pyridine ligands to the TBA that are able to coordinate to a Cu^{II} ion. The ligand modified TBA, without the Cu^{II} ion being present, was not able form the G4 structure and thrombin inhibition was not possible. However, the square planar metal coordination with Cu^{II}, in the presence of a Na^+/K^+ cations, led to increased stabilisation of the modified G4 structure, allowing it to bind and inhibit thrombin. Therefore, the ability of the modified TBA to slow down the proteolysis of fibrinogen was found to be inefficient in the absence of copper (**Figure 3.7**).[42]
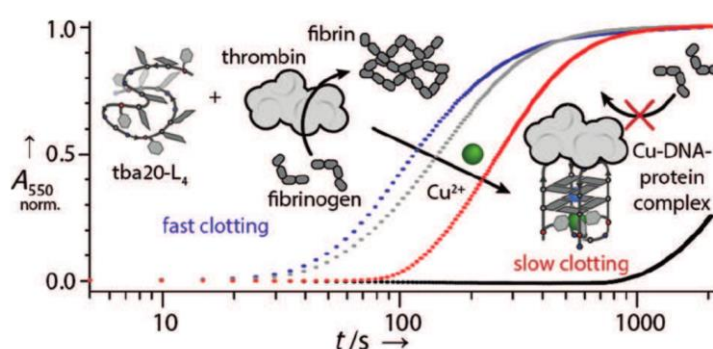
Figure 3.7 *A time dependent clotting study carried out by Clever et al., demonstrating that a modified thrombin binding aptamer (tba-20-L4) slows down blood clotting in the presence of Cu^{II} ions. The red line represents the clotting time in the presence of Cu^{II}, whereas the blue line represents the clotting time in the absence of Cu^{II}. The black line is the clotting reaction with unmodified TBA and the grey line is the reaction without any DNA present.[42]*

Recently Mo *et al.* demonstrated the control of thrombin activity using the photochemical properties of an azobenzene modified TBA. Azobenzene is capable of trans-cis isomerism upon irradiation of UV light and the modification of the TGT loop of TBA with 4,4'-bis(hydroxymethyl) azobenzene resulted in the photoregulation of thrombin and therefore the ability of the thrombin to bind fibrinogen.[43]

3.5 Project Aims

It was hypothesised that a DNA aptamer modified with anthracene could be used for photo-control over its binding to a target protein. For this purpose, two anthracene units, attached to a D-threoninol linker, were to be incorporated into the TBA sequence using automated DNA synthesis. This chapter demonstrates how the antithrombotic activity of TBA can be controlled using anthracene photochromism.

The original aims can be separated into three key milestones:

1) The design and synthesis of a modified thrombin binding aptamer containing two anthracene units.

2) To study the structural properties of the modified aptamer and in particular its ability to bind thrombin in its open and closed (photodimerised) forms.

3) If the binding studies were positive, to carry out thrombin:fibrinogen clotting assays to determine whether the formation of a blood clot could be photocontrolled.

3.6 Results and Discussion

3.6.1 Modified aptamer design

Two important considerations in the successful design of the photo-switchable aptamer were the position of the two anthracene groups in the TBA sequence (**Figure 3.8A**) and which bases they would replace. In particular, the guanines partaking in G4 formation had to be retained as this motif gives the required tertiary structure for strong thrombin binding. Furthermore, it was reasoned that replacing two thymines (T) in both top TT loops would adversely affect thrombin binding in its un-photodimerised form as this face binds to the protein. Therefore, one anthracene moiety was introduced into one top loop, with the other replacing a thymine in the bottom TGT loop, giving the sequence of M3 (**Figure 3.8B**). It was anticipated that this strand would retain the ability to bind thrombin but with its two anthracene groups in close enough proximity (separated by two bases) to undergo intramolecular photodimerisation. In addition to M3, M4 (**Figure 3.8C**) containing only one anthracene in the bottom TGT loop was to be synthesised as a control to examine whether the observed effects could result from other entities in the system.

5'-GGTTGGTGXGGYTGG-3'

TBA: X = T,   Y = T
M3: X = An, Y = An
M4: X = An, Y = T
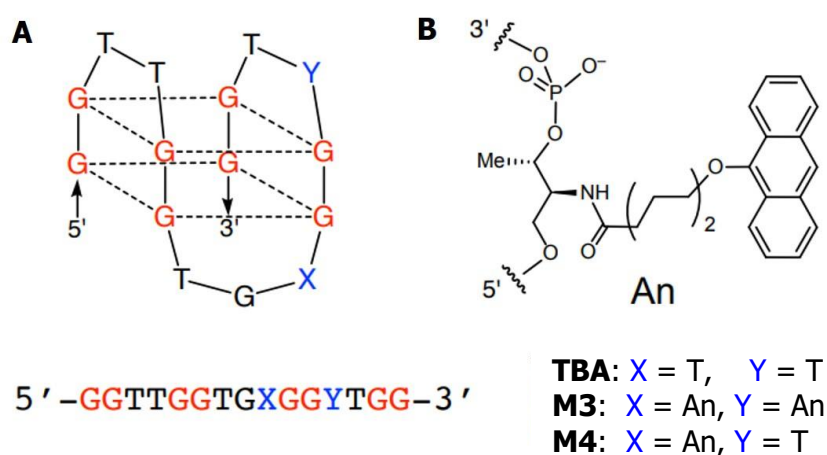
*Figure 3.8 Diagrammatic representations of **A)** TBA G4 structure held together by hydrogen bonds at the guanine residues which are indicated in red and the potential modification locations indicated in blue and **B)** The anthracene modification introduced into the aptamer with a D-threoninol linker (denoted as An). M3 contained a An modification at both position Y and X and M4 contained an An modification only in position X.*

3.6.1.1 Aptamer purification and characterisation

The anthracene phosphoramidite was synthesised as per the Tucker group protocol and characterised by another member of the group.[44] Each oligonucleotide strand with the anthracene modifications was purified using reverse phase high performance liquid chromatography (RP-HPLC) and characterised by negative mode electrospray ionisation (ESI) mass spectrometry (the data can be seen in **Table 3.1**). RP-HPLC and mass spectrometry results can be seen in **Appendix Section 7.1.1** and **Section 7.1.2**.

Table 3.1 *The aptamer and control sequences used within this research including a non-specific (NS) control. The X represents an anthracene modification. The NS control was chosen as previous work within the group had determined that it did not bind to thrombin.*

Name	Sequence (5' → 3')	Expected mass	Observed mass	RP-HPLC purity (%)
Native-TBA	GGT TGG TGT GGT TGG	4726	4726	97
M3	GGT TGG TGX GGX TGG	5057.7	5060	97
M4	GGT TGG TGX GGT TGG	4891.9	4894	100
NS Control	TGA AAA TGG AAC CTC GCC AAA TGT CA	7972	7971	100

3.6.2 Photoirradiation studies

As discussed in the introductory chapter, the anthracene units give a characteristic absorption spectrum of three bands between 350-400 nm. Upon photodimerisation of two anthracene molecules, the conjugated structure of the anthracene begins to disappear, which results in a decrease in its characteristic absorption spectrum. This process allows for the monitoring of the photodimerisation reaction by ultraviolet visible (UV-vis) spectroscopy. To determine whether M3 could undergo photodimerisation samples of M3, at 2 μM in TBA buffer (20 mM Tris-HCl, 1 mM $MgCl_2$, 120 mM NaCl, 10 mM KCl, 2 mM $CaCl_2$, pH 7.4), were subjected to UV-vis irradiation (using a 365 nm bandpass filter to protect the nucleotides), over a period of 4 hours. Over this time, the characteristic anthracene absorbance band centred at ca. 370 nm decreased by 73%, indicating successful photodimer formation (**Figure 3.9**). In contrast, the corresponding spectrum of sequence M4, containing only one anthracene unit, did not change significantly over the same period of time (**Figure 3.10**). This confirmed that the light-induced reaction was an intramolecular process. The isolation of the photodimerised M3 from the

un-photodimerised M3 was attempted using RP-HPLC but this was not possible due to the two having the same retention time (**Appendix, Section 7.1.4**).
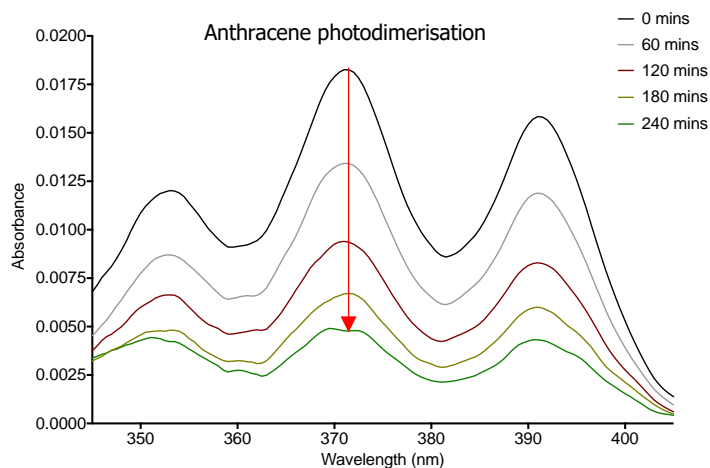
Figure 3.9 *Overlaid absorbance spectra over four hours, 340 nm – 410 nm region of the M3 aptamer at a concentration of 2 µM aptamer in TBA buffer, at room temperature (RT).*
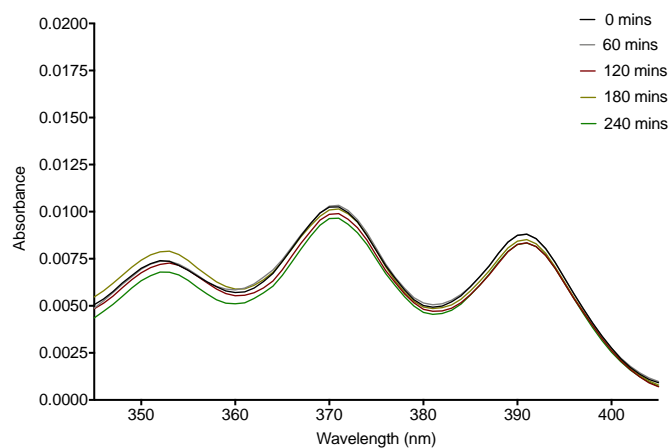
Figure 3.10 *Overlaid absorbance spectra over four hours, 340 nm – 410 nm region of the M4 aptamer at a concentration of 2 µM aptamer in TBA buffer, at room temperature (RT).*

3.6.3 Characterisation of the strands

The function of the unmodified TBA is inherently linked to the maintenance of a 3D structure stabilised by a number of non-covalent interactions. Even minor perturbations of this structure can lead to a reduction, or even a complete loss of binding activity. In this study it was hoped that the substitution of the two undimerised anthracenes into the TBA sequence would produce a minimal disturbance of the structure and hence the function of the TBA. By contrast, it was hoped that the photodimerisation of the two anthracene residues would perturb the M3 structure enough to affect binding to thrombin. In the following sections, the binding properties of the modified TBA to thrombin are explored.

3.6.3.1 DNA:protein binding studies

A common method used to determine whether an aptamer is binding to a protein is an electromobility shift assay (EMSA) (**Chapter 2**).[45] The successful formation of a complex between the modified TBA and thrombin should reduce its rate of migration down the gel and as the concentration of thrombin increases across the gel there should be a titration effect whereby an increase in concentration of native TBA should be seen at the top of the gel. The results in **Figure 3.11** shows that as you increase the concentration of thrombin from 0 to 2.5 µM the binding of native-TBA increases, demonstrated by the appearance of DNA bands at the equivalent point as the thrombin on the gels. The un-photodimerised aptamer (**Figure 3.12**) demonstrated thrombin binding according to that of native-TBA, which shows that the open form of M3 is still is still able to bind thrombin. However, the open form of M3 bound less strongly to thrombin than native TBA until the thrombin concentration was at 2.5 µM, where a similar binding intensity is seen. Conversely, a photodimerised sample of M3 did not show any significant bandshift on the EMSA in the presence of thrombin (**Figure 3.13**). This provides the evidence that the photodimerised M3 strand is unable to bind thrombin under these conditions. The process of photodimerisation of the two spatially separated anthracene units must result in sufficient distortion to the G4 structure that binding to the thrombin active site is disrupted.

In contrast, EMSA studies of a sample of M4 (**Figure 3.14**), irradiated under the same conditions as those used for M3, also demonstrated similar thrombin binding characteristics to those of

native TBA, as expected. However, M4 does not bind as strongly to thrombin as native TBA but showed improved binding between 1-2 µM concentrations of thrombin than the open form of M3. The results indicated that the anthracene photodimerisation of M3 is intramolecular in nature. The concentrations of aptamer and protein used in these gel studies are presented in **Table 3.2**. The protein stain of the gels all demonstrate extra bands and this is because the thrombin sample (Helena, UK) comes as prothrombin. The bands seen in the gel are likely to be due to the different states of thrombin once it has been reconstituted and cleaved to become the active thrombin.[46] This also made determining the binding affinities of the modified aptamers difficult and although calculating the K_d values using the EMSA studies was attempted it was deemed unsuccessful and a more qualitative approach was adopted.

Table 3.2 *The concentrations of components in the EMSA in Figures 10-13.*

Well	Thrombin (µM)	Aptamer (µM)	BSA control (µM)
a	0	1.0	0
b	0.2	1.0	0
c	0.5	1.0	0
d	1	1.0	0
e	1.5	1.0	0
f	2	1.0	0
g	2.5	1.0	0
h	0	1.0	1
i	1	NS Control (1.0)	0
j	Blank	Blank	Blank
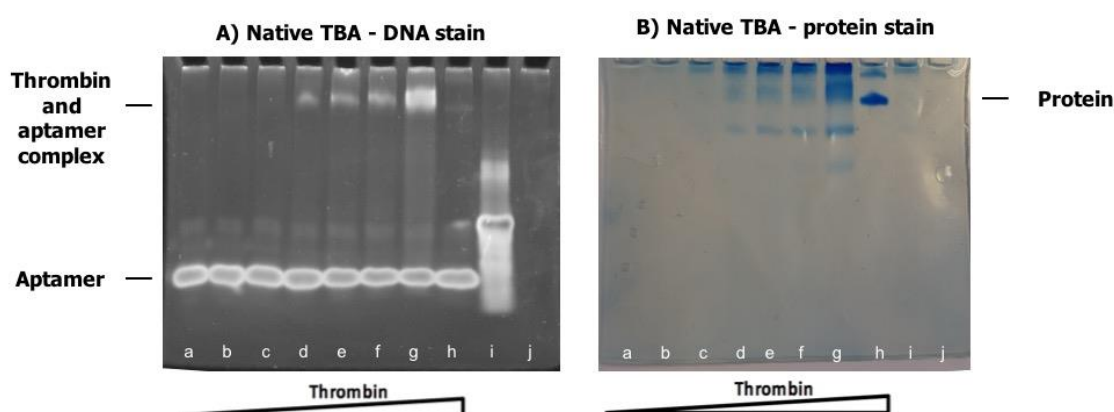
Figure 3.11 *EMSA results of the native TBA with thrombin. Gel A shows the DNA stain prior to staining for protein and Gel B shows the same gel under a protein stain. Contents of the gels can be seen in* **Table 3.2**. *All aptamers were in TBA buffer (defined earlier).*
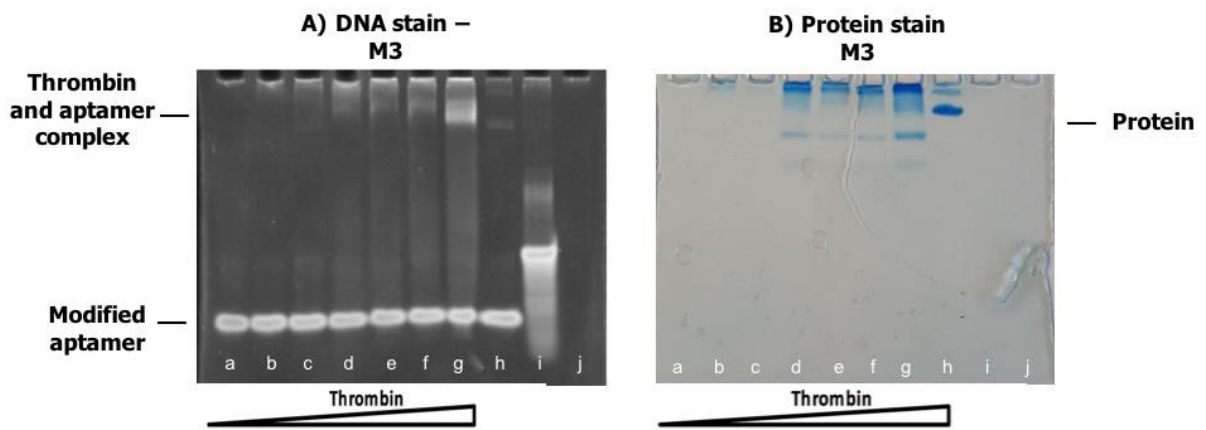
Figure 3.12 EMSA results of the un-photodimerised M3 with thrombin. Gel A shows the DNA stain prior to staining for protein and Gel B shows the same gel under a protein stain. Contents of the gels can be seen in **Table 3.2**. All aptamers were in TBA buffer.
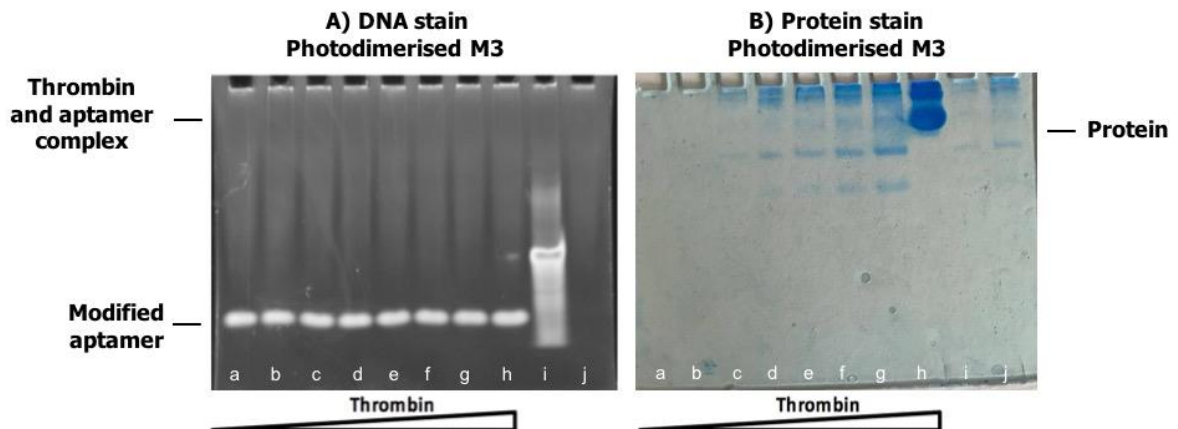
Figure 3.13 EMSA results of the photodimerised M3 with thrombin. Gel A shows the DNA stain prior to staining for protein and Gel B shows the same gel under a protein stain. Contents of the gels can be seen in **Table 3.2**. All aptamers were in TBA buffer.
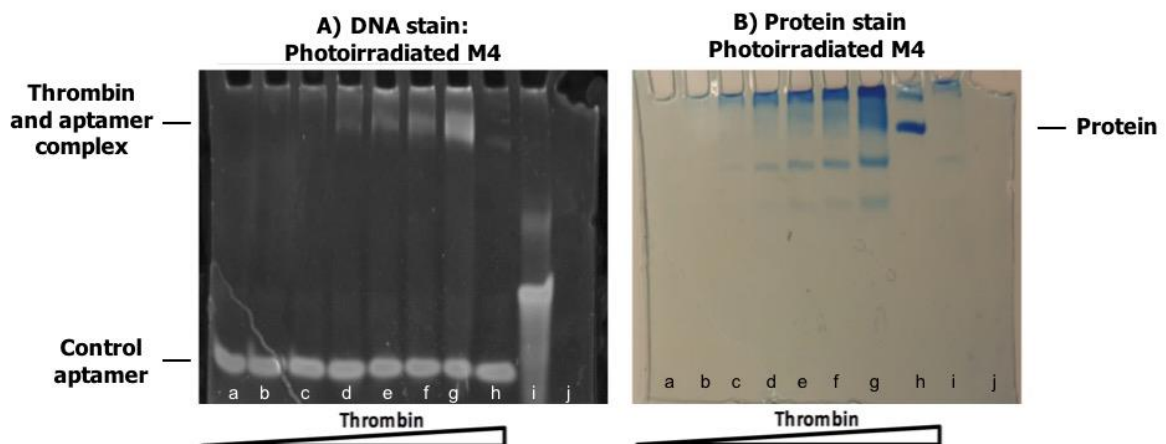
Figure 3.14 EMSA results of the photoirradiated M4 with thrombin. Gel A shows the DNA stain prior to staining for protein and Gel B shows the same gel under a protein stain. Contents of the gels can be seen in **Table 3.2**. All aptamers were in TBA buffer.

3.6.3.2 Circular dichroism studies

Circular dichroism (CD) spectra[47] were recorded to assess the extent to which the G4 tertiary structure of TBA was affected by anthracene modification and photodimer formation. Although it gave a much weaker spectrum than that of the unmodified TBA or control M4 strand, M3 showed characteristic CD signals of a G4 structure, with positive peaks at 295 nm and 245 nm and a negative peak at 265 nm (**Figure 3.15**).[48] The photodimerised sample of M3 gave an even weaker signal, with the peaks at 245 nm and 265 nm shifted to slightly higher wavelengths. Notwithstanding the presence of un-photodimerised M3 in the sample, as the photodimerisation reactions only gave 73% conversion, this data indicates that the photoadduct also possesses a tertiary (i.e. folded G4-type) structure, albeit slightly altered from its open form.
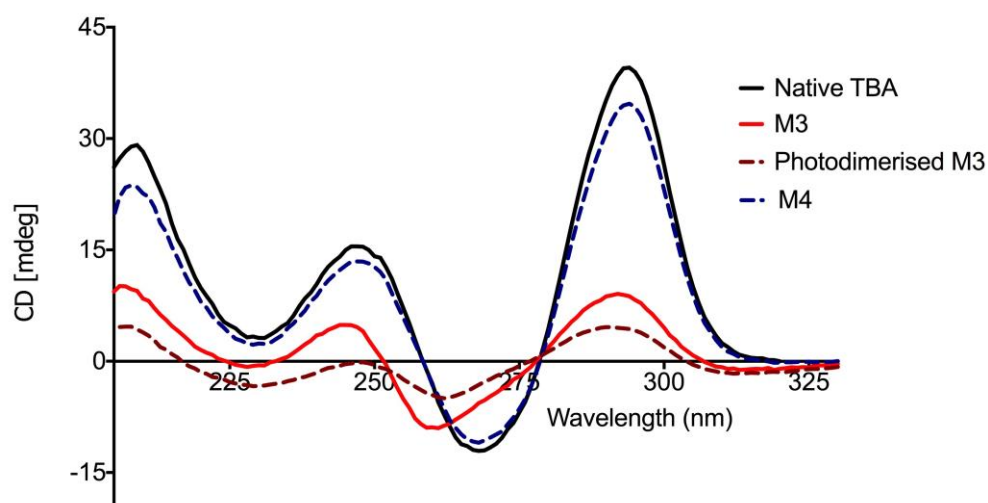
Figure 3.15 *CD results of the native TBA, the un-photodimerised M3 aptamer, the photodimerised M3 aptamer, and the M4 aptamer. All CD studies were carried out at 2 µM in TBA buffer, at RT.*

3.6.3.3 Thermal melting studies

The melting temperature (T_m) of an oligonucleotide gives information about its binding properties as well as its secondary and tertiary structures (detailed in **Chapter 2**).[49-50] In order to probe the intramolecular folding properties of these strands further, T_m values were determined using variable temperature CD (VT-CD). In each case, the data (**Figure 3.16**) showed a single co-operative unfolding transition. The T_m value of 49 °C for TBA, which was similar to the literature value,[51] was higher than that of M3 (41 °C) but lower than that of M4 (56 °C). This indicates that while the presence of one anthracene in the lower TGT loop is stabilising, an additional anthracene in the top loop is significantly destabilising (**Figure 3.15**). However, while the photoirradiated sample of M4 gave no significant change in T_m value (54 °C), the sample of M3 rose to 51 °C after photoirradiation, indicating a significant enhancement in thermal stability. This can be explained by the unfolding of the tertiary structure being hampered by the presence of the intramolecular covalent crosslinks provided by the anthracene photodimer.
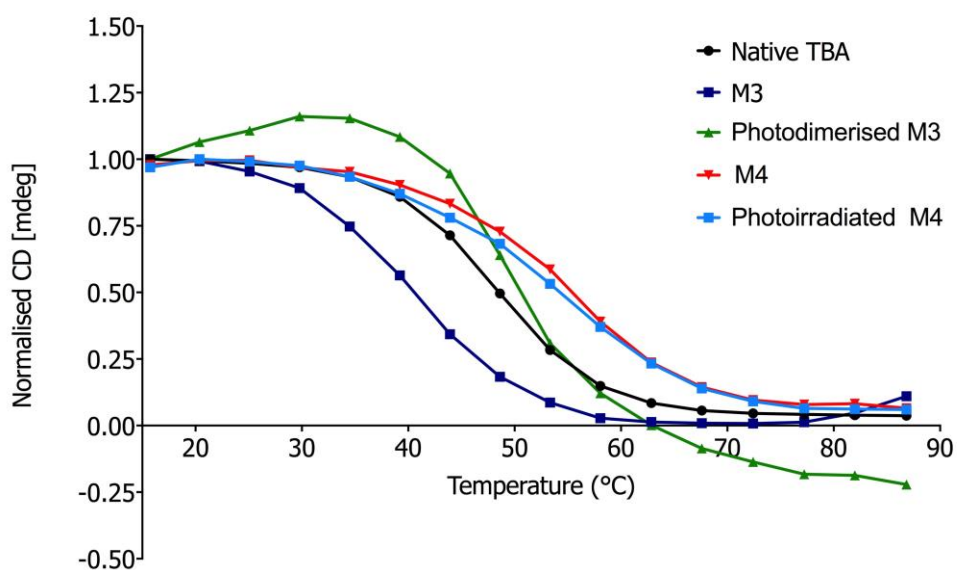
Figure 3.16 *Normalised CD melting curves at 292 nm using an aptamer concentration of 2 µM in TBA buffer.*

3.6.4 Clotting studies

The third aim of this project was to use the M3 aptamer as a photo-switchable inhibitor of blood coagulation. To achieve this, first the open form of the aptamer had to bind to the thrombin and inhibit its ability to cleave fibrinogen into fibrin (**Figure 3.17**). This research utilised the Clauss assay[52] which works by the addition of thrombin and fibrinogen, with the formation of a turbid clot then observed by monitoring the percentage decrease in UV-vis transmission, at a fixed wavelength.
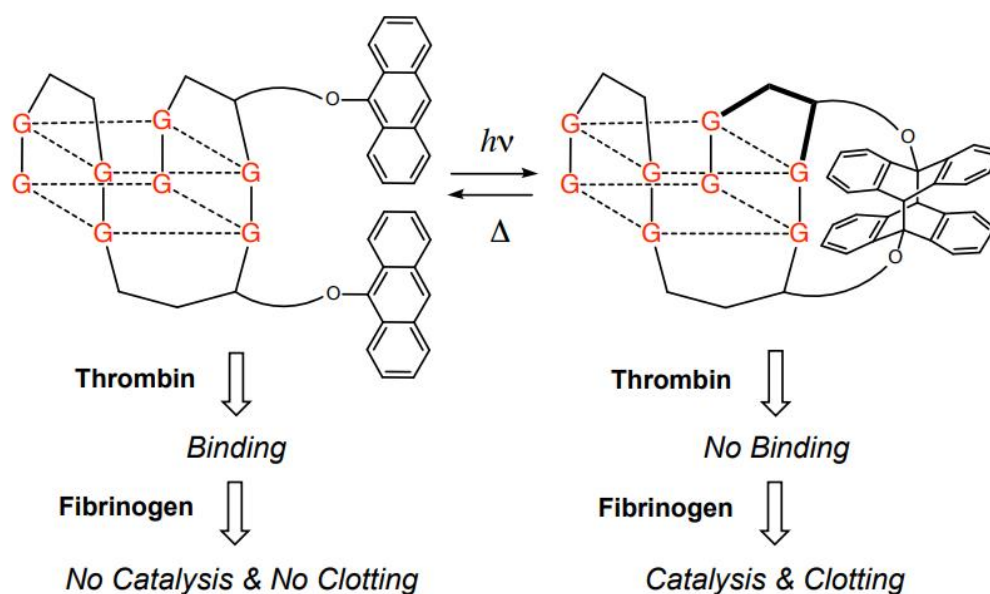
Figure 3.17 *Diagrammatic representation of anthracene photochromism in aptamer M3, forming a head-to-tail isomer. Distortion of one top TT loop, depicted in bold, prevents binding to thrombin, triggering catalysis and fibrin clot formation.*

3.6.4.1 Native-TBA clotting studies

First of all, the assay was undertaken in the presence and absence of the unmodified aptamer, native-TBA, to check that the assay was working effectively. The data showed that the presence of TBA reduced the interaction between thrombin and fibrinogen, and therefore clot formation by an average of 96% (±0.8) (**Figure 3.18**), when the decrease in UV-vis transmission of the thrombin and fibrinogen alone is taken as 100% clot formation. This observation was expected and as consistent with TBA binding to the exosite where fibrinogen would normally bind, which prevents fibrinogen:thrombin complex formation.

Thrombin	+	+
Fibrinogen	+	+
Native-TBA		+

Figure 3.18 *The results from the Clauss assay for native TBA. The graph shows the difference in % UV-vis transmission at 450 nm (40 minutes after addition of thrombin to fibrinogen). All Clauss assay experimentation involved a 1:1 ratio of thrombin to aptamer in TBA buffer (1 µM) in a 1:9 dilution of fibrinogen to Owren's buffer. Each test was done in triplicate and the error bars represent one standard deviation.*

3.6.4.2 M3 clotting studies

A similar experiment carried out with the open form of M3 showed that this modified version of TBA displays thrombin inhibition activity that is very similar to the unmodified TBA, with clot formation by inhibited by an average of 93% (±0.9) when compared to the native-TBA strand. This correlates with the EMSA data, which indicitated that binding occurs between thrombin and un-photodimerised M3. This gives further evidence tha the addition of anthracene groups to the TBA backbone has a negligible effect on its anti-thrombotic activity. The next step was to investigate whether the photodimerisation of the two anthracenes in M3 would reduce thrombin inhibitory activity. Data in **Figure 3.19** shows that a solution of photodimerised M3 was indeed much less effective at preventing clotting, with a reduction in signal intensity that approached the amount found in the absence of aptamer.

Thrombin	+	+	+	+
Fibrinogen	+	+	+	+
Native-TBA		+		
M3			+	
Photodimerised M3				+

Figure 3.19 *The results from the Clauss assay for the M3. The graph shows the difference in % UV-vis transmission at 450 nm (40 minutes after addition of thrombin to fibrinogen). All Clauss assay experimentation involved a 1:1 ratio of thrombin to aptamer in TBA buffer (1 μM) and a 1:9 dilution of fibrinogen to Owren's buffer. Each test was done in triplicate and the error bars represent one standard deviation.*

3.6.4.3 Clotting studies with M4

The assay was then repeated in the presence of the control strand M4. This modified aptamer also demonstrated similar thrombin inhibition activity to that of native TBA and un-photodimerised M3 (**Figure 3.20**). As the formation of a clot was inhibited it was concluded that the M4 strand could still bind to the thrombin (at 90% (±2.1) inhibition for M4 and 93% (±0.219) for the photoirradiated M4 inhibitory activity). Importantly, the irradiated sample also showed the same behaviour, supporting the gel studies which indicated the same binding profile after photo-irradiation.

Thrombin	+	+	+	+
Fibrinogen	+	+	+	+
Native-TBA		+		
M4			+	
Photoirradiated M4				+
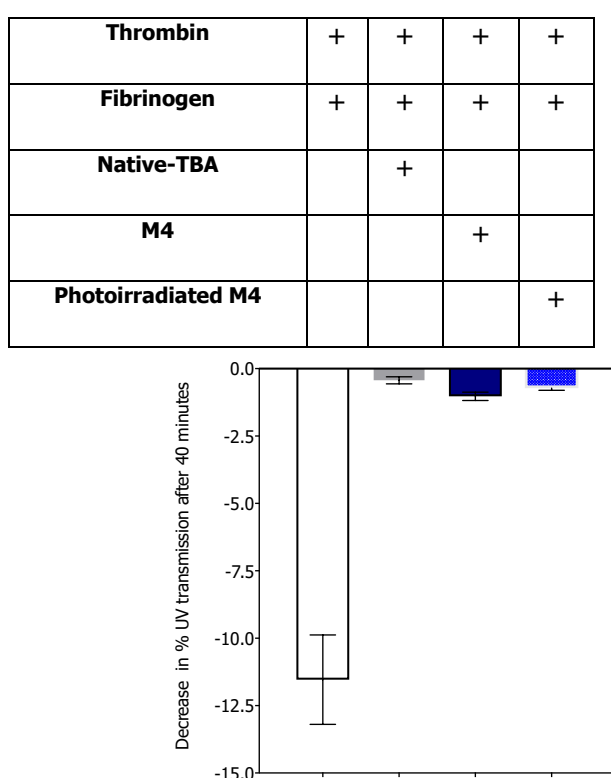
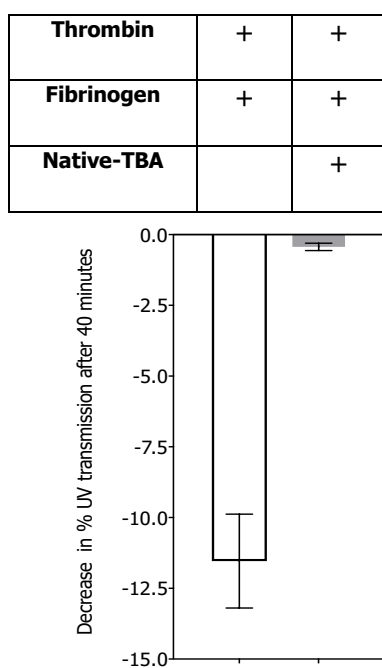**Figure 3.20** *The results from the Clauss assay for the M4. The graph shows the difference in % UV-vis transmission at 450 nm (40 minutes after addition of thrombin to fibrinogen). All Clauss assay experimentation involved a 1:1 ratio of thrombin to aptamer in TBA buffer (1 μM) and a 1:9 dilution of fibrinogen to Owren's buffer. Each test was done in triplicate and the error bars represent one standard deviation.*

3.6.5 Heat reversion studies

To determine whether the photo-triggered effect observed with the M3 aptamer was reversible, the photodimerised sample was heated to 80 °C. After this time, the solution was allowed to cool in order to allow the aptamer secondary structure to reform. The characteristic anthracene bands reappeared on the UV-vis spectrum to give a 60% return after 12 hours of heating (**Figure 3.21**).
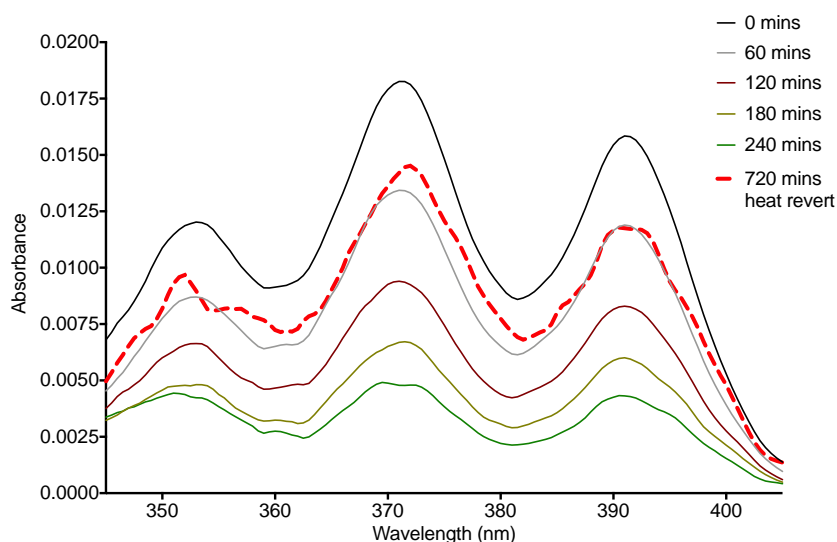
Figure 3.21 *UV-vis absorbance monitoring result of the heat reverted M3 aptamer that had been photoirradiated for 360 minutes and subsequent reversion of the anthracene signal after 12 hour (720 minute) heat exposure at 80 °C. All aptamer samples were in TBA buffer, at RT.*

CD signal studies on the photodimerised, un-photodimerised and the heat reverted M3 strands (**Figure 3.22**) showed that heat reverted strand more closely resembled the original M3, albeit with some additional signals indicating some possible degradation of the aptamer.
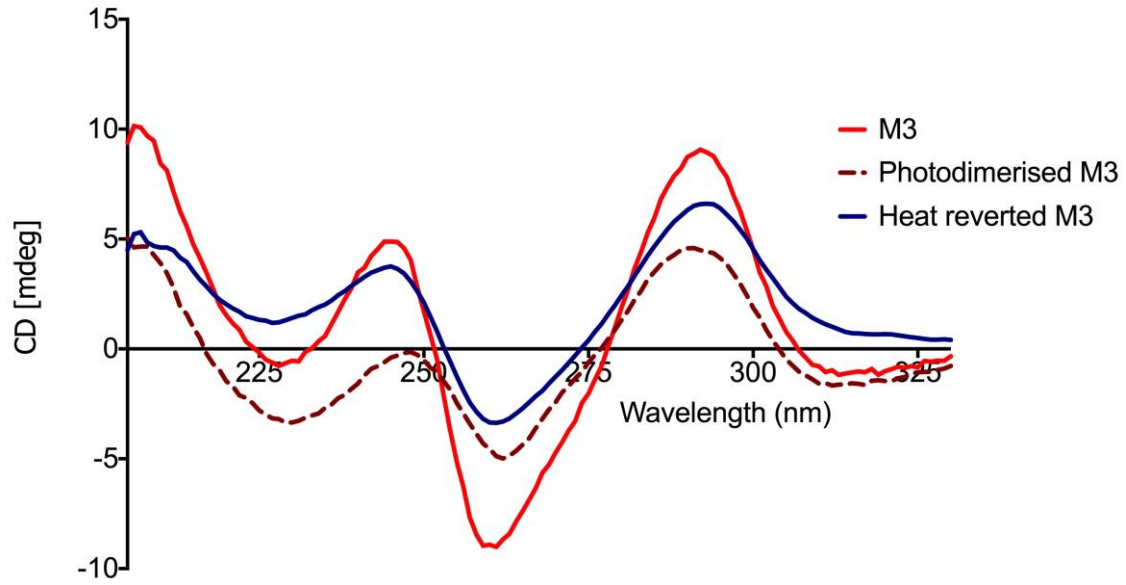
Figure 3.22 *CD results of the native TBA, the un-photodimerised M3, the photodimerised M3, the M3 after 12 hours of heat reversion. All CD studies were carried out at 2 µM in TBA buffer, at RT.*

The heat reverted aptamer was also analysed on an EMSA gel (**Figure 3.23**) which demonstrated that thrombin binding was again occurring. The concentrations of aptamer and protein used in these gel studies seen in **Figure 3.23** are presented in **Table 3.3**.

Table 3.3 *The concentration of components in the each well of the EMSA in* **Figure 3.20**.

Well	Thrombin (µM)	Aptamer (µM)
a	0	1.0
b	0.2	1.0
c	0.5	1.0
d	1	1.0
e	1.5	1.0
f	2	1.0
g	2.5	1.0
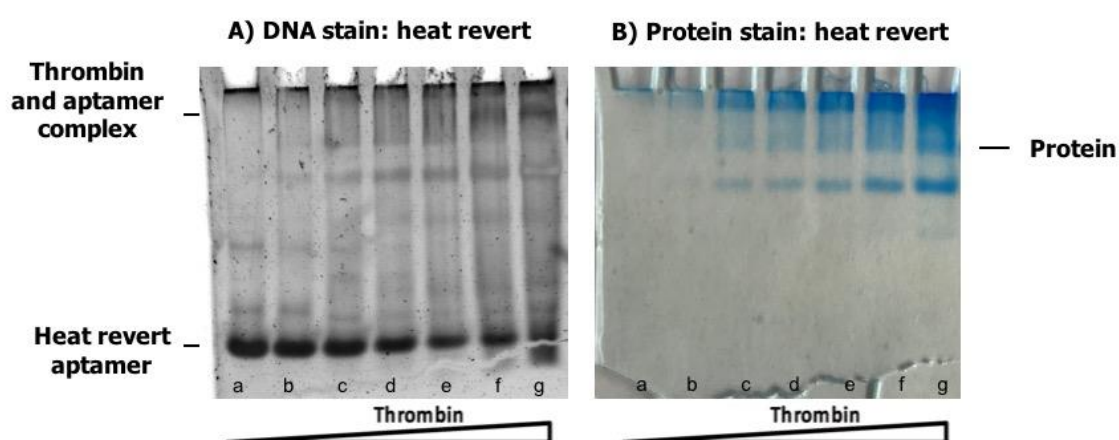
Figure 3.23 *EMSA results of the heat reverted M3 with thrombin. EMSA results of the un-photodimerised M3 with thrombin. Gel A shows the DNA stain prior to staining for protein and Gel B shows the same gel under a protein stain. Contents of the gels can be seen in* **Table 3.3**. *All aptamers were in TBA buffer.*

Finally the heat reverted sample was tested for thrombin inhibitory activity and much of the inhibitory activity of M3 could be restored, with the level of clotting product lowered to 21% (±2.7) (**Figure 3.24**), when the decrease in UV-vis transmission of the thrombin and fibrinogen alone is taken as 100% clot formation.. This data therefore consolidates the evidence that the heat reverted sample has regained some of its TBA-like properties in terms of structure and binding profile.

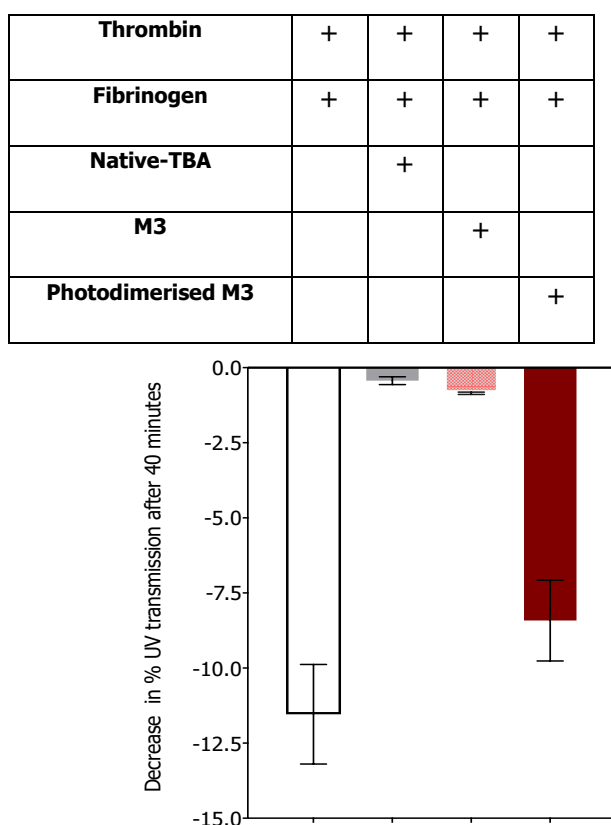| Thrombin	+	+	+	+	+
Fibrinogen	+	+	+	+	+
Native-TBA		+			
M3			+		
Photodimerised M3- TBA				+	
Heat reverted M3					+
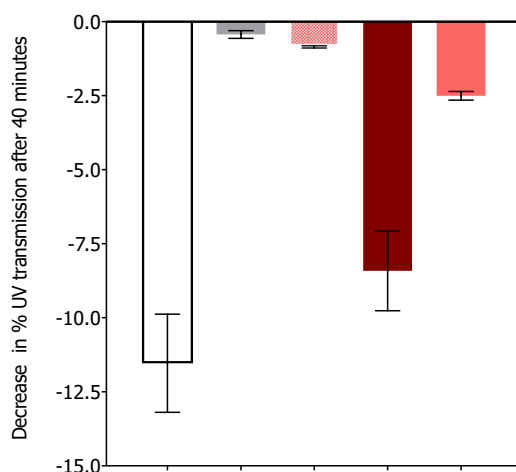
Figure 3.24 *The results from the Clauss assay for the heat reverted M3. The graph shows the difference in % UV-vis transmission at 450 nm (40 minutes after addition of thrombin to fibrinogen). All Clauss assay experimentation involved a 1:1 ratio of thrombin to aptamer in TBA buffer (1 µM) and a 1:9 dilution of fibrinogen to Owren's buffer. Each test was done in triplicate and the error bars represent one standard deviation.*

3.7 Conclusions

In conclusion, this work has demonstrated that a TBA modified with a photochromic anthracene system enables photo-control of thrombin-based clotting activity. This is brought about by intramolecular structural changes by anthracene photodimerisation that prevents its binding of thrombin and enables it to catalyse fibrinogen formation. While being relevant to the development of smart anticoagulation therapies, such an approach also has the potential to be applied more widely to other photocontrollable pharmacological processes.

3.8 Future Work

Due to the amount of sample, it was not possible to undertake a fuller study whereby the M3 sample undergoes more than one photodimerisation and heat reversion cycle. Future work would involve carrying out several light and heat reversion cycles to establish the fatigue properties of the system.

Although it was briefly attempted, photodimerisation studies could not be carried out in the presence of thrombin to assess whether photodimerisation could cause release of the bound aptamer. This was because the absorbance band of the protein masked the anthracene signals.

Future work could involve the modification of this or other aptamers with anthracene photochromic groups in order to establish whether in-situ, and reversible, light-triggered release of biological molecules would be possible.

3.9 References

1. Ecker, D. M.; Jones, S. D.; Levine, H. L., The therapeutic monoclonal antibody market. *MAbs* **2015,** *7*, pp. 9-14.

2. Beharry, A. A.; Woolley, G. A., Azobenzene photoswitches for biomolecules. *Chemical Society Reviews* **2011,** *40*, pp. 4422-4437.

3. Dunbar, W. B.; Wilson, N. A.; Schaeffer, J.; Klavins, E.; Bishop, J.; Tanner, B. C. W. In *Dynamics and control of biomolecules: Research venues and opportunities*, 2007 46th IEEE Conference on Decision and Control **2007**; pp. 3297-3307.

4. Travers, A., DNA-binding proteins. In *Encyclopedia of Genetics*, Brenner, S.; Miller, J. H., Eds. Academic Press: **2001**; pp. 541-544.

5. Song, K.; Lee, S.; Ban, C., Aptamers and their biological applications. *Sensors (Basel, Switzerland)* **2012,** *12*, pp. 612-631.

6. Van Damme, J.; Du Prez, F., Anthracene-containing polymers toward high-end applications. *Progress in Polymer Science* **2018,** *82*, pp. 92-119.

7. Manchester, J.; Bassani, D. M.; Duprey, J. H. A.; Giordano, L.; Vyle, J. S.; Zhao, Z. Y.; Tucker, J. H. R., Photocontrolled binding and binding-controlled photochromism within anthracene-modified DNA. *J Am Chem Soc* **2012,** *134*, pp. 10791-4.

8. Breton, G. W.; Vang, X., Photodimerization of Anthracene. *Journal of Chemical Education* **1998,** *75*, pp. 81.

9. Koo, B.; Nofen, E.; Chattopadhyay, A.; Dai, L., Dimeric anthracene-based mechanophore for damage precursor detection in epoxy-based thermoset polymer matrix: Characterization and atomistic modeling. *Computational Materials Science* **2017,** *133*, pp. 167-174.

10. Baysak, E.; Durmaz, H.; Tunca, U.; Hizal, G., Synthesis of Activated Ester Functional Polyesters through Light-Induced [4+4] Cycloaddition Polymerization. *Macromolecular Chemistry and Physics* **2017,** *218*, pp. 1600572.

11. Ozguc Onal, C.; Nugay, T., UV induced reversible chain extension of 1-(2-anthryl)-1-phenylethylene functionalized polyisobutylene. *Designed Monomers and Polymers* **2017,** *20*, pp. 514-523.

12. Beyeler, A.; Belser, P.; Cola, L. D., Rhenium Complexes with a Photochemically Variable Anthracene Subunit: A Molecular Switch. *Angewandte Chemie International Edition in English* **1997,** *36*, pp. 2779-2781.

13. Jin, T., Photocontrol of Na transport across a phospholipid bilayer containing a bisanthroylcalix[4]arene carrier. *Chemical Communications* **2000,** *15*, pp. 1379-1380.

14. Bullen, G. A.; Tucker, J. H.; Peacock, A. F., Exploiting anthracene photodimerization within peptides: light induced sequence-selective DNA binding. *Chemical communications* **2015,** *51*, pp. 8130-3.

15. Ihara, T.; Fujii, T.; Mukae, M.; Kitamura, Y.; Jyo, A., Photochemical ligation of DNA conjugates through anthracene cyclodimer formation and its fidelity to the template sequences. *J Am Chem Soc* **2004,** *126*, pp. 8880-1.

16. Reese, C. B., Oligo- and poly-nucleotides: 50 years of chemical synthesis. *Organic & Biomolecular Chemistry* **2005,** *3*, pp. 3851.

17. Kosuri, S.; Church, G. M., Large-scale de novo DNA synthesis- technologies and applications. *Nature Methods: Focus on Synthetic Biology* **2014,** *11*, pp. 499-507.

18. Bouas-Laurent, H.; Desvergne, J.; Castellan, A.; Lapouyade, R., Photodimerization of anthracenes in fluid solutions: (part 2) mechanistic aspects of the photocycloaddition and of the photochemical and thermal cleavage. *Chemical Society Reviews* **2001,** *30*, pp. 248-263.

19. Manchester, J.; Bassani, D. M.; Duprey, J. H. A.; Giordano, L.; Vyle, J. S.; Zhao, Z.; Tucker, J. H. R., Photocontrolled binding and binding-controlled photochromism within anthracene-modified DNA. *Journal of the American Chemical Society* **2012,** *134*, pp. 10791-10794.

20. Macaya, R. F.; Schultze, P.; Smith, F. W.; Roe, J. A.; Feigon, J., Thrombin-binding DNA aptamer forms a unimolecular quadruplex structure in solution. *Proceedings of the National Academy of Sciences of the United States of America* **1993,** *90*, pp.3745-3749.

21. Deng, B.; Lin, Y.; Wang, C.; Li, F.; Wang, Z.; Zhang, H.; Li, X.-F.; Le, X. C., Aptamer binding assays for proteins: The thrombin example—A review. *Analytica Chimica Acta* **2014,** *837*, 1-15.

22. Davie, E. W.; Fujikawa, K.; Kisiel, W., The coagulation cascade: initiation, maintenance, and regulation. *Biochemistry* **1991,** *30*, pp. 10363-10370.

23. Bode, W., Structure and interaction modes of thrombin. *Blood Cells Mol Dis* **2006,** *36* (2), 122-30.

24. Coughlin, S. R., Protease-activated receptors in hemostasis, thrombosis and vascular biology. *Journal of Thrombosis and Haemostasis* **2005,** *3*, pp. 1800-14.

25. Chen, Q.; Lord, S. T.; Lentz, B. R., Construction, properties and specific fluorescent labeling of a bovine prothrombin mutant engineered with a free C-terminal cysteine. *Protein Eng* **1996,** *9*, pp. 545-553.

26. Bode, W.; Mayr, I.; Baumann, U.; Huber, R.; Stone, S. R.; Hofsteenge, J., The refined 1.9 A crystal structure of human alpha-thrombin: interaction with D-Phe-Pro-Arg chloromethylketone and significance of the Tyr-Pro-Pro-Trp insertion segment. *Embo j* **1989,** *8*, pp. 3467-75.

27. Bock, L. C.; Griffin, L. C.; Latham, J. A.; Vermaas, E. H.; Toole, J. J., Selection of single-stranded DNA molecules that bind and inhibit human thrombin. *Nature* **1992,** *355*, pp. 564.

28. Burge, S.; Parkinson, G. N.; Hazel, P.; Todd, A. K.; Neidle, S., Quadruplex DNA: sequence, topology and structure. *Nucleic Acids Res* **2006,** *34*, pp. 5402-15.

29. Nagatoishi, S.; Nojima, T.; Galezowska, E.; Juskowiak, B.; Takenaka, S., G quadruplex-based FRET probes with the thrombin-binding aptamer (TBA) sequence designed for the efficient fluorometric detection of the potassium ion. *Chembiochem* **2006,** *7*, pp. 1730-7.

30. Phan, A. T., Human telomeric G-quadruplex: structures of DNA and RNA sequences. *FEBS J* **2010,** *277*, pp. 1107-17.

31. Lipps, H. J.; Rhodes, D., G-quadruplex structures: in vivo evidence and function. *Trends in Cell Biology* **2009,** *19*, pp. 414-422.

32. Jing, N.; Zhu, Q.; Yuan, P.; Li, Y.; Mao, L.; Tweardy, D. J., Targeting signal transducer and activator of transcription 3 with G-quartet oligonucleotides: a potential novel therapy for head and neck cancer. *Mol Cancer Ther* **2006,** *5*, pp. 279-86.

33. Kelly, J. A.; Feigon, J.; Yeates, T. O., Reconciliation of the X-ray and NMR structures of the thrombin-binding aptamer d(GGTTGGTGTGGTTGG). *J Mol Biol* **1996,** *256* (3), 417-22.

34. Diculescu, V. C.; Chiorcea-Paquim, A.; Eritja, R.; Oliveira-Brett, A. M., Thrombin-binding aptamer quadruplex formation: AFM and voltammetric characterization. *Journal of Nucleic Acids* **2010,** *2010*, pp. 8.

35. Proske, D.; Blank, M.; Buhmann, R.; Resch, A., Aptamers—basic research, drug development, and clinical applications. *Applied Microbiology and Biotechnology* **2005,** *69*, pp. 367-374.

36. Krauss, I. R.; Merlino, A.; Giancola, C.; Randazzo, A.; Mazzarella, L.; Sica, F., Thrombin–aptamer recognition: a revealed ambiguity. *Nucleic Acids Research* **2011,** *39*, pp. 7858-7867.

37. Krauss, I. R.; Merlino, A.; Randazzo, A.; Novellino, E.; Mazzarella, L.; Sica, F., High-resolution structures of two complexes between thrombin and thrombin-binding aptamer shed light on the role of cations in the aptamer inhibitory activity. *Nucleic Acids Research* **2012,** *40*, pp. 8119-8128.

38. Paborsky, L. R.; McCurdy, S. N.; Griffin, L. C.; Toole, J. J.; Leung, L. L., The single-stranded DNA aptamer-binding site of human thrombin. *Journal of Biological Chemistry* **1993,** *268*, pp. 20808-20811.

39. Griffin, L. C.; Tidmarsh, G. F.; Bock, L. C.; Toole, J. J.; Leung, L. L., In vivo anticoagulant properties of a novel nucleotide-based thrombin inhibitor and demonstration of regional anticoagulation in extracorporeal circuits. *Blood* **1993,** *81*, pp. 3271-6.

40. Licari, L. G.; Kovacic, J. P., Thrombin physiology and pathophysiology. *Journal of Veterinary Emergency and Critical Care* **2009,** *19*, pp. 11-22.

41. Weinberger, J., Adverse effects and drug interactions of antithrombotic agents used in prevention of ischaemic stroke. *Drugs* **2005,** *65*, pp. 461-71.

42. Engelhard, D. M.; Nowack, J.; Clever, G. H., Copper-Induced Topology Switching and Thrombin Inhibition with Telomeric DNA G-Quadruplexes. *Angewandte Chemie (International ed. in English)* **2017,** *56*, pp. 11640-11644.

43. Mo, M.; Kong, D.; Ji, H.; Lin, D.; Tang, X.; Yang, Z.; He, Y.; Wu, L., Reversible Photocontrol of Thrombin Activity by Replacing Loops of Thrombin Binding Aptamer using Azobenzene Derivatives. *Bioconjugate Chemistry* **2019,** *30*, pp. 231-241.

44. Duprey, J. H. A. Studies on anthracene tagged oligonucleotides. Thesis. University of Birmingham, **2010**.

45. Hellman, L. M.; Fried, M. G., Electrophoretic mobility shift assay (EMSA) for detecting protein-nucleic acid interactions. *Nature Protocols* **2007,** *2*, pp. 1849-1861.

46. Chen, Q.; Lord, S. T.; Lentz, B. R., Construction, properties and specific fluorescent labeling of a bovine prothrombin mutant engineered with a free C-terminal cysteine. *Protein Engineering, Design and Selection* **1996,** *9*, pp. 545-553.

47. Woody, R. W., Circular dichroism. In *Methods in enzymology*, Academic Press: **1995**; Vol. 246, pp. 34-71.

48. Kelly, S. M.; Jess, T. J.; Price, N. C., How to study proteins by circular dichroism. *Biochim Biophys Acta* **2005,** *1751*, pp. 119-39.

49. von Hippel, P. H.; McGhee, J. D., DNA-Protein Interactions. *Annual Review of Biochemistry* **1972,** *41*, pp. 231-300.

50. Reese, E.; Krishnan, V. V., Classification of DNA sequences based on thermal melting profiles. *Bioinformation* **2010,** *4*, pp. 463-467.

51. Kankia, B. I.; Marky, L. A., Folding of the thrombin aptamer into a G-quadruplex with Sr(2+): stability, heat, and hydration. *Journal of American Chemical Society* **2001,** *123*, pp. 10799-804.

52. Clauss, A., Rapid physiological coagulation method in determination of fibrinogen. *Acta Haematologica* **1957,** *17*, pp. 237-46.

Chapter 4 – BRAF detection system

4.1 Introduction

Research on the human genome has resulted in many advances in the way scientists understand, diagnose and treat disease, and the development of oligonucleotide-based diagnostics has revolutionised the way disease and infection are detected (**Chapter 1**). The term "molecular marker" encompasses fragments of the genome that can be studied to identify certain characteristics about a particular individual. One key molecular marker can be a base at a single locus within the genome: a change at such a base is considered to be a single nucleotide polymorphism (SNP) if the frequency of the least recurrent allele is 1% or greater.[1] Point variants can be inherited or be a result of somatic mutations that leads to two different base types within genomes. Any mutations that have occurred as a result of external stimuli, but can now be passed on during cell division, are known as somatic mutations. The base changes/mutations can be purine-purine (adenine (A) <-> guanine (G)) or pyrimidine-pyrimidine (cytosine (C) <-> thymine (T)) transitions and they are called a transversion when the change is from a purine to a pyrimidine or a pyrimidine to a purine (A <-> C, A <-> T, G <-> C, G <-> T).[2] Despite the definition given above, there is an ongoing debate about the definition of SNPs.[3] For this reason, all the base changes in this introduction will be referred to as point variations rather than mutations or SNPs, but whatever they are named, the methods to detect them are the same.

A point variation within an individual's chromosomes can either be homozygous or heterozygous for the base. If an individual is homozygous only one type of base pair will be present at this position. However, if it is heterozygous, then two different base-pairs will be present (**Figure 4.1**).
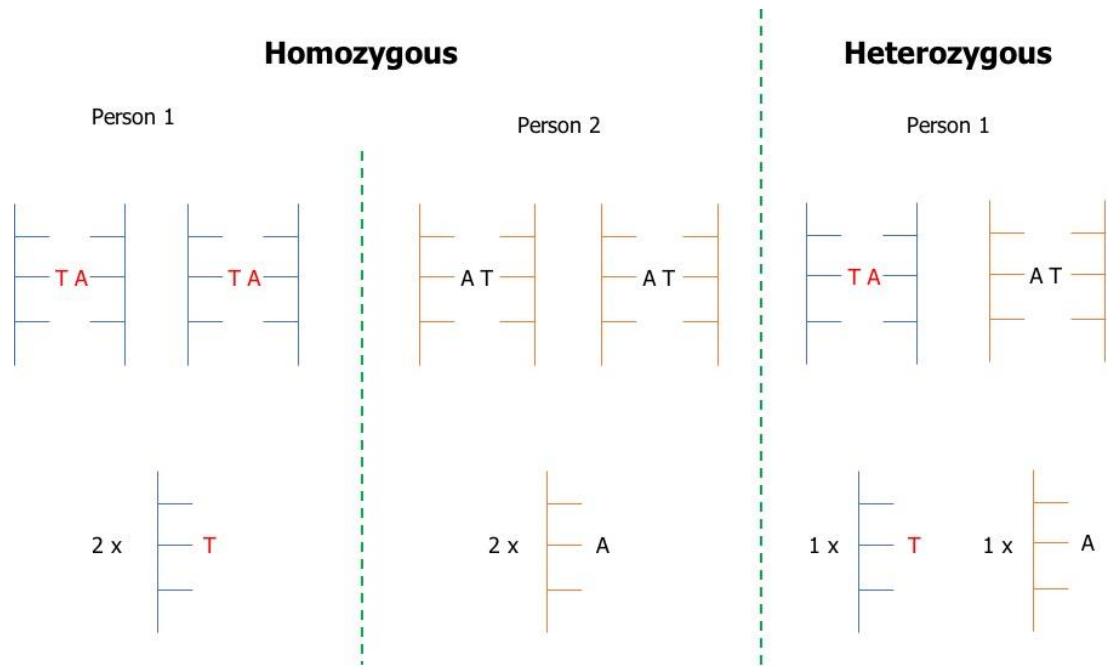
Figure 4.1 *A diagrammatic representation of homozygous vs heterozygous point variation sites in pairs of chromosomes. The individual will either have one base pair variant on both chromosomes (homozygous) or they will have two base pair variants, one on each chromosome, making them heterozygous.*

For example, the BRAF mutation, focused on within this chapter, is as a result of a point variation from a T to an A base. This somatic mutation, implicated in certain cancers, is homozygous for the wild-type (WT) (i.e. T-A, T-A) and heterozygous for the cancerous form (T-A, A-T). However, the heterogeneity of a single stranded DNA (ssDNA) sample from a patient with cancer originally from a BRAF mutation (**Figure 4.1**) might not be a simple 50% A and 50% T mix. The ratio is dependent upon the somatic mixture that occurs as a tumour develops. In other words, the ratio of T:A in the DNA of the local cell population will change as more WT DNA is converted to mutant DNA and as a result certain areas within the tumour will contain the A mutation and some areas will not.[4]

Point variations across the genome can result in amino acid changes in proteins that result in differences between patients in the efficacy and/or the toxicity of medicines. There is therefore a need for personalised medicine and treatment plans that aim to elucidate the differences in these effects based upon the genetic information from a patient.[5] Heterozygous point variations in the genome can be difficult to quantify and diagnose correctly and this can lead to diagnostic complexity. In the case of

BRAF, mutations can result in an increase in sensitivity of patients to inhibitor medication.[6] Therefore knowing the specific genetic ratio of the mutation can allow for a treatment plan that can lead to improved survival rates.

As detailed in the introductory **Chapter 1,** there are several commercial assays available that are used to identify point variants within a gene. The diagnostic assays currently available are useful for the detection of heterozygous alleles from the corresponding homozygous alleles (i.e. giving a binary heterozygous or homozygous answer). However, what these assays lack is the ability to quantify alleles that contain an unequal ratio of the nucleobases. Within the Tucker Group, anthracene containing oligonucleotide probes for genes containing a point variation that codes for prostate cancer have previously been designed.[7-8] In this chapter a similar probe was designed in order to detect the A to T point variation within the BRAF gene and given the issues with the commercial assays outlined above, the probe was also tested to assess whether a linear correlation could in the signal read-out could be obtained, as a measure of the heterozygous nature of the sample.

4.2 Cancer

Cancer is the second leading cause of mortality in the world and encompasses more than 277 cancerous diseases.[9] Statistics published in 2017 stated that in the United States, over 1.5 million new cancer cases and around 600,000 cancer related deaths occurred in 2017.[10] The disease occurs as a result of the uncontrollable proliferation of cells within the body, referred to as malignancy. The cause of this pathogenicity of an individual's own cells is often as a result of mutations in the genome that cause cancer cells to proliferate uncontrollably, become immortal, undergo angiogenesis, apoptosis, and finally the most lethal of cancer traits, metastasise to other parts of the body. These traits of a cancer cell are known as the hallmarks of cancer and define the difference between a normal cell and a malignant cancer cell.[11]

Cancer causing mechanisms are of a genomic nature and therefore any phenotypic changes in cells are commonly as a result of; mutation, insertion, deletion and genetic recombination of bases in DNA sequences.[12] Point variations where this has occurred then become molecular markers that can help indicate cancer formation and development.

4.2.1 BRAF gene

The Raf gene is responsible for the production of an enzyme, which is also referred to as Raf. It is a serine/threonine-protein kinase that phosphorylates signalling molecules that cause cell proliferation, survival and differentiation. For the activation of the WT form of the protein a phosphorylation event is required from another serine/threonine-protein kinase known as Ras (**Figure 4.2**). This is triggered when cell proliferation and growth is required from a growth factor outside the cell.[13] This signalling pathway involving Ras/Raf/Mek and Erk is mutated in around 30% of cancers and the Raf gene is mutated to B-raf (BRAF) in 7% of cancers.
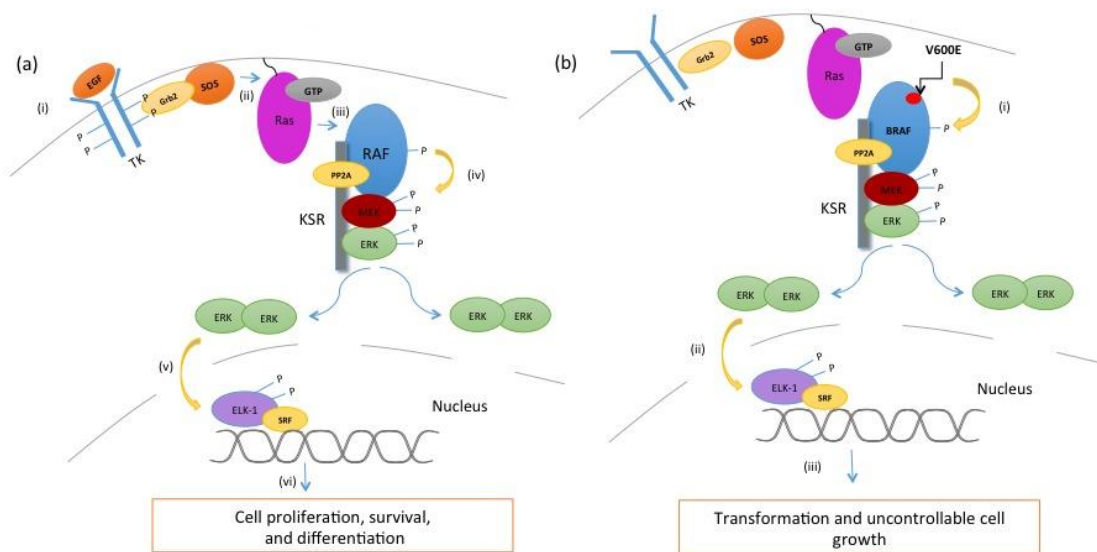
Figure 4.2 *A figure representing the signalling difference in the a) wild type form and b) mutated form of the RAF protein.*

In the mutated form of the protein, the signal is innately in the 'on' form and therefore causes phosphorylation of the signalling molecules within the pathway, leading to cell transformation and uncontrollable cell growth without external signals. The Raf to BRAF mutation involves a base substitution in exon 1799 from a T to an A base causing a change in the amino acid position of the protein from a valine (Val) to a glutamic acid (E).[13] The kinase domain of the Raf protein has two lobes that are separated by a catalytic area. When the protein is in its inactive conformation, the Glycine (Gly) 595 to Val600 area is close to the Gly463 to Val470 area. The hydrophobic interactions between these two areas result in the catalytic area being unable to be accessed by other proteins. When the activation area of the kinase is phosphorylated the hydrophobic segment becomes destabilised and the catalytic area becomes accessible. The BRAF mutation causes the replacement of the Val600 to Glutamic acid (E). Glutamic acid has a bulkier, negatively charged side chain, at pH 7, compared to the smaller hydrophobic side chain of the valine residue.[13] The hydrophobic interactions causing the catalytic pocket to remain closed are now disrupted, resulting in the protein being consistently in the active form. This

gene mutation can be responsible for cancers that include malignant melanoma (MM) and colorectal cancer.[14]

Malignant melanoma (MM) is a type of skin cancer that occurs due to the uncontrollable growth (malignancy) of melanocytes. Melanocytes are the cells, predominantly found on the skin, that are responsible for pigmentation.[15] MM, although only accounting for 1% of skin cancer[16], is the most lethal type of skin cancer and has an extremely high rate of mortality when compared with other cancers and commonly results in metastasised tumours.[14, 17] Colorectal cancer (CRC), commonly known as bowel cancer, occurs when the epithelial cells from the colon region of large intestine become malignant. CRC is the third most common type of cancer in the world and is also a prominent cause of cancer related death.[18]

The risk of CRC and MM can be environmental, genetic or a complicated combination of both.[17] Although there are many therapies available for the treatment of these cancers[19], early detection of these cancers is important to ensure the treatment required is minimal and the chance of acquiring a secondary tumour is reduced, ultimately resulting in a better chance of survival.

4.2.2 Anthracene as a fluorophore

The modification of oligonucleotides using polycyclic aromatic hydrocarbons as nucleobase replacements has been described by Ren *et al.*, using naphthalene, phenanthrene and pyrene with the view of creating biophysical probes.[20] The synthesis of modified bases that do not significantly disrupt the hybridisation of probes to their target has resulted in the advent of base discriminating probes (BDPs). BDPs contain fluorescent base replacements that can aid in identifying the bases opposite or adjacent, either in the 5'- or the 3'- direction, to them.[21] The fluorescence emission changes upon the hybridisation to the probes are monitored in order to determine what base is present.

An example of base adjacent sensing has been demonstrated by Seitz *et al.*,[22] using Peptide Nucleic Acids (PNAs) that contained a thiazole orange fluorophore. The thiazole orange acted as a nucleobase replacement sensor for point variants. Upon binding of the modified PNA strand to the target strand the thiazole orange modification (**Figure 4.3A**) intercalated with DNA and subsequently gave a high fluorescence signal. The tag showed increased fluorescence when the base adjacent was complementary, as the modification took on a more fixed coplanar organisation. When a mismatch was adjacent to the tag the fluorescence signal decreased compared to the fully matched duplex.

In the previous chapter (**Chapter 3**) the research focused on anthracene being utilised as a photochemical moiety that can undergo photodimerisation upon irradiation with UV light. This chapter focuses on the photophysical properties of anthracene. Conjugated molecules often fluoresce and anthracene, being a fully conjugated polyaromatic compound fluorescing in the wavelength region of 390-550 nm, is a perfect example of this. The fluorescence properties of anthracene have been used in sensing applications within chemistry[23], medicinal biology[7] and materials science.[24]

The Brown group had previously synthesised a thymidine base with anthracene based, anthracenylethynyl (AeT) (**Figure 4.3B**) and anthracenylbuta-1,2-diynyl (AeeT) (**Figure 4.3C**), modifications and incorporated these into oligonucleotides. The anthracene modifications were synthesised to have a linker group at the carbon 9 position using either one (AeT) or two (AeeT) ethynyl linker groups. An increase in fluorescence emission was seen when the target strands had complete

complementarity and a decrease in fluorescence emission was seen when the base opposite to the

modified thymine was a guanine.[25]

A   Thiazole orange-PNA monomer   B   10-anthracenylethynyl dT (**AeT**)   C   10-(buta-1,3-diynyl)anthracenyl dT (**AeeT**)
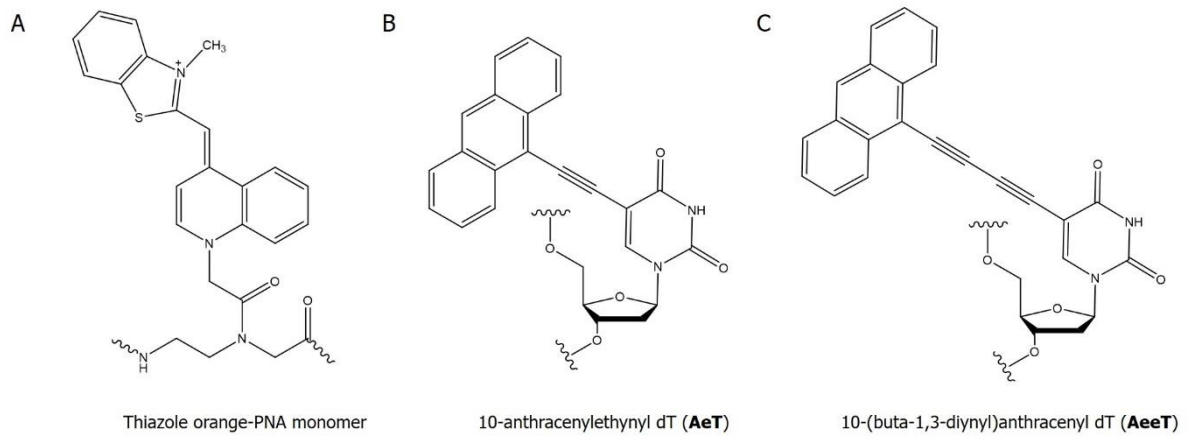
Figure 4.3 A) *The thiazole orange-PNA monomer by Seitz et al.,[22]* ***B)*** *The AeT monomer and* ***C)*** *The AeeT monomer, both reported by Brown et al.[25]*

4.2.3 Previous work

Oligonucleotides modified with anthracene have been developed within the Tucker group for similar fluorescence sensing systems based on DNA hybridisation. This sensing technology can identify different bases opposite the tag in target DNA.[8, 26-27] The anthracene fluorescence signal, normally monitored at 426 nm, either decreases or increases upon duplex formation depending on the identity of the base opposite it (**Scheme 4.1**). Differences in emission can be explained by the extent to which the anthracene can insert itself into the duplex.
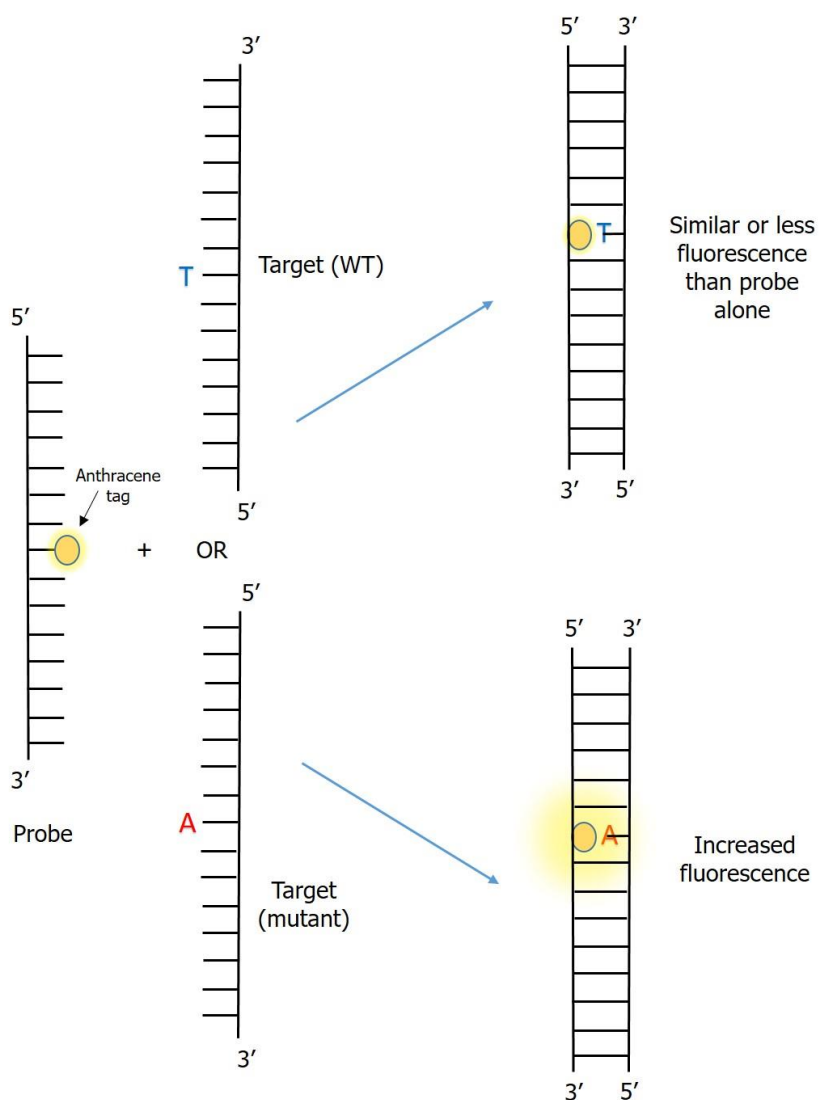
Scheme 4.1 *A schematic describing the base opposite sensing. The anthracene oligonucleotide probe binds complementary strands with a different base opposite the tag (here shown as T and A).*

4.2.3.1 Linker length and stereochemistry

The anthracene tag contains a threoninol unit (**Figure 4.4**), which functions as a linker group allowing the tag to be incorporated into the backbone of DNA as a phosphoramidite. The modification does not significantly disrupt the formation of the DNA duplex.[28]
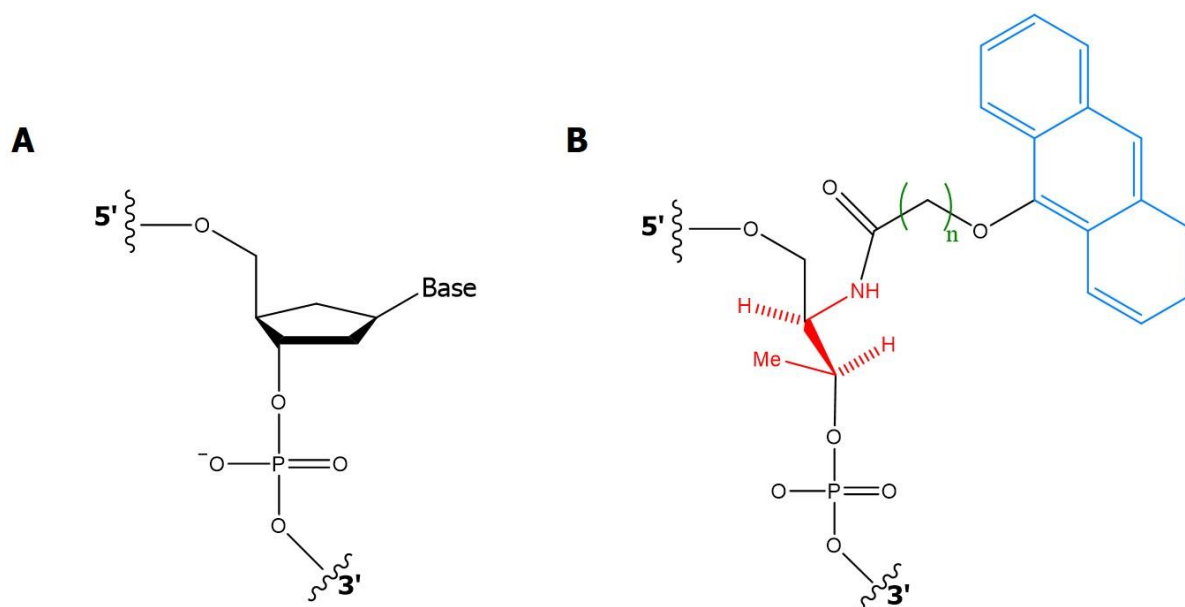
Figure 4.4 *The comparison of the natural DNA nucleotide (**A**) and the Tucker group anthracene nucleotide base mimic (**B**); in red is the threoninol unit that where the stereochemistry can be controlled between the L or D form, in green is the carbon linker chain where the carbon length (represented by n) and the anthracene can be seen in blue.*

The alkyl linker length between the peptide bond and the ether can be varied and be anything in length from 1 ($n = 1$) to 7 ($n = 7$) carbons long (apart from $n=2$). The reason for the n=2 linker length not working are currently not known. In addition, the stereochemistry of the threoninol linker (L or D isomers) can be changed and this, along with the linker length affects how the probe interacts with the targets, which consequently affects the sensing signal. The work within this chapter is based on base-opposite detection, which generally works well with longer linker lengths.[29]

4.2.3.2 Previous work

Previously within the Tucker group the optimum linker length and stereoisomer for the base opposite sensor had been established[29] and as a result the n = 5 carbon linker length with the stereochemistry L (denoted 5L) anthracene was chosen for the so-called BRAF probe. Initial studies within the Tucker Group determined that 15 base length (15-mer) synthetic targets of the BRAF gene containing either the T or A point variation opposite the tag could be detected using this probe. Its sequence is the following where the **X** represents the 5L anthracene as the 7th "base" in the 15-mer sequence:

5' - AGA TTT C**X**C TCT AGC - 3'

The target sequences, based on the SNP within the BRAF gene, are displayed in (**Figure 4.5**).

Figure 4.5 *The complementary target sequences to the BRAF probe.*

When the base opposite to the anthracene was T, the fluorescence decreased, relative to the probe alone, whereas it increased when the base was an A. Importantly, the data also showed a linear dependence on the emission as a function of allelic ratio using these 15-mer targets in combination with this BRAF probe (**Figure 4.6**).

122

This sensing technique was also able to provide fluorescence read-outs at temperatures up to the melting temperature of the duplex. This BDP approach works since the technique relies on monitoring differences in intensity of the fluorescence signal upon probe binding rather than the extent to which the probe binds to the target at a particular temperature. This eliminates the need for identifying certain temperature windows in which one target is bound and the other is not, as is the case for commercial assays such as TaqMan®.[30]
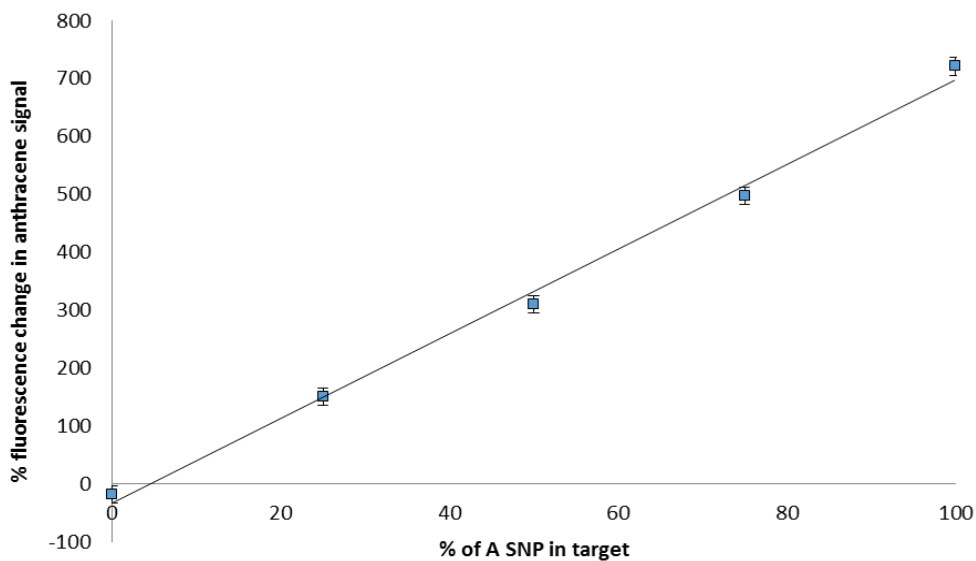
Figure 4.6 *Previous work within the group demonstrating the linear correlation plot gained from the fluorescence emission at 426 nm of the 5L BRAF probe with the 15-mer BRAF targets. All studies were carried out using 1 µM of the BRAF probe and 1 µM of the 15-mer target (the 15-mer strands were added in varying ratios of T/A). The samples were in 10 mM sodium phosphate buffer, 100 mM NaCl at pH 7. All studies were carried out at room temperature (RT). The λ_{ex} = 350 nm, room temperature (RT), λ_{em} = 426 nm, room temperature.[31]*

4.3 Project Aims

The aim of this work was to examine an oligonucleotide probe with an anthracene modification for targeting the cancer-causing T to A point variation within the BRAF gene and to begin to assess its viability for use in a clinical setting.

The primary aim of this project involved undertaking similar fluorescence emission studies to those done previously but with longer, 173 nucleobases long (173-mer), synthetic targets. These would be similar to the lengths of target seen after the amplification of genomic patient DNA using the polymerase chain reaction (PCR). PCR is required to generate enough target sample to achieve a strong enough sensing signal (**Chapter 1**). If the longer targets did hamper probe binding and emission enhancement, then probes longer than the normal 15-mer length would have to be synthesised for use with any amplified PCR products. Following this, the next step would be the production of a linear dependence plot of percentage change in emission of varying amounts of A vs T in a sample using synthetic 173-mer targets with either, the A or T mutation.

In order to further the work discussed in **Section 4.2.2** a secondary aim of this project was to determine the capabilities of the BRAF probe in distinguishing between the A and T mutation in real patient DNA samples. As described in **Figure 4.7**, the first step would be to extract the genomic DNA from both healthy tissue and cancerous patient tissue. The genomic DNA would undergo PCR in order to amplify the region containing the mutation. This PCR product would then be digested to the single strand containing the point variant to allow hybridisation with the anthracene-containing probe strand.
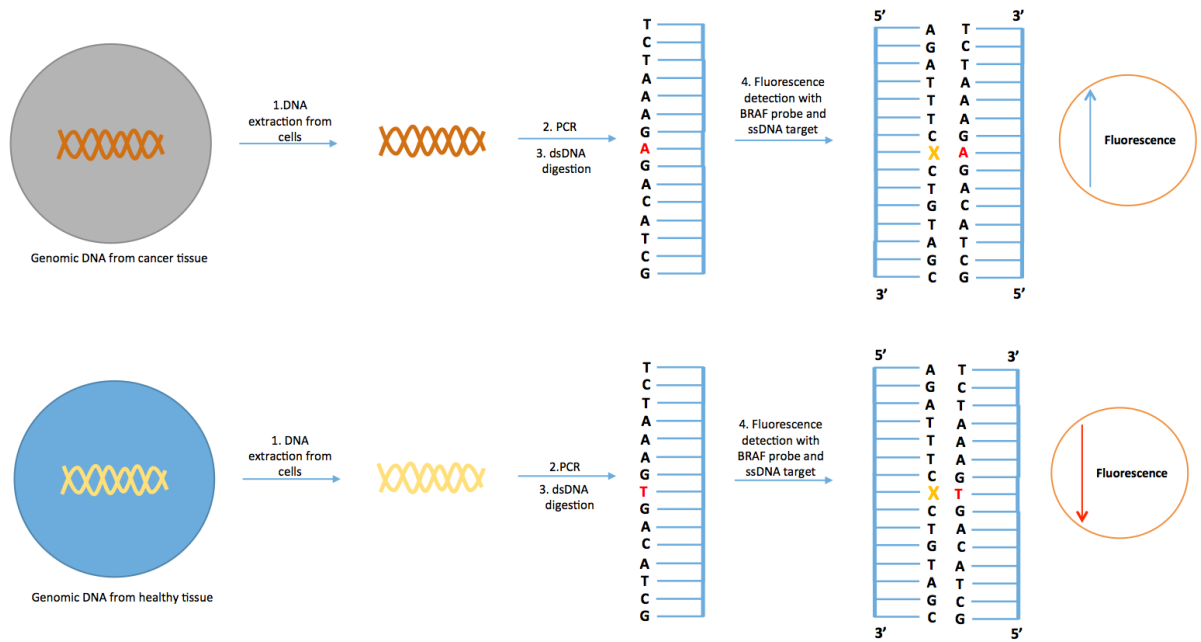
Figure 4.7 *The secondary aims within the project. 1. Involves the extraction of the DNA from the cells, 2. PCR of the genomic DNA, 3. dsDNA digestion, 4. Fluorescence studies of the PCR amplified genomic DNA with the BRAF probe.*

4.4 Results and Discussion

4.4.1 Anthracene synthesis

The anthracene oligonucleotide phosphoramidite was synthesised as per the research established by Jean-Louis Duprey within the Tucker Group and characterised by another member of the group.[29]

4.4.2 Oligonucleotide probe synthesis and characterisation

The anthracene phosphoramidite was incorporated into an oligonucleotide strand using solid phase oligonucleotide synthesis (**Chapter 2**). The 15-base target strands with the A and T point variant are referred to as 15-A and 15-T respectively. Likewise, the 173-base target strands with the A and T point variant are referred to as 173-A and 173-T respectively. The two longer synthetic targets were purchased by IDT-DNA and the sequence can be seen in **Appendix 7.2.2**.

Once the probe and the two targets had been synthesised, they were purified by reversed-phase high performance liquid chromatography (RP-HPLC) and the resulting strands characterised using negative mode electrospray ionisation (ESI) mass spectrometry. The results are presented in **Table 4.1**.

Table 4.1 *The three oligonucleotides synthesised using solid-phase synthesis during this project and their percentage purity and observed mass. The X represents the anthracene modification.*

Strand	Sequence (5' → 3')	Expected Mass	Observed mass	% purity
BRAF probe	AGA TTT C**X**C TCT AGC	4711.3	4710.70	98.053
15-T	GCT ACA G**T**G AAA TCT	4576	4575.8	100
15-A	GCT ACA G**A**G AAA TCT	4585.1	4585.9	100

4.4.2.1 Thermal melt data

Duplex formation between the BRAF probe and the 15-mer and 173-mer targets was monitored using variable temperature ultraviolet visible (UV-vis) spectroscopy (**Chapter 2**). The resulting melting data (**Table 4.2**) showed that duplexes with both the 15-mer and 173-mer targets had very similar thermal stabilities. This was consistent with the results obtained previously within the Tucker group showing that varying the base opposite the 5L anthracene tag has little effect on duplex stability.[29] This is in contrast to work with probes that target base adjacent changes.[21] This can be explained by the system here not going from a match to a mismatch, so there are no changes in the number of base pairs present, resulting in similar stabilities of the duplexes. Using a T_m prediction tool[32] the predicted T_m of the unmodified, fully complementary, probe was 50 °C. As expected, this was slightly higher than the results for the modified duplexes due to the extra H-bonding between the base present in the unmodified system.

Table 4.2 *The thermal melting temperatures of the BRAF probes hybridised with the the 15-mer or 173-mer targets. The 15-mer values All samples were at 5 μM in 10 mM sodium phosphate buffer, 100 mM NaCl at pH 7, and data shows one repeat.*

Duplex content		T_m (°C)
BRAF probe	15-A	45.5
BRAF probe	15-T	46
BRAF probe	173-A	44
BRAF probe	173-T	43

4.4.2.2 15-mer synthetic targets

The fluorescence studies that were to be carried out with the 173-mer were first repeated on the 15-mer. As expected, the addition of an equimolar amount of 15-A resulted in a 577% increase in fluorescence emission whereas that for 15-T resulted in a 27% decrease (**Figure 4.8**).
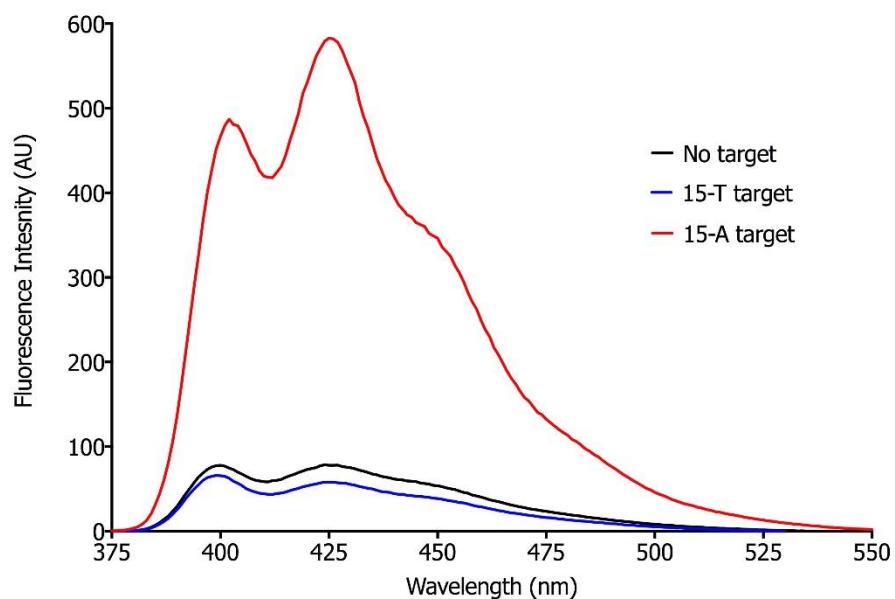
Figure 4.8 *The fluorescence emission gained with a 1:1 ratio of probe to target (both at 1 µM in 10 mM sodium phosphate buffer, 100 mM NaCl at pH 7, at RT). The λ_{ex} = 350 nm, room temperature (RT), λ_{em} = 426 nm, room temperature.*

4.4.2.3 173-mer synthetic targets

Two longer 173-mer targets were then hybridised in the same way, one with the A point variant (173-A) and one with the T point variant (173-T). As expected, a similar trend was observed (**Figure 4.9**) whereby a 220% increase and 12% decrease was seen with 173-T and 173-A respectively.
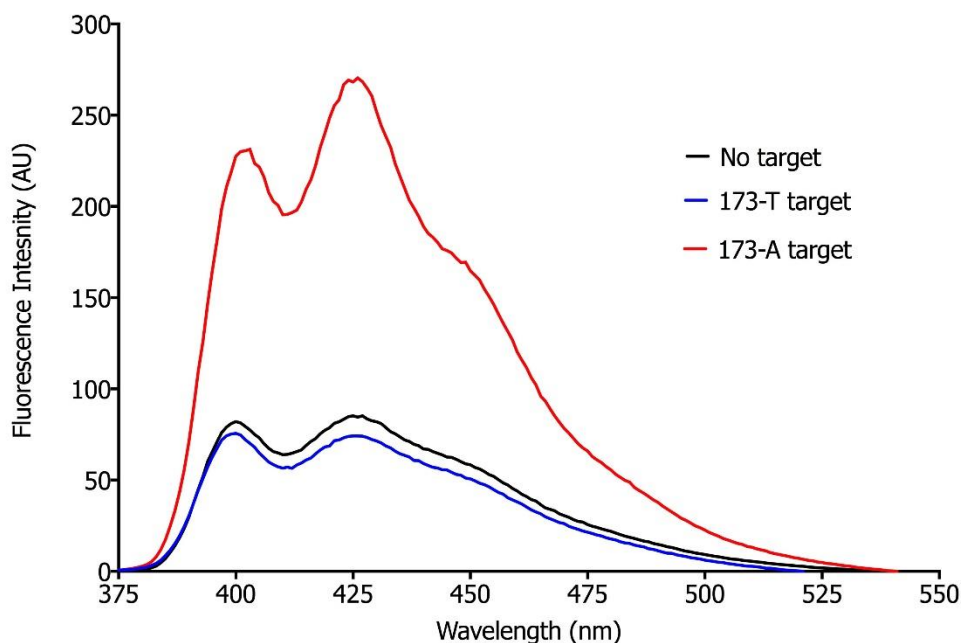
Figure 4.9 *The fluorescence emission gained with a 1:1 ratio of probe to target (both at 1 μM in 10 mM sodium phosphate buffer, 100 mM NaCl at pH 7, at RT). The red line presents the emission increase when the 173-A target is added and the blue line presents the emission decrease when the 173-T target is added. The λ_{ex} = 350 nm, room temperature (RT), λ_{em} = 426 nm, room temperature.*

A previous titration with the 15-mer targets showed a linear dependence for sub-stoichiometric amounts of target before levelling off at more than one equivalence.[31] Interestingly, for the larger target (173-A), while saturation was also observed, now a curved profile was apparent for sub-stoichiometric amounts (**Figure 4.10**). This can be explained by additional non-specific binding interactions between the probes (when in excess) and the target due to the latter having longer flanking regions.
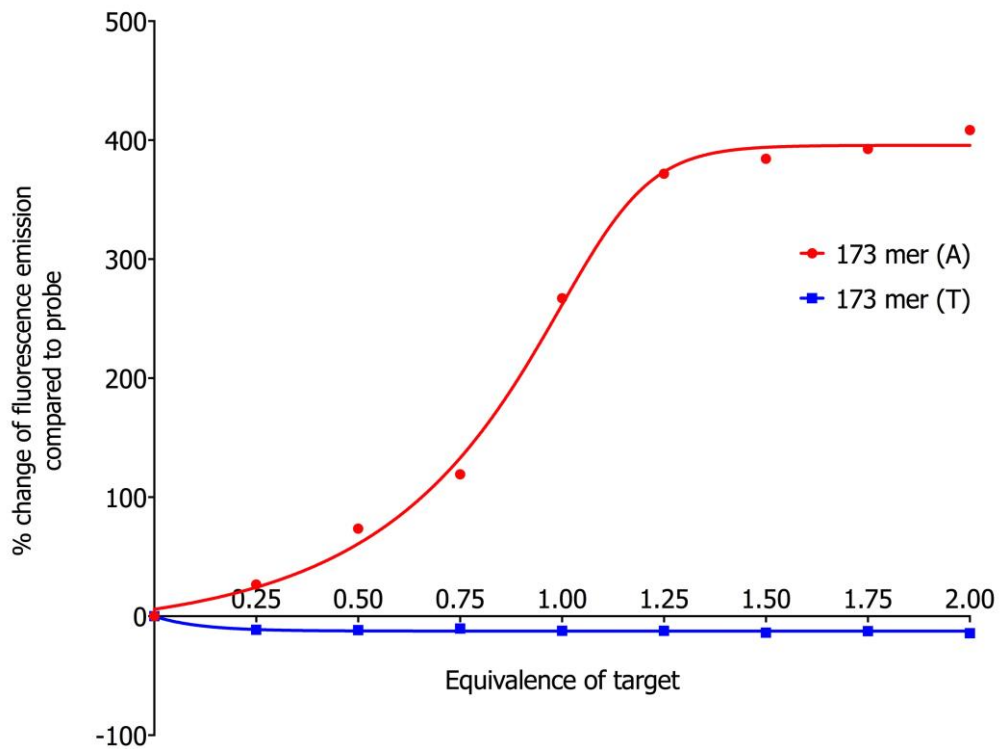
Figure 4.10 *The percentage change in fluorescence emission at 426 nm of 15-A (in red) and 15-T (in blue) compared to the probe when varying equivalance of target is present. All samples were in 10 mM sodium phosphate buffer, 100 mM NaCl at pH 7, at RT. The data were fit to a non-linear asymmetric sigmoidal best fit curve. The λ_{ex} = 350 nm, room temperature (RT), λ_{em} = 426 nm, room temperature.*

4.4.2.4 Comparison of 15-mer vs 173-mer fluorescence

A comparison of the percentage changes in fluorescence emission between the 15-mer targets and the 173-mer targets at one equivalence to the BRAF probe, at 1 µM, is presented in **Table 4.3**. The 15-A target gave approximately a two-fold fluorescence increase over its 173-mer counterpart. This difference can be explained by the local environment experienced by the anthracene probe when it is bound to a target with longer flanking sequences. It is possible that these ends can interact with the tag in a non-specific manner, which reduces the overall emission intensity.

Table 4.3 *The comparison of the percentage change in emission at 426 nm of the BRAF probe with one equivalance of the 15-mer targets and the same probe with one equivalane of the 173-mer targets (1 µM concentration of probe with 1 µM conentration of target in 10 mM sodium phosphate buffer, 100 mM NaCl at pH 7, at RT). The λ_{ex} = 350 nm, room temperature (RT), λ_{em} = 426 nm, room temperature.*

Target	Percentage change in fluorescence at one equivalence	
	Target A	Target T
15-mer	+ 577	- 27
173-mer	+ 220	- 12

The fluorescence studies were successful in demonstrating that even with the longer target lengths, there was a sufficiently large enhancement in fluorescence emission intensity when the BRAF probe hybridised to 173-A. This data, along with the T_m results, indicated that despite the targets being longer in length they would not hamper the binding of the target which would allow PCR products of a similar length originating from patient DNA to be studied effectively.

4.4.2.5 173-mer oligonucleotide linear plot

The next step was to determine whether the correlation initially observed with the 15-mer synthetic oligonucleotide targets was also seen with the longer 173-mer targets. It was hypothesised that the longer targets, truer to the length of PCR products from genomic samples, would display the same behaviour. A fluorescence linear dependence study as a function of allelic ratio, varying the amount of 173-A compared to the 173-T targets, was accordingly carried out on the synthetic target sequences. The results showed that it was indeed possible to construct a linear plot from the data (**Figure 4.11**). Since the mutation for the BRAF allele is heterozygous, (i.e. there is not 100% conversion from T to A but 50%), more data points were obtained between 0 to 50% of 173-A within the allelic sample mix. From this data, it was concluded that strands similar in length to a typical PCR product, could be used to determine allelic ratios in unknown DNA samples from patients.
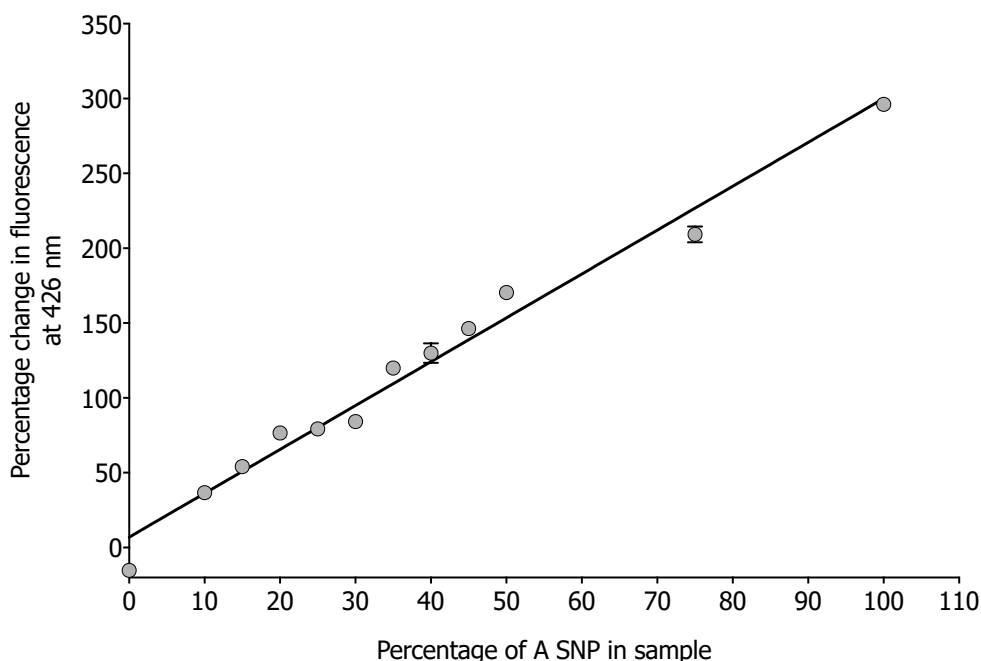
Figure 4.11 *The linear correlation data from the 173 base synthetic oligonucleotide strands. The error bars demonstrate one standard deviation from 3 experimental repeats. The error bars on all points show one standard deviation from 3 experimental repeats. All samples were made up to 1 µM in 10 mM sodium phosphate buffer, 100 mM NaCl at pH 7. The λ_{ex} = 350 nm, room temperature (RT), λ_{em} = 426 nm. The graph shows a linear regression line of best fit. The Pearson's correlation coefficient value was at 0.99.*

4.4.3 Genomic studies from patient samples

After successful detection of 173-mers using the BRAF probe and the generation of a linear dependence plot the next milestone involved generating similar length ssDNA targets from both WT and mutant genomic patient samples. The first step was to amplify the region of interest, containing the point variant, using PCR. Already known forward and reverse BRAF primers, based on the genome sequence of the BRAF gene (**Table 4.4**) were purchased, with the reverse primer containing a phosphorothioate modification at the 5'- end. The detection system relies on there being a ssDNA target produced in excess that can hybridise to the fluorescent probe strand. The product of a PCR reaction is dsDNA and therefore a procedure is required to digest the complementary strand of DNA that is not to be detected, leaving the single strand of target DNA. The digestion was carried out using a T7 exonuclease DNA polymerase that is not able to recognise and digest the strand containing the phosphorothioate modification. As a result, the ssDNA after digestion is the strand elongated using the forward primer containing the 5'- phosphorothioate modification, i.e. the target strand. The ssDNA PCR products would then be checked using DNA sequencing before any fluorescence studies were undertaken.

Table 4.4 *The sequence of the forward and reverse primers donated from the Beggs group along with the patient DNA samples. The forward primer contains a 5'- phosphorothioate modification (noted as PTO in the sequence) to ensure this strand is the ssDNA target after digestion of the PCR product. The T_m values were for the hybridisation of the complementary region of DNA to the primers.*

	Sequence (5' → 3')	T_m (°C)
Forward primer	**PTO** – TGC TTG CTC TGA TAG GAA AAT G	50
Reverse primer	CCA CAA AAT GGA TCC AGA CA	58

4.4.3.1 PCR amplification of patient DNA

To determine whether the PCR cycles had been successful, the samples were run on 3% agarose gels using gel electrophoresis. This technique, previously discussed in detail in **Chapter 2,** is used to separate large fragments of double stranded DNA. One of the main issues faced with PCR reactions is being able to generate dsDNA in sufficient quantities for sensing purposes. Each PCR amplification cycle is sequence and primer specific and therefore protocols require optimisation for different sequences.

The annealing temperatures of the PCR cycle (**Chapter 1**) are often based on the predicted T_m of the DNA duplex. However, this is not always the optimum annealing temperature for generating the maximum amount of product. The optimal temperature gives the highest yields that can be visualised using gel electrophoresis. As well as changing the temperature, the number of PCR cycles can be modified to optimise the yield.

The predicted T_m temperatures for the primers were 58 °C for the forward primer and 50 °C for the reverse primer. The lower temperature for the reverse primer, at 55 °C, was initially chosen as the annealing temperature but in order to optimize the reaction, this was modified to 50 °C as a lower temperature can often be favorable for annealing.[33] The different temperatures and cycles chosen during the optimization procedure are presented in **Table 4.5**.

Table 4.5 *A table with the PCR conditions that were varied for the optimisation of the reaction. In 1 to 3 the number of cycles were changed and from lanes 4 to 6 the annealing temperature was changed along with the 3 different cycling conditions.*

Condition	Temperature (°C)			
	Heat	Anneal	Heat	Cycles
Original	94	55	72	36
1	94	55	72	38
2	94	55	72	40
3	94	55	72	42
4	94	50	72	38
5	94	50	72	40
6	94	50	72	42

The resulting gel data is shown in **Figure 4.12A** Figure **4.12B**. Interestingly, although modifying the cycling number did not bring about any successful PCR reactions, reducing the annealing temperature to 50 °C ensured a successful reaction every time (**Figure 4.12C** and **D**). The optimum condition that produced the highest amount of product can be seen in entry 4 of **Table 4.5** and in the corresponding gel in **Figure 4.12C**.
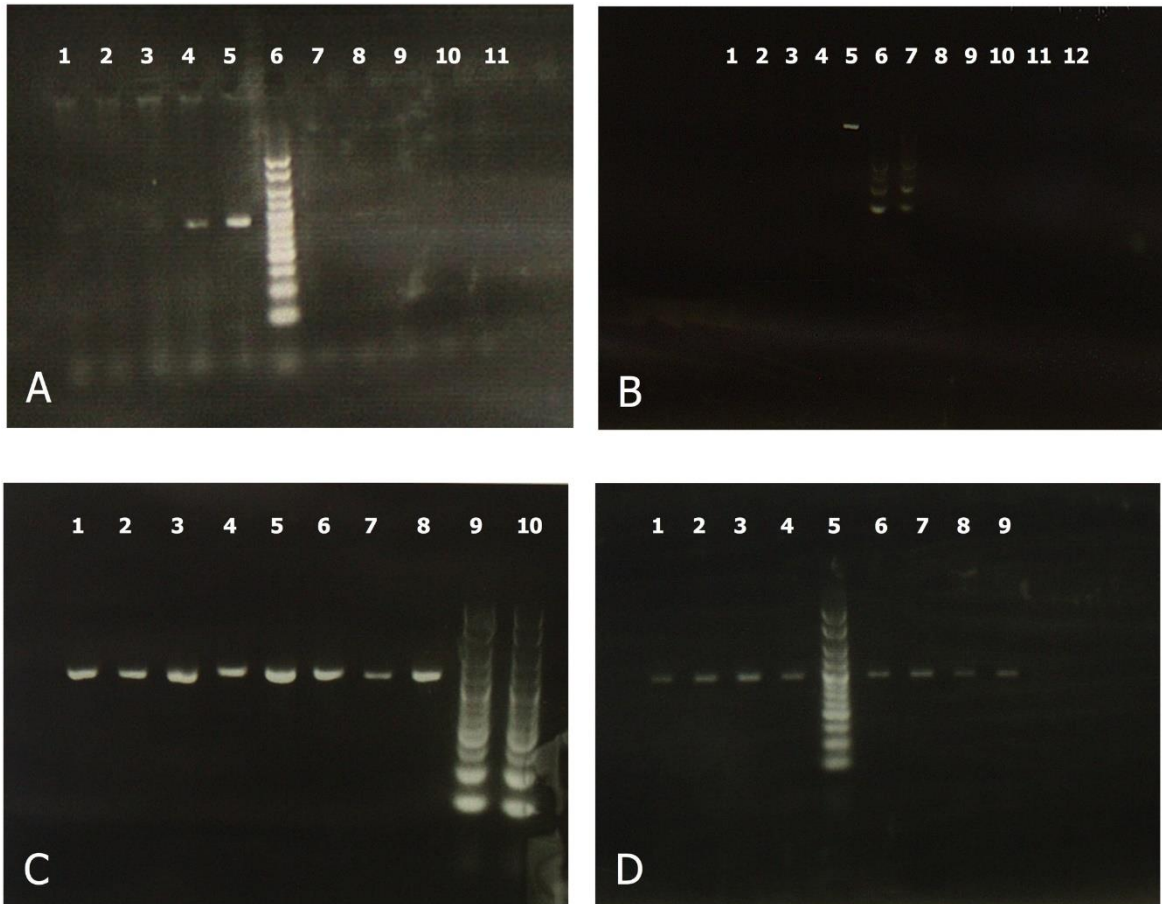
Figure 4.12 *An example of 4 gels demonstrating the result from the six different conditions attempted the PCR reactions. The samples were run on 3% agarose to show the ~150 base pair PCR product. Gels A and B show the failed PCR attempts from conditions 1 and 3 respectively and gels C and D show the successful PCR reactions from conditions 4 and 5 respectively. Lanes 2 and 6 had no visible PCR products and therefore the images have not been included here (Table 4.5). The contents of the samples in each lane can be seen in Table 1 of Appendix 7.2.2.*

4.4.3.2 Sequencing results

To undertake any fluorescence studies on the PCR products the samples were digested from dsDNA to ssDNA. The phosphorothioate modification on the forward primer used during the PCR amplification process ensured that the modified strand was not digested by the exonuclease enzyme used during the digestion process.
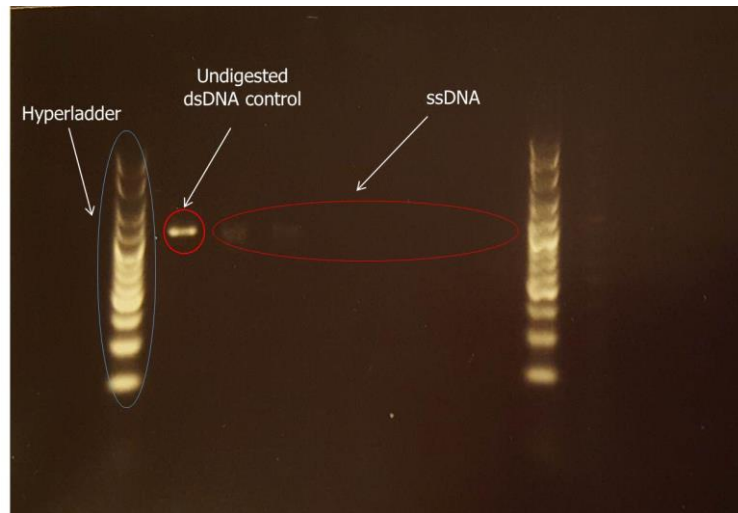
Figure 4.13 *The agarose gel image of the digested PCR products. The dye used to stain and visualise the PCR products will only bind dsDNA. The samples were run on 3% agarose to show the ~150 bp ssDNA products.*

Once the double stranded PCR product had been digested to ssDNA evidenced by agarose gel electrophoresis (**Figure 4.13**), the samples were submitted for sequencing to ensure the correct target sequence was present in both the healthy and mutant genomic DNA samples. The sequencing results can be seen in **Figure 4.14** and **Figure 4.15**. The point variation that occurs in malignant melanomas has been circled within the figure. As expected, the WT tissue demonstrates DNA containing the T base at its position (**Figure 4.14**). Initially, it was thought that the mutant samples were homozygous for the A base, i.e. the sequencing results should be showing the A base only at the base variation position. However, after several PCR and sequencing attempts it was seen that both the A and the T base were seen in the sequencing data. This was initially thought to be contamination of the healthy sample with the mutant sample however, literature searches later revealed that the BRAF V600E mutation is known to be 100% T (homozygous) for the WT-DNA and 50% T and 50 A in the mutant DNA (heterozygous).[4]

As a result of this the mutant tissue demonstrates both A and the T bases at its position (**Figure 4.15**). The sequencing of the PCR amplified product was repeated several times to confirm that the correct ssDNA was obtained within the PCR product and the mutated patient sample was indeed heterozygous for the A/T point variations. The full sequence for both WT and mutant patient samples can be read in the **Appendix 7.2.3**.
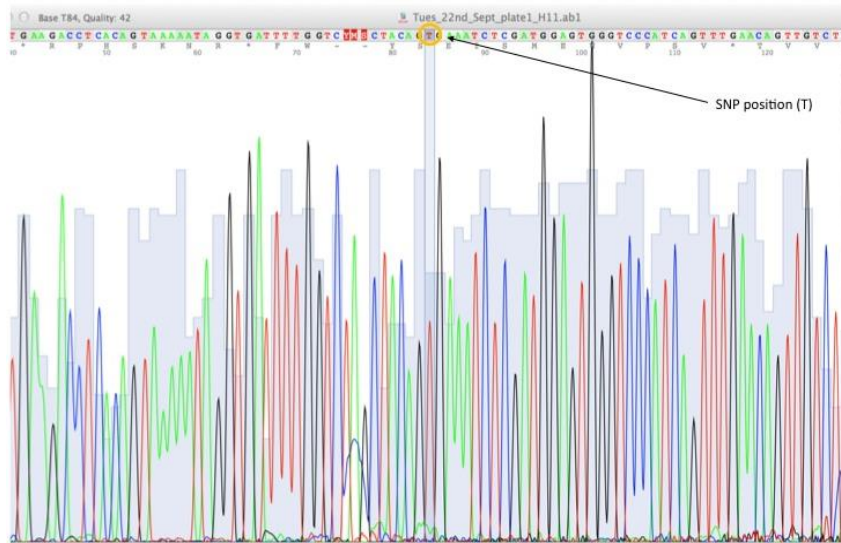
Figure 4.14 *Sequencing data of the PCR product from the genomic DNA from healthy tissue after the digestion step and subsequent purification. The SNP position is seen to be a T showing that the sample is from healthy tissue.*
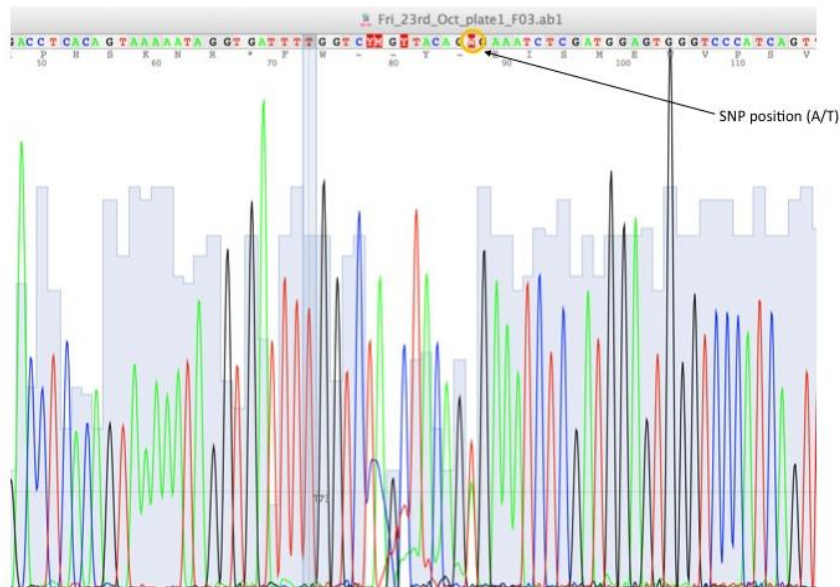
Figure 4.15 *Sequencing data of the PCR product from the genomic DNA from tumour tissue after the digestion step and subsequent purification. The W represents to alleles (A and T) in the SNP base position.*

4.4.3.3 Fluorescence studies of genomic samples

To determine whether the technique was viable on patient DNA, fluorescence studies were undertaken on the samples that had been produced from the PCR of genomic DNA. The fluorescence studies required equimolar concentrations at 1 µM of both the BRAF probe and the target PCR product. Each time the PCR product was purified, firstly after the initial PCR reaction and subsequently after the digestion of the strands to ssDNA, the yield dropped by ca. 85%. This meant that unfortunately only very small amounts of purified sample were being produced and the fluorescence studies had to be undertaken on unpurified ssDNA. Initial studies with the unpurified sample (**Figure 4.16A**) showed an increase in fluorescence at 426 nm for both the mutant and the WT. This led to some control studies whereby the BRAF probe alone was compared to the probe together with the components resulting from the PCR and digestion process that remained in the samples (**Figure 4.16B**). This data showed that there was a fluorescence increase upon addition of the probe to these components. In order to account for the fluorescence increase, the components (**Appendix Figure 7.7**) were added to the BRAF probe one by one and it was seen that the increase was due to the formamide, used to deactivate the T7 exonuclease, and 2xQ mastermix provided as part of the PCR protocol (**Figure 4.16C**).

However, upon addition of the mutant sample, a 1.2-fold fluorescence *increase* could still be seen after taking into account the fluorescence emission increases due to the formamide and 2xQ mastermix (**Figure 4.16D**). Significantly, there was also a fluorescence *decrease* observed with the WT target when compared to the probe in the reaction mix.

There could be several reasons as to why the increase in fluorescence using the PCR product was not as high as is normally seen using the synthetic targets. Firstly, this could be due to the concentration of the PCR target not being in excess compared to the probe. However it is worth noting that, the PCR product from the mutant DNA contains both the A and the T alleles, as the mutant sample is heterozygous leading to a fluorescence emission dampening from the T base.
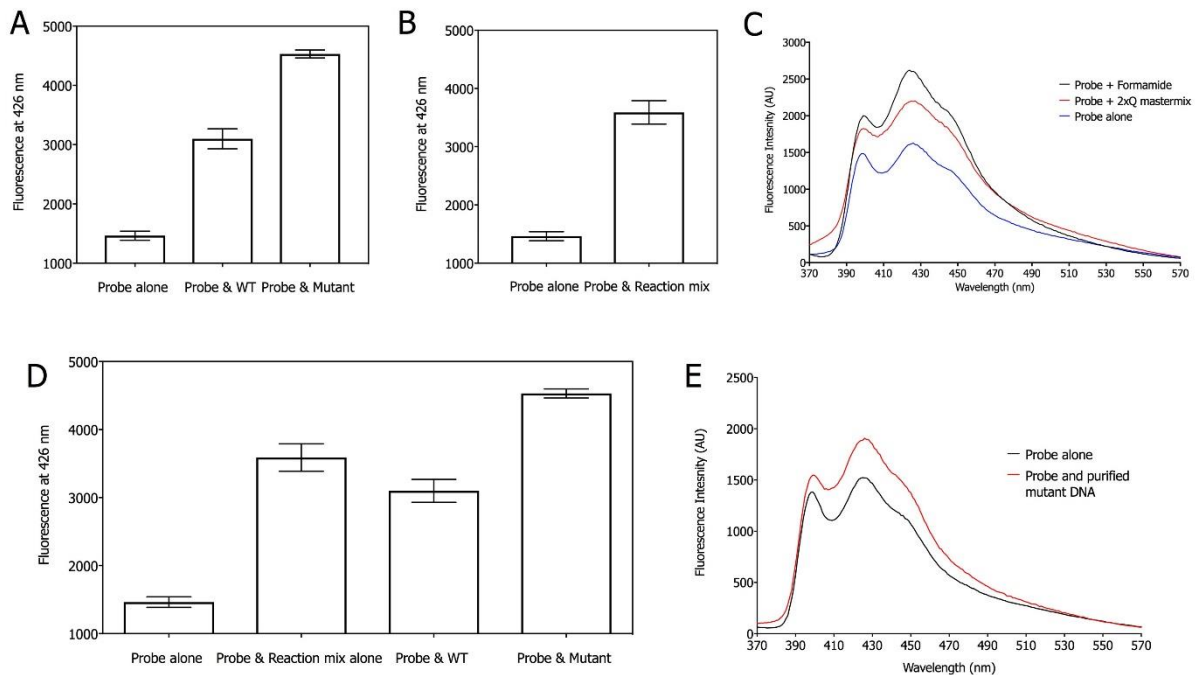
Figure 4.16 A) *The emission data from the study of the unpurified PCR samples compared to the emission of the probe alone,* **B)** *the emission data from the study of the probe alone compared to the emission of the probe in the reaction mix,* **C)** *the emission data from the study of the probe with formamide or 2xQ mastermix, demonstrating the components that caused a fluorescence increase in the probe,* **D)** *the emission data from the study of; the probe alone, the probe and the reaction mix and the PCR samples. All samples except the probe alone were still present in the reaction mix in A-D and finally* **E)** *shows the emission data from the study of the purified mutant genomic PCR sample at (0.03 µM) and the probe at 1 µM (0.03 equivalence). The purified products were in 10 mM sodium phosphate buffer, 100 mM NaCl at pH 7. The λ_{ex} = 350 nm, RT, λem = 426 nm, room temperature. The error bars show one standard deviation from three experimental repeats.*

A small amount of purified mutant target was obtained and added to the probe. However, only at 0.03 equivalence addition could be added. Nevertheless, a small increase in emission was observed as expected (**Figure 4.16E**). This demonstrated that even at a low concentrations, the purified mutant target produced an increase in fluorescence emission compared to the probe alone. Both the studies on the unpurified and purified mutant target added to the evidence for the effectiveness of this anthracene based BRAF probe in detecting point variants from PCR products.

4.5 Conclusions

Although genomic analysis and DNA sequencing technologies are well established there are still avenues to be explored that include obtaining accurate and quantitative data concerning allelic ratios. This project has attempted to address this issue using BDP technology. It has been proven possible to detect and distinguish between the A and T base difference between the mutant and WT BRAF gene in real patient DNA samples. This project has also established that having longer target sequences does not adversely affect the ability of the probe to identify a point variant correctly. Furthermore, a linear dependence for the A and T base ratio has been established with the longer target sequences. This provides evidence that it is possible to establish a fluorescence-based detection system whereby the ratio of different alleles in a mixture of cells can be quantitatively established using a linear calibration curve.

4.6 Future work
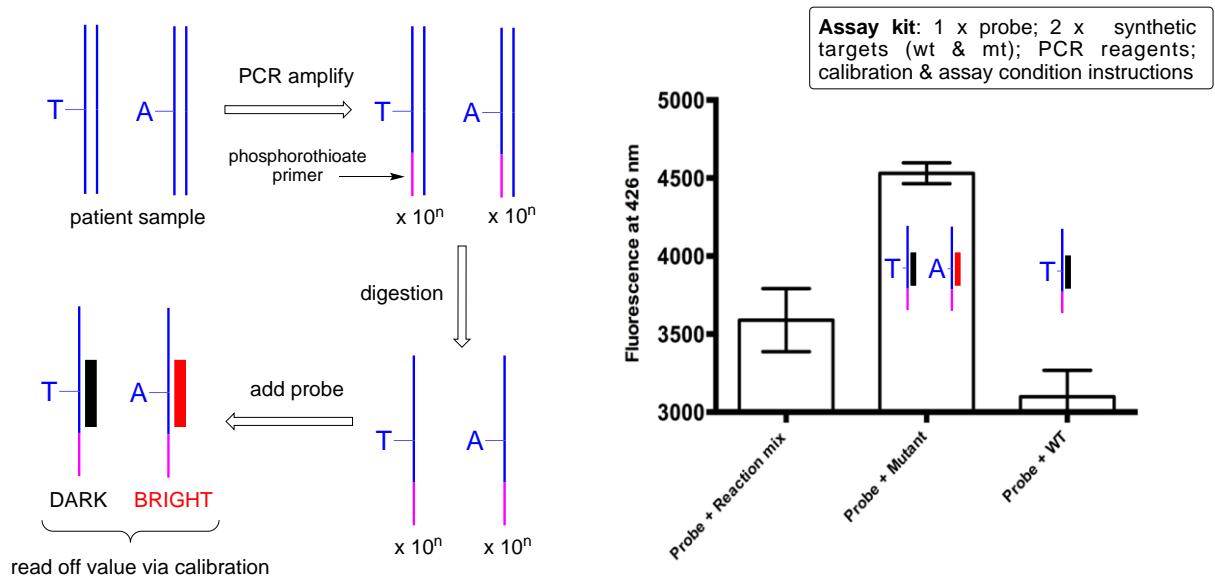
Figure 4.17 A diagrammatic representation of the future goal to create an assay kit that allows the determination of allelic ratios of PCR amplified genomic samples using a calibration plot.

The future of this project will involve the development of an assay kit (**Figure 4.17**) that is viable for the detection of SNP changes in patient samples. Initially, the PCR reaction will be automated, using an automated liquid handler linked to a PCR thermocycler, in order to produce genomic products in sufficient quantities. The fluorescence emission testing will be repeated with the purified PCR products and the ratio of the A/T bases within the samples will be read off using a calibration plot similar to that produced within the work described in this chapter.

4.7 References

1. Sachidanandam, R.; Weissman, D.; Schmidt, S. C.; Kakol, J. M.; Stein, L. D.; Marth, G.; Sherry, S.; Mullikin, J. C.; Mortimore, B. J.; Willey, D. L.; Hunt, S. E.; Cole, C. G.; Coggill, P. C.; Rice, C. M.; Ning, Z.; Rogers, J.; Bentley, D. R.; Kwok, P. Y.; Mardis, E. R.; Yeh, R. T.; Schultz, B.; Cook, L.; Davenport, R.; Dante, M.; Fulton, L.; Hillier, L.; Waterston, R. H.; McPherson, J. D.; Gilman, B.; Schaffner, S.; Van Etten, W. J.; Reich, D.; Higgins, J.; Daly, M. J.; Blumenstiel, B.; Baldwin, J.; Stange-Thomann, N.; Zody, M. C.; Linton, L.; Lander, E. S.; Altshuler, D., A map of human genome sequence variation containing 1.42 million single nucleotide polymorphisms. *Nature* **2001,** *409*, pp. 928-33.

2. Vignal, A.; Milan, D.; SanCristobal, M.; Eggen, A., A review on SNP and other types of molecular markers and their use in animal genetics. *Genetics, selection, evolution : GSE* **2002,** *34*, pp. 275-305.

3. Karki, R.; Pandya, D.; Elston, R. C.; Ferlini, C. J. B. M. G., Defining "mutation" and "polymorphism" in the era of personal genomics. *BMC Medical Genomics* **2015,** *8*, pp. 37.

4. Willmore-Payne, C.; Holden, J. A.; Hirschowitz, S.; Layfield, L. J., BRAF and c-kit gene copy number in mutation-positive malignant melanoma. *Human Pathology* **2006,** *37*, pp. 520-7.

5. Evans, W. E.; Relling, M. V., Pharmacogenomics: Translating functional genomics into rational therapeutics. *Science* **1999,** *286*, pp. 487-491.

6. Flaherty, K. T.; Infante, J. R.; Daud, A.; Gonzalez, R.; Kefford, R. F.; Sosman, J.; Hamid, O.; Schuchter, L.; Cebon, J.; Ibrahim, N.; Kudchadkar, R.; Burris, H. A.; Falchook, G.; Algazi, A.; Lewis, K.; Long, G. V.; Puzanov, I.; Lebowitz, P.; Singh, A.; Little, S.; Sun, P.; Allred, A.; Ouellet, D.; Kim, K. B.; Patel, K.; Weber, J., Combined BRAF and MEK inhibition in melanoma with BRAF V600 mutations. *New England Journal of Medicine* **2012,** *367*, pp. 1694-1703.

7. Moran, N.; Bassani, D. M.; Desvergne, J.; Keiper, S.; Lowden, P. A. S.; Vyle, J. S.; Tucker, J. H. R., Detection of a single DNA base-pair mismatch using an anthracene-tagged fluorescent probe. *Chemical Communications* **2006,** 48, pp. 5003-5005.

8. Zhao, Z.; San, M.; Duprey, J. H. A.; Arrand, J. R.; Vyle, J. S.; Tucker, J. H. R., Detection of single nucleotide polymorphisms within a sequence of a gene associated with prostate cancer using a fluorophore-tagged DNA probe. *Bioorganic & Medicinal Chemistry Letters* **2012,** *22*, pp. 129-132.

9. Hassanpour, S. H.; Dehghani, M., Review of cancer from perspective of molecular. *Journal of Cancer Research and Practice* **2017,** *4*, pp.127-129.

10. Siegel, R. L.; Miller, K. D.; Jemal, A., Cancer statistics, 2017. *CA: A Cancer Journal for Clinicians* **2017,** *67*, pp. 7-30.

11. Hanahan, D.; Weinberg, R. A., Hallmarks of Cancer: The Next Generation. *Cell* **2011,** *144*, pp. 646-674.

12. Shen, H.; Laird, P. W., Interplay between the Cancer Genome and Epigenome. *Cell* **2013,** *153*, pp. 38-55.

13. Cantwell-Dorris, E. R.; O'Leary, J. J.; Sheils, O. M., BRAFV600E: implications for carcinogenesis and molecular therapy. *Mol Cancer Ther* **2011,** *10*, pp. 385-94.

14. McCourt, C.; Dolan, O.; Gormley, G., Malignant melanoma: A pictorial review. *The Ulster Medical Journal* **2014,** *83*, pp. 103-110.

15. Rastrelli, M.; Tropea, S.; Rossi, C. R.; Alaibac, M., Melanoma: epidemiology, risk factors, pathogenesis, diagnosis and classification. *In Vivo* **2014,** *28*, pp. 1005-11.

16. Domingues, B.; Lopes, J. M.; Soares, P.; Pópulo, H., Melanoma treatment in review. *ImmunoTargets and Therapy* **2018,** *7*, pp. 35-49.

17. Bandarchi, B.; Ma, L.; Navab, R.; Seth, A.; Rasty, G., From melanocyte to metastatic malignant melanoma. *Dermatology Research and Practice* **2010,** *2010*, 8.

18. De Rosa, M.; Pace, U.; Rega, D.; Costabile, V.; Duraturo, F.; Izzo, P.; Delrio, P., Genetics, diagnosis and management of colorectal cancer (Review). *Oncology reports* **2015,** *34*, pp. 1087-96.

19. Leonardi, G. C.; Falzone, L.; Salemi, R.; Zanghì, A.; Spandidos, D. A.; McCubrey, J. A.; Candido, S.; Libra, M., Cutaneous melanoma: From pathogenesis to therapy (Review). *International Journal of Oncology* **2018,** *52*, pp. 1071-1080.

20. Ren, R. X. F.; Chaudhuri, N. C.; Paris, P. L.; Rumney, S.; Kool, E. T., Naphthalene, Phenanthrene, and Pyrene as DNA Base Analogues: Synthesis, Structure, and Fluorescence in DNA. *Journal of the American Chemical Society* **1996,** *118*, pp. 7671-7678.

21. Duprey, J.-L. H. A.; Bassani, D. M.; Hyde, E. I.; Jonusauskas, G.; Ludwig, C.; Rodger, A.; Spencer, N.; Vyle, J. S.; Wilkie, J.; Zhao, Z.-Y.; Tucker, J. H. R., Rationalisation of a mechanism for sensing single point variants in target DNA using anthracene-tagged base discriminating probes. *Organic & Biomolecular Chemistry* **2018,** *16*, pp. 6576-6585.

22. Köhler, O.; Seitz, O., Thiazole orange as fluorescent universal base in peptide nucleic acids. *Chemical Communications* **2003,** 23, pp. 2938-2939.

23. Mariappan, M.; Maiya, B. G., Effects of anthracene and pyrene units on the interactions of novel polypyridylruthenium(II) mixed-ligand complexes with DNA. *European Journal of Inorganic Chemistry* **2005,** *2005*, pp. 2164-2173.

24. Chen, M.; Yan, L.; Zhao, Y.; Murtaza, I.; Meng, H.; Huang, W., Anthracene-based semiconductors for organic field-effect transistors. *Journal of Materials Chemistry C* **2018,** *6*, pp. 7416-7444.

25. Xiao, Q.; Ranasinghe, R. T.; Tang, A. M. P.; Brown, T., Naphthalenyl- and anthracenyl-ethynyl dT analogues as base discriminating fluorescent nucleosides and intramolecular energy transfer donors in oligonucleotide probes. *Tetrahedron* **2007,** *63*, pp. 3483-3490.

26. Duprey, J.-L. H. A.; Bullen, G. A.; Zhao, Z.-Y.; Bassani, D. M.; Peacock, A. F. A.; Wilkie, J.; Tucker, J. H. R., Single Site Discrimination of Cytosine, 5-Methylcytosine, and 5-Hydroxymethylcytosine in Target DNA Using Anthracene-Tagged Fluorescent Probes. *ACS Chemical Biology* **2016,** *11*, pp. 717-721.

27. Duprey, J. H. A.; Zhao, Z. Y.; Bassani, D. M.; Manchester, J.; Vyle, J. S.; Tucker, J. H., Detection of DNA base variation and cytosine methylation at a single nucleotide site using a highly sensitive fluorescent probe. *Chemical communications* **2011,** *47*, pp. 6629-31.

28. Manchester, J.; Bassani, D. M.; Duprey, J. H. A.; Giordano, L.; Vyle, J. S.; Zhao, Z.; Tucker, J. H. R., Photocontrolled binding and binding-controlled photochromism within anthracene-modified DNA. *Journal of the American Chemical Society* **2012,** *134*, pp. 10791-10794.

29. Duprey, J.-L. Studies on Anthracene Tagged Oligonucleotides. University of Birmingham, 2010.

30. McGuigan, F. E.; Ralston, S. H., Single nucleotide polymorphism detection: allelic discrimination using TaqMan. *Psychiatric Genetics* **2002,** *12*, pp. 133-6.

31. Hay, J. The use of an anthracene probe to undertake fluorescent studies detecting SNPs in DNA and the stabilising benefits of using modified 2'OMe and DNA attached to gold nanoparticles. Dissertation. *University of Birmingham* **2015**.

32. Integrated DNA Technologies, I. OligoAnalyzer Tool. https://www.idtdna.com/calc/analyzer (accessed 2015-2018).

33. Integrated DNA Technologies, I. How do you calculate the annealing temperature for PCR? https://www.idtdna.com/pages/support/faqs/how-do-you-calculate-the-annealing-temperature-for-pcr- (accessed August 2016).

Chapter 5 – A multiplexed DNA detection assay

5.1 Introduction

In agriculture, the spread of pathogenic viral strains from one country to another can cause significant economic damage. Therefore, techniques that accurately detect such viruses are of paramount importance to prevent disease being rapidly spread across wide areas of the globe.

The potato (*Solanum tuberosum*) is in the top four of all food crops by volume.[1] As of 2016, ca. 377 million metric tonnes of potato were being produced and consumed annually.[2] Potatoes are known to be affected by approximately 40 different viruses,[3] with these infections having a serious effect on potato production. *Potato virus Y* (PVY, genus *Potyvirus*, family *Potyviridae*) is one of the few potato viruses that is found to cause worldwide loss of potato yield and production quality.[4] This is particularly acute if the virus contaminates the potato seed supplies. To address this the European Commission has begun to create High Grade (HG) seed potato production areas across Europe. To create this HG system, it is important to have rapid monitoring systems of potato seed to ensure fast and accurate diagnosis of potato viruses.[5] This can aid in controlling viruses entering the HG seed potato areas.

This introduction will discuss the viruses used within this project and later will compare some well-established biomolecular detection techniques. The final section will discuss the results from an innovative virus detection method employing M13 bacteriophage (M13) as a scaffold for the conjugation of deoxyribonucleic acid (DNA). This DNA-based assay detects the presence of potato virus DNA using the technique linear dichroism (LD) spectroscopy.

5.2 Potato viruses

5.2.1 Potatoes

The potato plant is one of the most versatile and important food crops and is a staple food item that is key to alleviate hunger in areas of poverty due to the high energy density of the crop. It also has nutritional value, being rich in carbohydrates, potassium, protein and certain vitamins such as vitamin C, B1, B3 and B6. Potatoes can in fact give provide up to 50% of the daily requirement of vitamin C intake.[6]

The increasing importance of potatoes has heightened efforts to study and control the risk of 'potato enemies' such as pests, bacterial wilt and viral diseases that affect the production of the crop. The focus of this project is on the detection of viruses that can cause yield reduction in the potato harvest. There are 40 known viral species that can infect potatoes and many cause problems in their yield and marketability.[3]

Viruses are assembled from nucleic acid material, this can be RNA or DNA, enveloped by a protein and/or lipid shell. The structure has evolved in a way such that the genetic material of the virus can be protected from external environments allowing the genetic information to be passed from one host cell to another.[7] The genetic material is the most significant part of the virus that enters the host in order for viral replication to occur.[8] Viral pathogenic pandemics can be lethal to populations of animals and plants as there are minimal ways known to fight viral infection.

5.2.2 *Potato virus Y (PVY)*

The largest international viral problem faced in the production of potatoes comes from PVY.[3] PVY infections in seed tubers can cause a loss of up to 85% of crop.[9] In 1931 Smith[10] first initiated a study on PVY and since then, it has become the 5th most important plant virus based on both economic and scientific significance.[11] For this reason, the regulation and control of PVY is of utmost importance to keep virus levels below set thresholds. PVY is transmitted by hemipteran insects, and within these insects it is the aphid species that transmits more than 50% of potato viruses.[12] The method of transmission of the viruses is an important factor in order to choose appropriate regulatory measures. The PVY virus has a non-persistent viral transmission mode. This involves a very short probing action; the inoculation process is normally minutes to hours as opposed to days to weeks with persistent transmission, and this is sufficient for the virus to enter the epidermis of plant tissue.[13-14] This transmission can be carried out by over 50 aphid species.[15] The short transmission time of the PVY virus is a key reason as to why these viruses and their vectors are incredibly difficult to limit and regulate.

5.2.3 Potato virus structure

PVY is a filamentous virus and its genetic material is a single stranded RNA (ssRNA). The virus is long, approximately 720-850 nm in length, and has a diameter of 12-15 nm (**Figure 5.1**).[16] The ssRNA genome is translated by the host cell into one long protein. This large polypeptide is then post-translationally and co-translationally modified by proteases encoded by PVY into varying functional proteins (**Table 5.1**). The RNA has a poly (A) tail at the 3' end and has a protein that is covalently bound to the 5' end of the genome.[17] The protein of interest that is often used for the detection of the virus is the coat protein (CP). The outer capsid proteins are vital in the detection of, and the ability to distinguish between, different viral species. It is copied approximately 2000 times in the PVY virus surrounding the RNA genome in a cylindrical inclusion body (CIb). The CP is a very important phenotypic feature that is used to distinguish between a potyvirus such as PVY and other potato virus species, such as potato virus A (PVA). For this reason, this project has utilised the coat protein genes that are specific to PVY and PVA respectively for the design of the detection system that will be discussed later.
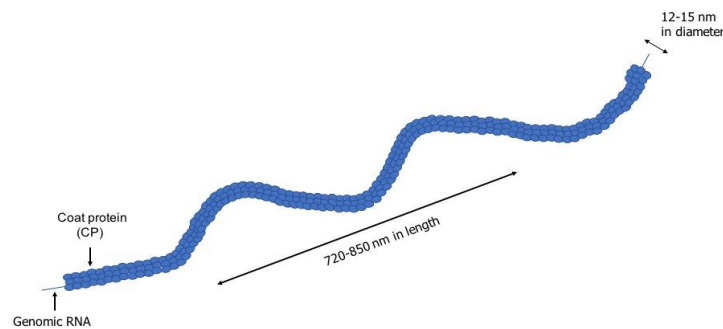
Figure 5.1 *The filamentous PVY virus structure containing the genomic RNA with repeat copies of the coat protein surrounding it in a cylindrical inclusion body.*

Table 5.1 *A summary of the proteins involved in the structure, replication and pathology of PVY.*

Protein	Protein Function
Viral genome linked protein (VPg)	Covalently binds to the phosphate of the 5'-nucleotide of the genome to initiate the replication system.[18-19]
First protein (P1)	Serine protease that is involved in the amplification of the genome and can supress HC-Pro.[20]
Helper component proteinase (HC-Pro)	Cysteine protease that plays a role in the replication and transmission of PVY.[21-22]
Third protein (P3)	Function is poorly understood but it is thought that the protein is necessary for the replication of PVY and the symptoms expressed by the virus.[23]
Potyviridae opening reading frame (PIPO)	This protein is associated with P3 and is involved in cell-to-cell movement.[24]
First 6 kilodalton protein (6K1)	The exact function of this protein is unknown.[22]
Cylindrical inclusion protein (CI)	RNA helicase that has a role in cell-to-cell movement.[25]
Second 6 kilodalton protein (6K2)	A protein involved in the anchoring of PVY to Endoplasmic Reticulum type membranes.[26]
Nuclear inclusion protein a (NIa)	Displays serine-like protease functions and is one of the main proteases within potyviruses.[27]
Nuclear inclusion protein b (NIb)	A RNA helicase that has RNA polymerase activity for the replication of PVY.[28]
Coat protein (CP)	Involved in the encapsidation and motion of the PVY virus. The virus is surrounded by 2000 copies of CP.[29]

5.2.4 Potato virus A (PVA)

The second virus to be detected in this project was chosen to be PVA, also from the *potyviridae* family of viruses. PVA is another virus that is known in all parts of the world that potatoes are produced. However, the importance of this virus is lower than that of PVY, due to its lower incidence level. However, it can also cause a loss in the production of tuber if the PVA infection reaches high levels.[30-31] Additionally, if the plants become co-infected with the potato virus X (PVX) it can cause potato crinkle and mosaic symptoms. The virus is also transmitted by aphid species in a non-persistent manner.[30] There are four major strain groups of the PVA virus and studies undertaken on the potato cultivar 'King Edward' demonstrated that the strains cause varying problems, from strains that cause necrotic lesions to strains that cause no symptoms leading to a difficulty in detection.[32] The genome organisation of the virus is similar to that of PVY discussed previously (**Figure 5.1**).

5.2.5 M13 bacteriophage as a DNA scaffold

Structurally, viruses are highly organised nanoparticles that can be deployed as biological scaffolds.[33-36] M13 bacteriophage (M13) is an example of a virus that has been manipulated as a scaffold for the use in chemistry, material science, and biological engineering.

M13 are filamentous viruses (**Figure 5.2**), from the *Inoviridae* family, that contain ssDNA as their genetic material. These phage are specific in only infecting the bacterium *Eschericia coli* (*E. coli*). The viral capsid is a protein filament comprising of 1 major coat protein, pVIII, and 4 minor coat proteins, pIII, pVI, pVII and pIX.[37] These proteins aid the virus in entry, exit and cell recognition upon contact with *E. coli*. The length of the virus depends on the size of the genome and consequently the number of pVIII proteins surrounding capsid. The ssDNA is coiled forming a tertiary structure of DNA within the surrounding capsid. The pVIII protein, which consists of 50 amino acids, can be modified and conjugated to oligonucleotides and the pVIII protein contains many amino acids that allow for bioconjugation reactions. The key modification sites (**Figure 5.2**) are:

1. The amine groups on the exposed Lysine 8, 40, 43, 44 and 48 and this is a result of these lysine residues being more exposed than the other amino acids with amine functional groups. [38]

2. Out of the four amino acids that contain carboxylic acid functional groups the carboxylic acid groups on glutamic acid and aspartic acid 4 or 5 are the most reactive. This is due to the fourth amino acid, glutamic acid 20, is more buried than the rest.[38]

3. The phenol groups are reactive to biotin modification at both tyrosines (21 and 24) in the PVIII protein.[38]
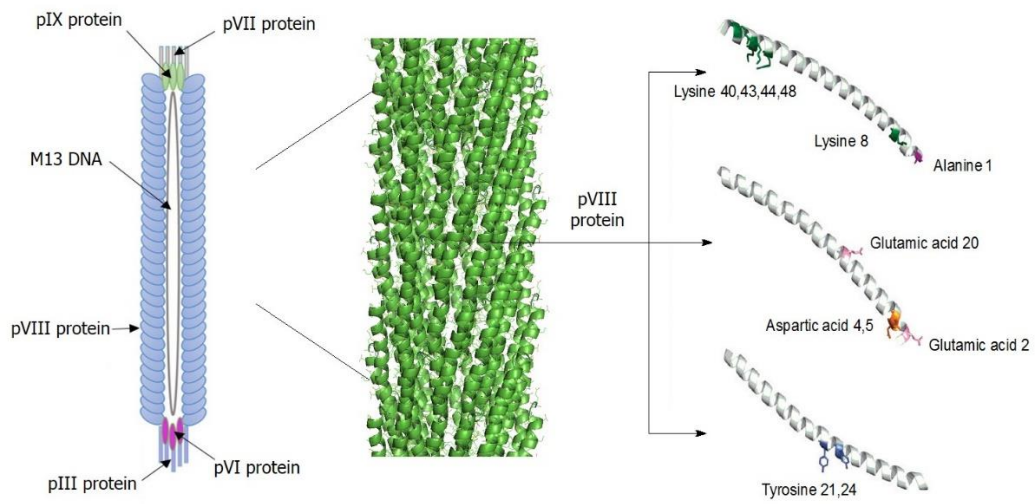
Figure 5.2 *An M13 virus labelled with the major coat proteins repeated along the length of the phage and the minor coat proteins on either end. In the centre is the ssDNA genome. The P8 protein and the key modification sites are also highlighted.*

5.3 Linear dichroism detection systems

LD spectroscopy is a technique that uses linearly polarised light to give information about molecules that are able to be artificially aligned along an orientation axis (**Chapter 2**). DNA and M13 bacteriophage, both being long and rigid, can be oriented in solution allowing electronic transition moments to be gathered and changes in the alignment to be monitored using LD. Changes in alignment would occur if a target or ligand, able to interact with them, was added to the solution as the target-probe complex would induce an aggregation event.

As implied above, the key feature of M13 that makes it ideal for an LD based assay is its shape. M13 is fibrous in morphology with a length of ca. 800 nm and a thickness of 8 nm. This morphology means that the virus can be artificially oriented using fluid flow; a pre-requisite for detection by LD. When aligned using Couette flow (**Chapter 2**) LD the M13 will give a distinct LD spectrum (**Figure 5.3**). Each constituent of the M13 structure can be analysed in order to understand the characteristic LD signal that it creates. When aligned under Couette flow the long axis of the M13 will align against the predefined orientation axis giving high amplitude LD spectra. The positive signals are the result of the transition moments that are parallel to the orientation axis. The negative signals are the result of the transition moments that are perpendicularly aligned against the orientation axis. The positive peak seen at higher wavelengths is due to short axis transition absorptions from the tryptophan and tyrosine residues within the pVIII protein (**Figure 5.3**). At the lower wavelengths, between 250 and 260 nm, a negative peak can be seen. This is due to the single stranded DNA (ssDNA) bases absorbing whilst being perpendicular to the long axis of the M13. At the lowest wavelength between the ranges of 222 to 226 nm the positive peak is predominantly due to the long axis transitional moments of the tryptophan residues within the major coat protein. The n - π^* transitions of the pVIII protein on causes the negative peak seen at 216 nm, with the peak at ca. 205 nm a result of π - π^* transitions.[39]
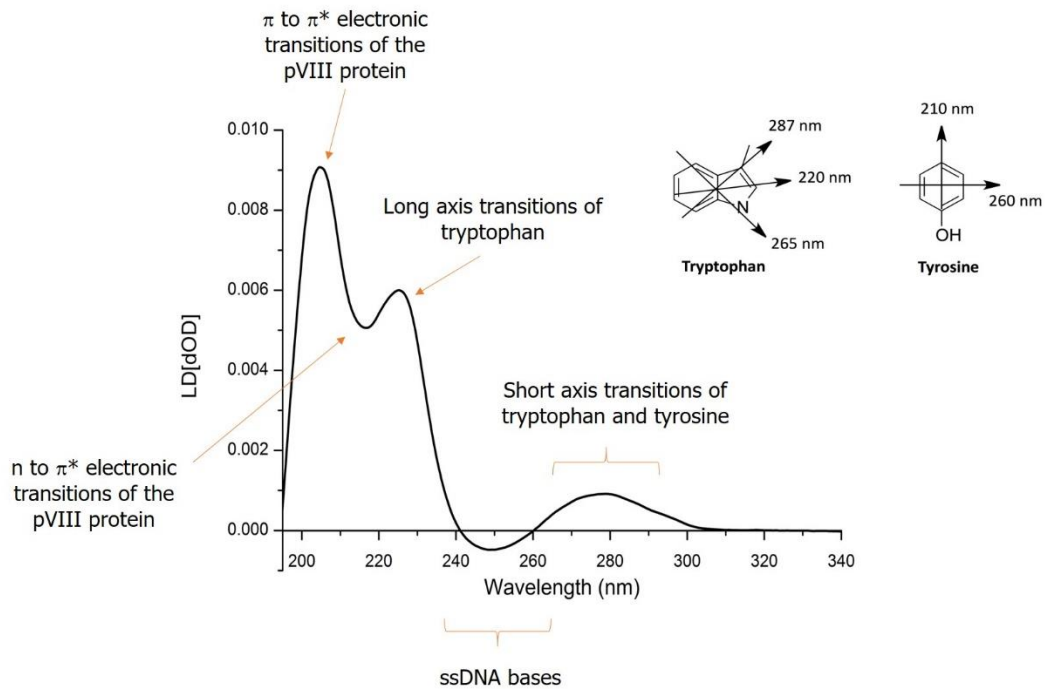
Figure 5.3 *The characteristic LD spectra seen by M13-phage by shear Couette flow and the transition moments that result in the signal.*

The oligonucleotide based sensing research using LD and M13 began when Carr-Smith and co-workers aimed to develop the M13 scaffold as a novel biomolecular PCR based DNA sensor.[40] The PCR based assay furthered the work in the group whereby a pathogenic *E. coli* bacterium was sensed using an M13 scaffold conjugated to antibodies specific to the *E. coli*.[41] The PCR based assay functioned by conjugating oligonucleotide primers to M13 able to anneal to a DNA target strand that encoded an antibiotic resistance protein and PCR amplification occurred only if this DNA target was present. The amplification of the target strand was monitored using LD spectroscopy by detecting decay in the alignment of the M13-primer conjugates. The next section will explore previous work by the group in developing a DNA based detection assay that becomes the basis of a novel potato virus assay detected in this chapter.

5.3.1 Bioconjugation of oligonucleotides to M13

M13 is easily modified, both chemically and genetically, for a variety of different functions. Phage display, first demonstrated by Smith *et al.*, in 1985, is a technique that involves the genetic modification of M13 allowing the "display" of foreign molecules on the surface of the viral proteins and has been used in many biological applications, for example imaging and sensing.[42-43]

However, the use of M13 as a scaffold with this research used a much simpler conjugation approach. In 2012 Lee *et al.*, demonstrated the conjugation of oligonucleotides to M13 for the hybridisation of these strands to oligonucleotide conjugated gold nanoparticles (referred to as DNA-AuNPs).[44] The bioconjugated system was then exploited to detect proteins. The method utilised within the Tucker and Dafforn groups of conjugating an oligonucleotide strand to the pVIII protein of the M13 has been published previously.[40] The first step involves the amine groups on the lysine residues of the major coat protein of the M13-bacteriophage (pVIII) forming a peptide bond to the functional NHS-ester group, on a heterobifunctional linker, succinimidyl-4-(N-maleimidomethyl)cyclohexane-1-carboxylate (SMCC) linker. The oligonucleotide probes are designed to have a thiol modification on either the 5'- or the 3'- end (**Figure 5.4**) and the thiol group is incorporated onto the strands as a disulphide (**Figure 5.5**) in order to protect inter-strand thiol linkages. Tris(2-carboxyethyl)phosphine (TCEP) is used in order for the disulphides to become reactive thiol groups. The thiol group on the oligonucleotide will bind the maleamide group on the SMCC linker allowing for the bioconjugation of the strand to the M13.[45]

SH-3'

5'-HS

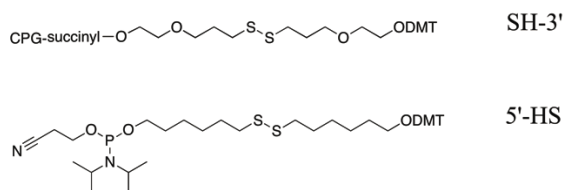**Figure 5.4** *The disulphide monomers synthesised onto oligonucleotide strands that aid in the conjugation to M13. The disulphide group is reduced using TCEP in order to give a reactive thiol group that will form a covalent linkage to the SMCC linker group on the PVIII protein of M13-phage.*
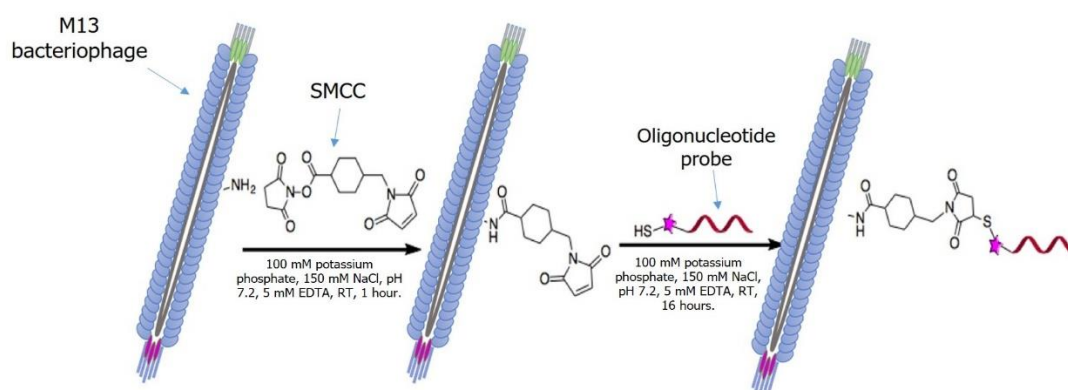
Figure 5.5 *The bioconjugation of the pVIII protein of M13 to a thiol modified oligonucleotide probe using the linker SMCC.*

5.3.2 Previous work

Previously within the Tucker and Dafforn groups, the M13 scaffold and its subsequent bioconjugation to antibodies or oligonucleotide probes has been used for detecting both pathogens and DNA targets.[40-41] The creation of a DNA biosensor was progressed by creating an M13 and oligonucleotide probe (M13-probe) system that acts as the basis for a DNA detection assay using LD spectroscopy. The detection system was designed to be a 'sandwich' assay (**Figure 5.6**). This involved one set of M13 phage conjugated to DNA probes designed for the 5'- end of the target sequence and another set of M13 phage conjugated to DNA probes designed for the 3'- end of the target sequence.[46]
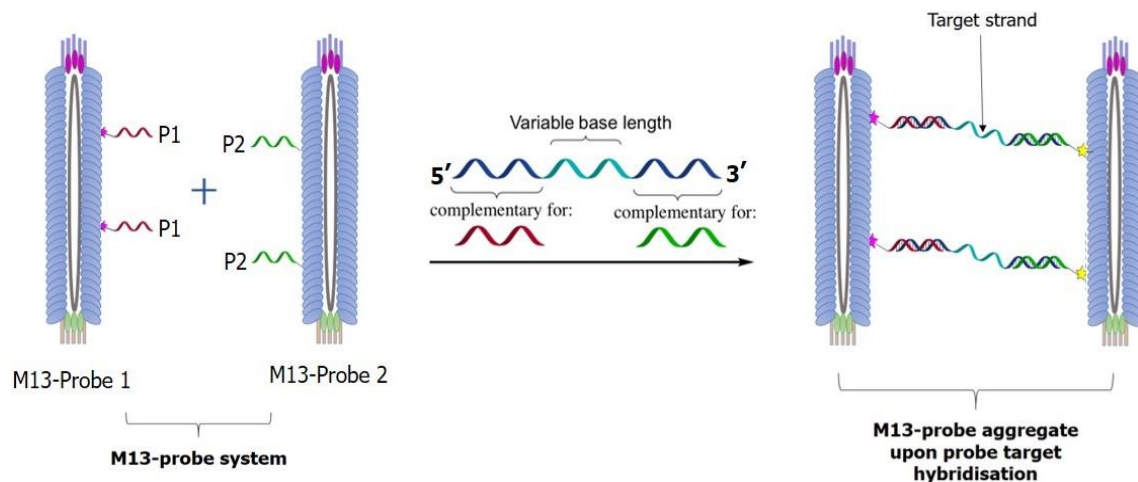
Figure 5.6 *The M13 'sandwich' assay. The left-hand side shows the M13-probes without target present and the right hand side shows the M13-probes when the correct target is present.*

Once the conjugation of the two probes to their respective M13 phages had occurred, the samples were purified using size exclusion chromatography (SEC) in order to separate the M13-probes from any free oligonucleotides (**Figure 5.7A**). In each case, the peak collected from the SEC purification was confirmed to be the M13 conjugated to the probes using gel electrophoresis (a technique discussed in detail in **Chapter 2**) (**Figure 5.7B**). Gel imaging revealed that this first peak contained some M13 bacteriophage with unconjugated pvIII proteins as well as the desired M13 bacteriophage with the conjugated pVIII proteins.[46]
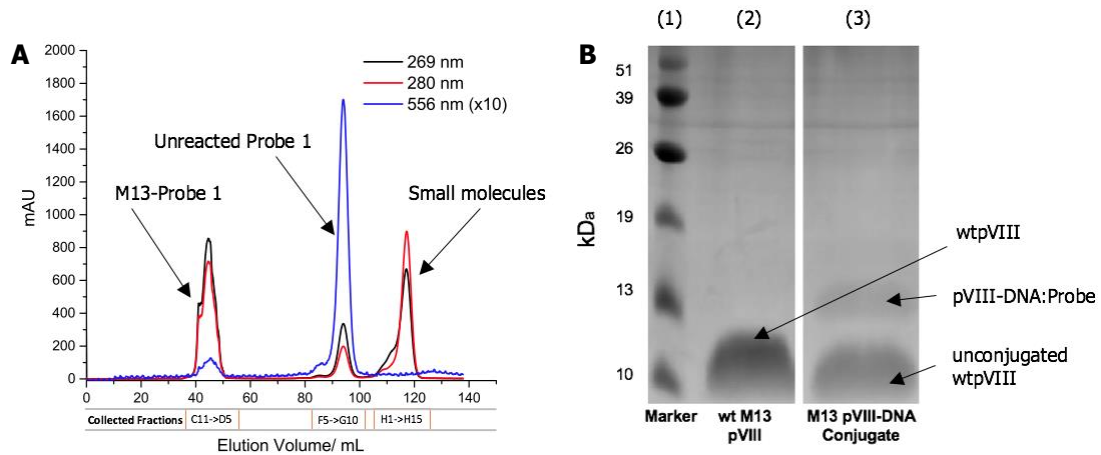
Figure 5.7 A) *An example of the SEC chromatogram after DNA (Probe 1) conjugation to M13 phage. Three different wavelengths are monitored: The wavelengths at 269 nm and 280 nm are indicative of the M13 DNA and proteins. At 556 nm the rhodamine tag on the probe can be monitored;* ***B)*** *sodium dodecyl sulphate-poly acrylamide gel electrophoresis (SDS-PAGE) of the denatured pVIII protein of WT-M13 (lane 2) vs the peak from the denatured pVIII protein of M13-probe conjugates (lane 3) and a marker in lane 1.*

In the presence of the correct target sequence, which is complementary for the two probes that are present in the sandwich assay system, a DNA hybridisation event caused the M13-probe systems to be bound together and aggregate (**Figure 5.8A**). This disturbed the alignment of the M13 in flow, causing a decrease in the signal (**Figure 5.8B**). When the experiment was repeated with a target that was non-complementary to the probes no change occurred in the LD signal.
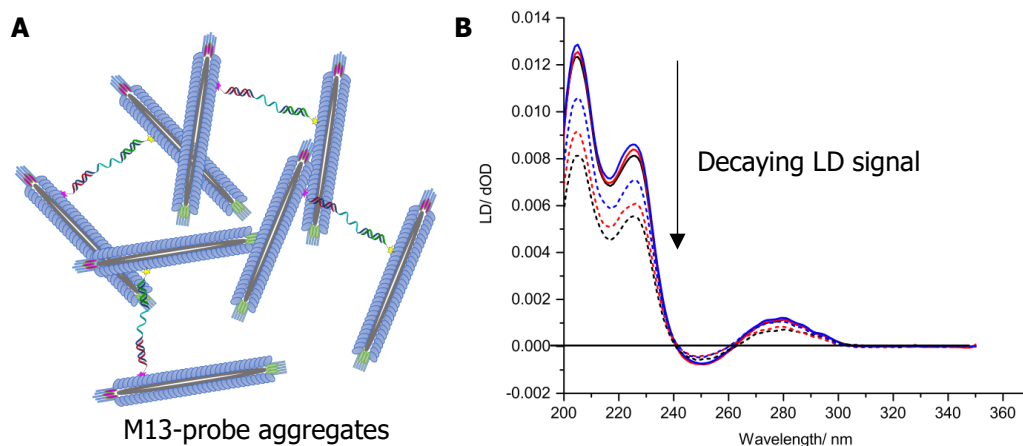
Figure 5.8 A) *the aggregation of M13-probes as the correct target causes hybridisation and duplex formation and* ***B)*** *the resulting decay in LD signal as increasing concentrations of target are added to the system.*

161

A proof-of-concept assay for the ampicillin resistance gene in the plasmid pBR322[47] was then designed in order to test its application. The assay was able to detect synthetic oligonucleotides at a sensitivity of 2 nM target concentration and was also able to discriminate between targets of varying lengths. Detection was also possible at temperatures as high as 65 °C, demonstrating that the assay was more robust than other DNA detection methods.

The decay in LD signal seen upon target binding was ascribed to the formation of an aggregated M13-probe structure. In order to determine whether this hypothesis was correct the M13-probe and target complexes were studied using transmission electron microscopy (TEM) on a copper nanogrid. The results can be seen in **Figure 5.9**. The TEM experiments proved that when the target was not present, or a non-specific target was present, the M13-probes did not form super structures. However, when the target was present, an aggregate was seen, which was consistent with the decay in LD signal being due to a decrease in alignment of the M13-probes and an increase in aggregation as a result of target binding.
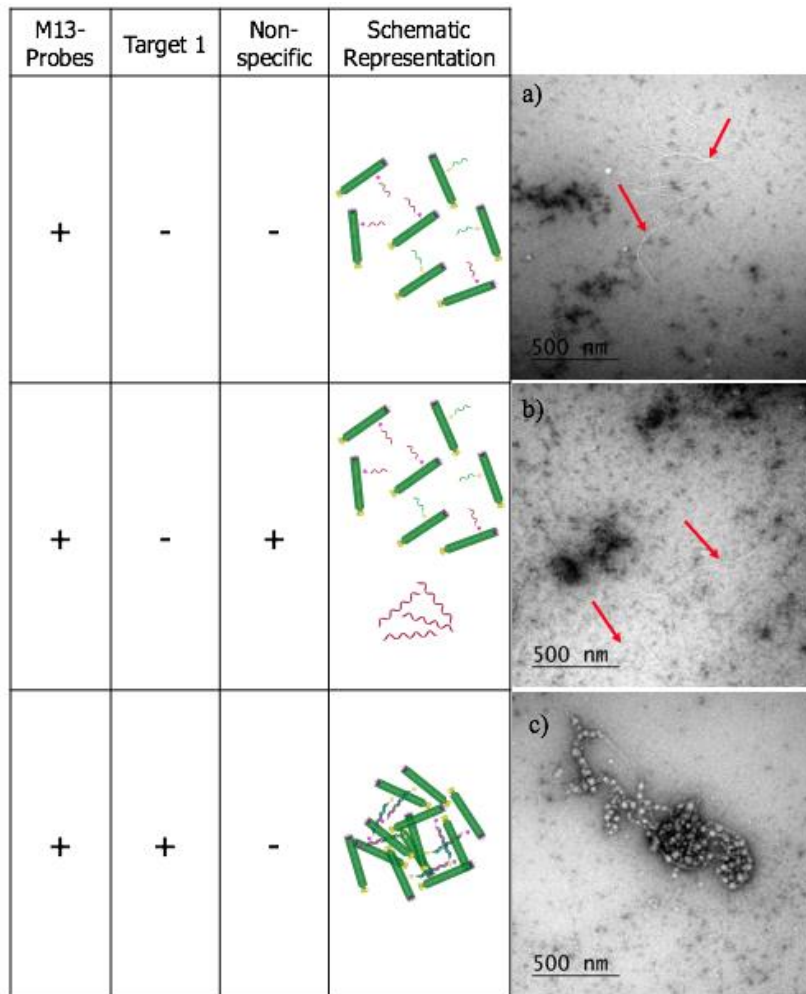
Figure 5.9 *TEM images of a) M13-probes with no target present, b) M13-probes with non-specifc DNA, and c) the M13-probes with the correct target present. The dark patches are hypothesied to be uranyl acetate precipitation due to residual buffer being left within the samples. The red arrows point to the M13-probes that can be seen by thin white lines demonstrating their filamentous structure.*

This study showed the potential of an LD based detection system for a wide range of targets and became the basis of the potato virus detection system in this chapter.

5.4 Aims of project

Despite the success of this proof-of-concept study, further aims were identified as follows:

A primary aim was to further develop the lab-based LD assay system to detect new targets. One of these was chosen to be the potato virus strain (PVY) both as a synthetic target and also the PVY coat protein (CP) gene within a dsDNA plasmid commonly utilised in industry to study the virus. A novel high-throughput assay method was also to be tested by using samples in a 96-well plate monitored at one wavelength (205 nm).

The secondary aim of this project was to simplify the system for in-the-field use by determining whether the assay could be multiplexed to detect two viruses at once (with the use of dyes conjugated to the M13-probe systems). This was a two-fold process and was carried out as follows:

1. The design of a novel system whereby both probes (probe 1 (P1) and probe 2 (P2)) for one target (e.g. just PVY) were to be added to one phage (**Figure 5.10**). If successful, this system would reduce the amount of oligonucleotide and bacteriophage material utilised and also decrease the steps required to create an M13-probe-dye conjugated system.
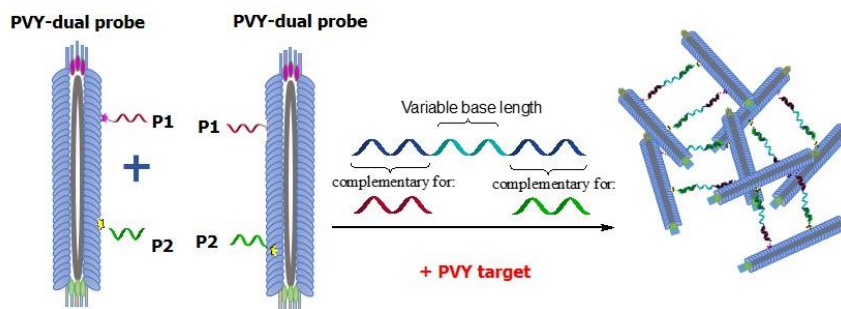
Figure 5.10 *The 2 probe, 1 phage sandwich assay where P1 and P2 are the probes for the PVY virus and are conjugated onto the same phage.*

2. A Cy3 dye was to be added to one bacteriophage system, discussed in the step above, that detects one target (the PVY virus) and a Cy5 dye to be added to another system that detects a second target (the PVA virus). The decrease in LD signal at a particular dye wavelength would then indicate which target is present in the system (**Figure 5.11**). This sensing system with the Cy3 and Cy5 dyes would also allow for the design of an assay that operates in the visible region leading to potential in-the-field devices that are simple and portable.
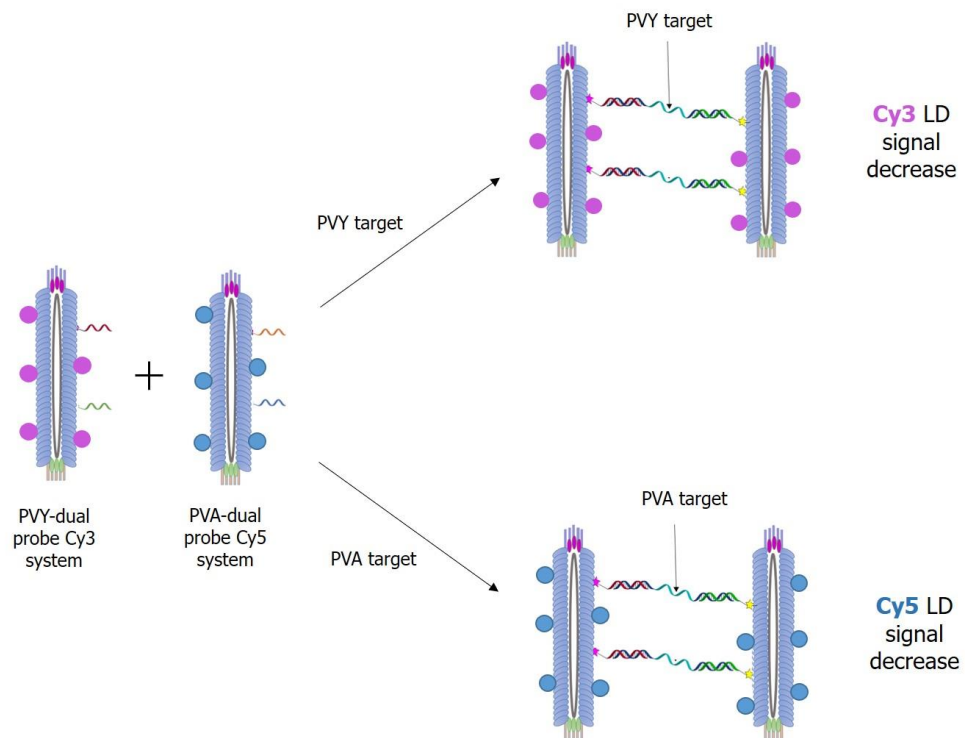
Figure 5.11 *The two probe, one phage system conjugated to either a Cy3 dye (pink) for the PVY target or Cy5 dye (blue) for the PVA target. When the PVY target is present a decrease would be seen in the Cy3 signal under LD and when the PVA target is present, a decrease in the Cy5 signal would be seen.*

5.5 Results and Discussion

5.5.1 PVY DNA sensor design, purification and characterisation

The PVY detection system was designed using the DNA probes and targets that are commonly used for PCR based reactions to detect potato viruses (**Table 5.2**).[4] The target was chosen to be the coat protein cDNA sequence generated after reverse transcription of the gene from the PVY virus. In order to easily determine whether the probes had conjugated to the M13, a fluorescent tag, fluorescein, was incorporated into both strands (**Figure 5.12**). These fluorescent tags would also enable the monitoring of the fluorophore absorption at 495 nm during the size exclusion chromatography (SEC) purification of the M13-probe systems.

The DNA probes were designed to be 21 bases long with poly thymine (polyT) linker bases on the 5'- end of probe 1 and the 3'- end of probe 2 in accordance with previous studies[46] that had established that this was the optimum length of probe for sensitive target detection. PVY probe 2 (**PVY-P2**) and the PVY target were synthesised using solid-phase oligonucleotide synthesis (**Chapter 2**) and PVY probe 1 (**PVY-P1**) was purchased from Sigma Aldrich. The purity of all oligonucleotides were checked using reverse phase high performance liquid chromatography (RP-HPLC). The purified oligonucleotides were characterised using negative electrospray ionisation mass spectrometry (ESI-MS) (negative mode). The RP-HPLC and ESI-MS results are displayed in **Table 5.2** and the resulting chromatograms and spectrums can be seen in **Appendix 7.3.1**.

Table 5.2 *The oligonucleotide sequences for the PVY probes and targets (including a non-specific (NS) target) used within this research. The **SH** represents a thiol modification and the **FAM** represents the fluorescein modification. The PVY-P1 was purchased from sigma Aldrich and so the mass and the HPLC purity have not been included here.*

Name	Sequence (5' -> 3')	Expected Mass	Observed Mass	HPLC purity (%)
PVY P1	**HS** – **FAM**- TTTTTTTTTTGAAAATGGAACC	7437	N/A	N/A
PVY P2	TCGCCAAATGTCATTTTTTTTT – **FAM** - **SH**	7554	7555.8	98
PVY Target	TGA CAT TTG GCG AGG TTC CAT TTT CA	7967.2	7966.24	98
NS control	TGA AAA TGG AAC CTC GCC AAA TGT CA	7972.51	7971.32	100

6-Fluorescein (6-FAM)

SH-3'

5'-HS
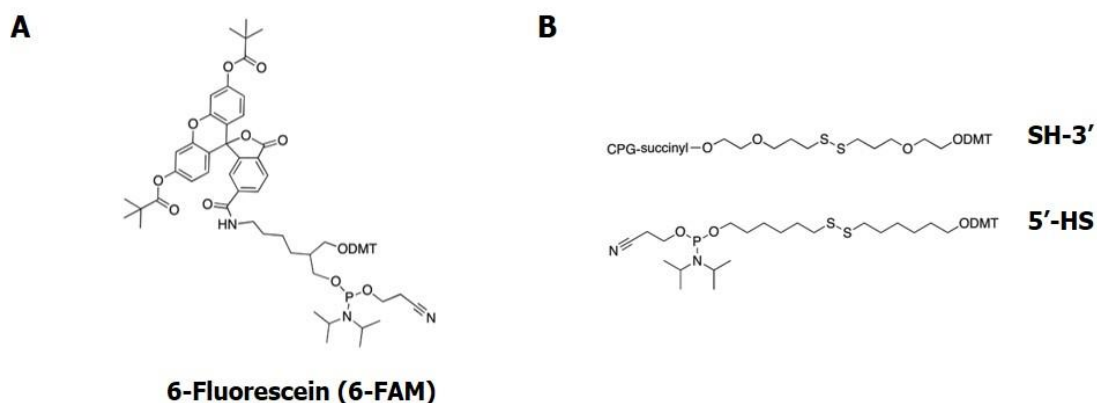
Figure 5.12 A) *the fluorescein phosphoramidite monomer used to tag the oligonucleotide probe for visualisation during the SEC purification procedure post conjugation of the probes to the M13. The DMT group represents the dimethoxytrityl protecting group and **B)** the disulphide monomers that are reduced to form thiol groups for the conjugation of the probes to the M13. The SH-3' is used for probe 2, to conjugate to the M13-phage from the 3'- end and the 5'-HS is used for probe 1, to conjugate to the M13-phage from the 5'-end. The DMT group represents the dimethoxytrityl (DMT) protecting group and the CPG is the controlled pore glass column used during solid phase oligonucleotide synthesis.*

5.5.2 M13 bacteriophage purification and characterisation

Once the DNA probes were made and purified, the next stage of the assay was to produce the M13 bacteriophage. The M13 was produced through infection of *Escherichia coli* (*E. coli*) with a small amount of seed virus. Upon overnight incubation the virus subverts the protein production machinery in the bacterium to produce many copies of its own structure, thereby amplifying the concentration of M13 in solution. Once this has occurred it is relatively straightforward to purify the phage from the broth using a well characterised set of extraction steps (**Chapter 6**).[46]

After M13 production its concentration was determined using UV-vis spectroscopy (**Figure 5.13A**) using λ_{max}=269nm, and assuming ε (at 269 nm) of 3.84 cm^{2}mg^{-1}.[48] A quality check was also carried using LD to determine whether the M13 was structurally intact. As the characteristic signal was seen (**Figure 5.13B**), the M13 was ready to be used in the later bioconjugation reactions with the oligonucleotide probes.
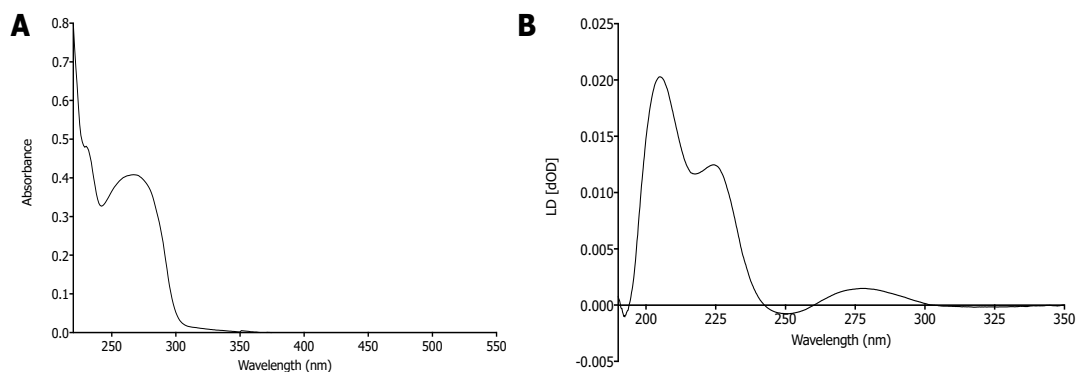
Figure 5.13 A) *The characteristic UV-vis spectrum of M13 and **B)** The characteristic LD spectrum of M13 under Couette flow alignment. The M13 samples were characterised in 100 mM potassium phosphate buffer, 150 nM NaCl, at pH 7.2, at room temperature (RT).*

Before conjugation of the DNA to the M13 it was important to determine whether the oligonucleotides modified with the thiol and fluorescein were still able to bind the synthetic PVY target sequence. To assess this native polyacrylamide gel electrophoresis (native-PAGE) (**Chapter 2**) binding studies were carried out (**Figure 5.14** and **Table 5.3**). After several repeats of the native-PAGE gels they were not showing intense or clean bands as desired however, the simultaneous binding of PVY-P1 and PVY-P2 to the target could still be evidenced by the

appearance of a higher band than that for both the probes and the target alone (**Lane D** of **Figure 5.14**). As this target sequence is commonly used in RT-PCR assays for the detection of the PVY virus it was assumed that the binding of this sequence to its target sequences will be sufficient enough to carry out further studies.[4]
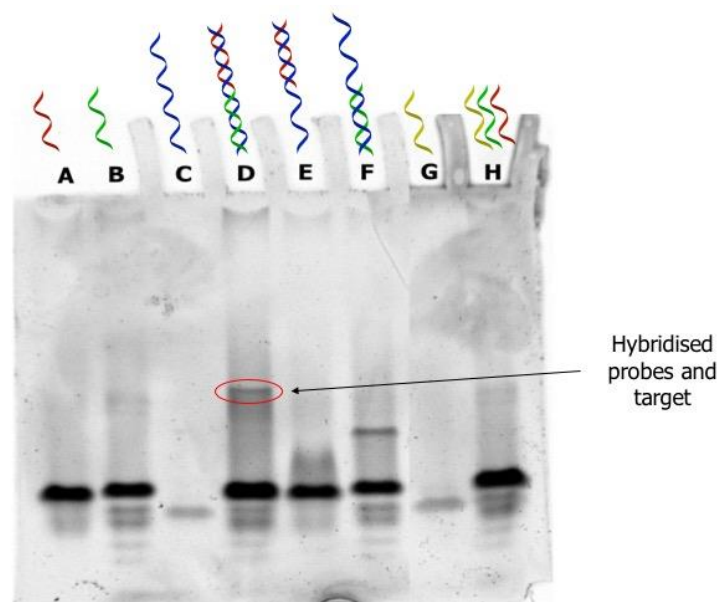
Figure 5.14 *A native-PAGE of the PVY probes and targets to provide evidence for probe hybridisation to the PVY CP target used in this assay. All binding studies were carried out at 1 μM DNA concentration 100 mM potassium phosphate buffer, 150 nM NaCl, at pH 7.2.*

Table 5.3 *The content and concentration of DNA in each well of the gel seen in* **Figure 5.14**.

Lane	DNA content	DNA concentration (μM) in 20 μL
A	PVY-P1	1
B	PVY-P2	1
C	PVY Target	1
D	PVY-P1 + PVY-P2 + PVY Target	1
E	PVY-P1 + PVY Target	1
F	PVY-P2 + PVY Target	1
G	NS control	1
H	PVY-P1 + PVY-P2 + NS control	1

5.5.3 M13 bacteriophage bioconjugation

Once the bioconjugation procedure[40] had been carried out, the M13-probe conjugates were purified to remove any DNA probes that had not undergone conjugation (see **Chapter 6** for more details). Purification was carried out using SEC, as discussed earlier in this chapter and in **Chapter 2**. During the elution procedure, three different wavelengths were monitored to determine which peaks contained the M13-probe conjugates and which contained any unreacted DNA or small molecules. The 269 nm signal provides information on the M13 bacteriophage (the protein capsid), the peak at 260 nm is indicative of DNA from both the virus and probes and the one at 495 nm corresponds to the fluorescein tag on the oligonucleotide probe (**Figure 5.15**). The peak for the fluorescein tag was used to identify the probes on the absorbance spectrum and to ensure that there was a way to provide quantitative evidence of the bioconjugation procedure.
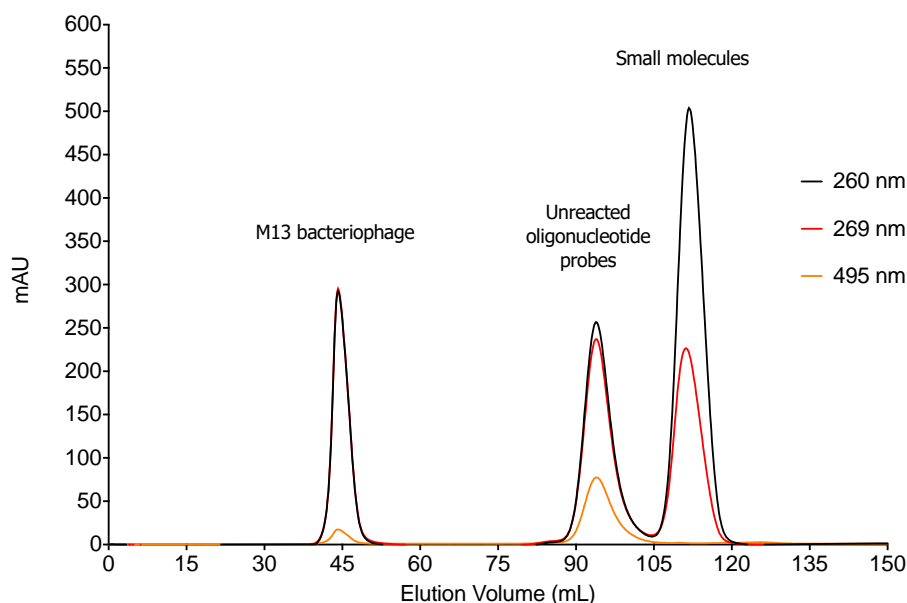
Figure 5.15 *An example of the size exclusion chromatogram produced during the purification of the M13-phage after conjugation to PVY P1. All samples were eluted into 100 mM potassium phosphate buffer, 150 nM NaCl, at pH 7.2, at RT.*

The samples eluted from each peak were confirmed by mass spectrometry by previous members of the Tucker group[46] and were found to be as follows: The first peak that eluted, at approximately 40 mL in the chromatogram, contained the desired M13-probe conjugates, along with any unconjugated M13 (referred to as wild type M13 (WT-M13)), as these have the largest

masses. This was confirmed by UV-vis spectroscopy and LD spectroscopy and the results can be seen in **Figure 5.16**. This was as expected as the M13-probe conjugates are less retarded on the column and are eluted first into what is known as the void volume (V_0). The second peak at approximately 90 mL represents unreacted oligonucleotide probe as indicated by the high intensity of the 495 nm signal. The final peak begins eluting at approximately 105 mL and consists of the other small molecules, for example L-cysteine, which was involved in the bioconjugation procedure. The chromatogram suggests that only a small number of oligonucleotide probes were conjugated to the M13 as the 495 nm absorbance peak of the fluorescein in fraction one compared to fraction two is very small. Previous work had established that approximately 100 SMCC groups are incorporated onto the M13-phage during each conjugation reaction.[46] Once the M13-probes had been purified, the concentration of sample was determined using UV-vis spectroscopy. The typical absorbance spectra of the M13-probe 1 conjugate can be seen in **Figure 5.16A**. The appearance of a fluorophore peak at λ_{max}=495nm, provides evidence for successful probe conjugation, compared to the M13 spectrum seen in **Figure 5.13A**.

The fractions eluted from the purification were run on a UV-vis spectrophotometer to determine the concentration of M13-probe in each fraction. LD spectroscopy was also undertaken to ensure that the M13-probe samples gave a characteristic LD spectrum, to confirm that the structure of the M13 was still intact after conjugation of the DNA probes. The higher the concentration of the M13-probe fraction under UV-vis spectroscopy (**Figure 5.16A**) the stronger the LD signal observed (**Figure 5.16B**).
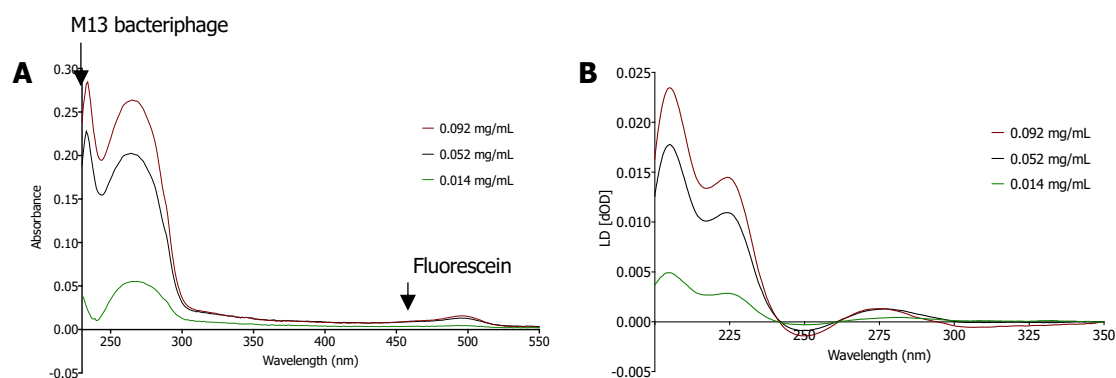
Figure 5.16 A) The UV-vis absorbance spectra of all the fractions eluted in peak 1 from the SEC purification in *Figure 15* and *B)* The corresponding LD spectra of all the eluted fractions of PVY M13-probe 1. All samples were in 100 mM potassium phosphate buffer, 150 nM NaCl, at pH 7.2, at RT.

5.5.3.1 Effect of bioconjugation on LD alignment

A potential problem with the assay was that conjugation of the DNA probes to the pVIII protein of the M13 could result in a disruption to the M13 alignment, resulting in a reduction in the LD signal. However, the data in **Figure 5.17** demonstrates only a small change in LD signal between WT-M13 and the PVY M13-probe system. The PVY M13-probe system refers to a sample mixture that contains both the M13 conjugated to probe 1 (M13-P1) and the M13 conjugated to probe 2 (M13-P2). This indicated that the phage alignment was not significantly affected by DNA conjugation. This was similar to the previous studies conducted.[46]
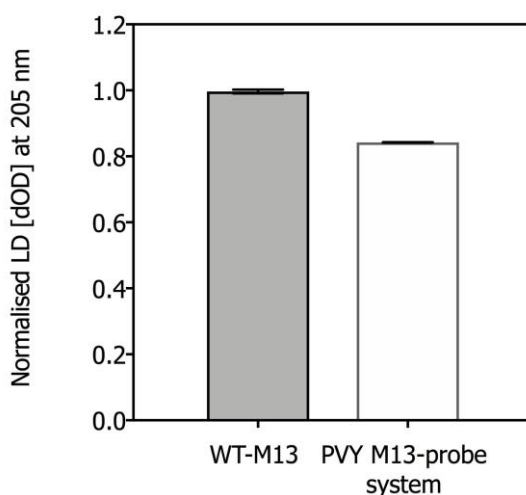
Figure 5.17 *The LD signal at 205 nm of WT-M13 versus the LD signal at 205 nm of the PVY M13-probe system (both samples were at 1 nM concentration of phage). All samples were in 100 mM potassium phosphate buffer, 150 nM NaCl, at pH 7.2, at RT. Data shows n=3 and one standard deviation.*

5.5.4 PVY detection studies

The main aim of this project was to determine whether the M13-probe system could be used as an assay to detect the PVY virus. Therefore, an important step in this process was to determine whether the LD signal of the conjugated M13 could change in the presence of the target, as outlined below.

5.5.4.1 Control studies

To ensure any decay in LD signal seen in the later experiments was due to the M13-probe system binding to the PVY target, and not any non-specific interactions, control studies were undertaken. The results showed that firstly no decay in LD signal, compared to the WT-M13 alone, when an equimolar amount of either the PVY target or the non-specific (NS) control was added to WT-M13 (**Figure 5.18A**). A similar result was seen when the NS control was added to the PVY M13-probe system (**Figure 5.18B**).
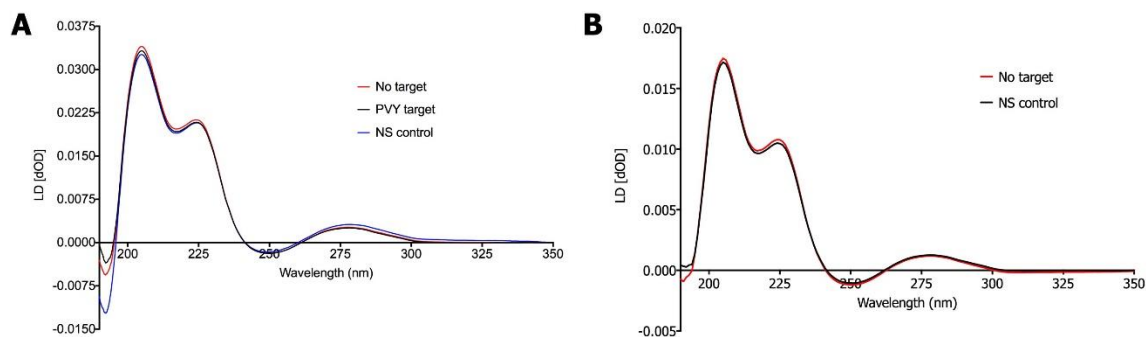
Figure 5.18 A) *The LD spectra of the WT-M13 (red), the WT-M13 with the PVY target (black) and the WT-M13 with the NS control (blue) and **B)** The LD spectra of the PVY M13-probe system with no target (red) and the NS control (black). The samples were at 1 nM in 100 mM potassium phosphate buffer, 150 nM NaCl, at pH 7.2 at RT.*

5.5.4.2 PVY detection

The next step was to determine whether the PVY target could be detected using LD spectroscopy. This was done by adding aliquots of target oligonucleotide to the PVY M13-probe system and monitoring the change in LD signal upon each addition. The signal was differentiated from the noise by defining a threshold based on the standard deviation (SD). If the signal was more than 4 times the SD then it could be read as signal as opposed to noise. All data presented in this chapter has been calculated to be above this signal to noise threshold. As expected, a decay in LD signal was observed as increasing concentrations of PVY target were added to the PVY M13-probe system (**Figure 5.19A**) The lowest concentration of PVY target that could be detected was 50 pM (or 0.05 nM) (**Figure 5.19B**). This is comparable to the limits of detection of immunological methods such as the lateral flow immunoassay (sensitivity at 0.1 nM)[49-50] and other DNA based detection methods (sensitivity at 2 nM)[51] that do not require amplification.
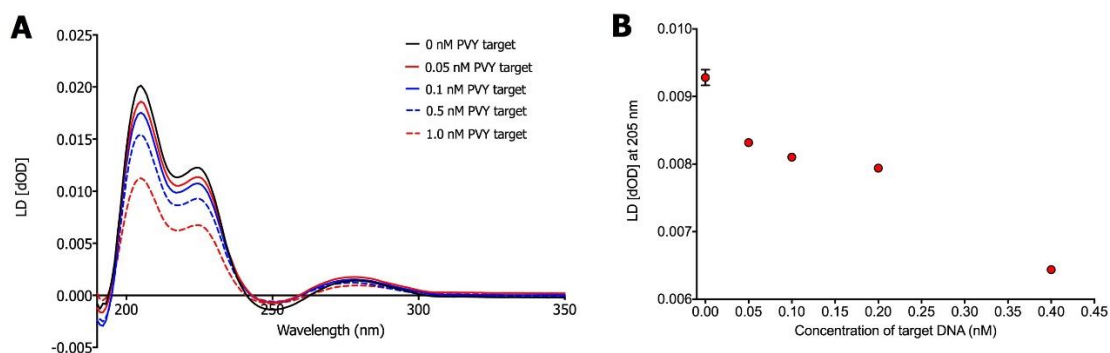
Figure 5.19 A) *The full LD signal decay of the PVY M13-probe system after the addition of increasing equivalence, up to 1 nM, of PVY-target compared to phage and **B)** the decay in LD signal at 205 nm of the PVY M13-probe system with increasing concentrations between 0 nM and 0.4 nM PVY-target for sensitivity studies. The concentration of the PVY M13-probe system was at 1 nM. The samples were in 100 mM potassium phosphate buffer, 150 nM NaCl, at pH 7.2, at RT. Data shows n=3 and one standard deviation.*

5.5.4.3 A novel high-throughput LD system

One of the benefits of ELISA tests is the ability to use a 96-well plate for detection which increases the number of samples that can be analysed at one time. Up to this point, all previous work on the LD assay system had involved the time-consuming process of recording an LD spectrum for each sample. However, in order to create a high throughput detection device, ideally there would be a set-up whereby changes at one specific wavelength can be monitored, rather than taking a whole spectrum. Also, the system should be able to detect more than one sample (multiplexing) without the need for manual insertion of samples, one by one.

A high-throughput system, based on 96 well plates (designed and assembled by Dr Charles Moore-Kelly within the Dafforn group) had previously been created that enables the detection of the samples at one wavelength, the M13 peak at 205 nm. Each sample is injected along a quartz capillary which induces alignment in the M13 with its long axis parallel to the flow direction in a Couette cell (**Figure 5.20**). Using this novel system, to begin with aliquots of the PVY target were added to WT-M13, set at a concentration of 1 nM. As expected, no change in LD signal was observed (**Figure 5.21A**).
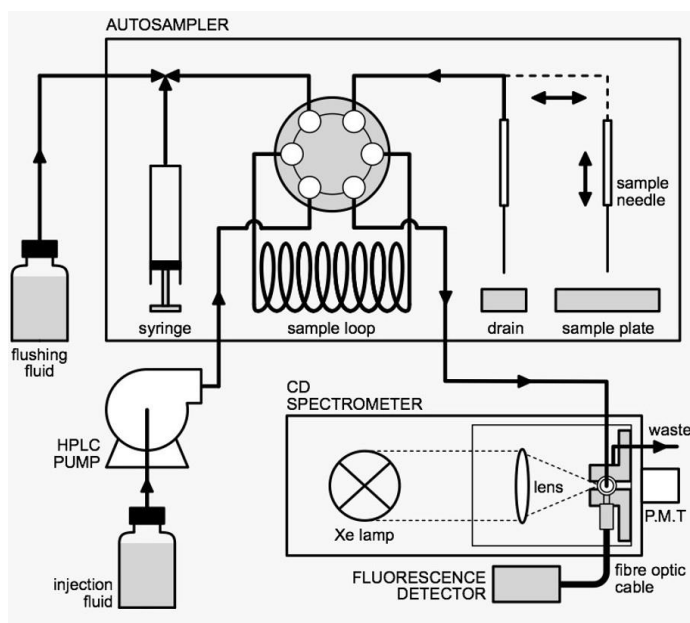
Figure 5.20 *A schematic that demonstrates the high-throughput LD system created by Dr Charles Moore-Kelly within the Dafforn group. The sample is sent from a 96-well plate by an autosampler using a HPLC pump into the LD spectrophotometer.*
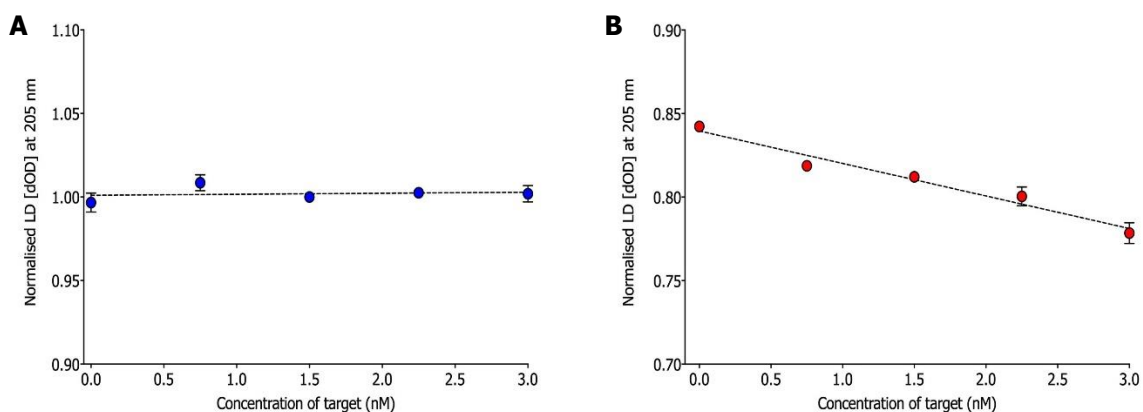
Figure 5.21 A) *The change in alignment of 1 nM WT-M13 without any probes conjugated with increasing equivalence of PVY target and **B)** the change in alignment of 1 nM of M13-P1 and M13-P2 with increasing equivalence of PVY target. All samples were in 100 mM potassium phosphate buffer, 150 nM NaCl, at pH 7.2, at RT. Data shows n=3 and one standard deviation with linear regression analysis and line of best fit.*

Then the PVY target was added in the same way to the PVY M13-probe system. LD data from these samples showed a concentration dependent decrease in LD signal amplitude (**Figure 5.21B**), which was consistent with binding to the PVY target by the PVY M13-probe system, causing a decrease in alignment.

5.5.4.4 Plasmid detection system

In order to make the assay more relevant to the detection of raw target samples, a double stranded DNA (dsDNA) target was required. In order to test the hypothesis that dsDNA could also be detected by the probe system a plasmid containing the same PVY CP gene was chosen. A small volume of such a plasmid was a kind donation by Dr Christophe Lacomme from the Science and Advice for Scottish Agriculture (SASA). Once it had been confirmed (through DNA sequencing) that the PVY CP gene sequence was present within the plasmid (**Appendix Section 7.3.2**), the same LD experiment was repeated. To facilitate melting of the plasmid, the solution was first heated to 85 °C, above which the M13 bacteriophage becomes unstable, to which the PVY M13-phage system was added before cooling to room temperature (RT). Plasmid detection was found to be possible using the maximum concentration of sample available (30 pM) as shown by the data in **Figure 5.22**. A control plasmid pUC19, which did not contain the PVY CP sequence, gave no change in signal under the same conditions.
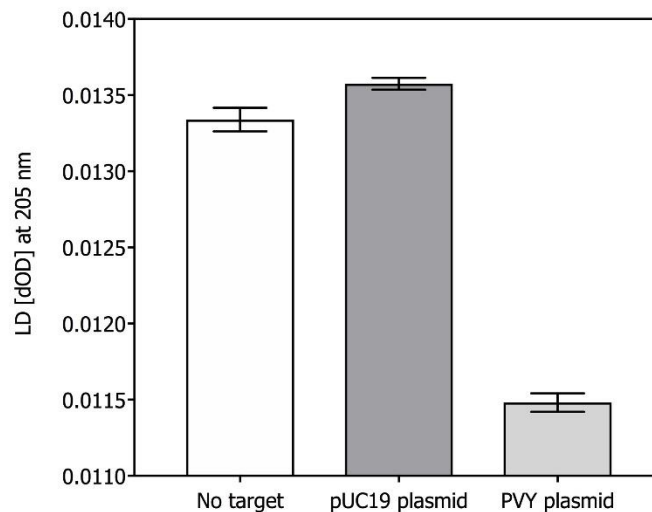
Figure 5.22 *The LD signal at 205 nm of the M13-probe system without target compared to after the addition of a control pUC19 plasmid (no decay in signal) and the PVY plasmid (decay in signal). The concentration of phage was at 1 nM and the concentration of the plasmids were at 30 pM. All samples were in 100 mM potassium phosphate buffer, 150 nM NaCl, at pH 7.2, at RT when the LD was monitored. Data shows n=3 and one standard deviation.*

5.5.5 Towards multiplexed systems

In the aims of this chapter, it was hypothesised that the detection of targets could be multiplexed to create a rapid yet simple detection device for potential in-the-field use. In order to test this, the simultaneous detection of PVY and PVA viruses was studied using an M13-probe dye conjugate system as outlined below.

5.5.5.1 PVA sensor design, purification and characterisation

As done previously for the PVY system, the PVA detection system was designed using probes and targets used for its detection in PCR based reactions within industry (**Table 5.4**).[4] The new PVA target has a completely different sequence to the PVY target (**Table 5.2**).

Table 5.4 The oligonucleotide sequences for the PVA probes and targets used for the assay. The **SH** represents a thiol modification and the **FAM** represents the fluorescein modification.

Name	Sequence (5' → 3')	Expected Mass	Observed Mass	HPLC % purity
PVA-Probe 1	SH – FAM- TTTCCACGCTTAAAATCAATG	7376	N/A	N/A
PVA-Probe 2	ACATCAAAACTGACACTTTTT–FAM-SH	7246	7247	100
PVA Target	AGTGTCAGTTTTGATGTCATTGATTTTAAGCGTGG	10853	10853	99.91
NS Control	TGA AAA TGG AAC CTC GCC AAA TGT CA	7972.51	7971.32	100

In order to determine whether the thiol and fluorescein modifications were still able to bind the PVA target, native gel electrophoresis binding studies were carried out as also done previously for the PVY system. The probes were designed to be 21 bases long with poly thymine (polyT) linker bases at the 5'- end of probe 1 and at the 3'- end of probe 2. In electrophoresis experiments, the binding of PVA probe 1 (**PVA-P1**) and PVA probe 2 (**PVA-P2**) to the complementary PVA target was evidenced by the appearance of a higher band than both the probes and the target alone (**Lane D** of **Figure 5.23**). The conditions in each well are given in **Table 5.5**.

179
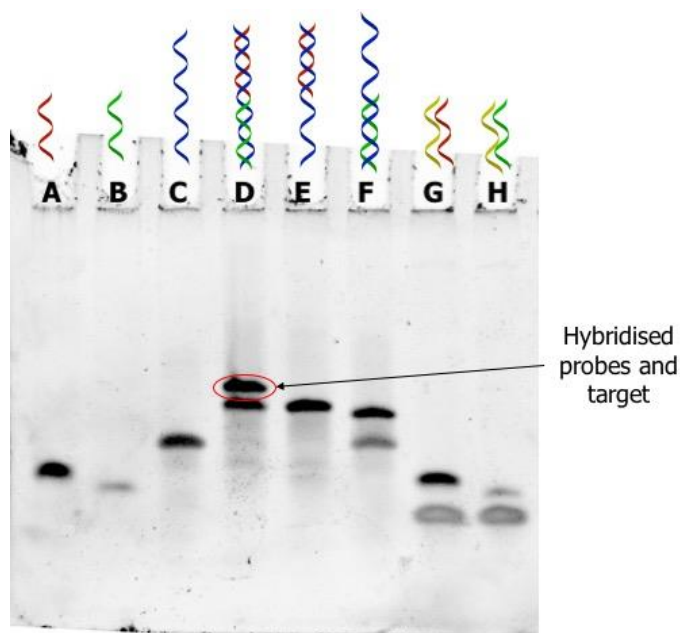
Figure 5.23 *A native-PAGE of the PVA probes and targets to provide evidence for probe hybridisation to the PVA CP target used in this assay. All binding studies were carried out at 1 µM DNA concentration 100 mM potassium phosphate buffer, 150 nM NaCl, at pH 7.2.*

Table 5.5 *The contents and concentration of DNA in each well of the native-PAGE gel in* **Figure 5.23**.

Lane	Lane content	DNA concentration (µM) in 20 µL
A	PVA-P1	1
B	PVA-P2	1
C	PVA Target	1
D	PVA-P1 + PVA-P2 + PVA target	1
E	PVA-P1 + PVA target	1
F	PVA-P2 + PVA target	1
G	PVA-P1 + NS control	1
H	PVA-P2 + NS control	1

5.5.5.2 Two probe, one phage system

As described in the aims section, for a multiplexed system it was hypothesised that the assay could be simplified by using a two probe, one phage system. In other words, a sandwich assay system was now considered whereby both probes (probe 1 and probe 2) for the target sequences of interest were conjugated to one M13 phage rather than two. The assay would work in the same way as described previously (**Figure 5.10**) except that less material would be used and the conjugation steps would be reduced, allowing for a less complicated system that could still be adapted for the addition of dye tags later.

M13 with two different DNA probes attached were therefore prepared with probe 1 and probe 2 for the PVY target conjugated to one phage and probe 1 and probe 2 for the PVA target conjugated to another (**Figure 5.10**). The systems were named PVY-dual probe and PVA-dual probe respectively. The hetero-functionalised phages were prepared and purified using the previously described bioconjugation procedure (details in **Chapter 6**). However, this time two different probe strands were added to the M13 at the same time. To determine whether this new system could function as desired, 1 nM of each M13-probe was treated with 1 nM of target. As expected, the alignment of the PVY-dual probe phage only decreased when the PVY target was present along with its complementary strand (**Figure 5.24A**). The same occurred for the PVA-dual probe phage in the presence of the PVA target only (**Figure 5.24B**).
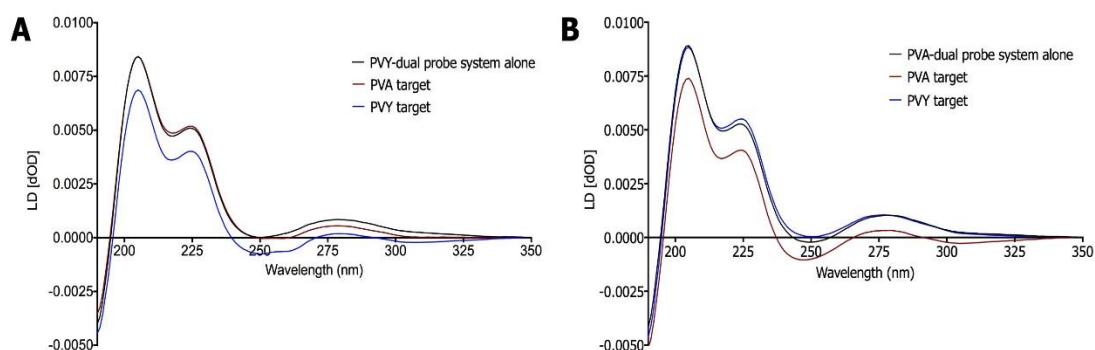
Figure 5.24 *LD spectra of the two probe, one phage system.* **A)** *PVY-dual probe phage demonstrating a decay in signal only when the PVY target is present;* **B)** *PVA-dual probe phage demonstrating a decay in signal only when the PVA target is present.* *All samples were in 100 mM potassium phosphate buffer, 150 nM NaCl, at pH 7.2, at RT.*

An interesting phenomenon can be seen in these LD results. If binding were leading to a universal loss in alignment then all the peaks would tend towards a zero value. In other words, the data should show all the positive peaks decreasing and all the negative peaks increasing until the LD d[OD] value becomes 0, showing a fully unaligned M13 aggregate. However, as can be seen in **Figure 5.24A** and **Figure 5.24B** all the peaks decrease towards more negative values when the probes bind their respective targets. A similar phenomenon was seen in the PCR-based assay designed previously within the group (discussed in **Chapter 1**).[40] The work published described the process of using PCR to amplify strands of DNA attached to an M13 scaffold in which PCR was triggered by DNA target binding. The presence of the amplified target strand resulted in an inversion of the LD signal (**Figure 5.25**) rather than its hypothesised disappearance.[40] If the original signals of the M13 under LD are examined, the pVIII protein is oriented at a 20° angle compared to the long axis of the virus. From the literature, it is known that if the virus aligns at exactly 54.7°, then no LD signal will be seen. In contrast, if the angle is aligned at less than or greater than 54.7°, a positive or negative LD signal will be seen respectively.[52] This means that with the pVIII protein angled at 20° all that is required for a negative signal is greater than 34.7° shift away from the orientation axis. The presence of a target might be expected to increase the rotational drag of the M13 against the orientation axis, which could cause an inversion of the LD signal, which could explain the data in **Figure 5.24**. This would suggest that although the target is being detected, it is not through a complete loss in alignment but in the creation of a new alignment triggered by aggregation.
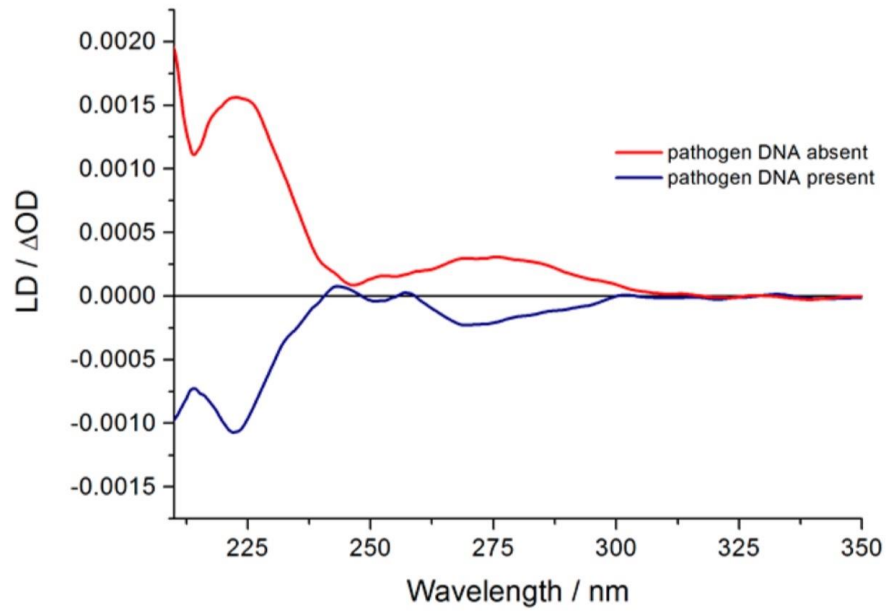
Figure 5.25 *The comparison of LD spectra published by Carr Smith et al.[40], from the target pathogen DNA being absent (red) vs the pathogen DNA being present (blue) where M13 is conjugated to primers specific to the pathogen DNA.*

5.5.6 Multiplexed detection using dye-tagged phage

With the 2 probe, 1 phage system being shown to work, the next step was to decide on two dyes that would bring the detection system into the visible region, to allow for smaller portable detection devices to be designed, and allow for the distinguishing of two DNA targets at once. The chosen dyes were Cyanine 3 (Cy3) and Cyanine 5 (Cy5), both commercially available with NHS-ester functional groups to allow for direct conjugation to the M13 after first conjugating the phage to the DNA probes. The conjugation was done in this order to ensure that the DNA probes had enough tether sites, as attaching DNA strands to phage is known to be inefficient.[46] From previous studies in the Dafforn group, Cy3 and Cy5 are known to conjugate efficiently onto M13 and align under Couette flow giving absorbance peaks of λ_{max} = 570 nm and λ_{max} = 650 nm respectively.[53] It was hypothesised that their absorption maxima would be sufficiently far enough apart that they could be used together in an assay system. The Cy3 dye was accordingly directly conjugated onto the PVY-dual probe system and the Cy5 dye conjugated onto the PVA-dual probe system by reacting the NHS-ester functionalised dyes with the the pVIII proteins of each phage. An example of what was to be the expected result can be seen in **Figure 5.26**.

PVY-dual probe **Cy3**
system

PVA-dual probe **Cy5**
system
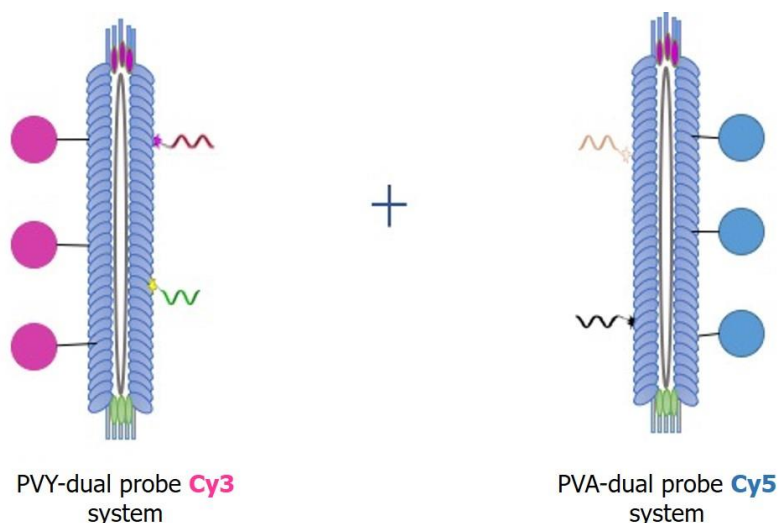
Figure 5.26 *A visual representation of the M13 with PVY probes 1 and 2 conjugated to the Cy3 dye (left) and the M13 with the PVA probes 1 and 2 conjugated to the Cy5 dye (right).*

5.5.6.1 UV-vis and LD studies of the phage-dye systems

Through UV-vis spectroscopy it could be seen that the PVY-dual probe phage Cy3 system gave a peak at 269 nm for the bacteriophage and two additional peaks at 500 nm and 550 nm attributable to the Cy3 dye (**Figure 5.27A**). Under alignment in Couette flow, the two Cy3 peaks can be observed in the LD spectrum at 515 nm and 555 nm (**Figure 5.27B**). This gave confirmation that the Cy3 had indeed been successfully conjugated onto the PVY-dual probe phage.
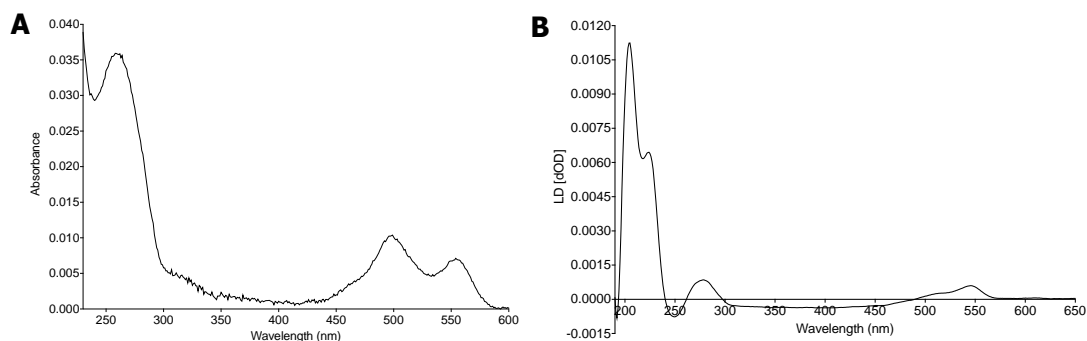
Figure 5.27 A) *The UV-vis spectrum of the PVY-dual probe phages with the Cy3 peak appearing between 550 nm and 600 nm confirming conjugation and **B)** The LD spectra of Cy3 conjugated to the PVY-dual probe phages. The appearance of peaks between 450 and 600 nm demonstrates the successful Cy3 conjugation to the PVY-dual probe phages. The sample was in 100 mM potassium phosphate buffer and 150 nM NaCl at pH 7.2 at RT.*

The same results were observed for the corresponding Cy5 system, whereby the PVA-dual phage Cy5 system gave absorption bands at 605 nm and 655 nm, attributable to the Cy5 dye (**Figure 5.28A**). Similarly, two peaks in a similar wavelength region (598 nm and 645 nm respectively) were seen in the corresponding LD spectrum (**Figure 5.28B**). This confirmed that the Cy5 had also been successfully conjugated onto the PVA-dual phage system.
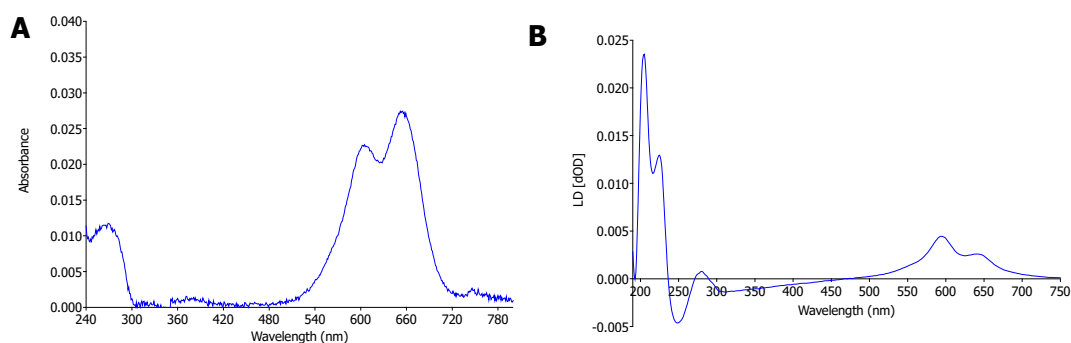
Figure 5.28 A) *The UV-vis spectrum of the PVA-dual probe phages with the Cy5 peak appearing between 550 nm and 700 nm confirming conjugation and **B)** The LD spectra of Cy5 conjugated to the PVA-dual probe phages. The appearance of peaks between 550 and 700 nm demonstrates the successful Cy5 conjugation to the PVA-dual probe phages. The sample was in 100 mM potassium phosphate buffer and 150 nM NaCl at pH 7.2 at RT.*

When comparing the absorption spectra of the PVY-dual phage Cy3 and to the PVA-dual phage Cy5 systems the ratios of dye/phage signal are considerably different suggesting more efficient conjugation of the Cy5 dye to the PVA-dual probe system. For both the Cy3 and Cy5 peaks seen in the UV absorbance and the LD spectra there are two peaks attributable to the dyes. This is known to be an indication of the dyes forming H-aggregates when bound to the bacteriophage. The H-aggregates could be as a result of covalent interactions of the dyes on the same virus or dyes on other virus particles.[54]

5.5.6.2 DNA detection with the phage-dye system

The ability of the new phage conjugates to sense target DNA was then tested. For both systems, the result was a decrease in the LD signals for both the dye and phage backbone regions of the LD spectrum in the presence of 1 nM of target DNA, confirming that the new constructs were indeed functional (**Figure 5.29A** and **Figure 5.29B**). In **Figure 5.29A** the LD peaks representing the bacteriophage backbone at 204 and 222 nm showed a decrease of 40% and 48% respectively and the LD peaks representing the Cy3 at 510 and 547 nm showed a decrease of 28% and 33% respectively.
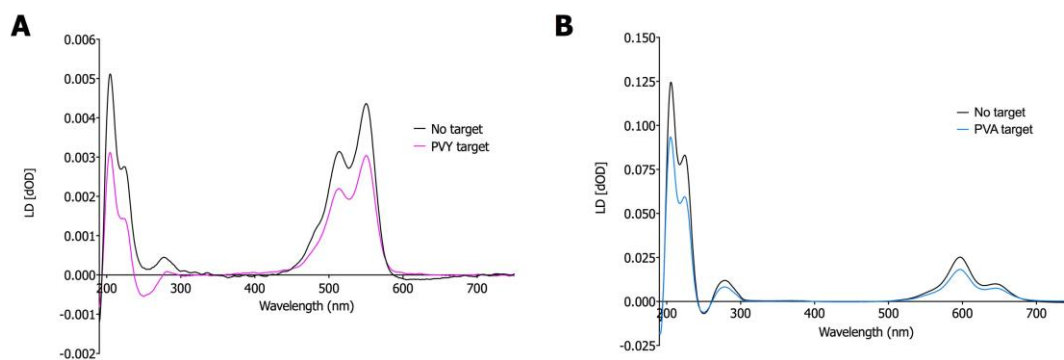
Figure 5.29 A) *The LD signal of the PVY-dual probe Cy3 system with no target present (black line) and with target present (pink line). The concentration of M13 to DNA target was 1 nM M13: 1 nM target and **B)** the LD signal of the PVA M13-probe Cy5 conjugates with no target present (black line) and with target present (blue line). The concentration of M13 to DNA target was 1 nM M13: 1 nM target. The samples were in 100 mM potassium phosphate buffer, 150 nM NaCl at pH 7.2 at RT.*

5.5.6.3 Multiplexed detection using the phage-dye systems.

The two phage-dye systems were then combined together in order to assess whether the simultaneous detection of two targets, (by comparing with the single phage spectra), was possible in one assay. The Cy3 and Cy5 peaks in the resulting LD spectrum are shown in **Figure 5.30**. The Cy3 dye is responsible for the 515 and 555 nm peaks and the Cy5 dye is responsible for the 598 nm and 650 nm peaks. Changes in the LD spectrum upon addition of the two DNA targets were then monitored at 555 and 598 nm for the Cy3 and Cy5 dye systems respectively. These peaks were chosen as they best represent the appropriate maxima of the two dyes (circled in **Figure 5.30**).
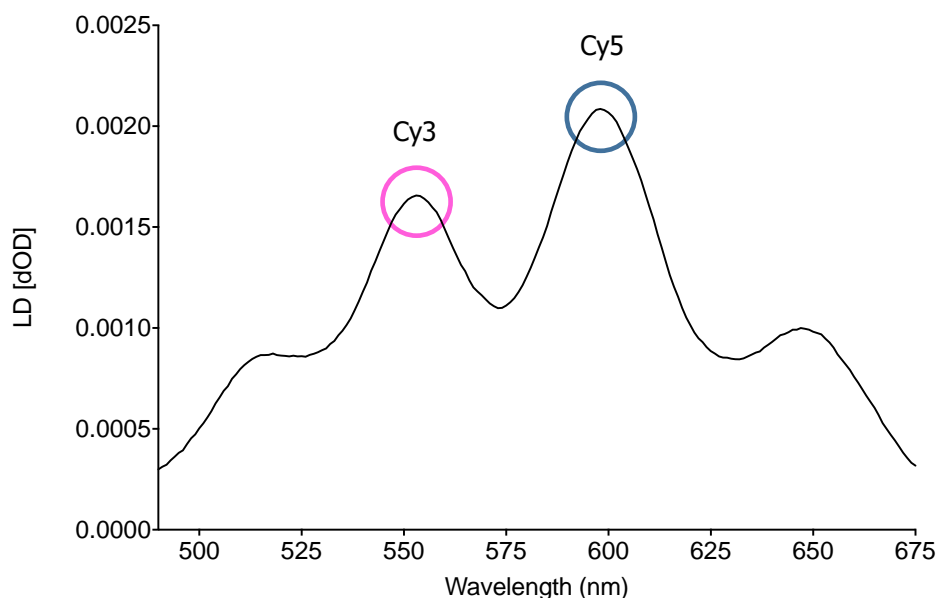
Figure 5.30 *An example of the spectra seen when the Cy3 and Cy5 M13-probes are mixed into one assay. The two highest peaks were chosen to be studied for the multiplex assay for simplicity of analysis. The two peaks can be seen circled; the pink at 550 nm is the Cy3 peak and the blue circle at 600 nm is the Cy5 peak. The samples were in 50 mM potassium phosphate buffer and 150 nM NaCl, pH 7.2 at RT.*

The change in LD alignment at these two wavelengths upon addition of PVY target (at 1 nM) to the combined system can be seen in **Figure 5.31A**. The peak at 555 nm shows a decrease of 28% in alignment, when compared to the spectra with no target, than the Cy5 peak which decreases by 8% which is as expected, indicating that the PVY target is being detected. Likewise, only the Cy5 peak shows a decrease of 24% upon the addition of the PVA target as shown in **Figure 5.31B**. A key experiment is the addition of both targets, presented in **Figure 5.31C**. In

this spectrum, both the Cy3 and the Cy5 peaks show a decrease in alignment, at 80% and 61% respectively, demonstrating that both the PVY and the PVA targets are being detected by the dye system. This shows not only can the visible region of the LD spectrum be used for target detection but crucially two DNA targets can be detected at the same time within the same assay system. In **Figure 5.31A** the PVA peak is seen to decrease along with the PVY peak which is best explained by overlap of the Cy3 and Cy5 absorbing regions. This suggests that further optimisation of the assay is required and some options are discussed in **Section 5.7**.
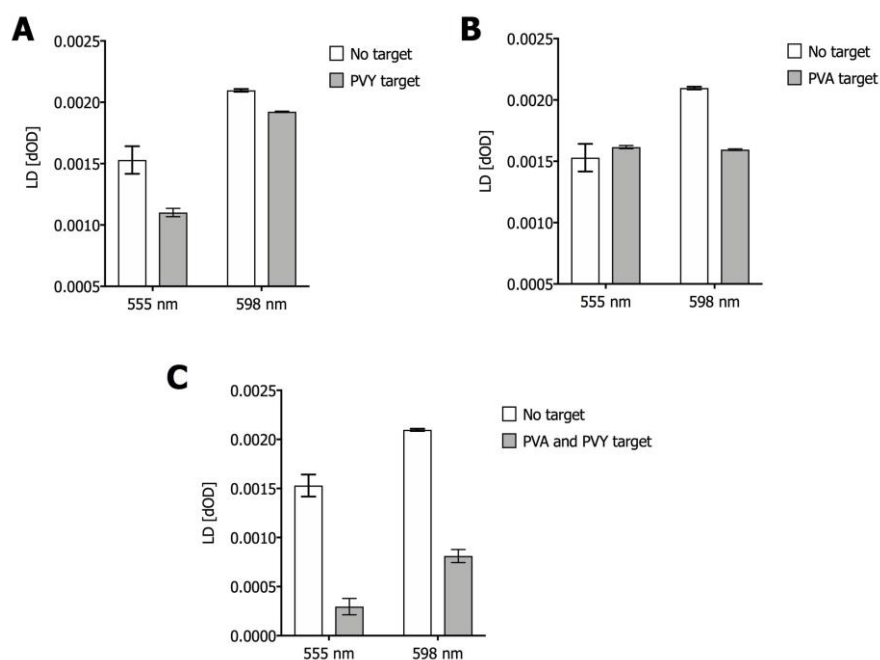
Figure 5.31 A) the LD spectra signal the combined phage-dye system with no target vs the same system with the PVY target *B)* the LD signal of the combined phage-dye system with no target vs the same system with the PVA target *C)* the LD signal of the combined phage-dye system with no target vs the system with both the PVA and PVY targets. All data show the 555 nm wavelength representing Cy3 dye and the 598 nm wavelength representing Cy5 dye. All data shows n=3 and one standard deviation. The samples were in 100 mM potassium phosphate and 150 nM NaCl at pH 7.2 at RT.

5.6 Conclusions

The successful introduction of a viral M13 DNA detection system using LD spectroscopy was demonstrated. In particular, a distinctive base sequence of the coat protein gene of the PVY potato virus was detected at a sensitivity of 50 pM. Following this, a novel 2 probe, 1 phage assay system was designed for the simultaneous detection of the PVY and PVA coat protein genes and the use of conjugated Cy3 and Cy5 dyes enabled signal read-out to occur in the visible region. Although the multiplex assay was able to detect both virus genes at once, further optimisation to make a commercially-viable assay is required.

5.7 Future Work

5.7.1 Whole Genome Viral RNA Detection

As discussed in the introduction, the PVY and PVA viruses contain an RNA genome. In order to truly test the efficiency of this assay it would be necessary to test the M13-probe system using an RNA target from the whole genome of the raw potato virus material. This would also enable the sensitivity of the LD based assay to be directly compared to other assays already available on the market for the detection of these viruses.

5.7.2 Isothermal amplification

Although the sandwich assay is sensitive down to the 30-50 pM range, certain other assays available today have lower limits of detection.[55] Furthermore, in order to create a portable in-the-field device using this assay, the instrumentation would need to be as small and simple as possible. One idea would be to incorporate an isothermal amplification method into the assay, which would not only allow for the design of simpler instrumentation with faster detection times, but also detection of targets at lower concentrations.

5.7.3 Multiplexing using different dyes

Although the absorbance spectra of the Cy3 and Cy5 dyes do not overlap significantly, they are close enough together to affect one another in the assay. The first step would be to measure the Cy3 and Cy5 at a different point by characterising the signal to noise ratio and determining whether the smaller peaks at 515 nm (Cy3) and 650 nm (Cy5) can be used for detection purposes. If this did not work, it would be beneficial to attempt the assay with dyes that have more separated absorbance spectra. Using such an approach and a greater variety of dyes would also enable the testing of more than two targets at once in order to test the limits of this multiplexing approach.

5.8 References

1. Davie, K.; Holmes, R.; Pickup, J.; Lacomme, C., Dynamics of PVY strains in field grown potato: Impact of strain competition and ability to overcome host resistance mechanisms. *Virus Research* **2017,** *241*, pp. 95-104.

2. FAO FAOSTAT: Crops. http://www.fao.org/faostat/en/#data/QC (accessed July 2017).

3. Valkonen, J. P. T., Elucidation of virus-host interactions to enhance resistance breeding for control of virus diseases in potato. *Breeding Science* **2015,** *65*, pp. 69-76.

4. Lacomme, C.; Holmes, R.; Evans, F., Molecular and serological methods for the diagnosis of viruses in potato tubers. *Methods in Molecular Biology* **2015,** *1302*, pp.161-76.

5. Lievens, B.; Thomma, B. P., Recent developments in pathogen detection arrays: implications for fungal plant pathogens and use in practice. *Phytopathology* **2005,** *95*, pp. 1374-80.

6. Brown, C. R., Antioxidants in potato. *J American Journal of Potato Research* **2005,** *82*, pp. 163-172.

7. Roger, H., *Comparative Plant Virology*. 2nd ed.; Elsevier: **2009**.

8. Taylor, M. W., What is a virus? In *Viruses and Man: A History of Interactions*, Taylor, M. W., Ed. Springer International Publishing **2014**; pp. 23-40.

9. Whitworth, J. L.; Nolte, P.; McIntosh, C.; Davidson, R., Effect of Potato virus Y on yield of three potato cultivars grown under different nitrogen levels. *Plant Disease* **2006,** *90*, pp. 73-76.

10. On the composite nature of certain potato virus diseases of the mosaic group as revealed by the use of plant indicators and selective methods of transmission. *Proceedings of the Royal Society of London. Series B, Containing Papers of a Biological Character* **1931,** *109*, pp. 251.

11. Scholthof, K. B.; Adkins, S.; Czosnek, H.; Palukaitis, P.; Jacquot, E.; Hohn, T.; Hohn, B.; Saunders, K.; Candresse, T.; Ahlquist, P.; Hemenway, C.; Foster, G. D., Top 10 plant viruses in molecular plant pathology. *Molecular Plant Pathology* **2011,** *12*, pp. 938-54.

12. Ng, J. C.; Perry, K. L., Transmission of plant viruses by aphid vectors. *Molecular Plant Pathology* **2004,** *5*, pp. 505-11.

13. Broadbent, L.; Tinsley T, W.; Buddin, W.; Roberts E, T., The spread of lettuce mosaic in the field *Annals of Applied Biology* **1951,** *38*, pp. 689-706.

14. Powell, G., Cell membrane punctures during epidermal penetrations by aphids: consequences for the transmission of two potyviruses. *Annals of Applied Biology* **1991,** *119*, pp. 313-321.

15. Radcliffe, E. B.; Ragsdale, D. W., Aphid-transmitted potato viruses: The importance of understanding vector biology. *American Journal of Potato Research* **2002,** *79*, pp. 353-386.

16. Mascia, T.; Gallitelli, D., Chapter 10 - Synergism in plant–virus interactions: A case study of CMV and PVY in mixed infection in tomato. In *Plant Virus–Host Interaction*, Gaur, R. K.; Hohn, T.; Sharma, P., Eds. Academic Press **2014**; pp. 195-206.

17. Chung, B. Y. W.; Miller, W. A.; Atkins, J. F.; Firth, A. E., An overlapping essential gene in the Potyviridae. *Proceedings of the National Academy of Sciences* **2008,** *105*, pp. 5897.

18. Wittmann, S.; Chatel, H.; Fortin, M. G.; Laliberte, J. F., Interaction of the viral protein genome linked of turnip mosaic potyvirus with the translational eukaryotic initiation factor (iso) 4E of Arabidopsis thaliana using the yeast two-hybrid system. *Virology* **1997,** *234*, pp. 84-92.

19. Leonard, S.; Plante, D.; Wittmann, S.; Daigneault, N.; Fortin, M. G.; Laliberte, J. F., Complex formation between potyvirus VPg and translation eukaryotic initiation factor 4E correlates with virus infectivity. *Journal of Virology* **2000,** *74*, pp. 7730-7.

20. Verchot, J.; Koonin, E. V.; Carrington, J. C., The 35-kDa protein from the N-terminus of the potyviral polyprotein functions as a third virus-encoded proteinase. *Virology* **1991,** *185*, pp. 527-35.

21. Torrance, L.; Andreev, I. A.; Gabrenaite-Verhovskaya, R.; Cowan, G.; Makinen, K.; Taliansky, M. E., An unusual structure at one end of potato potyvirus particles. *J Mol Biol* **2006,** *357*, pp. 1-8.

22. Revers, F.; Garcia, J. A., Molecular biology of potyviruses. *Adv Virus Res* **2015,** *92*, pp. 101-99.

23. Rodriguez-Cerezo, E.; Ammar, E. D.; Pirone, T. P.; Shaw, J. G., Association of the non-structural P3 viral protein with cylindrical inclusions in potyvirus-infected cells. *J Gen Virol* **1993,** *74*, pp. 1945-9.

24. Chung, B. Y.; Miller, W. A.; Atkins, J. F.; Firth, A. E., An overlapping essential gene in the Potyviridae. *Proceedings of the National Academy of Sciences USA* **2008,** *105*, pp. 5897-902.

25. Sorel, M.; Garcia, J. A.; German-Retana, S., The Potyviridae cylindrical inclusion helicase: a key multipartner and multifunctional protein. *Mol Plant Microbe Interactions* **2014,** *27*, pp. 215-26.

26. Schaad, M. C.; Jensen, P. E.; Carrington, J. C., Formation of plant RNA virus replication complexes on membranes: role of an endoplasmic reticulum-targeted viral protein. *The EMBO Journal* **1997,** *16*, pp. 4049-4059.

27. Carrington, J. C.; Dougherty, W. G., Small nuclear inclusion protein encoded by a plant potyvirus genome is a protease. *Journal of Virology* **1987,** *61*, pp. 2540-8.

28. Hong, Y.; Hunt, A. G., RNA polymerase activity catalyzed by a potyvirus-encoded RNA-dependent RNA polymerase. *Virology* **1996,** *226*, pp. 146-51.

29. Rojas, M. R.; Zerbini, F. M.; Allison, R. F.; Gilbertson, R. L.; Lucas, W. J., Capsid protein and helper component-proteinase function as potyvirus cell-to-cell movement proteins. *Virology* **1997,** *237*, pp. 283-295.

30. Shattock, R., *Compendium of potato diseases* Second Ed.; Wiley/Blackwell **2002**; Vol. 51, pp. 520-520.

31. Khouadja, F.; Glais, L.; Tribodet, M.; Kerlan, C.; Fakhfakh, H., Incidence of potato viruses and characterisation of Potato virus Y variability in late season planted potato crops in Northern Tunisia. *European Journal of Plan Pathology* **2010**; 126, pp. 479-488.

32. Rajamäki, M.; Merits, A.; Rabenstein, F.; Andrejeva, J.; Paulin, L.; Kekarainen, T.; Kreuze, J. F.; Forster, R. L. S.; Valkonen, J. P. T., Biological, serological, and molecular differences among isolates of potato A potyvirus. *Phytopathology* **1998,** *88*, pp. 311-321.

33. Mao, C.; Liu, A.; Cao, B., Virus-based chemical and biological sensing. *Angewandte Chemie* **2009,** *48*, pp. 6790-810.

34. Souza, G. R.; Christianson, D. R.; Staquicini, F. I.; Ozawa, M. G.; Snyder, E. Y.; Sidman, R. L.; Miller, J. H.; Arap, W.; Pasqualini, R., Networks of gold nanoparticles and bacteriophage as biological sensors and cell-targeting agents. *Proceedings of the National Academy of Sciences of the USA* **2006,** *103*, pp. 1215-1220.

35. Wu, C.; Barnhill, H.; Liang, X.; Wang, Q.; Jiang, H., A new probe using hybrid virus-dye nanoparticles for near-infrared fluorescence tomography. *Optics Communications* **2005,** *255*, pp. 366-374.

36. Petrenko, V. A.; Sorokulova, I. B., Detection of biological threats. A challenge for directed molecular evolution. *Journal of Microbiological Methods* **2004,** *58*, pp. 147-68.

37. Scott C Meyer, I. G., *Recognition receptors in biosensors: Phage display technology in biosensor development*. Springer **2010**.

38. Li, K.; Chen, Y.; Li, S.; Nguyen, H. G.; Niu, Z.; You, S.; Mello, C. M.; Lu, X.; Wang, Q., Chemical Modification of M13 Bacteriophage and Its Application in Cancer Cell Imaging. *Bioconjugate Chemistry* **2010,** *21*, pp. 1369-1377.

39. Norden, B.; Rodger, A.; Dafforn, T. R., *Linear Dichroism and Circular Dichroism: A textbook on Polarized-Light Spectroscopy*. 1 Ed.; Royal Society of Chemistry **2010**.

40. Carr-Smith, J.; Pacheco-Gómez, R.; Little, H. A.; Hicks, M. R.; Sandhu, S.; Steinke, N.; Smith, D. J.; Rodger, A.; Goodchild, S. A.; Lukaszewski, R. A.; Tucker, J. H. R.; Dafforn, T. R., Polymerase Chain Reaction on a Viral Nanoparticle. *ACS Synthetic Biology* **2015,** *4*, pp. 1316-1325.

41. Pacheco-Gomez, R.; Kraemer, J.; Stokoe, S.; England, H. J.; Penn, C. W.; Stanley, E.; Rodger, A.; Ward, J.; Hicks, M. R.; Dafforn, T. R., Detection of pathogenic bacteria using a homogeneous immunoassay based on shear alignment of virus particles and linear dichroism. *Analytical chemistry* **2012,** *84*, pp. 91-7.

42. Henry, M.; Debarbieux, L., Tools from viruses: Bacteriophage successes and beyond. *Virology* **2012,** *434*, pp. 151-161.

43. Li, K.; Nguyen, H. G.; Lu, X.; Wang, Q., Viruses and their potential in bioimaging and biosensing applications. *Analyst* **2010,** *135*, pp. 21-27.

44. Lee, J. H.; Domaille, D. W.; Cha, J. N., Amplified Protein Detection and Identification through DNA-Conjugated M13 Bacteriophage. *ACS Nano* **2012,** *6*, pp. 5621-5626.

45. Hermanson, G. T., Chapter 3 - The Reactions of Bioconjugation. In *Bioconjugate Techniques (Third Edition)*, Hermanson, G. T., Ed. Academic Press **2013**; pp. 229-258.

46. Little, H. A. The development of novel diagnostic sensors based on linear dichroism spectroscopy. Thesis. University of Birmingham, England, **2016**.

47. Sutcliffe, J. G., Nucleotide sequence of the ampicillin resistance gene of Escherichia coli plasmid pBR322. *Proceedings of the National Academy of Sciences USA* **1978,** *75*, pp. 3737-3741.

48. Berkowitz, S. A.; Day, L. A., Mass, length, composition and structure of the filamentous bacterial virus fd. *Journal of Molecular Biology* **1976,** *102*, pp. 531-547.

49. Sajid, M.; Kawde, A.; Daud, M., Designs, formats and applications of lateral flow assay: A literature review. *Journal of Saudi Chemical Society* **2015,** *19*, pp. 689-705.

50. Lindsley, M. D.; Mekha, N.; Baggett, H. C.; Surinthong, Y.; Autthateinchai, R.; Sawatwong, P.; Harris, J. R.; Park, B. J.; Chiller, T.; Balajee, S. A.; Poonwan, N., Evaluation of a newly developed lateral flow immunoassay for the diagnosis of cryptococcosis. *Clinical infectious diseases : an official publication of the Infectious Diseases Society of America* **2011,** *53*, pp. 321-5.

51. Wu, Z.-S.; Jiang, J.-H.; Fu, L.; Shen, G.-L.; Yu, R.-Q., Optical detection of DNA hybridization based on fluorescence quenching of tagged oligonucleotide probes by gold nanoparticles. *Analytical Biochem* **2006,** *353*, pp. 22-29.

52. Clack, B. A.; Gray, D. M., Flow linear dichroism spectra of four filamentous bacteriophages: DNA and coat protein contributions. *Biopolymers* **1992,** *32*, pp. 795-810.

53. Tridgett, M.; Moore-Kelly, C.; Duprey, J. H. A.; Iturbe, L. O.; Tsang, C. W.; Little, H. A.; Sandhu, S. K.; Hicks, M. R.; Dafforn, T. R.; Rodger, A., Linear dichroism of visible-region chromophores using M13 bacteriophage as an alignment scaffold. *RSC Advances* **2018,** *8*, pp. 29535-29543.

54. Tridgett, M.; Moore-Kelly, C.; Duprey, J.-L. H. A.; Iturbe, L. O.; Tsang, Chi W.; Little, H. A.; Sandhu, S. K.; Hicks, M. R.; Dafforn, T. R.; Rodger, A., Linear dichroism of visible-region chromophores using M13 bacteriophage as an alignment scaffold. *RSC Advances* **2018,** *8*, pp. 29535-29543.

55. Sanavio, B.; Krol, S., On the slow diffusion of point-of-care systems in therapeutic drug monitoring. *Frontiers in Bioengineering and Biotechnology* **2015,** *3*, pp. 20.

Chapter 6 - Experimental

6.1 Materials

The reagents and materials used within this thesis were purchased from Sigma Aldrich (Gillingham, UK) or Fisher Scientific (Loughborough, UK) and if this was not the case the supplier has been stated. All the reagents for the synthesis of the oligonucleotides were purchased from Link Technologies Ltd (Bellshill, UK) unless otherwise stated. Once the reagents or materials had been purchased no further purification was carried out.

6.2 Oligonucleotide synthesis

6.2.1 Synthesis conditions

Oligonucleotides, unless stated otherwise, were synthesised on an Applied Biosystems 394 DNA/RNA synthesizer. The DNA synthesis was carried out using the phosphoramdite method (**Chapter 1**).[1] The anthracene phosphoramidites (**Chapter 3**) were also incorporated into the relevant oligonucleotide strands using the same phosphoramidite method. The phosphoramidites are all made up to a concentration of 0.1 M.

The DNA synthesis is done in a 3′ to 5′ direction and is a cyclic process involving the following steps:

1) The first base required was attached using a controlled-pore glass resin column (CPG) and the resin washed with acetonitrile before any coupling took place.

2) A 3% trichloroacetic acid (TCA) in a dichloromethane (DCM) solvent system was used to deprotect the DMT protected bases at the 5′ end of the sequence.

3) The following phosphoramidite base, at a concentration of 0.1 M, was activated using 0.5 M Ethylthiotetrazole (ETT) and coupled to the previous base for 25 seconds.

4) If an oligonucleotide had not reacted it was capped with tetrahydrofuran (THF)/pyridine/acetic anhydride at a 70:15:15 ratio and 10% methyl imidazole in THF.

5) The resulting strand was oxidised using 0.02 M iodine THF:pyridine:water at a ratio of (70:15:15) for the formation of a phosphotriester.

6) Once all the phosphoramidites in the sequence were coupled, the oligonucleotide was cleaved from resin using an ammonia hydroxide solution (28-30% ammonium hydroxide) for 90 minutes and this was heated to 65 °C for 6 hours for the removal of the protecting groups.

Finally, the ammonia hydroxide within the solution was then removed *in vacou* and the DNA was stored at -18 °C until required.

6.2.2 Purification with reverse phase- high performance liquid chromatography (RP-HPLC)

All oligonucleotide strands were purified using Reversed Phase-High-Performance Liquid Chromatography (RP-HPLC) on a Phenomenex Clarity 5 μm Oligo RP 250 x 10 mm column on an Agilent Technologies 1260 Infinity System. A thousand microliters of sample were loaded onto the columns and the elutions were monitored using absorbance spectroscopy with the following wavelengths; 260 nm for all oligonucleotides, 495 nm for the fluorescein modified oligonucleotide strands, and 360 nm for the anthracene modified oligonucleotide strands. Once the samples were collected they were dried *in vacuo* before being dissolved in 1.0 mL of MilliQ water.

All RP-HPLC purification methods have been developed within the Tucker group in order to purify the specific modified and unmodified oligonucleotide strands synthesised within the group. All flow rates during the purifications of the oligonucleotides were set to 3 mL/min. The buffer used in all purification steps was named Buffer D and contained 0.1 M triethylammonium acetate (TEAA) in HPLC grade H_2O. A DMT-ON method was used if there were two anthracene modifications present where the solvent gradient ran from: 15-60% acetonitrile over a period of 30 minutes (85-40% of Buffer D), then 100 % acetonitrile for 10 minutes, and finally 15% Acetonitrile for 10 minutes. If only one anthracene modification was present the FcAnth method was used in which the solvent gradient ran from: 15-25% Acetonitrile over a period of 30 minutes (85-75% of Buffer D), then 100 % Acetonitrile for 10 minutes, and finally, 15 % Acetonitrile for 10 minutes. Any unmodified oligonucleotides were purified using the Short Oligo method which ran from: 5-18% Acetonitrile over a period of 30 minutes (85-82% of Buffer D), then 100 % Acetonitrile for 10 minutes, and finally, 5% Acetonitrile for 10 minutes.

The samples were desalted using a NAP-10 column (GE Healthcare). One millilitre of sample was added to the column and eluted in 1.5 mL of MilliQ® water. The purity of the oligonucleotide was

confirmed using an analytical RP-HPLC on the same Agilent system with a Phenomenex Clarity 5 μM Oligo-RP LC 250 x 4.6 mm column using the same solvent gradient as with the prior purification of the strand and a flow rate of 1 mL/min. All samples were deemed pure if the purity of the sample was above 95%.

6.2.3 Characterisation using mass spectrometry

The oligonucleotide was characterised using negative mode electrospray ionistion mass spectrometry (ESI MS). Twenty microliters of purified oligonucleotide samples (at 6 μM in MilliQ® water) were analysed on a Walters XEVO G2-XS Time of Flight (TOF) mass analyser, fitted with an Acquity UPLC C18 1.7 μM chromatography system. The predicted masses and extinction coefficients for each oligonucleotide were calculated using the online IDT OligoAnalyser tool[2] or the software ChemDraw. The oligonucleotide deconvolution was conducted using Promass (Novatia) using the deconvolution algorithm ZNova.

6.3 Polymerase chain reaction (PCR)

Any genomic DNA samples, along with the forward and reverse primers used in **Chapter 4** were donated by Dr Andrew Beggs, University of Birmingham. The PCR was carried out using the Qiagen Multplex kit (Qiagen, Germany) on a PCR thermocycler (G-Storm GS1 Thermocycler). The reaction mixture included 1 μL mutant or wild type genomic DNA both at 50 ng/μL, 0.5 μL of forward and reverse oligonucleotide primer at 0.1 μM, 25 μL of 2 x Qiagen mastermix, 10 μL of 5 x Q-solution and 14 μL of MilliQ H$_2$O. The PCR reaction was started by a 95 °C hot start for 15 minutes. The cycling conditions were at 94 °C for 20 seconds, 55 °C for 30 seconds, 72 °C for 30 seconds. This cycle was repeated 40 times and the reaction was completed at 72 °C for 5 mins.

The PCR product was purified using a DNA clean and concentrator 5 (Zymo Research, U.S.A) as per the protocol provided. The PCR product was then eluted into 15 μL of MilliQ water. The concentration of the samples was determined using a NanoDrop® 1000 spectrophotometer.

6.3.1 Agarose gel electrophoresis

The presence of PCR products, and the efficiency of the PCR reactions, were determined by agarose gel electrophoresis. A 5 μL sample of PCR product was run on a 3% agarose gel (1.5 g) in 1 X Tris/Borate/Ethylenediaminetetraacetic acid (EDTA) (TBE) buffer using UltraPure Agarose 1000 (Thermo Fisher Scientific, U.S.A). One microlitre of 5X xylene cyanol loading dye was mixed with the 5 μL of sample and loaded onto the. One lane on the gel was loaded with 5 μL of Bioline Hyperladder 25 bp (Bioline, UK) alone. The gel was run for 1 hour at 100 V. The gels were stained with ethidium bromide and visualised using a UV transluminator linked to a polaroid camera.

6.3.2 Digestion of PCR product

PCR products are double stranded but to carry out fluorescence studies single stranded DNA was required. To obtain single stranded DNA the PCR product was digested using a T7 exonuclease. To allow the samples to be digested so only the target single strand of DNA was left intact, the forward primer was modified with a phosphorothioate group on the 5' end of the sequence that blocked the T7 exounclease from binding and digesting the target strand. The samples were digested using a T7 exonculease in the 10X NEB reaction buffer provided with the enzyme (New England BioLabs, UK) overnight at 37 °C, and the enzyme reaction was stopped using formamide. The samples were sequenced using the Biosciences sequencing facility using an ABI 3730 capillary sequencer using the Sangar sequencing method. The digested samples were further purified using the same DNA clean and concentrator 5 as before (Zymo Research, U.S.A).

6.4 Ultraviolet-visible (UV-vis) spectroscopy

6.4.1 Oligonucleotide concentration determination

A Shimadzu UV-1800 UV spectrophotometer was used to measure the concentration of all the oligonucleotides that were synthesised in this project. The absorbance of the sample at 260 nm was measured in a quartz cuvette (Starna Scientific Ltd, UK) with a path length of 1.0 cm (parameters can be seen in **Table 6.1**). The extinction coefficients of the oligonucleotides were determined using IDT OligoAnalyser tool[2] and the extinction coefficient of anthracene was taken to be ε_{375nm} = 6300 $M^{-1}cm^{-1}$ from the literature.[3] To calculate the concentration of the strands the Beer Lambert law was used (**Chapter 2**).

Table 6.1 *The parameters used for the UV-vis concentration determination of all oligonucleotides.*

Range	200 – 800 nm
Response	Fast/Medium
Data pitch	0.5 nm
Scan speed	200 nm/min
Band width	1.0 nm

6.4.2 M13 bacteriophage concentration determination

To determine the concentration of the M13 bacteriophage after it had been synthesised, a Jasco V-550 UV/Vis spectrophotometer was used. The absorbance of the sample at 269 nm was measured in a Quartz cuvette (Hellma Quartz Suprasil®, Germany) with a path length of 1.0 cm.   The parameters for the absorbance measurements can be seen in **Table 6.2**. The Beer Lambert law was used calculate the concentration of the M13 bacteriophage (**Chapter 2**). The bacteriophage extinction coefficient has been calculated to be 3.84 cm^2mg^{-1}.[4]

Table 6.2 *The parameters for the UV-vis concentration determination of the M13-bacteriophage.*

Range	200 – 800 nm
Response	Medium
Data pitch	0.5 nm
Scan speed	200 nm/min
Band width	1.0 nm

6.4.3 Thermal melting of DNA (T_m)

The oligonucleotide thermal melting studies in **Chapter 4** were carried out on a Cary 5000 (Agilent Technologyies Ltd, Chesire, UK) UV-vis spectrophotometer. The instrument was fitted with a Peltier temperature controller for temperature control. The samples were monitored in a quartz cuvette with a 10 mm pathlength (Starna Scientific Ltd, UK). The cuvette cells were sealed at the top in order to stop any evaporation of sample and subsequent concentration changes. The samples were heated at 0.5 °C per minute from 15-85 °C. The absorbance of the DNA was monitored at 260 nm. All samples were at 5 µM in a buffer consisting of 100 mM NaCl and 10 mM sodium phosphate buffer (pH 7.0). Each thermal denaturation run consisted of 3 denaturation and 2 annealing ramps.

6.4.4 *Anthracene photoirradiation*

For photoirradiation of the anthracene modified aptamer samples the samples were made up to 2.0 µM in TBA buffer (content of buffer noted below). All samples were de-gassed using argon for 10 minutes before irradiation with a UV lamp with a 365 nm bandpass filter (Edmund Optics), with a 10 nm bandwith, to avoid oxidation of the anthracene to anthraquinone. The irradiation was done at 30-minute intervals with an absorbance spectrum of the samples being taken at each interval. The absorbance spectrum was obtained between 200 and 600 nm using a Shimadzu UV-1800 UV spectrophotometer with an interval scan of 1 nm (parameters in **Table 6.3**). All samples were irradiated until the absorbance decay at 392 nm had plateaued.

Table 6.3 *The parameters for the UV-vis monitoring of the anthracene photodimerisation.*

Range	200 – 600 nm
Response	Fast/Medium
Data pitch	0.5 nm
Scan speed	200 nm/min
Band width	1.0 nm

For **all** thrombin binding aptamer (TBA) studies throughout this thesis the DNA was in TBA buffer consisting of 20 mM Tris-HCl, 1 mM $MgCl_2$, 120 mM NaCl, 10 mM KCl, 2 mM $CaCl_2$, pH 7.4 as this buffer had been determined to give optimum folding of the aptamer and optimum binding to thrombin.[5]

6.4.5   Thrombin clotting studies

As per the protocol provided with the Helena biosciences Clauss assay,[6] the thrombin(100 NIH/mL) was made up to 2 mL with MilliQ water and left for 10 minutes before use. Once reconstituted, the thrombin is only active for 8 hours at room temperature. The fibrinogen was made up to 1 mL in the buffer provided and left for 15 minutes, and then diluted to a 1:9 dilution of fibrinogen and stored on ice throughout the clotting studies as the reconstituted fibrinogen is only active for 4 hours when stored between 2-8 ºC. To ensure optimal DNA-protein interaction each sample of aptamer and thrombin was incubated for 30 minutes at 37 °C. The DNA was in TBA buffer in order to allow for optimum aptamer folding and thrombin:aptamer binding. A 0.1 mL solution of either the thrombin alone or the thrombin:aptamer sample was added to 0.4 mL of the 1:9 dilution of fibrinogen. The clotting reaction was monitored using the percentage change in UV-vis transmission of the sample at 450 nm over a period of 40 minutes using a Jasco V-550 UV/Vis spectrophotometer.[7]

6.5 Fluorescence spectroscopy

All fluorescence emission studies were carried out on a Jasco FP-800 Fluorometer. All samples had an equal equivalence of DNA probe to target (at 1 µM in 50 µL). The samples were made up in MilliQ water, with 0.1 M NaCl to aid duplex formation and 10 mM phosphate buffer (PB) to replicate a cellular environment. A three-window sub-micro quartz cuvette (Starna Scientific Ltd, UK) was used with a 3 mm pathlength. The settings used can be seen in **Table 6.4** below:

Table 6.4 *The parameters used for the fluorescence emission studies of the anthracene modified oligonucleotide probe.*

Range	370 – 570 nm
Data interval	1 nm
Excitation bandwith	5 nm
Emission bandwith	5 nm
Response	50 msec
Sensitivity	High
Excitation wavelength	350 nm
Data interval	1 nm
Scan speed	200 nm/min

6.6 Gel electrophoresis

6.6.1 Native (non-denaturing) polyacrylamide gel electrophoresis

Native gel studies were performed using 12% polyacrylamide gels using 0.8% (w/v) bis-acrylamide. The gel was made up to 20 mL using 5x Tris/Borate/EDTA (TBE) buffer, MilliQ water, 10% Ammonium persulphate (APS) (150 µL) and 15 µL tetramethylethylenediamine (TEMED). Gels were cast using glass plates with 1 mm separation. Once the gels had set, they were immersed in *ca.* 1 L of 1 x TBE buffer. Each sample was made up to 40 µL using 2 µL of 6X 30% glycerol, 2 µL of 6X loading dye (New England Biolabs, UK), and MilliQ water according to the concentration of DNA utilised (1 µM). The gels were run at 100 V (14 mA) for 45 minutes. DNA was stained for 15 minutes using Diamond™ Nucleic Acid Dye (Promega, USA) and visualised using an excitation wavelength of 480 nm on an ultraviolet (UV) transilluminator (Alpha Innotech, AlphaImager HP) fitted with an ethidium bromide filter.

6.6.2 Gel electrophoretic mobility shift assay (EMSA)

All EMSA studies used a similar protocol to the native gels. The gels were made using 12% polyacrylamide gels using 0.8% (w/v) bis-acrylamide. The gel was made up to 20 mL using 10 mM KCl, 5x TBE buffer, MilliQ water, 10% APS (150 µL) and 15 µL of TEMED. Once set, the gels were immersed in *ca.* 900 mL of 1 x TBE buffer + 10 mM KCl in an electrophoresis tank. Each sample was made up to 20 µL using 2 µL of 6X 30% glycerol and TBA buffer according to the concentration of thrombin and DNA required. The gels were run at 100 V (14 mA) for 45 minutes. The DNA was stained for 15 minutes using Diamond™ Nucleic Acid Dye (Promega, USA) and visualised using an excitation wavelength of 480 nm on an UV transilluminator (Alpha Innotech, AlphaImager HP) fitted with an ethidium bromide filter. The proteins were stained with InstantBlue™ Ultrafast protein stain for 30 minutes, after which they were destained with deionised water for 30 minutes.

6.7 Circular dichroism (CD) spectroscopy

All aptamer CD studies were done on a Jasco J-1500spectropolarimeter (Jasco, Japan) using a 2 µM concentration of DNA in a 10 mm pathlength 6Q quartz cuvette. The high tension (HT) voltage limit was set to 400 V. The final data produced was an accumulation of spectra using the parameters in the table below (**Table 6.5**). The aptamer was studied in the TBA buffer mentioned earlier. All data were baseline corrected from a buffer baseline.

Table 6.5 *The parameters for the CD analysis of the aptamer G-quadruplexes.*

Photometric mode	CD
Measure range	350 – 200 nm
Data pitch	0.5 nm
Bandwidth	1.00 nm
Scanning speed	200 nm/min
Accumulations	8

6.7.1 *Variable temperature CD*

All thermal VT-CD studies of the aptamers were done on a Jasco J-1500 spectropolarimeter. The aptamer samples were at 2 µM in TBA buffer in a 10 mm pathlength 6Q quartz cuvette. Thermal studies were performed using a Jasco PTC-517 Peltier cell holder in the same spectropolarimeter. A CD spectrum was recorded at every 5 °C temperature interval from 15 °C to 85 °C at a bandwith of 1.00 nm at 292 nm (**Table 6.6**). Each data set was normalised to 1 (fully folded) at 15 °C, and the data for the temperatures between 15-85 °C were normalised relative to this in order to allow comparison of the thermal melting curves between the data sets.

Table 6.6 *The VT-CD parameters for the thermal melting study of the aptamer G-quadruplexes.*

Photometric mode	CD
Wavelength	292 nm
Data pitch	0.5 nm
Temperature range	15-85 °C
Bandwidth	1.00 nm
Scanning speed	200 nm/min

6.8 M13 bacteriophage synthesis[5]

The inoculation of the bacterial culture in which M13 (New England Biolabs, UK) is produced was carried out in 400 mL of 25 g/L NB2 (Oxoid) solution. This was inoculated with 400 µL of 5 mg/mL of tetracycline dissolved in ethanol and all inoculation procedures were under sterile conditions. A 500 µL solution of One Shot Top10F' _E. coli_ (F' [_lad_q, _Tn_10(Tet^R]) (Invitrogen, California, USA) and 0.04 mg of M13 bacteriophage in 50 mM potassium phosphate (at pH 8.0) was added to the same flask. The culture was then incubated for 16 hours, at 200 rpm, 37 °C in an orbital shaker. After the 16 hour incubation the culture was sedimented (Avanti J-24, Beckman Coulter USA centrifuge with a JLA 10.5 rotor) at 10000 g for 20 minutes at 4 °C. To ensure all the _E. coli_ had been removed the supernatant is taken and the same sedimentation step was repeated. After the second sedimentation step 80% of the supernatant was then taken from the tubes and added to a beaker. The M13 was precipitated using a 2.5% w/v solution of polyethylene glycol (PEG) 6000 and 2.5 M NaCl (5:1 ratio of PEG 6000/supernatant). The solution was left to stir at 4 °C for 1 hour. The precipitated solution was sedimented, using the same method as the sedimentation after the 16 hour incubation, but for 25 minutes instead of 20 minutes. After the supernatant had been discarded the pellet was resuspended in 1 mL of 100 mM potassium phosphate buffer, 150 nM NaCl, at pH 7.2 in a microcentrifuge tube. To remove any remaining _E. coli_ cells in the solution the tubes were sedimented for a further 5 mins at 14000 rpm (FX241.5p rotor, Microfuge® 16, Beckman Coulter, USA) and the pellet was discarded.

Finally, the PEG/NaCl precipitation was repeated at a ratio of 5:1 PEG 6000/supernantant. The resulting solution was sedimented in a bench top centrifuge (FX241.5p rotor, Microfuge® 16, Beckman Coulter, USA) at 14000 rpm for 15 minutes. The resulting supernatant was discarded, and the pellet was resuspended in 200 µL of 100 mM potassium phosphate buffer, 150 nM NaCl, at pH 7.2. The M13 sample was stored at 4 °C until required.

6.9 Bioconjugation

6.9.1 Bioconjugation of thiol functionalised oligonucleotides to M13 bacteriophage

All the oligonucleotides used as probes for the M13 bacteriophage system were synthesised with a 5'
or 3' thiol linker group. The thiol linker groups were added to the oligonucleotides as disulphide
phosphoramidites and these were reduced prior to the conjugation reactions by adding a 5:1 molar
ratio of 5 mM TCEP:DNA-SH, by leaving to react for 1 hour whilst stirring at RT. A heterobifunctional
crosslinker, succinimidyl-4-(*N*-maleimidomethyl) cyclohexane-1-carboxylate (SMCC), was used to
conjugate the oligonucleotides to the M13 bacteriophage. A a reaction volume of 500 µL, 25 µL of a 10
mg/mL of SMCC was added to 0.5 mg/mL of M13 bacteriophage in 100 mM potassium phosphate, 150
mM NaCl, 5mM EDTA, pH 7.2. This was left to react for 1 hour whilst stirring at RT. A MiniTrap G25
Sephadex column (GE Healthcare) was used to remove any unreacted SMCC and eluted back into the
conjugation buffer. One mL of sample was added to the column and eluted in 1.5 mL of 100 mM
potassium phosphate buffer, 150 nM NaCl, at pH 7.2. The M13-SMCC was combined with the reduced
oligonucleotide strands and left to react for 16 hours at RT whilst stirring. L-cysteine, at a 5X excess
over SMCC, was added to the sample to quench any unreacted SMCC and was left at RT for 15 mins.
The reagents in this procedure were degassed before use and all reactions were carried out under a
nitrogen atmosphere. The two probe, one phage bioconjugations used the same reaction conditions
except both probes were added to the same M13 bacteriophage sample.

6.9.2 Bioconjugation of Cy3 and Cy5 dyes to the M13 bacteirophage

Once the oligonucleotide probes had been conjugated to the M13, the samples to be used in the multiplexing experiments were further conjugated to either Cy3-NHS ester or Cy5-NHS ester (Lumiprobe). For the M13 to be in an optimum buffer for dye conjugations the samples in conjugation buffer were buffer exchanged into 50 mM potassium phosphate buffer (at pH 8) using a MiniTrap G25 Sephadex column. One mL of sample was added to the column and eluted in 1.5 mL of conjugation buffer. The M13 with the probes for the potato virus Y (PVY) were conjugated to the Cy3 dye and the M13 with the probes for the potato virus A (PVA) were conjugated to the Cy5 dye. A solution of 0.5 mg/mL of the M13-DNA conjugates were left to react overnight, at RT, with 10 µL of a 10 mg/mL solution of dye in DMSO. Any unconjugated dye remaining was removed using a MiniTrap G25 Sephadex column as above and the M13-probe dye conjugates were buffer exchanged back into the conjugation buffer to allow for optimum probe:target DNA duplex formation.

The Cy5 conjugation to the M13 had to be modified as the concentration of dye (10 mg/mL) used in the initial conjugation reaction did not produce a strong enough signal under linear dichroism (LD) spectroscopy so double the concentration (20 mg/mL) was used in order for enough dye to conjugate to the M13 in order to be detectable under LD.

6.10 Size exclusion chromatography

Once the M13 bacteriophage samples had been conjugated to the oligonucleotide probes they were purified using SEC[8] on an ÄKTA Explorer 10 purification system. The column (a Superdex S200 HiLoad 16/60 SEC column) was initially washed with 1.2 column volumes of MilliQ® water and then 1.2 column volumes of a reaction buffer, consisting of 100 mM potassium phosphate buffer, 150 mM NaCl, pH 7.2, in order to equilibrate the column. A flow rate of 1.0 mL/min was used for the purification with 1.2 column volumes of the reaction buffer. Three absorbances were monitored during the purification; A_{269} (M13 bacteriophage), A_{280} (protein peak), and A_{495} (oligonucleotide tagged fluorophore peak). Two mL fractions were collected using a Frac-950 auto sampler (Amersham Pharmacia Biotech). The oligonucleotide conjugated M13 bacteriophage fractions were combined and kept at 4 °C until use.

6.11 Plasmid production

6.11.1 Transformation of plasmid

The PVY plasmid used in the LD detection studies was a kind donation from the Science & Advice for Scottish Agriculture (SASA). The plasmid map can be seen in **Figure 6.1**. In order to check the sequence of the plasmid and create further stocks a transformation protocol was undertaken.

One vial of XL-10 gold competent cells (donated by Dr Ian Cadby at the University of Birmingham) kept at -80 °C were thawed on ice. Five nanograms of DNA in a volume of 5 μL was added to the cells. The cells were mixed with the DNA by gentle tapping. The solution was left on ice to incubate for 30 minutes. The cells were then exposed to heat shock by placing the cells in a 42 °C water bath for exactly 30 seconds. This aided the uptake of the DNA into the cells. The cells were then placed onto ice again. Super optimal broth with catabolite repression (SOC) medium was pre-warmed and 250 μL was added to the cells. This was done using aseptic technique to avoid any contamination of the SOC medium. The vial was left to shake in an orbital shaking incubator (New Brunswick™ Innova 44 Incubator Shaker) at 37 °C for one hour at 225 rpm. Two lysogeny broth (LB) agar plates with ampicillin (100 μg/mL) for plasmid selection were prepared in advance. Two hundred microlitres of the either cells with DNA or cells without DNA were plated onto two separate LB plates. One plate was to be used for the cells with plasmid DNA and one plate was used as a negative control with cells that did not contain any DNA. As a result of the antibiotic on the plates, cells would only grow on the plate containing the plasmid with the antibiotic resistance gene. The plates were inverted and incubated at 37 °C overnight. One successful transformant colony was then picked using a sterile tooth pick from the plates and cultured in 100 mL of LB media containing 100 μg/mL ampicillin. The colony was grown in a shaking incubator at 37 °C overnight shaking at 180 rpm.
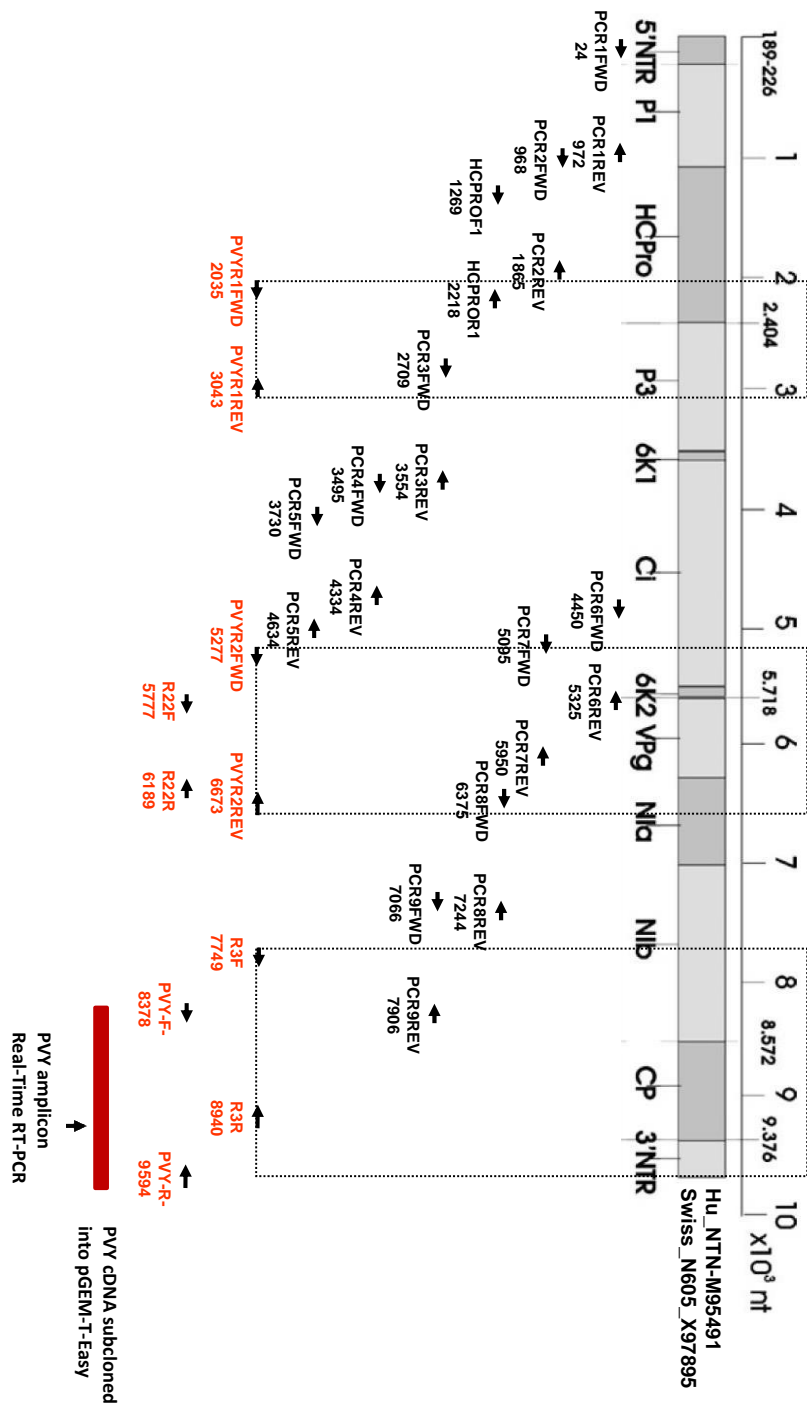
Figure 6.1 *The plasmid map of the PVY coat protein gene subcloned into the pGEM-T-Easy plasmid.*

6.11.2 Glycerol stock production

A glycerol stock was prepared from the small-scale starter culture (**Section 6.11.1**) in order to create stocks for future use. A 50% glycerol (25 mL glycerol with 25 mL dH$_2$0) stock was created and filter sterilised using a 0.45 µM Supor® membrane. A 400 µL volume of starter culture was added, using aseptic technique, to a 1.8 mL cryogenic freezer tube. To this tube 600 µL of 50% glycerol stock was added and the solution was mixed gently by inversion. These stock cultures were then stored at -80 °C until required.

6.11.3 Mini-prep of the plasmid

To extract the plasmid from the cells a QiAprep Spin Miniprep Kit (Qiagen, Germany) was used and the procedure was also provided within the kit. The bacterial cells were harvested by pelleting 1 mL of glycerol stock culture for 30 seconds at 11, 0000 g. The supernatant was discarded and as much liquid as possible was recovered from the sample. The cells were lysed by the addition of 250 µL of Resuspension Buffer P1 and the sample was vortexed in order to resuspend the cell pellet. A volume of 250 µL of Lysis Buffer P2 was then added to the mix. The sample was inverted 6 to 8 times in order to allow mixing to occur. The sample was then left to incubate at room temperature until the lysate appeared to become clear (ca. 5 minutes). Three hundred microlitres of Neutralisation Buffer P3 was added to the sample and mixed by inverting 6 to 8 times. The lysate was then clarified at room temperature by sedimenting for 5 minutes at 11, 000 g and the pellet was discarded. The ISOLATE II plasmid mini spin column was inserted into a collection tube and 750 µL of the sample was added onto the column. The column was centrifuged for 1 minute and 11, 000 g and the sample that flowed through the column was discarded. This left plasmid DNA bound to the column. The silica membrane was then washed by adding 600 µL of Wash Buffer PW2. The column was then centrifuged again for 1 minute at 11, 000 g. The flow through was discarded. The DNA was elutied by the addition of a 50 µL amount of Elution Buffer P onto a membrane made of silica. This was incubated at room temperature for one minute and was then sedimented for 1 minute at 11,000g. The resulting plasmid solution was then stored at -20 °C until use. The samples were sequenced using the Biosciences sequencing facility using an ABI 3730 capillary sequencer.

6.12 Linear dichroism spectroscopy

6.12.1 Measurement of LD spectra using the normal method

LD spectroscopy experiments were done on a Jasco J-1500 spectropolarimeter (Jasco, Japan), which had been modified to measure LD. Samples (100 µL) were placed into a micro-Couette (**NB** note this apparatus is a Couette and not to be confused with Cuvette) cell apparatus[9] within the sample chamber of the instrument. A baseline was recorded (with a non-rotating capillary) and was subtracted from the sample with a Couette rotating (driven by a potential difference (PD) of 3V) and the signal zeroed at 750 nm. All spectra measurements were conducted with the following parameters:

Table 6.7 *The parameters used for the study of M13 using LD spectroscopy.*

Range	190-800 nm
Sensitivity	0.1 dOD
Data pitch	1.0 nm
Scanning mode	Continuous
Scan speed	200 nm/min
Band width	2 nm
Accumulation	3

To detect the plasmid samples the plasmid DNA was heated to 85 °C, as any higher would compromise the M13 bacteriophage, for 30 seconds to allow for double stranded DNA denaturation. The PVY M13-probe system was immediately added to the plasmid sample and the sample was left to cool to RT to allow for the probes to anneal to the denatured plasmid sample. The LD detection studies followed the same protocol as above.

6.12.2 Measurement of LD spectra using a high-throughput method (ht:LD)

The ht:LD was developed by Mr Charles Moore-Kelly within the Dafforn group. The samples were loaded onto a 96-well plate and transferred to the LD machine using a Jasco AS2055 autosampler. An extra 20 μL of sample is carried ahead of the 100 μL of the sample for the purpose of preventing the M13 bacteriophage sample adhering to the polyetheretherketone (PEEK) tubing. The samples were injected through a quartz capillary where the alignment occured through extension flow using a Jasco PU1580 HPLC pump with a flow rate of 1 mL/min. The flow cell capillary was a 220 μM i.d. fused silica capillary (PolyMicro Technologies). Two quartz rod lenses were used to focus the light behind and forward of the capillary.

The flow cell was connected to the PEEK tubing of the HPLC pump via a 1/16"-360 μm union. Optical components of the flow cell were held in a 3D printed housing unit, which was positioned immediately ahead of the PMT in a Jasco J1500 CD spectrometer. A 5 cm biconvex lens was positioned in the sample chamber to focus light onto the outfacing rod lens of the flow cell. Samples were measured using a wavelength of 205 nm, bandwidth of 2 nm, data pitch of 0.2 seconds and a digital integration time of 0.25 seconds.

6.13 Data analysis methods

All spectra were examined and manipulated using the data analysis and graphing software application GraphPad 7.
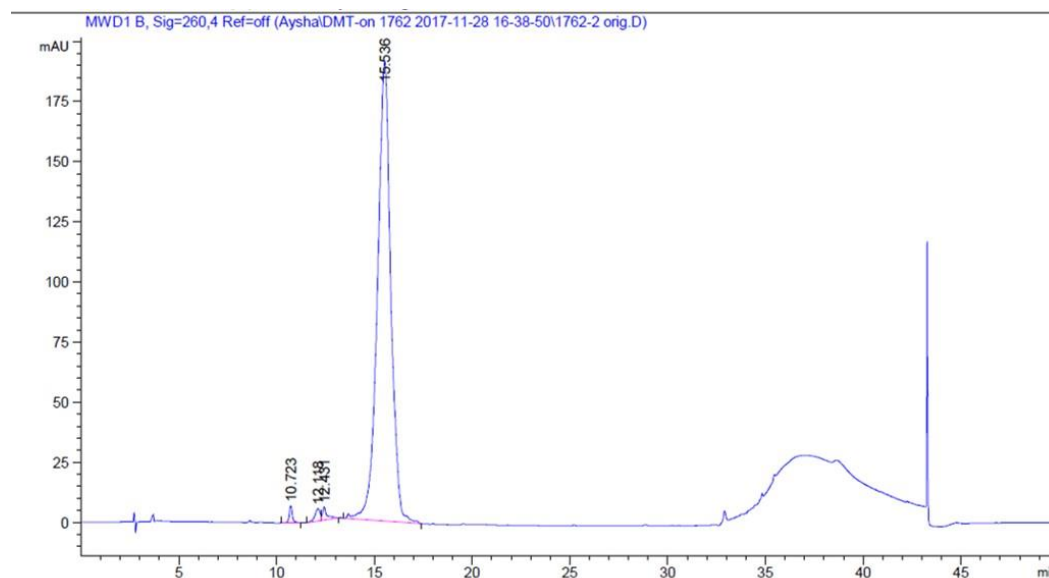
6.14 References

1. Brown, T.; Brown, T. J., Nucleic Acids Book. 2013. http://www.adtbio.co./nucleic-acids-book (accessed 20 July 2015).

2. Integrated DNA Technologies, I. OligoAnalyzer Tool. https://www.idtdna.com/calc/analyzer (accessed 2015-2018).

3. Lakowicz, J. R., *Principles of Fluorescence Spectroscopy*. Springer: Singapore, 2006; Vol. 3, p 960.

4. Berkowitz, S. A.; Day, L. A., Mass, length, composition and structure of the filamentous bacterial virus fd. *Journal of Molecular Biology* **1976,** *102*, pp. 531-547.

5. Little, H. A. The development of novel diagnostic sensors based on linear dichroism spectroscopy. Thesis, University of Birmingham, 2016.

6. Clauss, A., Rapid physiological coagulation method in determination of fibrinogen. *Acta Haematologica* **1957,** *17*, pp. 237-46.

7. Miesbach, W.; Schenk, J.; Alesci, S.; Lindhoff-Last, E., Comparison of the fibrinogen Clauss assay and the fibrinogen PT derived method in patients with dysfibrinogenemia. *Thrombosis Research* **2010,** *126*, pp. 428-433.

8. Sørensen, S.; Justesen, S. J.; Johnsen, A. H., Purification and characterization of osteopontin from human milk. *Protein Expression and Purification* **2003,** *30*, pp. 238-245.

9. Marrington, R.; Dafforn, T. R.; Halsall, D. J.; MacDonald, J. I.; Hicks, M. R.; Rodger, A., Validation of new microvolume Couette flow linear dichroism cells. *Analyst* **2005,** *130*, pp. 1608-1616.

7 Appendices

7.1 Chapter 3 Appendix

7.1.1 Purification and characterisation of M3 aptamer

7.1.1.1 Reversed-phase high performance liquid chromatography (RP-HPLC)


```
=================================================================
                        Area Percent Report
=================================================================

Sorted By          :      Signal
Multiplier         :      1.0000
Dilution           :      1.0000
Do not use Multiplier & Dilution Factor with ISTDs

 Signal 1: MWD1 B, Sig=260,4 Ref=off

Peak RetTime Type  Width     Area       Height     Area
  #   [min]        [min]   [mAU*s]      [mAU]       %
----|-------|----|-------|----------|----------|--------|
   1  10.723 BB   0.1691   80.05295    7.12271   0.8576
   2  12.118 BV   0.2730   92.89185    5.13644   0.9951
   3  12.431 VB   0.2098   84.87343    5.56993   0.9092
   4  15.536 VV R 0.7058 9076.92676  191.22037  97.2381

Totals :                 9334.74498  209.04944


=================================================================
                        *** End of Report ***
```

Figure 7.1 *The RP HPLC data of the purified M3-aptamer, eluted into MilliQ water, synthesised using solid-phase oligonucleotide synthesis showing 97.1 % purity. The aptamer was purified using the DMT-ON method discussed in chapter 6.*

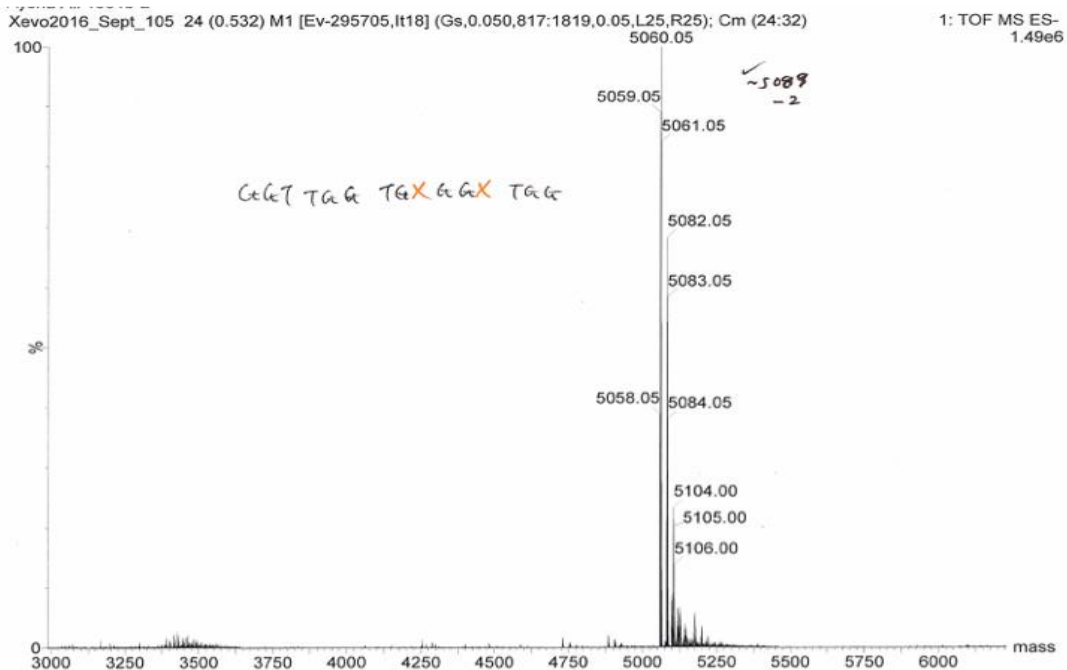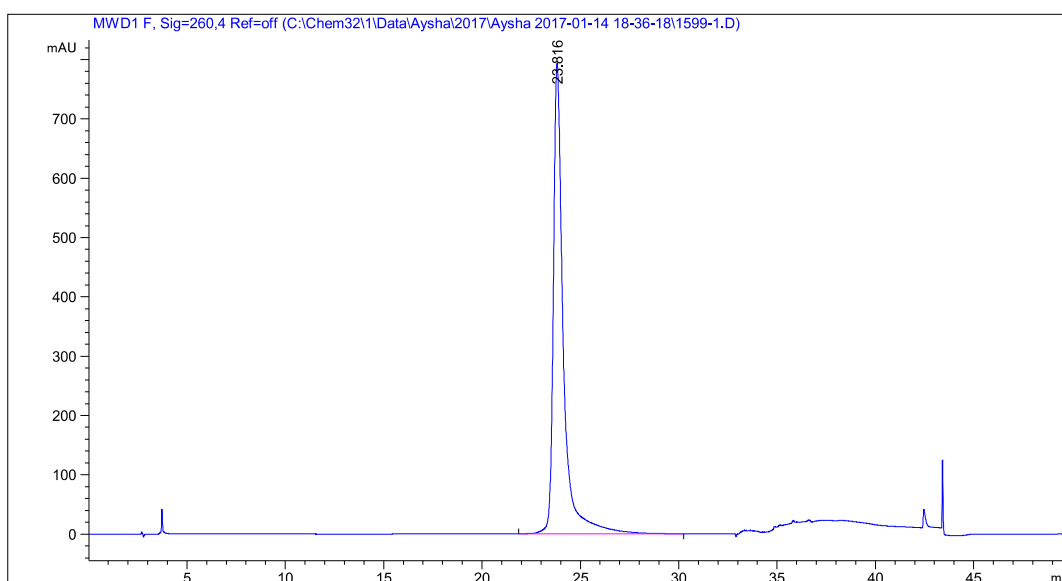### 7.1.1.2 M3 aptamer mass spectrometry analysis

Figure 7.2 The electrospray ionisation mass spectrometry (ESI MS) analysis of the purified M3-aptamer the purification of which is seen in **Figure 7.1**. The correct mass was seen at 5060.0 Da.

7.1.2   Purification and Characterisation of M4 strand

7.1.2.1   RP-HPLC purification analysis of the M4 strand


```
====================================================================
                        Area Percent Report
====================================================================


Sorted By             :      Signal
Multiplier            :      1.0000
Dilution              :      1.0000
Do not use Multiplier & Dilution Factor with ISTDs



Signal 1: MWD1 F, Sig=260,4 Ref=off

Peak RetTime Type  Width     Area       Height     Area
  #   [min]        [min]   [mAU*s]      [mAU]       %
----|-------|----|-------|----------|----------|--------|
   1  23.816 BB    0.5184 2.80315e4   793.08112 100.0000

Totals :                   2.80315e4   793.08112
```

Figure 7.3 *The RP HPLC data of the purified* **M4** *aptamer, eluted into MilliQ water, synthesised using solid-phase oligonucleotide synthesis showing 100.0 % purity. The aptamer was purified using the Fc-Anth method discussed in chapter 6.*

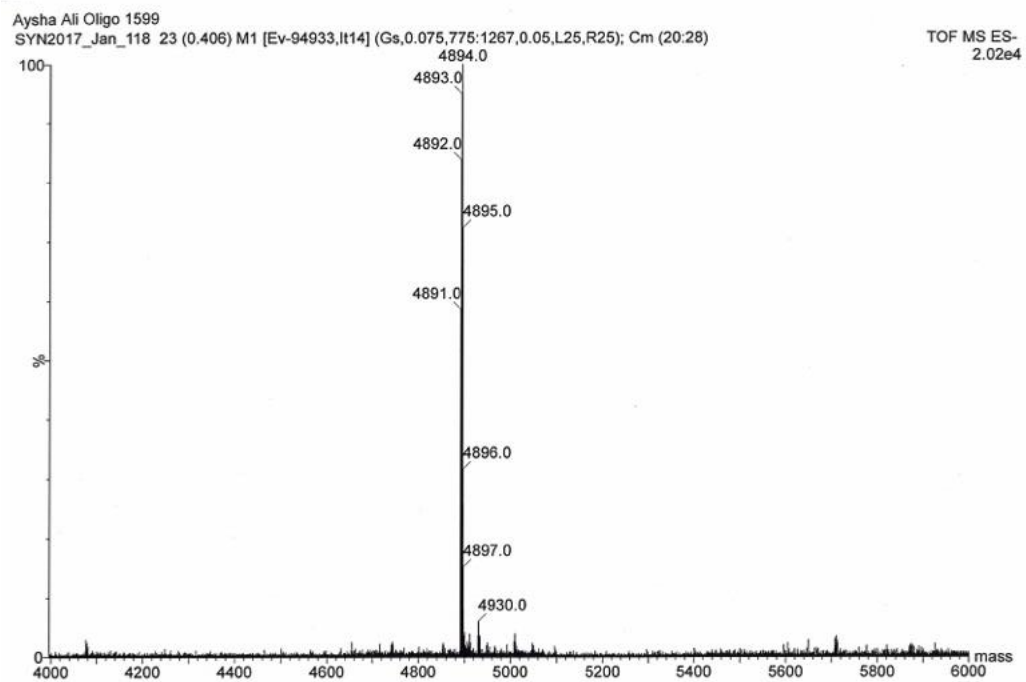224

7.1.3   M4 strand mass spectrometry analysis

Figure 7.4 *The negative electrospray ESI MS analysis of the purified M4-aptamer the purification of which is seen in **Figure 7.3**. The correct mass was seen at 4894.0 Da.*

7.1.4   Isolation of the photodimerised M3 from the unphotodimerised M3

During the M3 aptamer photoirradiation studies in Chapter 3 the sample did not undergo full photodimerisation, i.e. there was still some unphotodimerised M3 left in the sample. RP-HPLC purification was undertaken to determine whether the photodimerised M3 sample could be isolated from the open form of the M3 aptamer. However, the isolation was not possible as the retention times for both the unphotodimerised M3 and the photodimerised M3 samples were the same (**Figure 7.5**). The optimum concentration for the photoirradiation reactions was at 2 μM however, this concentration was too low to allow sufficient optimisation of the method allow separation of the photodimerised M3 aptamer. A dilution series of the native thrombin binding aptamer (TBA) can be seen in **Figure 7.6**, this data demonstrates that the lowest concentration before a sample peak can be distinguished from the buffer peaks is 5 μM.
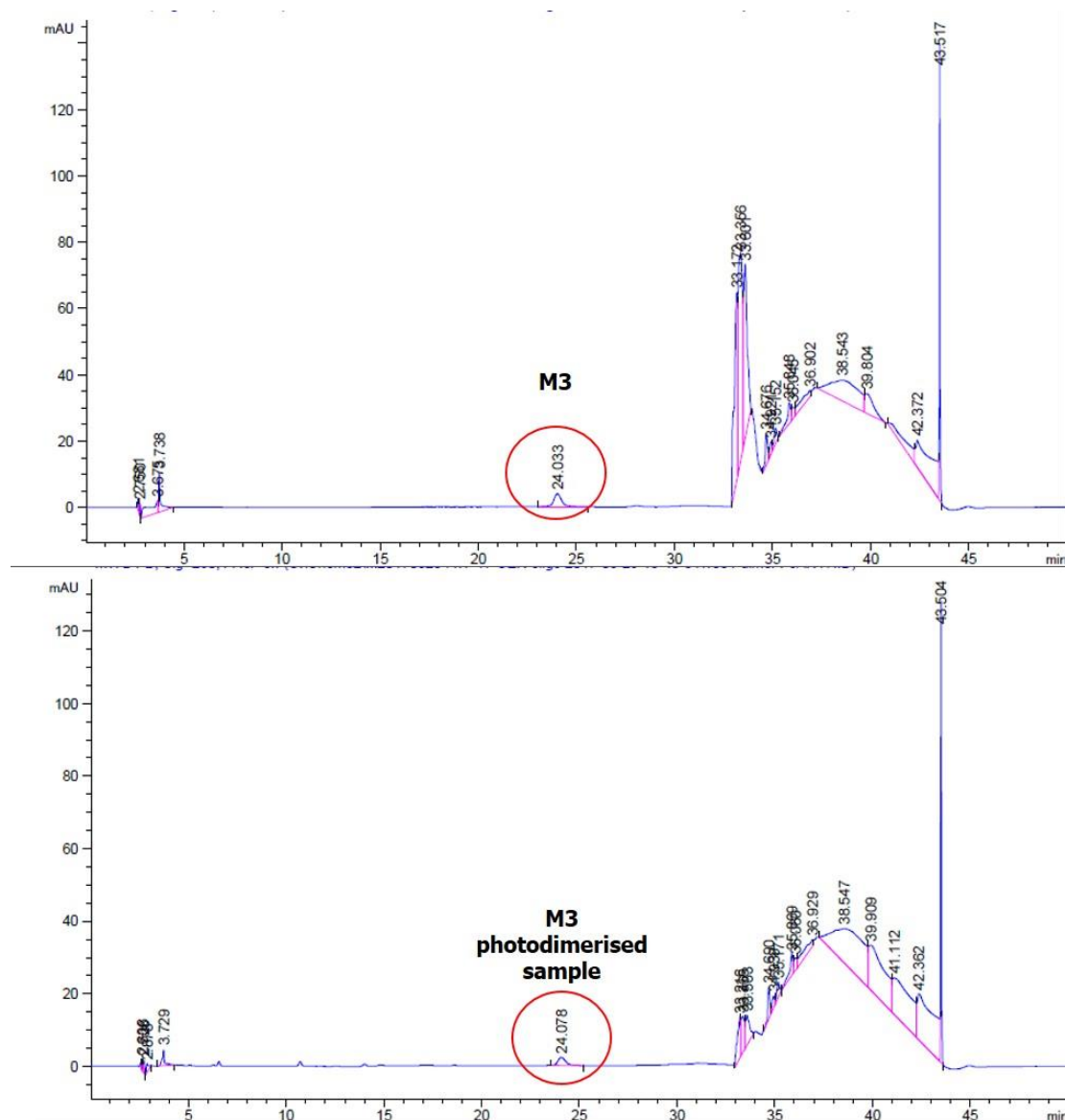
Figure 7.5 *The RP-HPLC isolation attempt of the M3 photodimerised sample in the mixture with the unphotodimerised sample using the DMT-ON method. The retention time of both the unphotodimerised M3 sample (above) and the M3 photodimerised sample (below) was the same so separation of the open form of the M3 from the photodimerised M3 was not possible.*
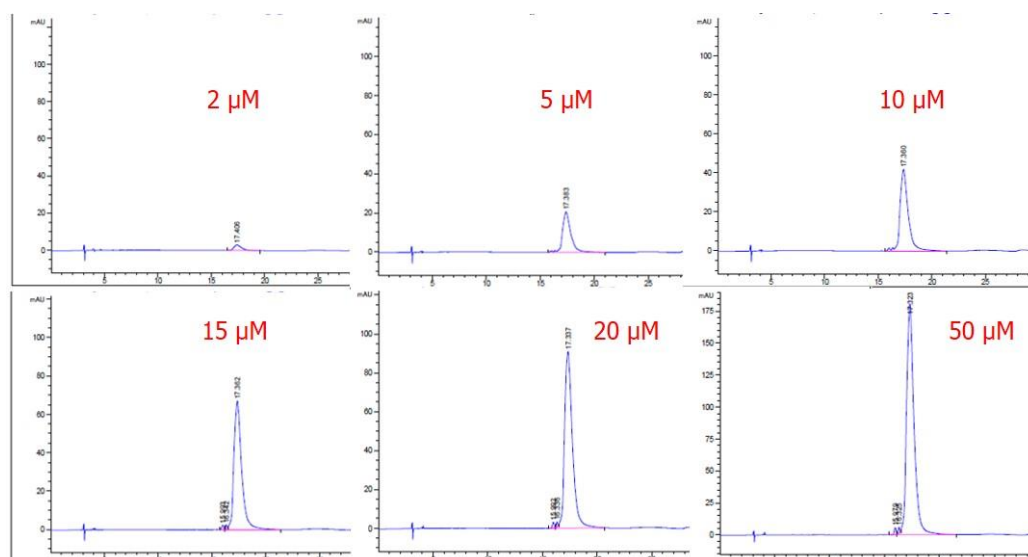
Figure 7.6 *A RP-HPLC dilution series, between 2 µM and 50 µM, of the native TBA demonstrating that the lowest concentration that can be monitored under RP-HPLC is 5 µM.*

7.2 Chapter 4 Appendix

7.2.1 Purification and Characterisation of BRAF probe

7.2.1.1 BRAF probe RP-HPLC purification analysis
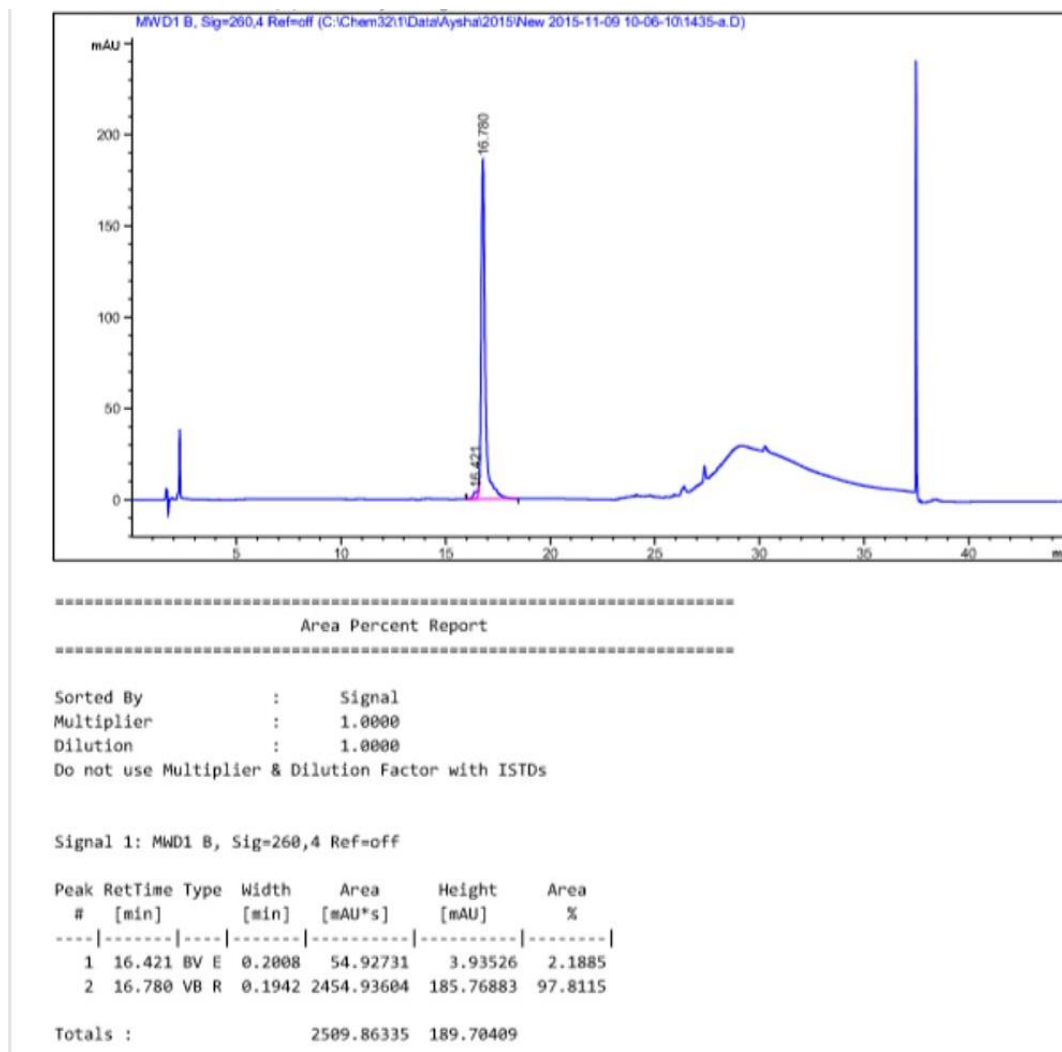

Figure 7.7 *The RP HPLC data of the purified BRAF probe, eluted into MilliQ water, synthesised using solid-phase oligonucleotide synthesis showing 97.8 % purity. The aptamer was purified using the Fc-Anth method.*

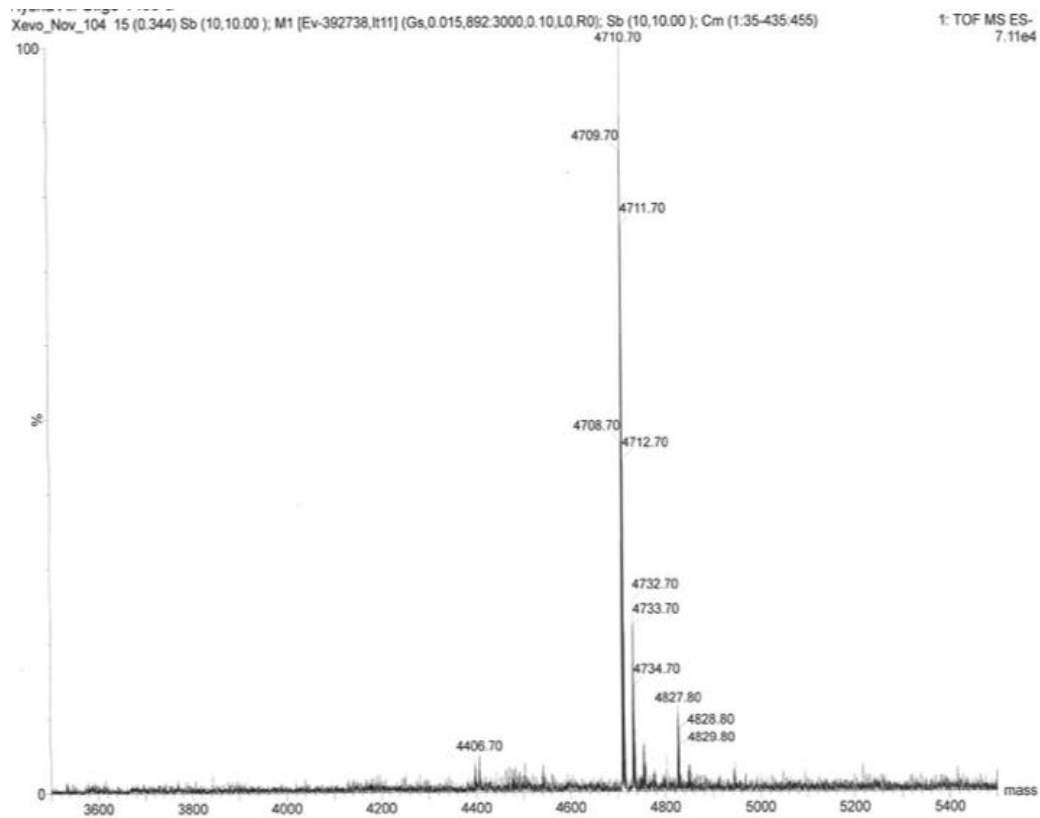### 7.2.1.2   Mass spectrometry analysis of the BRAF probe

Figure 7.8 *The negative electrospray ESI MS analysis of the purified BRAF probe, the purification of which is seen in* **Figure 7.7**. *The correct mass was seen at 4710.70 Da.*

7.2.2 Sequences of 173 base targets

Target with T base variant (healthy samples) (173-T):

TCC ACA GAG ACC TCA AGA GTA ATA ATA TAT TTC TTC ATG AAG ACC TCA CAG TAA AAA TAG GTG ATT TTG GTC TA
GCTACAGTGAAATCTCG ATG GAG TGG GTC CCA TCA GTT TGA ACA GTT GTC TGG ATC CAT TTT GTG GAT GGC ACC AGA
AGT CAT CAG AAT GCA AGA TAA A

Target with A base mutation (tumour samples) (173-A):

TCC ACA GAG ACC TCA AGA GTA ATA ATA TAT TTC TTC ATG AAG ACC TCA CAG TAA AAA TAG GTG ATT TTG GTC TA
GCTACAGAGAAATCTCG ATG GAG TGG GTC CCA TCA GTT TGA ACA GTT GTC TGG ATC CAT TTT GTG GAT GGC ACC AGA
AGT CAT CAG AAT GCA AGA TAA A

7.2.3 Polymerase chain reaction (PCR) of genomic samples

The contents of the agarose gels run in **Figure 4.13** of **Chapter 4** (**Table 7.1**). WT represents
the wild type samples, M represents the mutant samples, and L represents the Ladder. In lanes 10
to 17 in Gel F contained WT samples from lanes 10 to 13 and mutant from lanes 14 to 11.

Table 7.1 The DNA contents of the gels seen in **Figure 4.13** of **Chapter 4**.

	Lane										
Gel	**1**	**2**	**3**	**4**	**5**	**6**	**7**	**8**	**9**	**10**	**11**
A	WT	WT	WT	WT	WT	L	M	M	M	M	M
B	L	WT	WT	WT	WT	M	M	M	M	L	-
C	-	WT	WT	WT	WT	L	L	M	M	M	M
D	WT	WT	WT	WT	L	M	M	M	M	-	-

7.2.4 Sequencing results of the PCR products

The sequencing results from the PCR of both the wild type and mutant genomic samples used in the fluorescence studies of **Chapter 4**.

Wild type sequence:

TYWGCTTTCTTTTACTTACTACACCTCAGATATATTTCTTCATGAAGACCTCACAGTAAAAATAGGTGATT TTGGTCYA**GCTACAGTGAAATCT**CGATGGAGTGGGTCCCATCAGTTTGAACAGTTGTCTGGATYYRTKK TGTGGTAGG

Mutant sequence:

CYYTGCTTTCTTTACTACTACACCTCAGATATATTTCTTCATGAAGACCTCACAGTAAAAATAGGTGATTTT GGTCYM**GCTACAGWGAAATCT**CGATGGAGTGGGTCCCATCAGTTTGAACAGTTGTCTGGATYYWKTT KKGTGGATT

7.2.5 Fluorescence studies of the components of the unpurified PCR products
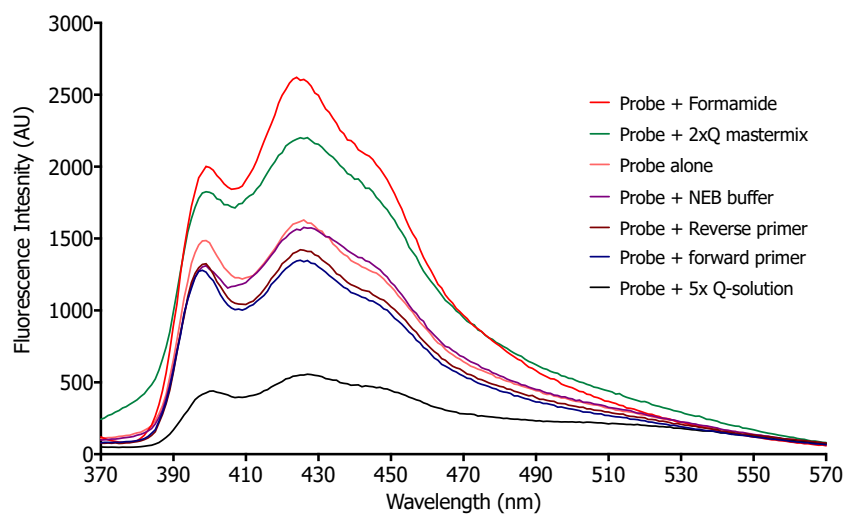

Figure 7.9 *The fluorescence emission data from the study of the probe with the components of the unpurified PCR product. The λ_{ex} = 350 nm, room temperature (RT), λ_{em} = 426 nm, room temperature.*

7.3 Chapter 5 Appendix

7.3.1 Purification of the PVY probes and targets

7.3.1.1 PVY probe 2 RP-HPLC purification analysis
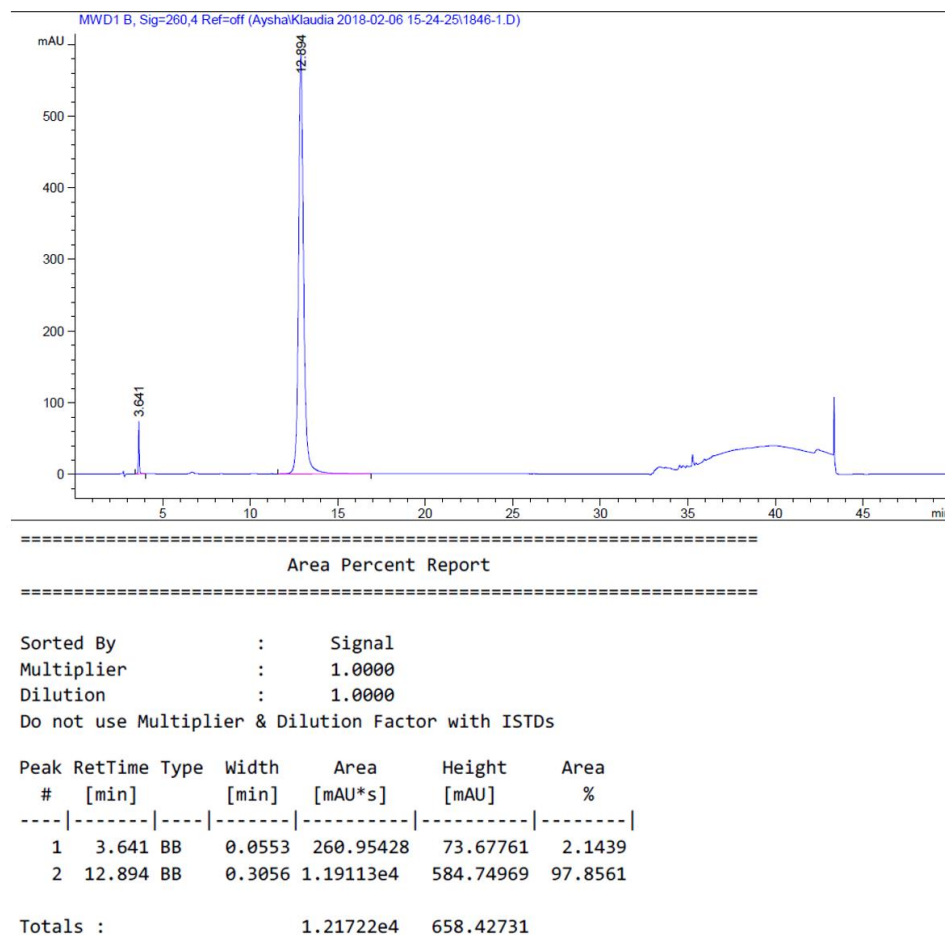

Figure 7.10 *The RP HPLC data of the purified PVY probe 2, eluted into MilliQ water, synthesised using solid-phase oligonucleotide synthesis showing 98 % purity. The strand was purified using the Short Oligo method.*

7.3.1.2 PVY probe 2 mass spectrometry analysis

Base Peak Mass (Da)	Intensity	Spectral Quality
7553.5	2.55E+005	ok

Figure 7.11 *The negative electrospray ESI MS analysis of PVY probe 2 after the RP-HPLC purification seen in **Figure 7.10**. The correct mass was seen at 7553.5 Da.*
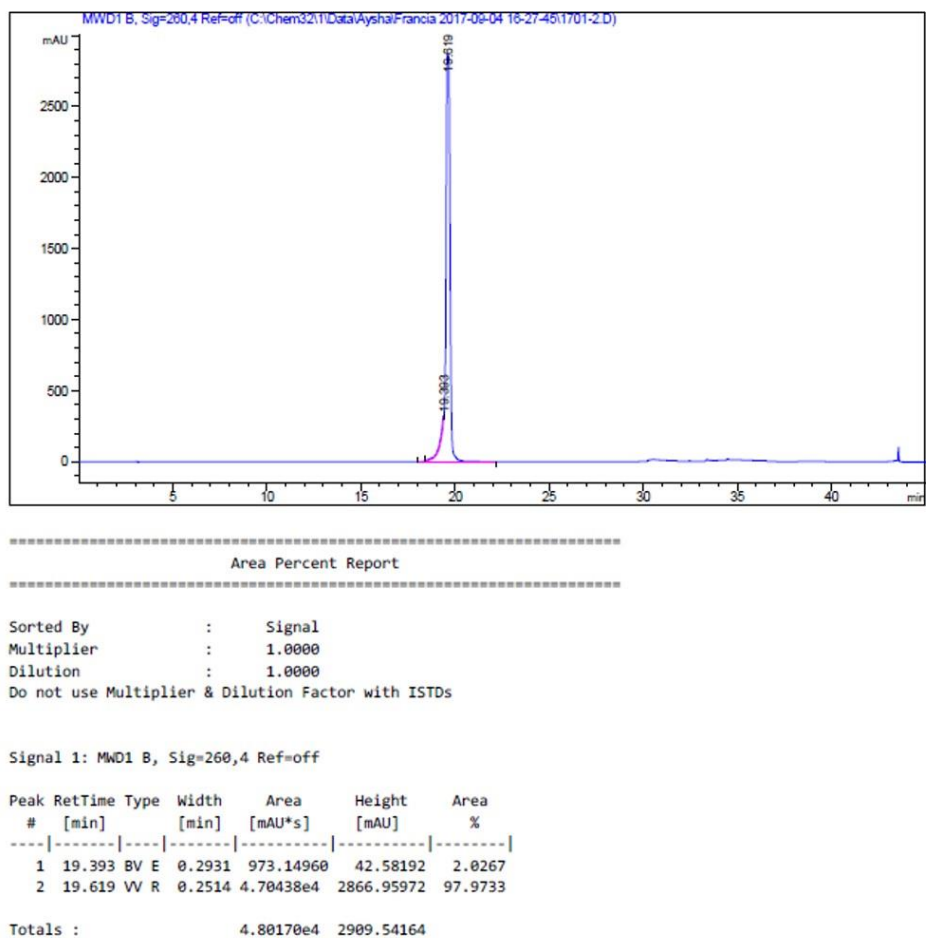
7.3.1.3 PVY target RP-HPLC purification analysis

Figure 7.12 *The RP HPLC data of the purified PVY target, eluted into MilliQ water, synthesised using solid-phase oligonucleotide synthesis showing 98 % purity. The strand was purified using the Short Oligo method.*

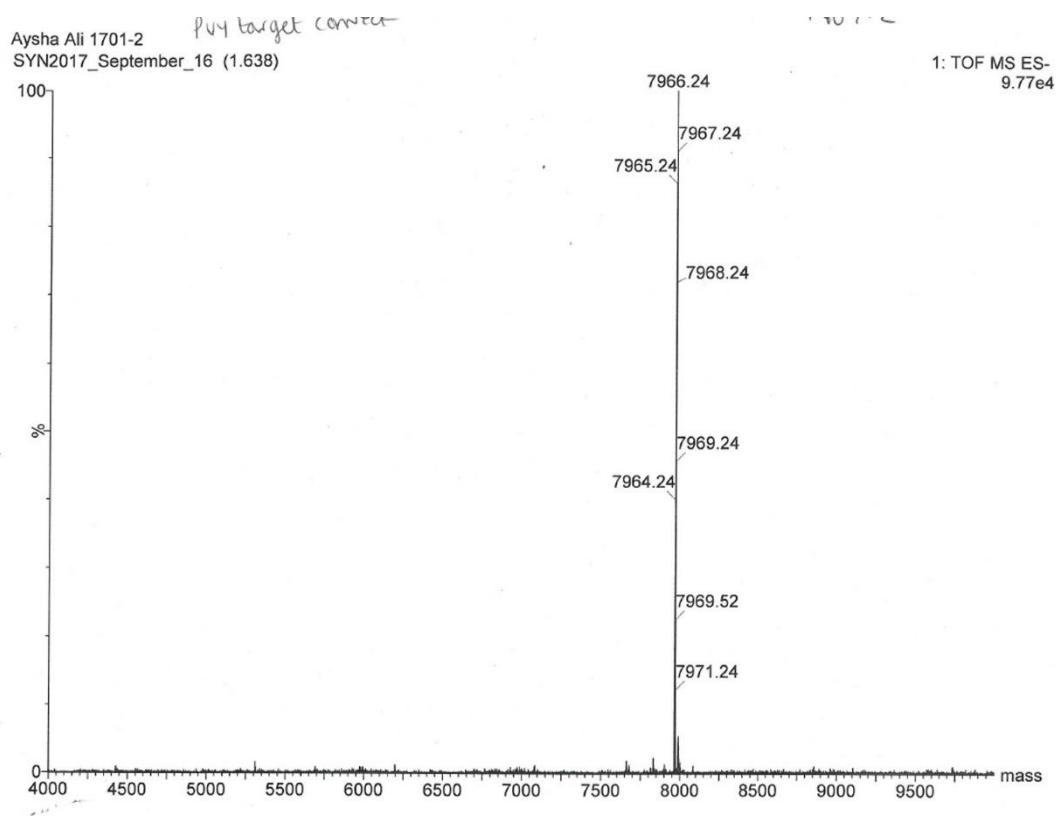### 7.3.1.4 PVY target mass spectrometry analysis

Figure 7.13 The negative electrospray ESI MS analysis of PVY target after the RP-HPLC purification seen in **Figure 7.12**. The correct mass was seen at 7966.24 Da.

7.3.1.5 Non-specific (NS) target RP-HPLC purification analysis


```
================================================================
                    Area Percent Report
================================================================

Sorted By          :      Signal
Multiplier         :      1.0000
Dilution           :      1.0000
Do not use Multiplier & Dilution Factor with ISTDs


Signal 1: MWD1 B, Sig=260,4 Ref=off

Peak RetTime Type  Width     Area       Height     Area
  #   [min]        [min]   [mAU*s]      [mAU]        %
----|-------|----|-------|----------|----------|--------|
  1  18.621 BV R  0.2770 5.34401e4  2855.32666 100.0000
```
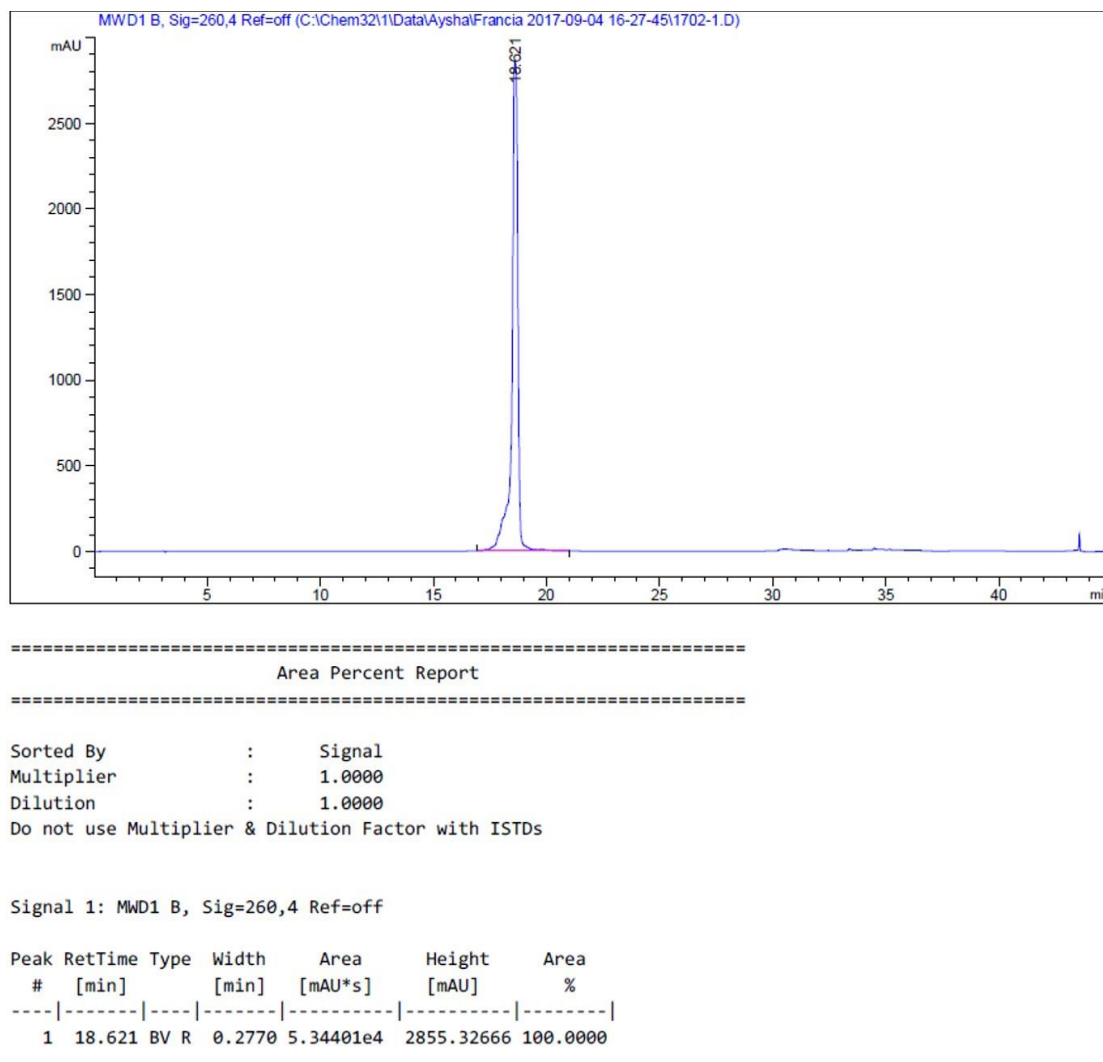
Figure 7.14 The RP HPLC data of the purified NS target, eluted into MilliQ water, synthesised using solid-phase oligonucleotide synthesis showing 100 % purity. The strand was purified using the Short Oligo method.
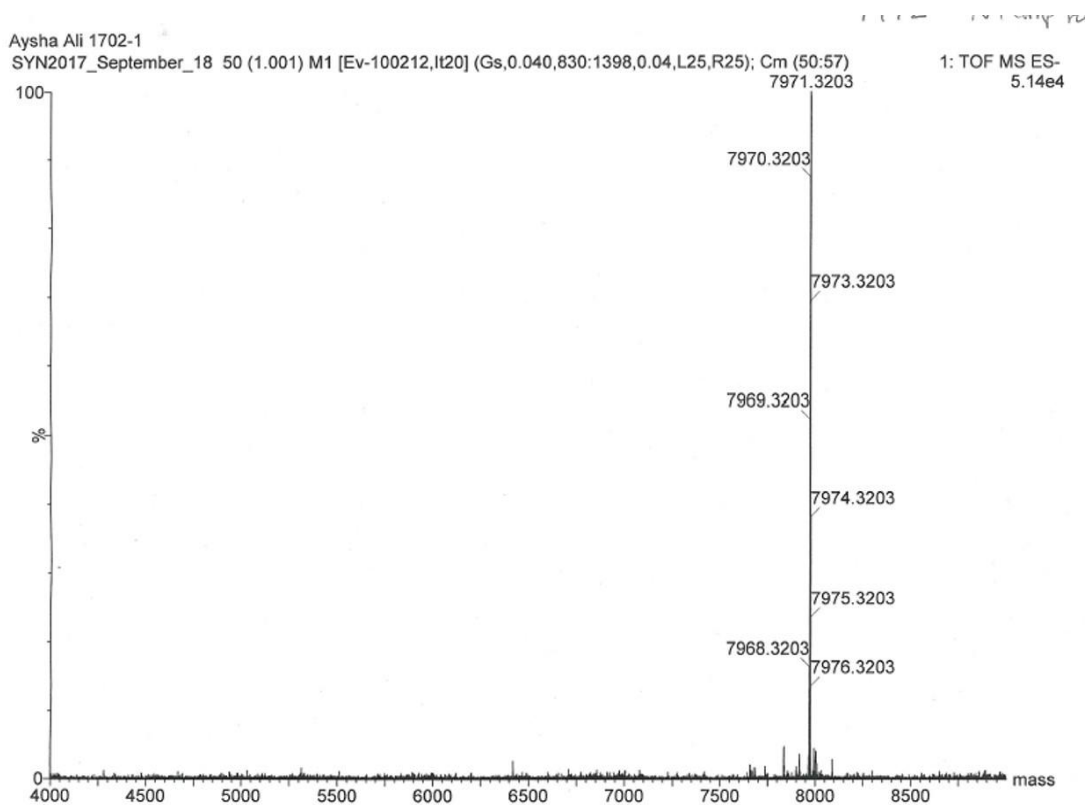
7.3.1.6 NS target mass spectrometry analysis

Figure 7.15 *The negative electrospray ESI MS analysis of NS target after the RP-HPLC purification seen in* **Figure 7.14**. *The correct mass was seen at 7971.3203 Da.*

7.3.1.7 PVA probe 2 RP-HPLC purification analysis

MWD1 B, Sig=260,4 Ref=off (Aysha\Klaudia 2018-02-07 16-55-09\1858-5.D)

```
=================================================================
                        Area Percent Report
=================================================================

Sorted By            :       Signal
Multiplier           :       1.0000
Dilution             :       1.0000
Do not use Multiplier & Dilution Factor with ISTDs


Peak RetTime Type  Width     Area      Height     Area
  #   [min]        [min]   [mAU*s]      [mAU]       %
----|-------|----|-------|----------|----------|--------|
  1  12.957 BB   0.3475 1.86755e4   779.48846 100.0000

Totals :                   1.86755e4   779.48846
```
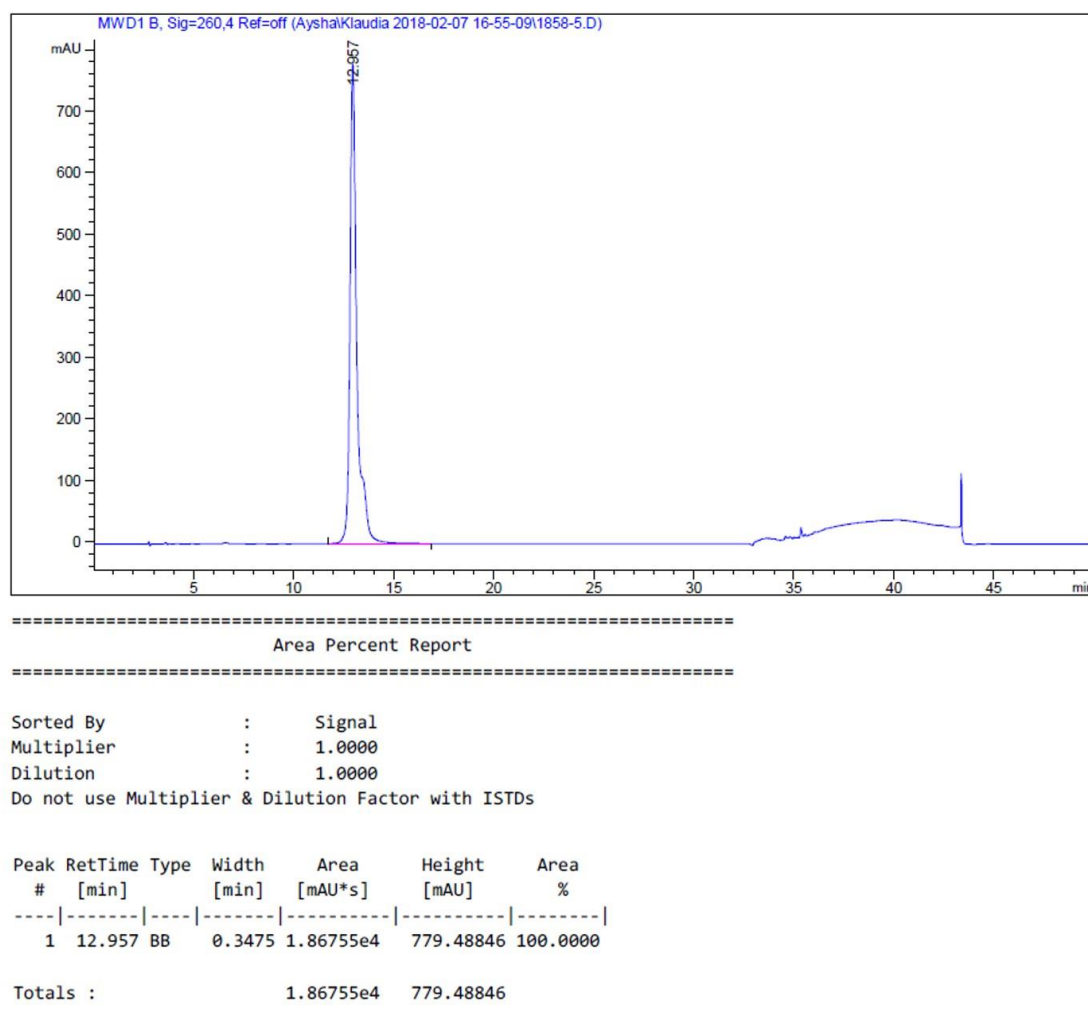
Figure 7.16 *The RP HPLC data of the purified PVA probe 2, eluted into MilliQ water, synthesised using solid-phase oligonucleotide synthesis showing 100 % purity. The strand was purified using the Short Oligo method.*

7.3.1.8 PVA probe 2 mass spectrometry analysis

Base Peak Mass (Da)		Intensity	Spectral Quality
7247.6		2.11E+006	ok

Figure 7.17 *The negative electrospray ESI MS analysis of PVA probe 2 after the RP-HPLC purification seen in **Figure 7.16**. The correct mass was seen at 7247.6 Da.*
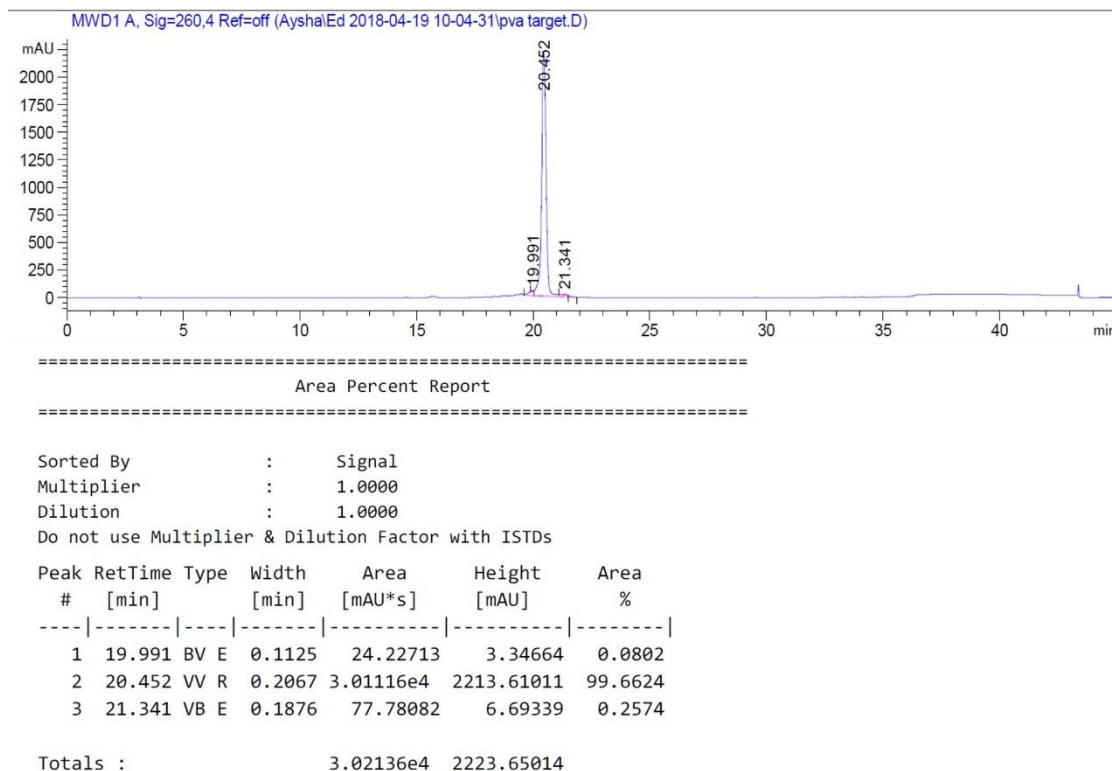
7.3.1.9 PVA target RP-HPLC purification analysis

Figure 7.18 The RP HLC data of the purified PVA target, eluted into MilliQ water, synthesised using solid-phase oligonucleotide synthesis showing 99.7 % purity. The strand was purified using the Short Oligo method.

7.3.1.10 PVA target mass spectrometry analysis

Figure 7.19 The negative electrospray ESI MS analysis of PVA target after the RP-HPLC purification seen in Figure 7.18. The correct mass was seen at 7553.5 Da.

7.3.2   Sequencing results of plasmid transformation

The sequencing results for the plasmid containing the potato virus Y (PVY) coat protein target can be seen below and the text in red showed the sequence was present within the plasmid.

5'- ATC TCA AAT ACT CGA GCA ACT CAA TCA CAG TTG ATA CGT GGT ATG AAG CGG TAC AAT TTG CAT ACG ACA TAG GAG AAA CTG AAA TGC CAA CTG TGA TGA ATG GGC TTA TGG TTT GGT GCA **TTG AAA ATG GAA CCT CGC CAA ACA TCA** ACG GAG TTT GGG TTA TGA TGG ATG GAG ATG AAC AAG TCG AAT ACC CAC TGA AAC CAA TCG TTG AGA -3'

7.3.3 RP-HPLC of Buffer D

All the RP-HPLC chromatograms in this appendix show a bump in the last 10 minutes of the chromatograms. The chromatogram from the buffer D blank (**Figure 7.20**) shows that the bumps are present within the buffer and not within the samples.
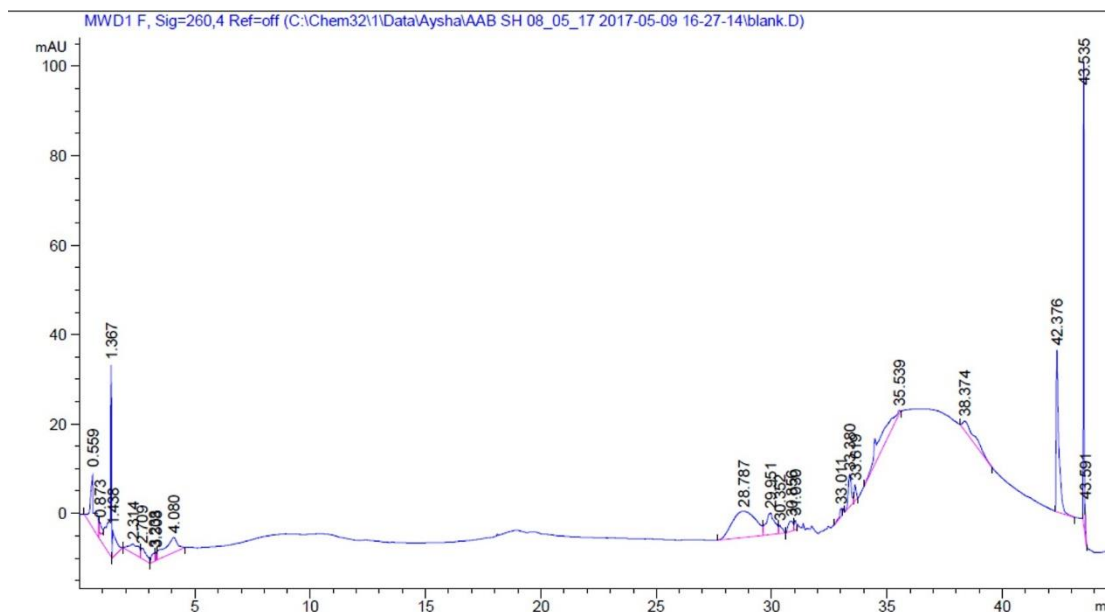

Figure 7.20 *The RP-HPLC chromatogram of the blank which is applicable to all the RP-HPLC analysis in this appendix.*